Spring 2024

Conceptual Design Methodology for the Fan-in-Wing VTOL Aircraft

Brock Steinfeldt
Embry-Riddle Aeronautical University, STEINFEB@my.erau.edu

CONCEPTUAL DESIGN METHODOLOGY

FOR THE FAN-IN-WING VTOL AIRCRAFT

By

Brock Steinfeldt

A Thesis Submitted to the Faculty of Embry-Riddle Aeronautical University

In Partial Fulfillment of the Requirements for the Degree of

Master of Science in Aerospace Engineering

April 2024

Embry-Riddle Aeronautical University

Daytona Beach, Florida

ACKNOWLEDGEMENTS

I would like to take this opportunity to thank the incredible support system that has guided me through my academic career and inspired me to complete this work. Though I cannot contain my gratitude for these people to a single page, I would like to use this space to acknowledge the biggest supporters of my research and thank them for their contributions to this endeavor.

To my thesis advisor, Dr. Richard Anderson, for his invaluable knowledge, expertise, and patience in guiding me through this project. To the members of my committee, Dr. Kyle Collins, Professor Kimberly Heinzer, and Dr. Alex Chaparro for their faith in my research and steadfast mentorship.

To the team at VerdeGo Aero, who graciously granted me their wisdom, tools, and financial resources to achieve this milestone. This company has completely transformed my career and fueled my passion for aviation.

To Embry-Riddle faculty members Dr. Hever Moncayo, Dr. Victor Huayamave, and Dr. Azizi Boutros for providing me undergraduate opportunities to excel and prove myself outside the classroom. I am especially grateful to the members of the Advanced Dynamics and Controls Laboratory for their generosity, advice, and friendship.

To my high school teachers who believed I could do anything I put my mind to. To coaches David Harms and Scott Patton for their profound impact on my character, and to Kevin Seidl, for going above and beyond to empower me as a student, athlete, and friend.

Most importantly, to my dearest friends and family. To my college roommate, David Vaden-Kiernan, for his enduring companionship. To my closest friends, with whom I share my most valuable memories and life goals. To my beloved mother and father, whom I am eternally indebted, and to my brothers Ben and Brody, who have always been by my side.

ABSTRACT

The Fan-In-Wing (FIW) aircraft concept is one of the most compelling solutions for missions demanding jet-like cruise speeds and Vertical TakeOff and Landing (VTOL) capability. However, despite years of interest and documented improvements in lift-fan technology, there exists little in the way of an adequate theory for conceptual design of a fan-in-wing aircraft. To address this issue, a general conceptual design methodology has been developed as a source of guidance for the FIW designer. Through this work, the top-level requirements ranking the fan-in-wing concept above other VTOL aircraft have been defined, while a cross-comparison between the FIW concept and conventional aircraft reveals major discrepancies in their design philosophies, constituting the need for a separate design algorithm. The final conceptual design methodology emerges from an elaborate technique of relating the FIW concept's major cruise and hover performance metrics to a physical disk area constraint imposed by the size of its wing reference area. Out of this process, a theoretical and practical design space for sizing the FIW concept has been defined, and as a result, the FIW aircraft designer is given an effective means of iterating on the initial size of their wings and lift fans to meet a set of cruise and hover performance requirements. A final demonstration of how the conceptual FIW design methodology is implemented in practice has been included using an example case study.

TABLE OF CONTENTS

LIST OF FIGURES

Figure **Page**

LIST OF TABLES

Table **Page**

NOMENCLATURE

The main symbols and their respective subscripts used throughout this text are listed below.

MAIN SYMBOLS

a_w	Wake contraction parameter
Ad	Disk area
Ad/S	Disk-to-wing area ratio
AR	Aspect ratio
b	Span
c	chord
c_t	Thrust specific fuel consumption
C	Coefficient
D	Drag
k	Induced power factor
K	Induced lift coefficient
L	Lift
L_x	Disk-to-wing area limiter
P	Power
P/W	Power-to-weight ratio
P_c/P_h	Cruise-to-hover power ratio
P_a/P_c	Available-to-cruise power ratio
P_a/P_h	Available-to-hover power ratio
S	Wing reference area
T	Thrust

T/A (DL)	Disk loading
T/W	Thrust-to-weight ratio
V	Velocity
w	Width
W	Weight
W/P (PL)	Power loading
W/S (WL)	Wing loading
β	Energy weight fraction
ϵ	Specific energy
η	Efficiency
Ω	Rotational speed
ρ	Density
σ	Solidity

SUBSCRIPTS & SUPERSCRIPTS

a	Available
Ad/S	Disk-to-wing area ratio
Bat	Battery
bz	Buffer zone
c	Cruise (required)
cs	Control surface
d	Drag (2D)
D	Drag (3D)
e	Equivalent

em	Electric motor
eng	Engine
f	Friction
F	Fuselage
g	Gas turbine
h	Hover (required)
i	Induced
lf	Lift-fan
l	Lift (2D)
L	Lift (3D)
m	Reference value
max	Maximum
p	Propeller
pack	Battery pack
r	Root
s	Stall
tip	Tip
T	Thrust (3D)
w	Wetted
x	Variable/Interchangeable
0	Initial/Profile (zero-lift)
/2	Semi-span

ABBREVIATIONS

AAM	Advanced Air Mobility
AFRL	Air Force Research Laboratory
AFWERX	Air Force Work Projects
ANCILARY	Advanced Aircraft Infrastructure-Less Launch and RecoverY
BRE	Breguet Range Equation
CFD	Computational Fluid Dynamics
CTOL	Conventional Takeoff and Landing
CV	Carrier Takeoff and Landing
DARPA	Defense Advanced Research Projects Agency
DoD	Department of Defense
eVTOL	Electric Vertical Takeoff and Landing
FAR	Federal Aviation Regulations
FARA	Future Attach and Reconnaissance Aircraft
FLRAA	Future Long Range Assault Aircraft
FIW	Fan-In-Wing
GE	General Electric
HOGE	Hover Out of Ground Effect
HSC	High-Speed Cruise
HSVTOL	High-Speed Vertical Takeoff and Landing
JSF	Joint Strike Fighter
LF	Lift-Fan
NASA	National Aeronautics and Space Administration

NATO	North Atlantic Treaty Organization
SPRINT	Speed and Runway Independent Technologies
STOVL	Short Takeoff and Vertical Landing
STOL	Short Takeoff and Landing
VFS	Vertical Flight Society
VTOL	Vertical Takeoff and Landing

1. Introduction

To prelude the momentum behind this research, a brief motivational section has been provided to introduce the subject matter.

1.1. Motivation

The United States military has been in pursuit of an aircraft as versatile in vertical flight as it is in high-speed cruise for decades. One of the most successful Department of Defense (DoD) efforts aimed at achieving this goal was the Joint Strike Fighter (JSF) program of the late 20th century. The objective of the JSF initiative was to support the development of a next-generation, multi-role warfighter to replace outdated fighter, strike, and ground attack aircraft [1]. Unlike conventional jets, the JSF program called for a two-in-one supersonic and Short TakeOff and Vertical Landing (STOVL) design. Despite the incredible challenge, Lockheed Martin's successful execution of the X-35 went on to make the F-35B the latest and most technologically advanced addition to the U.S. fleet of stealth combat aircraft. However, the declaration of a JSF winner was only the beginning of a much larger and more demanding U.S. search for High-Speed Vertical TakeOff and Landing (HSVTOL) platforms.

Since the JSF program, a number of new federal HSVTOL initiatives have been backed by the U.S. Army, including the former Joint Multi-Role (JMR) program that has since become Future Vertical Lift (FVL). The goal with FVL is to phase out the Army's aging fleet of UH-60 Black Hawk, AH-64 Apache, CH-47 Chinook, and OH-58 Kiowa helicopters with aircraft of improved speed and range [2]. Development programs under FVL include the FARA (Future Attack and Reconnaissance Aircraft) and FLRAA (Future Long Range Assault Aircraft) competitions, which have motivated designs like the Bell Valor V-280 tiltrotor and the Sikorsky/Boeing Raider X compound helicopter.

Other major HSVTOL initiatives have been led by the Air Force's innovation division (AFWERX) in conjunction with the Air Force Research Laboratory (AFRL). The Agility Prime and HSVTOL competitions were two of their latest calls for transformative military aircraft. While the former focused on state-of-the-art HSVTOL designs, the latter has been devoted to electric Vertical TakeOff and Landing (eVTOL) type aircraft. Furthermore, the Defense Advanced Research Projects Agency (DARPA) has supported the Air Force with additional VTOL development initiatives. In 2023, DARPA announced its intentions to kick off two X-plane projects: the SPeed and Runway INdependent Technologies (SPRINT) and AdvaNced aircraft Infrastructure-Less Launch and RecoverY (ANCILLARY) projects. As the SPRINT program targets scalability and efficiency in high-speed VTOL aircraft, the ANCILLARY project will seek new developments of unmanned VTOL aircraft requiring minimal operational infrastructure.

Table 1.1 shows a timeline of the major HSVTOL initiatives set forth by the U.S. in recent years, alongside their program requirements. Considering most of these programs were only announced within the last six years, Table 1.1 indicates that the relevancy and urgency behind HSVTOL development in the U.S. has reached unprecedented levels. Moreover, the objectives of these programs are staggering. In comparison to the "jet-like" target speeds of 400 knots, today's combat ready, high-speed rotorcraft such as the AH-64 Apache and V-22 Osprey are only capable of reaching 158 to 300 knots, respectively. Although building an HSVTOL aircraft in and of itself is an ambitious feat, adding range, survivability, payload, and maneuverability requirements only burdens the task with even more complexity. Achieving the desired HSVTOL program objectives, therefore, will require rethinking existing aircraft propulsion and state-of-the-art blending technology to balance efficient hover performance with the higher-speed cruise requirement.

Table 1.1 Program requirements of various U.S. HSVTOL initiatives in recent years.

Program		JSF	HSVTOL	FARA	FLRAA	Agility Prime eVTOL AOI-3	SPRINT	ANCILLARY
Year Announced		1996	2017	2018	2019	2020	2023	2023
Requirements	Dash Speed	>Mach 1.5	"Jet-like speeds" (400 kts)	180-200 kts	250-280 kts	>173 kts	400-450 kts	"High-Speed"
	Combat Radius	>400 nmi	>300 nmi	>200 nmi	200-300 nmi	>87 nmi	>200 nmi	"Long range"
	Endurance	NA	NA	NA	NA	>1.6 hr	>1.5 hr	"Long endurance"
	Survivability	HCE	HCE	Operable in harsh, dense, and complex environments	Operable in hot & cold conditions via MIL-STD-810	NA	NA	"Operable in adverse weather"
	Payload Weight	Internal >10k lb	>5,000 lb	MGTOW <14,000 lb	Internal 3.5-4k lb External 6-8k lb	>500 lb MGTOW >1,320 lb	>5,000 lb	~60 lb MGTOW 250-350 lb
	Volume	NA	Internal 1-2 std. pallets	Rotor diameter <40 ft	Internal seating for 10-12	NA	Internal 2-2.5 std. size cargo pallets	Compact
	Hover	STOVL capable	Low downwash 4k/95 HOGE @ MGTOW	VTOL capable	6k/95 HOGE @ MGTOW	VTOL capable	VTOL capable Stable in hover	VTOL capable
	Misc.	Multi-variant Stealth-driven design	Scalable In-air refueling capability	Maximum 3,000 shp	In-air refueling capable Inter-operability Operable for at least 30 min. with organic maintenance support	NA	Scalable	Autonomous

The motivation behind HSVTOL aircraft in the military stems primarily from a national defense vantage point. To compete with global superpowers, the U.S. is under constant pressure to adapt and innovate on warfighting technologies. Likewise, the U.S. is in a race against time to come up with high-performance replacements for its aging fleet of helicopters. At the time of Vietnam and various ongoing wars throughout the 1960s-90s, international conflict drove a serious

demand for a combat search and rescue aircraft that could infiltrate highly contested airspace to retrieve and extract downed personnel much quicker than available helicopters could. HSVTOL aircraft were also desirable for navigating the various Pacific Island chains without a dependency on long runways, as well as recovering reentry crew capsules to assist NASA's space program. This led to a surge of experimentation with VTOL aircraft design and resulted in the development of over 45 unique concepts, shown in Figure 1.1 from the Vertical Flight Society (VFS), each with mixed success. While a select few did lead to full-scale production, a fully operational aircraft that satisfies all HSVTOL requirements has yet to be seen.

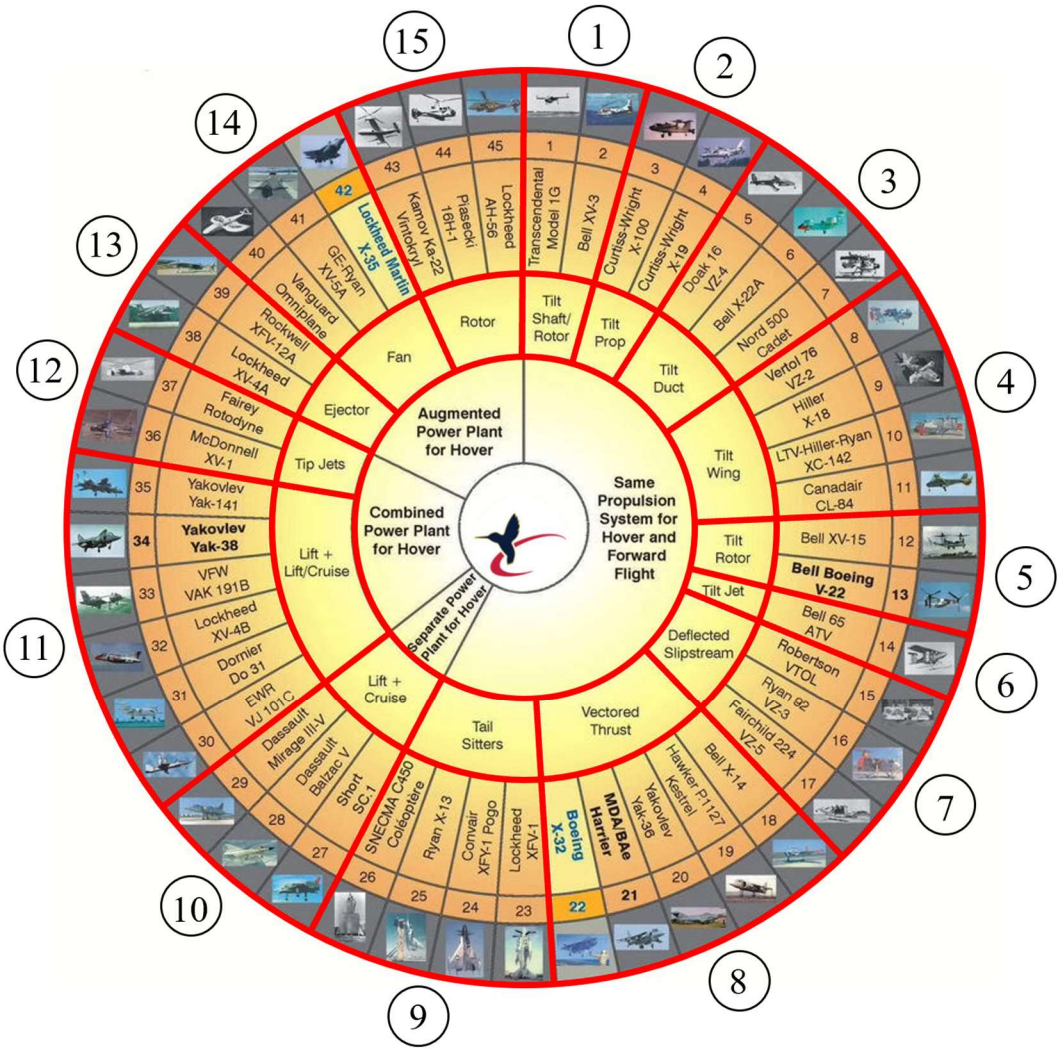

Figure 1.1 The VFS V/STOL Aircraft and Propulsion Concepts Wheel [3].

Unexpected changes in the geopolitical climate further reinforce the need to not only replace existing systems, but to update and amplify weapon systems for the future. A major concern with large runways is their vulnerability to security threats from readily available satellite imagery and enemy intelligence communities. If adversaries were able to locate and eliminate a military's critical ground support systems, its air defense and strike capabilities would be compromised. However, by reducing aircraft takeoff and landing requirements, not only would the enemy spy efforts and destruction potential be dampened, but it would also improve the military's aerial mobility by enabling aircraft to deploy from offshore rigs, aircraft carriers, and unimproved terrain. Furthermore, the fact that it takes decades to develop next-generation aircraft is all the more reason to advocate for designs now. As General Eisenhower once famously said, "in preparing for battle, I have always found that plans are useless, but planning is indispensable" [4].

Recognizing the strong incentives that exist for HSVTOL design, in addition to the extensive history of past HSVTOL programs, raises important questions for aircraft designers of the future. For instance, why, after all this time, have there been so few successful HSVTOL designs? Moreover, why are we now witnessing a sudden resurgence in HSVTOL initiatives? If future aircraft designers are expected to build upon past lessons learned, what guidance will they follow in developing the most advanced HSVTOL systems of all time?

Instead of looking to the past, perhaps the answers lie in forward thinking. Many would argue the late 20th century experimental VTOL aircraft were limited in success because of inadequate propulsion systems. Others would suggest it was the flight controls of the time that were not responsive enough or yet capable of reducing the high pilot workload these aircraft required. Some might first point out that structures were the primary limitation, citing the excessive weight and

mechanically complexities of early VTOL systems, while others would indicate that high technical risks and unaffordable program costs were the ultimate demise of early HSVTOL design efforts.

In reality, all of these factors had a part to play in grounding the HSVTOL demonstrators of the late 20th century. However, a major difference in the motivation behind current HSVTOL programs is the idea that many hindrances of the past can now be surmounted with modern technologies. Today, advances in high lift devices and distributed electric propulsion may offer new pathways to achieving vertical flight. Automation through fly-by-wire control systems has also been widely adopted to improve controllability as well as static and dynamic stability. Similarly, breakthroughs in light-weight composite structures are leading to significant reductions in empty weight fraction. Together, these improvements in aerospace technology could reshape the way aircraft are designed and renew lost hopes of a viable HSVTOL concept.

Furthermore, advancements in aerospace technologies have enticed designers to revive failed concepts of the past with novel advances in aerodynamics, propulsion, controls, and structures. Many speculate that if some of the unsuccessful VTOL designs making up the VFS V/STOL Wheel were to be reattempted today with modern technology, a good portion of them could prove to be viable. As a result, hundreds of individuals and organizations alike have been inspired to revamp past designs and conceptualize entirely new concepts leveraging distributed electric propulsion and modern design principles. According to the VFS eVTOL aircraft directory [5], the total number of proposals for electrically powered, vertical flight aircraft has surpassed 800.

While the number of proposed concepts is significant, what is more striking about the VFS eVTOL directory is the amount of concepts which feature embedded lift fans. The embedded lift-fan (LF) design – also known as the or “vertifan” or “Fan-In-Wing” (FIW) concept when the fans are located in the wings – is a classification of VTOL aircraft that features cutouts in its structure

to support vertical lift fans and occupies a separate or augmented propulsion system for thrust production [6]. Among all the various VTOL propulsion types, like conventional rotorcraft, tiltrotors, folding rotors, etc., one undeniable observation is that the FIW concept has persisted as a top VTOL aircraft design over the years.

Statistically, the embedded lift-fan or lift-rotor design makes up approximately 16.5% of all aircraft cataloged to date in the Vertical Flight Society's eVTOL aircraft directory. While the current VFS directory is somewhat convoluted with unspecific concepts, variation repeats, and those blurred between multiple classifications, estimated totals have been made upon close review and thoroughly filtering out disqualified entries. In total, there are roughly 845 concepts listed at the time of this writing, of which 817 are manned aircraft and 699 are unique concepts from 467 unique organizations. Of the 699 unique concepts, at least 116 involve some type of embedded lift fan, while 286 related vectored thrust and 352 ducted fan concepts have been accounted for.

In translation, this would imply that if the 15 different propulsion types specified in Figure 1.1 were each to take up an even share of the total eVTOL market, the embedded fan concept would occupy 247% of its allotted market share. Furthermore, lift-fan concepts were identified originating from all ranges of interested parties, including private hobbyists, university student project teams, and even well-known companies. Among the high-profile sponsors were automakers Aston Martin, Cadillac, Porshe, and Subaru, as well as aerospace groups Leonardo Helicopters, Pipistrel, Horizon Aircraft, Urban Aeronautics, Jetoptera, Valkyrie, and the XTI Aircraft Company. Although only a select number of LF concepts are portrayed in Figure 1.2, the complete breakdown of the lift-fan classification from the VFS eVTOL aircraft directory is provided in Table 6.1 of Appendix A.

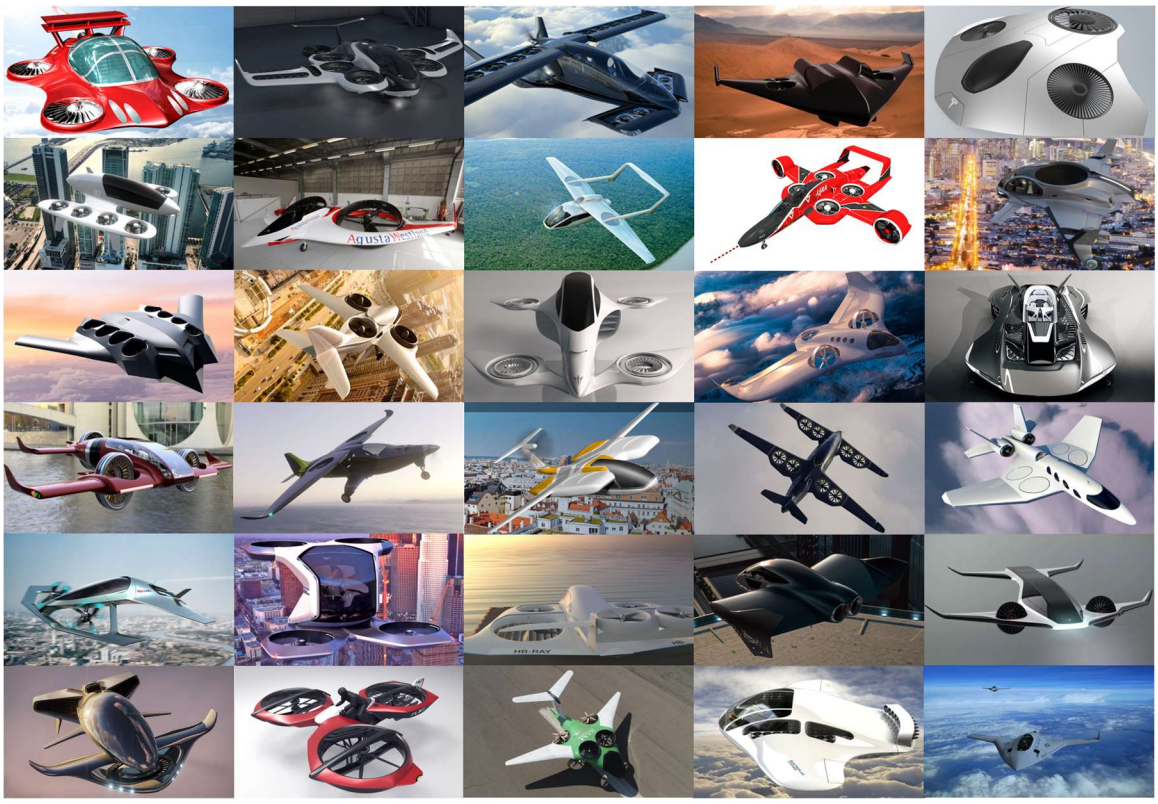

Figure 1.2 Collage of modern-day lift-fan concepts, images from the VFS [5].

Surviving the rigorous trials and tests of many decades, it is clear the LF and FIW concepts remain prominent in HSVTOL design. However, what is less clear is the design methodology behind the fan-in-wing concept required to uphold its timeless appeal. With only a few full-scale LF aircraft in the world to ever have flown, there is little guidance supporting new aircraft designs around a lift-fan propulsion system. A general conceptual design methodology proposed by Figure 1.3 can be adopted from conventional design processes to fulfil this task, but the present gaps surrounding the LF and FIW specific design criteria has left HSVTOL program initiators, decision makers, engineers, and design students alike wondering how exactly one might approach a FIW aircraft design from scratch. To better make sense of this pressing question, an in-depth review of the relevant literature around lift-fan aircraft has been conducted.

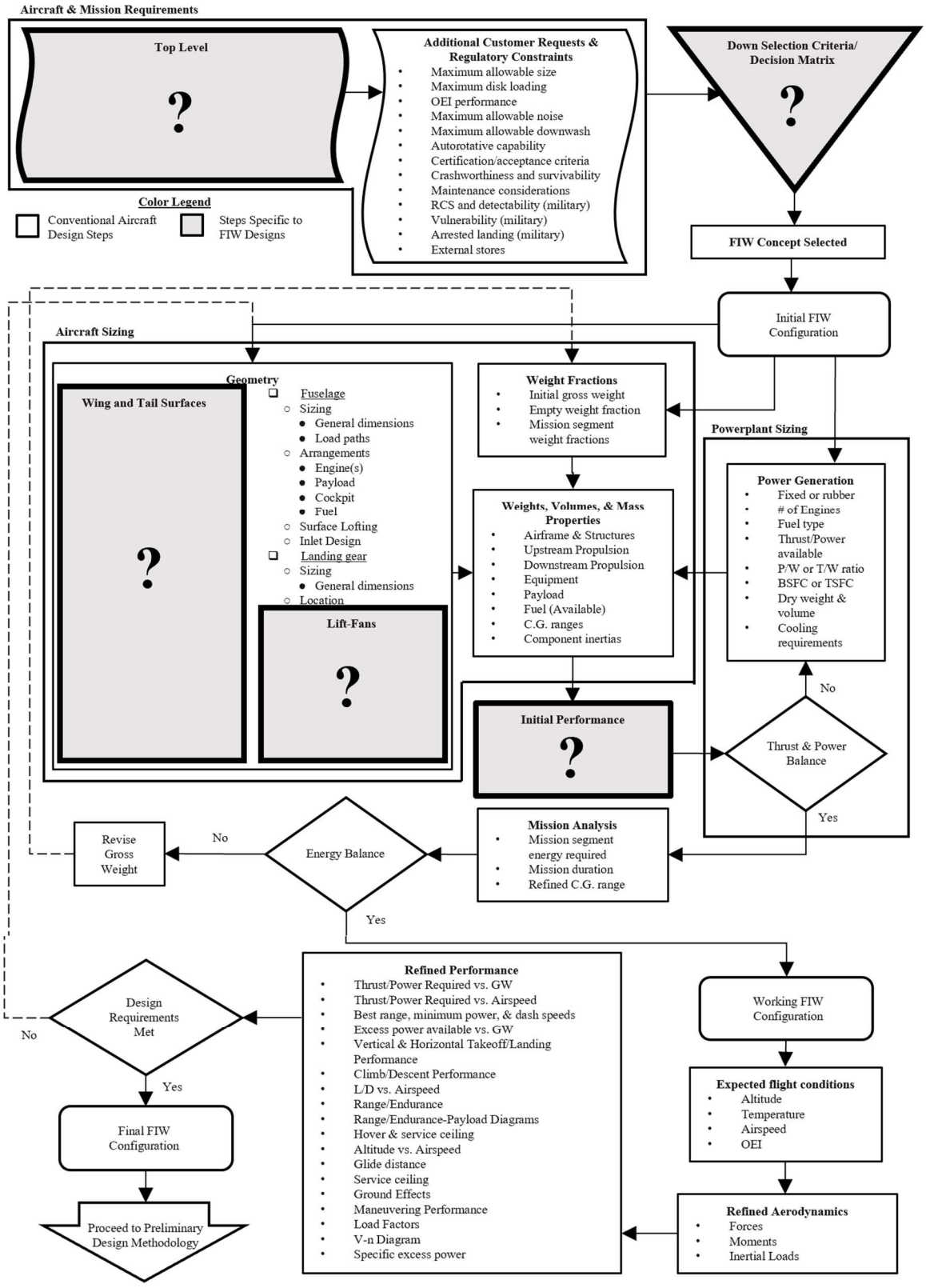

Figure 1.3 Possible conceptual design methodology for FIW aircraft with gaps specific to FIW designs (in gray) that must be addressed, adapted from [7].

2. Review of the Relevant Literature

The starting point for any aircraft design, regardless of configuration, mission, or end goal, is typically a review of similar past concepts. Designers begin by referencing historical designs to both rationalize their initial estimates and to familiarize themselves with what has and has not worked in the past. An overall lack of successful lift-fan designs, however, presents a significant barrier to the entry of new FIW aircraft, because the large database required to piece together sizing trends does not exist for the FIW concept like it does for conventional airplanes and helicopters.

Of all the FIW concepts extensively investigated in the late 20th century, only a select number were ever fully built, underwent wind tunnel testing, and recorded real flight test data. Even fewer yet have made their data available in the public domain. To this day, there exists only one true lift-fan aircraft that ever went into mass production – the F-35B Lightning II – and as a result, a conceptual design methodology adequately capturing the FIW design process has yet to be seen. Thus, the next best place to seek guidance on future FIW designs is to review the most historically significant lift-fan concepts, additional design work, and related VTOL concepts to date.

2.1. Historically Significant Lift-Fan Aircraft

The earliest experimental lift-fan aircraft concepts appeared around the 1950s, a time when post-WWII economic expansion and mounting political tensions between global superpowers aligned as catalysts for driving technological progression. Among the arrival of the first televisions, nuclear bombs, and space satellites, a push for air superiority and improved mobility also motivated designs for high-performance VTOL aircraft. The U.S. military was particularly concerned with the next European war involving an exchange of nuclear weapons that would destroy most airbases and render conventional takeoff and landing (CTOL) fighters useless. NATO

needed a runway independent, second-strike capability, and thus a great push for VTOL aircraft ensued.

Among the earliest lift-fan aircraft built was the VZ-9-AV "Avrocar" [8]. Led by chief engineer John "Jack" Frost from the Avro Canada group, the Avrocar was a decade-long development program of a disk-shaped supersonic VTOL fighter. The design emerged from Frost's work on a new type of turbine engine in the late 1940s, which featured a turbine-driven compressor using gearing rather than a shaft. This idea was intended to simplify Frank Whittle's reverse flow design by using flame cans directly outside the centrifugal compressor's outer rim. As a result, Frost's engine took the form of a large disk, with the inlet in the center and jet thrust directed around the outer rim. While the design was poorly suited for conventional jets, Frost believed it was a great contender for military VTOL applications.

Between 1952 and 1961, Frost and the Avro Canada group struggled to contend with competing VTOL designs, but they managed a number of government contracts to keep the project alive. By 1958, Frost had the U.S. Army and Air Force invested in his aircraft, and the Avrocar was developed as a proof-of-concept test vehicle. Between 1959 and 1961, much was learned about the performance of an annular lift-fan aircraft, including ground effect and hot gas reingestion [9]. However, no reports explaining how to replicate the design ever emerged, and the vehicle itself never rose more than a few feet off the ground. Before long, funds for the Avrocar project dried up and all flying saucer programs were officially cancelled.

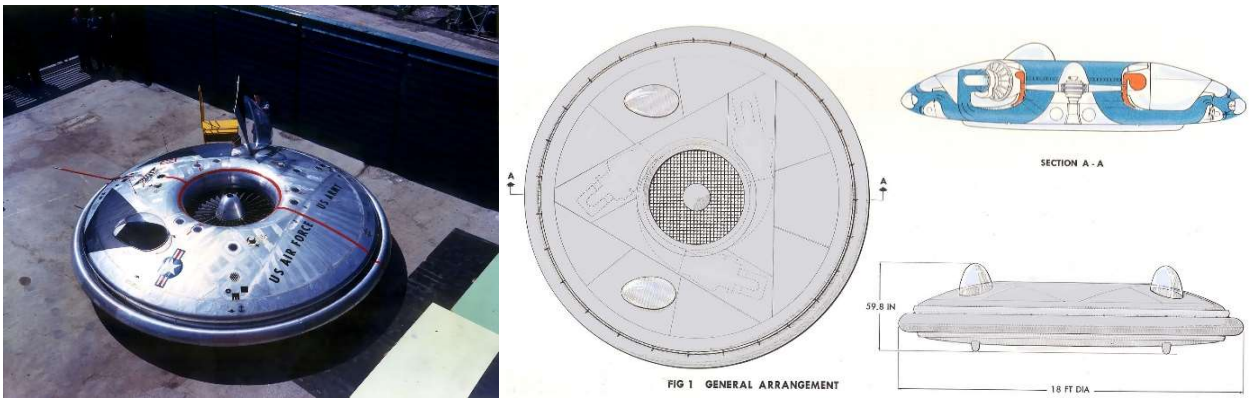

Figure 2.1 The VZ-9-AV "Avrocar" (1950s) from [10] (left) and [11] (right).

In 1959, former Piasecki engineers Edward J. Smith. Vanderlip and John L. Schneider founded the Vanguard Air and Marine Corporation with the goal of building a fixed wing aircraft with rotors embedded in its wings to combine the unique capabilities of airplanes and helicopters [12]. Supported by the U.S. Air Force and NASA, their first demonstrator aircraft, the Vanguard Omniplane 2C, was built that summer. It featured two, three-bladed, counter rotating propellers inside annular cutouts of its wings for vertical lift, while a ducted pusher prop at the tail section was meant to generate the thrust for forward flight. The Omniplane was a rather light and compact demonstrator at less than 25 feet long and a gross takeoff weight of 2,600 pounds, but the aircraft could only accommodate 1-2 people and was largely dependent on many conventional systems.

Over the next two years, the Omniplane underwent various wind tunnel experiments and tethered hover tests, receiving several upgrades and a model designation change from 2C to 2D. However, a hover test incident in early 1962 caused considerable damage to the Omniplane. Although the repairs were manageable, the Air Force and NASA considered the necessary restoration work inappropriate, claiming the design had not shown appreciable advantages over other VTOL classes of the time, and the government had collected enough data to assess the aircraft's overall performance. Nevertheless, much of this data remains hidden from the public or

lost in time, as there are still relatively few reports detailing the Vanguard Omniplane and its design approach available today [13].

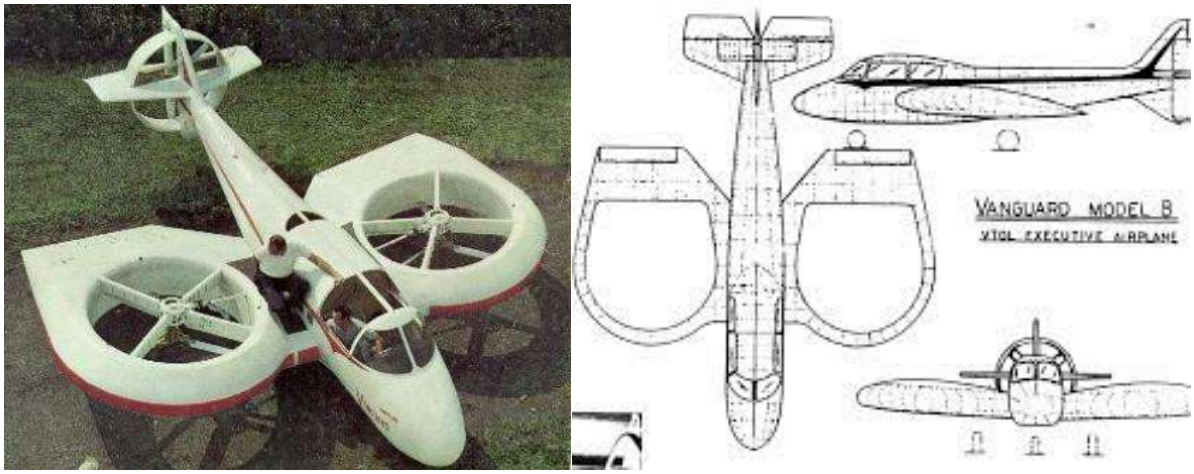

Figure 2.2 The Vanguard Omniplane (1959) from [14] (left) and [15] (right).

In 1961, the U.S. Armed Forces continued to accept proposals for VTOL aircraft under the Tri-Service Assault Transport program, with a specific interest in transporting soldiers and light weapons [16]. Although unable to get into the competition that was later won by the Ling-Temco-Vought XC-142 tiltwing concept, one designer by the name of Alexander Krivka used the program as motivation to pursue his own idea for a vertical lift aircraft – the Verticraft Verticar. As founder of the small Verticraft Corportion, Krivka envisioned the Verticraft Verticar to be a true flying car that was as equally airworthy as it was roadworthy.

Essentially, the Verticar was an extremely low aspect ratio flying wing VTOL with two lifting rotors embedded in its front and aft sections, respectively. The final design featured tilting louvers to vector the rotor thrust aft and transition to forward flight on the airfoil shaped fuselage, with a claimed 35,000 lb max takeoff weight and max speed of 420 kt, but this of course was never demonstrated. Only a single fan, subscale demonstrator was ever built and used in tethered hover testing. Despite many attempts, Krivka was unsuccessful in getting the military interested in his

design. Due to a lack of funds and resources, the Verticar project was abandoned, and the Verticraft Corporation eventually went under. Consequently, the design process behind the Verticraft Verticar remains largely undocumented [17].

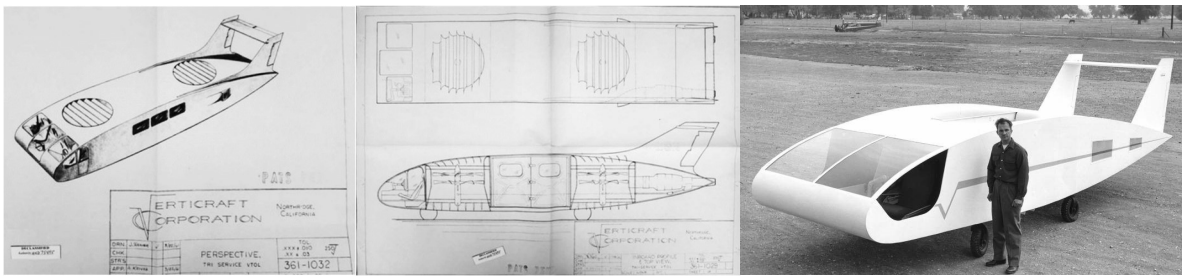

Figure 2.3 The Verticraft Verticar (1961) from [17] (left), and [18] (right).

At the same time the Verticar failed to gain military traction, the U.S. Army was actively supporting a separate lift-fan design: the GE-Ryan XV-5A [19]. From about 1961 to 1966, this experimental FIW – designated XV-5A – served as an Army testbed for assessing the performance of a lift-fan aircraft, and up until 1971, NASA continued to test a modified version of the aircraft: the XV-5B. The XV-5A utilized diverted exhaust gas from two J-85 jet engines to power two tip-turbine lift fans in its wings and a separate pitch fan in the aircraft's nose section for vertical flight. For maneuvering and transitioning to horizontal flight, the XV-5A leveraged a louvered shade system similar to the Verticraft Verticar for thrust spoiling and thrust vectoring. Once the aircraft gained enough forward velocity, the louvers were designed to completely enclose the fans, allowing the aircraft to operate as a normal airplane.

The thrust augmentation enabled the XV-5A to nearly triple the amount of thrust it could produce in hover, and consequently, it achieved a fuel burn rate in hover comparable to that in cruise. In 1965, an XV-5A test pilot suffered a fatal accident believed to have been initiated by an improperly mounted control switch, and a second XV-5A pilot was killed during a test flight in 1966 when a recuse sling was ingested by one of the wing fans. In both cases, the cause of death

was not determined to be related a lift-fan system failure, but rather a malfunction with the ejection seats. Nevertheless, the XV-5 program had succumb to budget cuts, like the lift-fan projects before it, and was effectively discontinued without any substantial algorithm published for replicating its design.

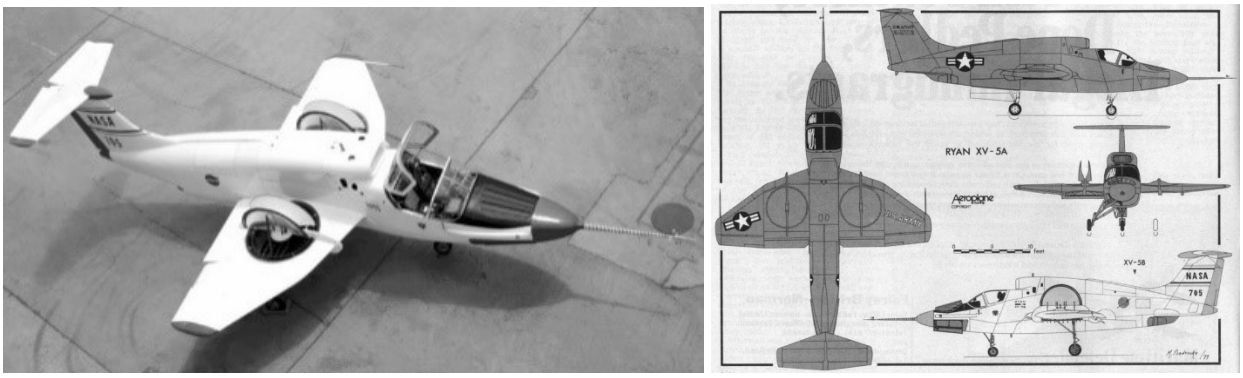

Figure 2.4 The XV-5A (1964) from [19] (left) and [20] (right).

The most successful lift-fan design ever produced was the product of several merged combat aircraft programs from the 1980s and 90s into what later became the Joint Strike Fighter (JSF) program [21]. Boeing and Lockheed Martin were selected to compete in this competition in 1997, proposing the X-32 and X-35 demonstrators respectively. While the X-32 employed a direct lift system with thrust augmentation, the STOVL variant of the X-35 made use of a patented shaft-driven lift fan in its forward fuselage section, which could be engaged via a clutch connected to its turbine engine. Each company was required to demonstrate conventional takeoff and landing (CTOL), carrier takeoff and landing (CV), and short takeoff vertical landing (STOVL), which Lockheed did by producing three separate variants of the X-35. The STOVL configuration was the only prototype with a lift-fan, and it utilized a swivel nozzle to vector engine exhaust gases vertically. Additionally, exhaust gas was vented to two roll posts under the wings for roll control. The X-35A first flew in 2000, shortly followed by the B and C variants, after which Lockheed was

announced the winner and received a contract to continue development of what would become the F-35. The F-35B flew for the first time in 2008, and to this day remains one of the most versatile fighters in the world. However, with the technical details of the F-35B's fan-driven lift system classified and steps documenting the F-35B's design absent from the public domain, designers are left to their own devices in trying to design HSVTOL systems of similar complexity.

Figure 2.5 The F-35B (2008) from [22] (left) and [23] (right).

Around the turn of the 21st century, Israeli aerospace company Urban Aeronautics began looking into a similar lift-fan configuration to the Verticraft Verticar [24]. Following the Lebanon War in 2006, chief designer Rafi Yeli wanted to create an unmanned VTOL aircraft that could perform search and rescue missions in highly contested airspace. To operate from unimproved terrain and confined areas more effectively than a helicopter, Yeli took inspiration from prior hovering platform designs like the Piasecki VZ-8 Airgeep, developing two "flying car" concepts he patented as "Fancraft." One of them would become the autonomous Cormorant (formerly "AirMule"), while the other was intended to be a multi-occupant version called the X-Hawk.

Although development of the Cormorant was led by Urban Aeronautics subsidiary Tactical Robotics Ltd. and work on the X-Hawk was undertaken by a separate subsidiary Metro Skyways

Ltd., the two vehicles originated from the same design. Like the Verticraft Verticar, the X-Hawk and Cormorant vehicles employ a tandem embedded-rotor lift system for VTOL and rely on airflow diversion around a streamlined fuselage for generating thrust and lift forces in forward flight. The first demonstration flight of Urban Aeronautics' fancraft concept took place in 2018, and while the company has expressed intentions to develop several variants for air taxi, emergency response, and law enforcement services, little has been shared on its development and general design philosophy.

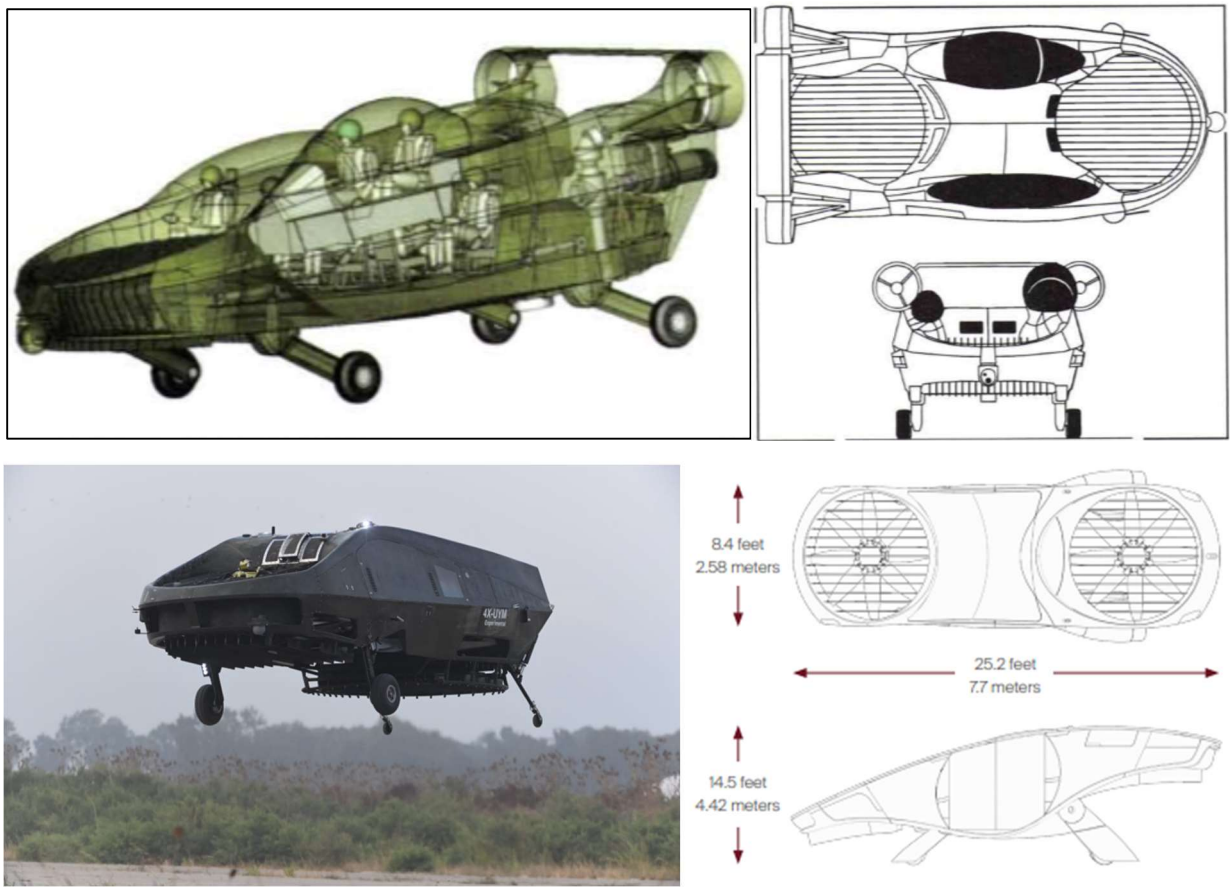

Figure 2.6 Urban Aeronautics X-Hawk (2008) from [24] (top) & Cormorant Fancraft (2016) from [25] (bottom).

Later, in 2013, Leonardo Helicopters (formerly AgustaWestland) went public with their work on a secret tilting FIW project – an unmanned eVTOL called Project Zero – under the direction of

James Wang [26]. Before the announcement, AgustaWestland had been conducting several hover tests and subscale test flights with this vehicle prior to 2013 at their Cascina Costa facilities, allowing them to refine their design of the rotor aerodynamics, rotating shroud, and electric propulsion system. While aesthetically appealing, Project Zero was purely designed to be an unmanned eVTOL technology testbed with no design mission or payload in mind.

To meet the technical readiness of rapidly advancing battery technology, AgustaWestland wanted a technology demonstrator that incorporated as many innovative design features as possible. The project name "Zero" came from the idea that this vehicle would look nothing like anything the company had developed prior. The all-electric embedded tiltrotor platform was designed without any swashplates, featured electric motors over mechanical transmission systems, and comprised of approximately 80% composite materials. In 2018, the vehicle was also slated to test hybrid-electric propulsion systems, but due to the secrecy of the project, little information has been shared about its design history, current whereabouts, or future plans.

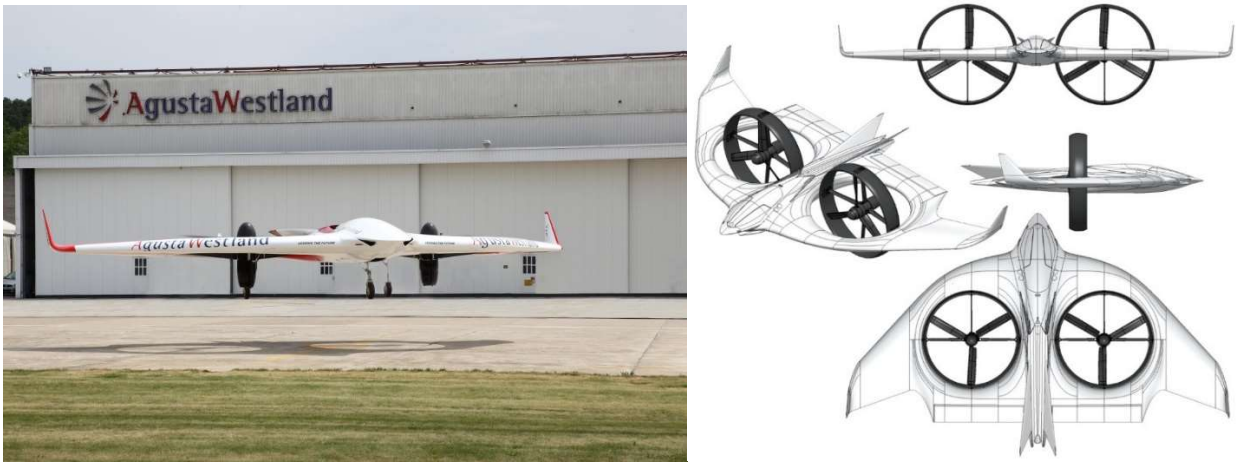

Figure 2.7 Project Zero (2013) from [26] (left) and [27] (right).

2.2. Additional Design Work

While the past 75 years or so has witnessed a handful of full-scale lift-fan demonstrators achieve vertical lift, there were many ongoing and simultaneous "behind-the-scenes" efforts involved with learning more about lift-fan technology. While none were found to explicitly detail a design methodology for lift-fan concepts, this section provides an overview of the most notable research efforts that helped accelerate the advancement of lift-fan technology.

In the 1960s, U.S. developments in lift-fan propulsion fueled by the military's interest in VTOL platforms were well under way, but only around this time did research on ducted fan and lift-fan experiments of the late 1940s and 50s start appearing in NASA technical reports and scientific journals in large quantities. In the age of the XV-5 research aircraft, a wave of flight test data, test flight experiences, and test pilot perspectives on the XV-5 emerged as progress was documented and later released to the public following declassification of the project [28-35]. In these early days, lift-fan pioneers attempted to describe the ground effects, wing leading-edge separation for induced lift, and oscillating propeller blade loads they had experienced [36]. Uncertainties surrounding scaling effects and aerodynamic interactions encouraged many researchers to advocate for larger scale lift-fan prototypes and wind tunnel testing, as shown in Figure 2.8. Furthermore, motivation from the XV-5's successes inspired many to begin contemplating the future use cases and applications of lift fan technology [29], [30-39].

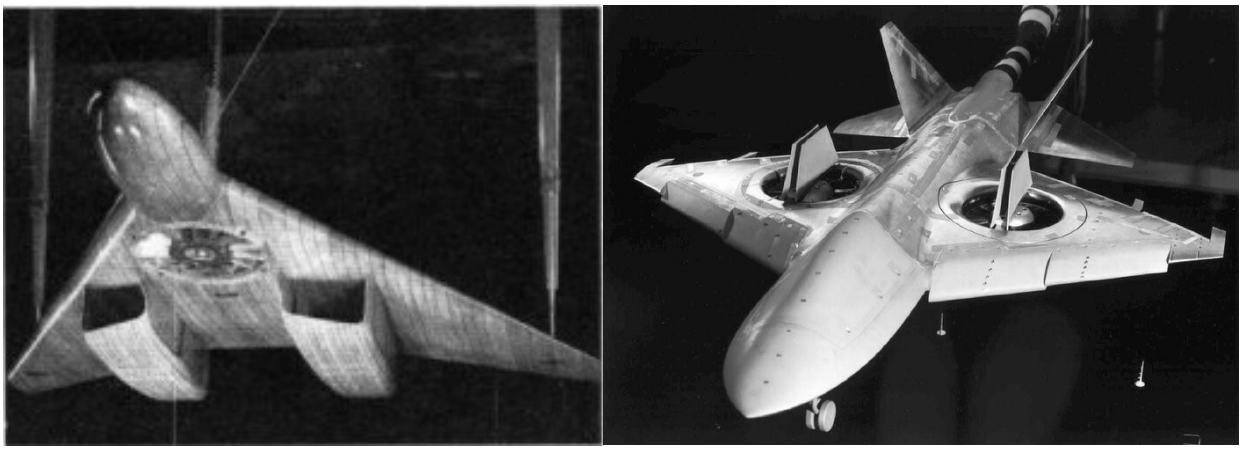

Figure 2.8 Wind tunnel models of the 3/25 scale 1950s Boulton Paul P.135 lift-fan design (left) [40] and scale model of the Grumman FAAV (G775) in 1964 (right) [41].

By the 1970s, published work on the XV-5 was everywhere. With the program freshly terminated, engineers had accumulated enough data to draw their final conclusions and perform overall assessments of the tip-turbine lift-fan system. Sentiments toward the XV-5's lift system were high enough to retain research interest in the concept, but technical concerns led many to search for improvements and alternative designs. Likewise, lessons learned from the whole XV-5 flight test experience continued to materialize, and engineers continued formulating equations that described aerodynamic effects specific to the lift-fan concept [42-44]. During this decade, a substantial amount of funding was also redistributed to investigate the feasibility of civilian jet transports utilizing lift-fan technology [45-49]. As a fundamental gap in lift-fan propulsion for commercial applications existed, researchers became increasingly interested in noise and controls implications [50-53]. Moreover, the economic, sociological, and political effects of lift-fan technology required considerable attention [54].

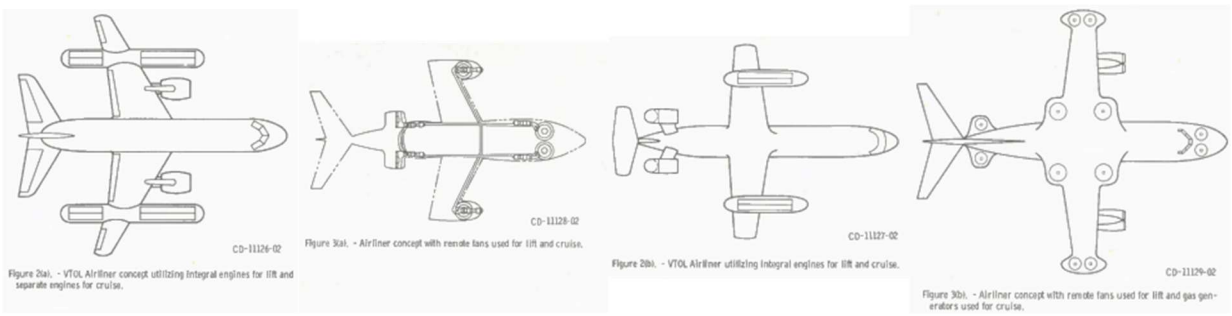

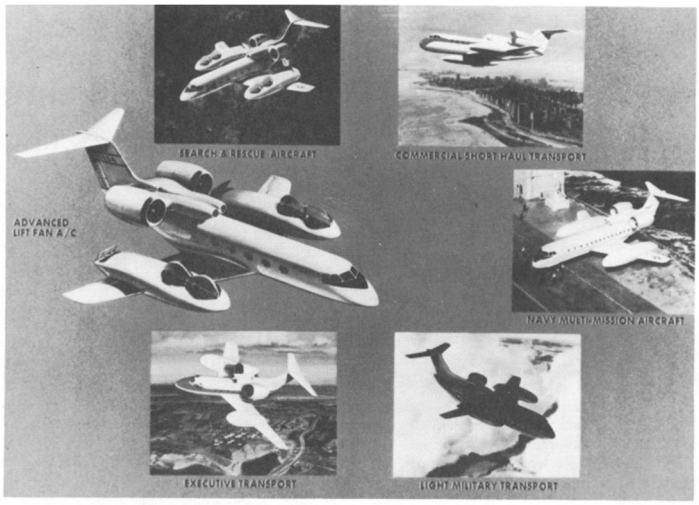

Fig. 1 - Lift-fan applications

Figure 2.9 Proposed lift-fan commercial transport concepts of the 1970s (top) from [46] and various applications (bottom) from [55].

In comparison, the 1980s saw a significant decline in publications on lift-fan technology, but the push for an HSVTOL aircraft was revitalized in the 90s leading up to the formation of the JSF program. This resurgence in HSVTOL designs led to a large number of papers summarizing the variety and updated status in vertical lift concepts that had emerged over the last half century. [56-60]. In particular, NASA produced a three-part document which thoroughly reviewed the mission requirements for a high-speed rotorcraft and reduced the massive VTOL design space down to a few of the most promising concepts [56]. While such works were milestones in defining top-level HSVTOL mission requirements, these efforts also reignited interest in the lift-fan design, leading researchers to work out similar requirements for a lift-fan aircraft [61] and [62]. Moreover, wind

tunnel tests carried on for understanding more about installation effects, distributed fans, and the contributions of various aerodynamic effects [63-65].

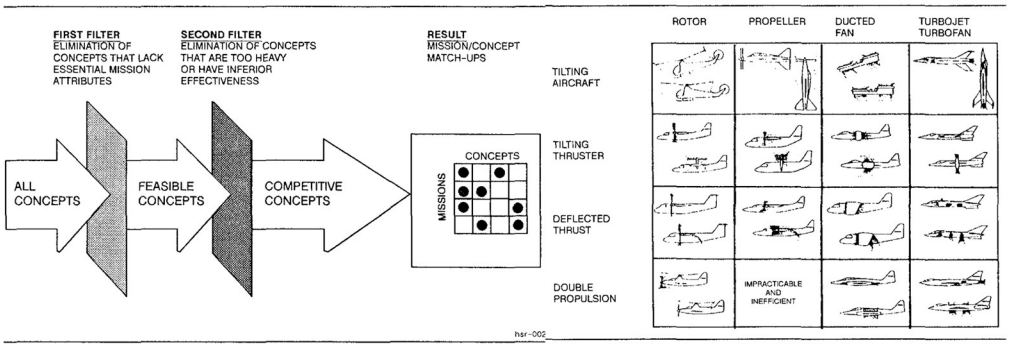

Figure 2 Mission–Concept Pair Selection Process

Figure 4 Matrix of VTOL Configurations

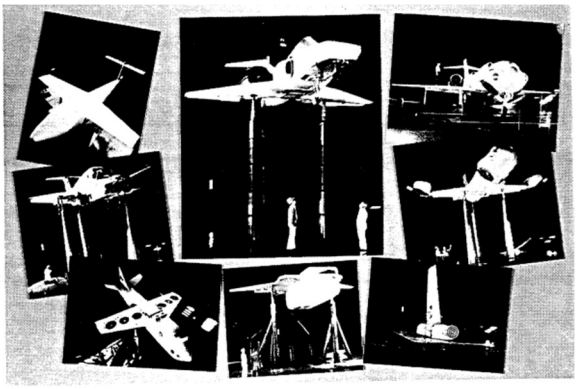

Figure 2.10 Down selection of competitive concepts in 1991 (top) from [56] and wind tunnel lift-fan summary from 1993 (bottom) from [62].

By the 2000s, modern developments in CFD [63-68] enabled higher precision simulation of lift-fan specific noise and aerodynamic effects, including details of the infamous horseshoe vortex formed by a FIW wake in crossflow [69-71]. After years went by and the F-35B program matured, descriptions of the shaft-driven lift fan were eventually circulating in the public domain [72]. However, as the crossing of autonomy, composites, and battery technology paths were soon recognized, yet another surge in VTOL aircraft erupted; this time, centered around all-electric designs (eVTOLs) and the new opportunities awaiting in Urban Air Mobility (UAM). This UAM "hype" drew massive amounts of capital and attention to revisiting previous VTOL designs with

a fresh perspective on sustainability and the versatility of electric motors. Such a movement evoked inspiration from students and industry members alike, and via ripple effect, many novel lift-fan concepts have since been proposed [73-81]. Although there have been no new prototype passenger or cargo carrying lift-fan aircraft, interest in the concept has remained steady in both commercial and military sectors of the AAM industry. Moreover, with the battery electric hype finally waning, new VTOL concepts have slowly begun to migrate toward hybrid-electric and hydrogen powered designs.

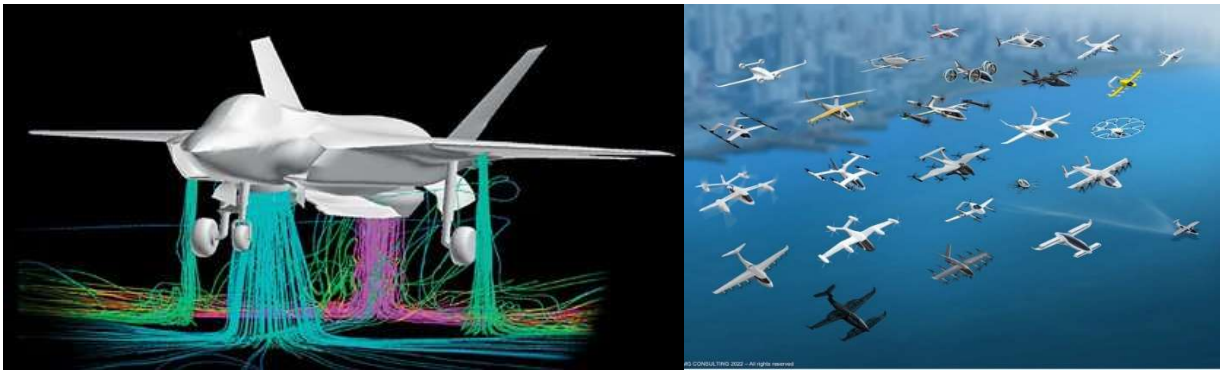

Figure 2.11 Recent F-35B CFD downwash simulation results (left) from [82] and the emergence of eVTOL designs (right) from [83].

2.3. Related VTOL Concepts

During the late 20th century boom in VTOL aircraft research, there were many competitors to the FIW configuration that emerged from similar design principles. Some of the most notable aircraft with related lift-fan technology included those of the combined-powered lift plus cruise category, as well as the ejector, tilt duct, vectored thrust, and hovering platform concepts. Due to their shared design characteristics, a brief historical review of these related VTOL concepts was conducted in search of existing design methodologies around similar concepts to the FIW VTOL aircraft.

2.3.1.Vectored Thrust

Vectored thrust concepts, which have historically been either jet or rocket powered, rely on the redirection of engine exhaust gases to go between VTOL and forward flight operating modes. One of the first jet powered vectored thrust concepts to demonstrate a full transition from hover to forward flight was the Bell X-14 in 1958. The X-14 was an experimental VTOL similar to the XV-5A in that it took off vertically in a horizontal attitude, which made it a member of the "flat-riser" jet club [19]. The X-14 featured twin turbojet engines near the center of gravity with thrust deflector vanes and reaction jets located at the wingtips and tail. The first X-14 prototype experienced a number of technical issues, including an adverse "suckdown" effect, insufficient thrust to weight ratio, and inadequate roll control. Modifications such as extended landing gear and new engines were implemented to alleviate these problems, and considerations to replace the wing tip jets with lift-fans to solve the roll issues were documented as shown in Figure 2.12.

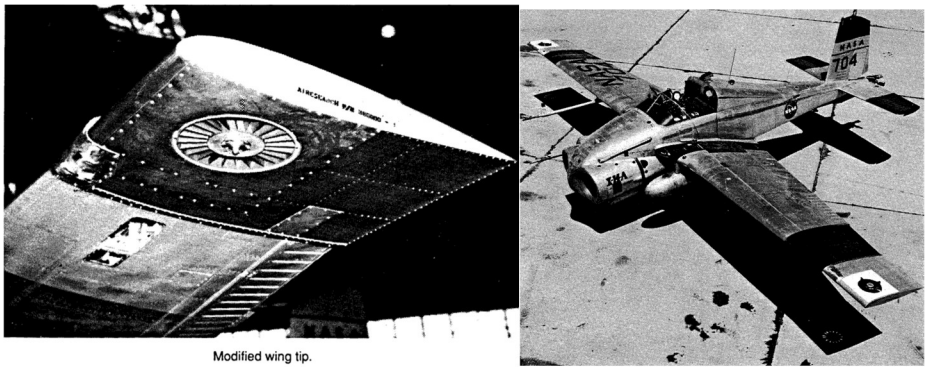

Figure 2.12 X-14A with tip-driven fans from [84].

Entering the 1960s, work began on the first-generation vectored thrust Hawker Sidley Harrier. The Harrier was designed around the late 1950s "Pegasus" engine of the former Bristol Engine Company, which possessed multiple, rotatable jet nozzles to vector and distribute thrust about the aircraft. Around the same time, the Soviets were working on a similar swivel nozzle demonstrator,

the Yakovlev Yak-36, which featured twin turbojets and a large nose air intake. While work on the Yak-36 inspired the designs of the Yak-38 and Yak-141, the Harrier design was highly successful and led to the development of the second-generation McDonnel AV-8B Harrier II later in the 1980s.

In 2001, Boeing also flew a vectored thrust STOVL fighter for the first time: the X-32. This direct competitor to Lockeed Martin's X-35B employed a direct-lift thrust vectoring system to compete with the X-35B's shaft-driven lift fan architecutre. The addition of a thrust vectoring module to the X-32's main engine was intended to simplify the propulsion system required for STOVL operation, but the decision resulted in a necessary C.G. shift and large air intake, introducing new issues with the design. In time, the X-35 was selected to become the U.S. military's next STOVL fighter over the X-32, and many of the British/American Harrier variants that once serviced all around the world have since been retired and replaced by the F-35B lift-fan aircraft.

However, as far as an overall design methodology for vectored thrust concepts goes, many existing publications only seem to detail aspects of the vectored thrust design process. For instance, works like [85] and [86] discuss individual control system and propulsion design methodologies for vectored thrust aircraft like the X-14, Harrier, and X-32, yet there appears to be a substantial gap between how the two aspects would integrate into a single design. If related FIW concepts are to benefit from the findings of vectored thrust concepts, a more general design methodology for vectored thrust aircraft must be developed.

2.3.2.Combined Lift-Plus-Cruise

The combined-powered lift-plus-cruise category pertains to aircraft with a combined powerplant for hover. This includes the traditional lift-jet and ejector concepts. Lift-plus-cruise aircraft are similar to lift-fan architectures in that they use a thrust augmenting principle for hover.

Germany was one of the earliest nations to extensively investigate the combined lift-plus-cruise VTOL design, flying three distinct prototypes in the 1960s. To continue rebuilding their post WWII military and scaling with the cold war threats, German sought to develop three nuclear war deterrents in the form of runway independent aircraft. Two of them were to be VTOL strike fighters, namely the subsonic VAK 191B and supersonic EWR VJ 101 C. With thrust vectoring exhaust nozzles similar to the Harrier, the VAK 191B's main Rolls-Royce/MAN Turbo RB. 193-12 engine provided both thrust for forward flight and lift in hover, but only when augmented by two additional Rolls-Royce lift engines could the vehicle produce enough lift for vertical flight.

The original EWR VJ 101 C prototype, the X-1, was outfitted with four engines in its tilting wingtip nacelles (two in each) and two engines vertically mounted behind the cockpit, for a total of six RB 145 engines. The EWR VJ 101 C made history as the first VTOL aircraft to break the sound barrier, and a second model (the X-2) was refitted with afterburners, but the program was later cancelled in 1968. Similarly, the thrust to weight ratio of the VAK 191B was negatively impacted by the dead weight of its additional lift engines, and in addition to political and managerial delays, plans for further production were effectively withdrawn.

A third 1960s combined lift-plus-cruise aircraft under German development was the Dornier Do 31: a cargo VTOL aircraft. The Do 31 occupied two specially modified thrust vectoring Bristol Pegasus engines inside a pair of inboard nacelles and housed eight RB162 lift engines (four on each wing) within wingtip pods. This aircraft was the first of its kind and the only VTOL jet transport to have ever flown, but suffered from high costs, high drag, and reduced payload capacity

compared to similarly sized CTOL transports. Due to a lack of support citing logistical concerns and low sales prospects, development of the Do 31 was eventually stopped altogether.

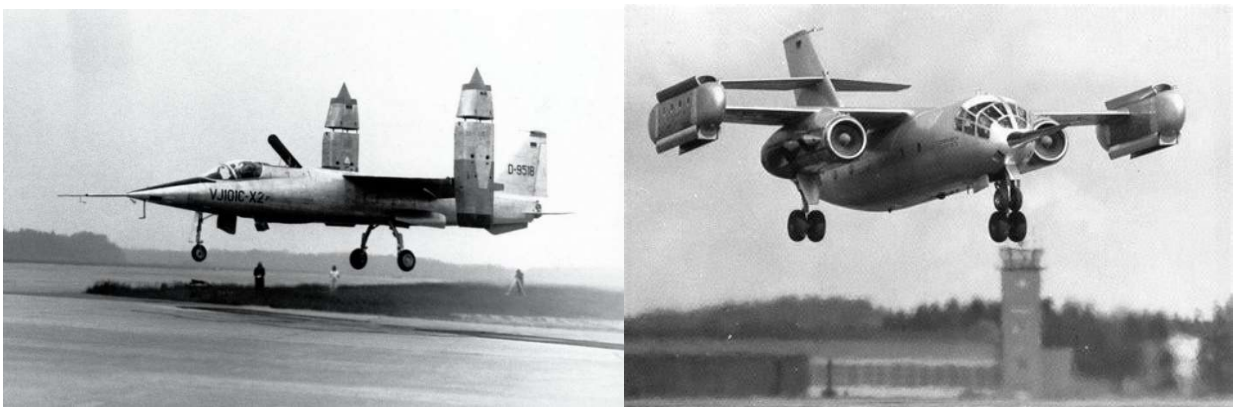

Figure 2.13 German lift-plus-cruise concepts EWR VJ 101 C (left) from [85] and Dornier D*o* 31 (right) from [88].

The Lockheed XV-4 was another 1960s VTOL endeavor funded by the U.S. army for aerial surveillance purposes. Competing to keep up with Britian's Harrier developments at the time, the XV-4A saw the use of two thrust-generating Pratt & Whitney JT12 turbojets and six lift-augmenting General Electric J85-GE-19 engines buried in the fuselage [89]. However, when the XV-4A fatally crashed during a test flight in 1964, a second XV-4B was radically reconfigured with only six GE J85 engines (two for cruise and four for hover). After a second accident with the XV-4B occurred in 1969, the Army was no longer interested in the XV-4.

Years later, Rockwell's XFV-12 thrust augmented wing concept won a request for proposals (RFP) for a supersonic U.S. Naval VSTOL fighter. The XFV-12 was designed around a single Pratt & Whitney F401-PW-400 afterburning turbofan and was expected to hover using thrust augmentation from exhaust gases ejected through openings in its large canard and aft primary wing. While the design was expected to exceed Mach 2.0, hover tests revealed inadequate hover capability compared to expectations from its paper and subscale model studies. With no affordable

and timely solution to increase the hover thrust to weight ratio, so too was the XVF-12 withheld from further development.

Following successful demonstration flights of the Yak-36, the Soviet Union proceeded to further develop a subsonic VTOL fighter known as the Yak-38 and later a supersonic VTOL fighter, the Yak-41 (misled to foreign nations as the Yak-141). Both subsonic and supersonic Soviet fighters were designed for carrier-based operations and adopted combined power cruise + lift propulsion platforms. The Yak-38 came first, with a Tumansky R-28 thrust vectoring engine performing like the Pegasus engine for cruise up to Mach 0.95 and two vertically positioned Rybinsk RD-38 turbojets buried forward in the fuselage to support VTOL flight. The first Yak-38 prototype was flown in 1970, and by the late 70s, production aircraft had entered service. The Yak-41 was designed to replace the Yak-38 and was under extensive work during the 1980s, but closely resembled its predecessor with the same three-engine layout. However, the Yak-41 possessed a Soyuz R-79V afterburning vectoring nozzle turbofan and two Rybinsk RD-41 turbojets slightly canted forward instead of vertically aligned. This configuration enabled the Yak-41 to achieve Mach 1.45, but state funding for further development was slashed in 1991.

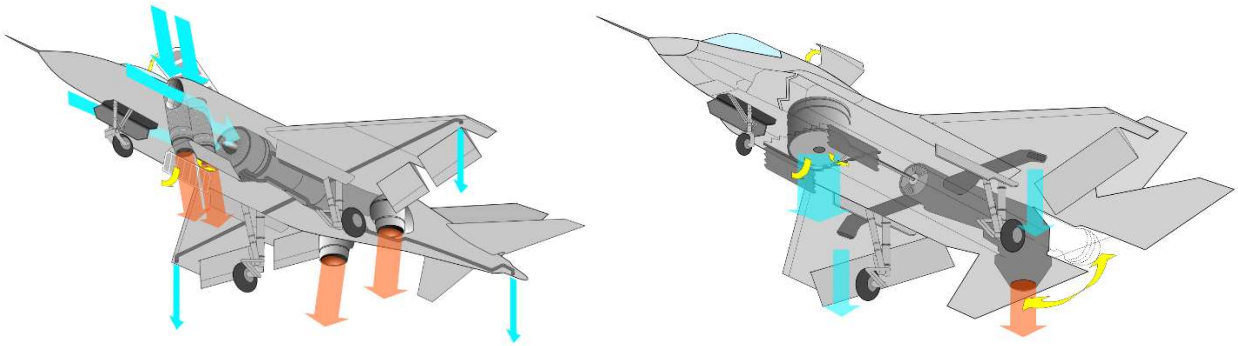

Figure 2.14 Differences in VTOL operation between the Yak-38 (left) from [90] and F35-B (right) from [91].

With many nations and concepts over the years adopting the combined-powered lift-plus-cruise VTOL architecture, a significant amount of work discussing general sizing methods and performance of the lift-plus-cruise aircraft category has been documented. NASA has contributed a great deal to this effort, responding to the latest surge in eVTOL aircraft proposals with several papers on optimization and sizing studies in electrified lift-plus-cruise propulsion [92-94]. It is possible that a related FIW design methodology might leverage design steps from this similar concept and the foundational theory that supports it.

2.3.3.Hovering Platforms

In the context of lift-fan designs, hovering platforms may encompass the original "flying" platforms, hovercraft, and all the annular disk "flying saucer" VTOL aircraft. The VZ-9 Avrocar falls in this category of flat-risers, as well as the previously mentioned Verticar, X-Hawk, and Cormorant concepts. These hovering platforms are essentially wingless lift-fan aircraft, or at least of the blended fuselage-wing variety. Their contributions to ducted fan research were pivotal to progressing the same types of technology used in more common FIW aircraft designs.

One of the first single-duct hovering platforms to take flight was the VZ-1 Pawnee from the former Hiller Aircraft company. Contracted under the Office of Naval Research in 1953, Hiller developed two models of a ducted, direct-lift coaxial hovering platform. One model, the 1032-A-1, drove its counter-rotating blades with two Nelson H-59 piston engines and a modified helicopter transmission while the pilot controlled the craft by standing and shifting their bodyweight overtop the platform. A second, slightly larger model, the VZ-1 Pawnee, sported three piston engines, an extended duct area, and required the pilot to sit while operating conventional helicopter controls. By the late 1950s, tandem ducted-fan platforms such as the Chrysler ZV-6 and Piasecki ZV-8 "Flying Jeeps" had also entered the design space through U.S. Army funding. Though flight tests

proved each of these hovering platform prototypes to be relatively stable, U.S. officials found them "unsuitable for the modern battlefield" and cancelled most concepts by 1960.

Other notable hovering platform designs that gained little success but considerable attention after the 1960s were those of aeronautical engineer Paul Moller. The most promising of his designs, the Moller M200G "Volantor," was a prototype "flying saucer" VTOL utilizing eight distributed lift-fans and eight Wankel rotary engines. Moller had been fascinated by hovercraft for years and marketed several hovercraft variants between 1970 and the early 2000s, including his Discojet and various Skycar models. However, Moller faced criticism for continually postponing developments and failing to meet deadlines. Most of his concepts never flew, and even the M200G was only proven to be a ground-effect capable during hover tests.

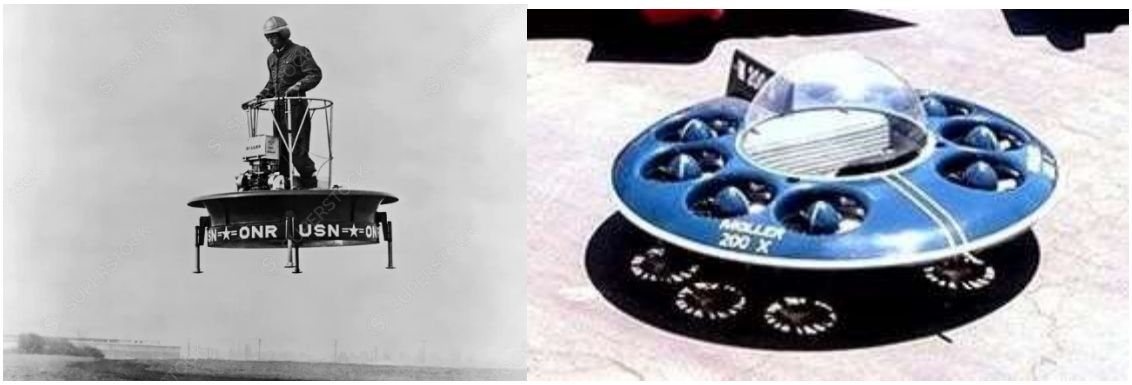

Figure 2.15 Hiller VZ-1 Pawnee (left) from [95] and the Moller M200G Volantor (right) from [96].

Although experimental reports on concepts like the VZ-9 and VZ-1 exist, there is relatively little research supporting a general design framework for hovering platforms compared to thrust vectoring and combined lift-plus-cruise concepts [97]. One may assume the absence of such design methodology correlates to the general failure of hovering platforms to fulfill any meaningful military or societal role, but the fact of the matter is, there is an evident void in the literature for design of hovering platforms, despite numerous concepts receiving funding and support over the

years. If one was to address this this gap, it is likely they would generate substantial material that is equally applicable to a FIW design methodology.

2.3.4.Tilt Ducts

The premise of the tilt duct concept is related to tiltrotors and proprotors in that the rotors on the aircraft are allowed to rotate about its lateral axis during transition between vertical and forward flight. However, the tilt duct design more closely resembles lift-fan configurations by housing its rotors or fans within ducted or shrouded structures.

The Doak VZ-4 (or Model 16) was an experimental ducted fan VTOL of the 1950s developed as a versatile helicopter replacement for the U.S. Army. Conceptualized by Edmund R. Doak Jr. of the former Doak Aircraft Company, the Doak VZ-4 was characterized by a pair of rotating wingtip-mounted fiberglass ducted fans attached to an otherwise conventional-looking airplane. Despite minor technical issues, flight tests in 1958 were rather successful, but after a few years of Douglas Aircraft taking over the project, the Army decided to cut funding for the program in favor of further helicopter development.

Nonetheless, by that time, ducted fans had already piqued the interest of the U.S. Navy, and in 1962, an RFP was released for a VTOL aircraft powered by four ducted fans. Already well versed in the VTOL design space, Bell Helicopters was awarded funding to develop the X-22 tilt duct VTOL. Their design featured four turboshaft engines atop a single aft wing, each of which was connected to one of four, three-bladed tilt duct rotors via mechanical shafting. When test flights began in 1966, the X-22 was able to demonstrate transition from hover to forward flight almost immediately. However, a crash occurred later that year, forcing the rebuild of a second prototype. Despite the potential the X-22 showed, the Bell ducted fan VTOL was cancelled and the required maximum speed was never reached.

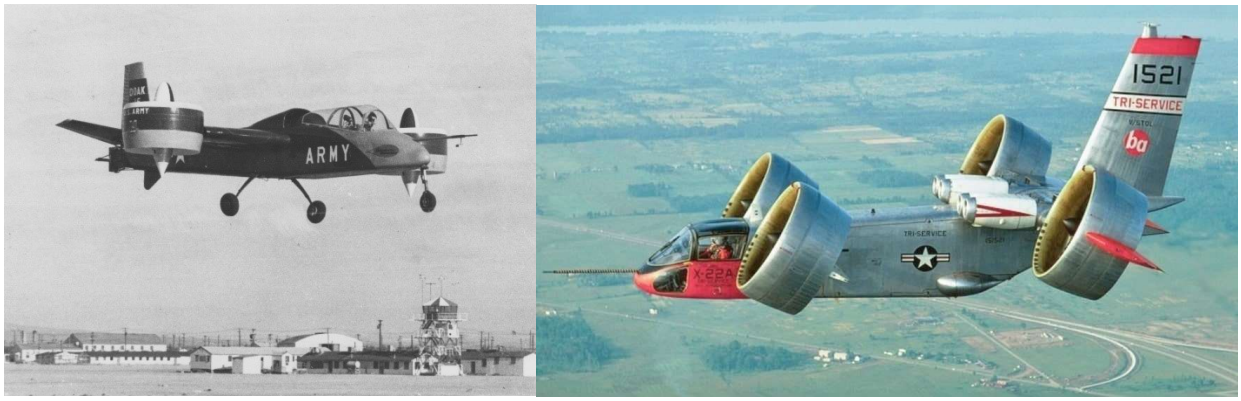

Figure 2.16 Doak VZ-4 (left) from [98] and Bell X-22 (right) from [99].

The tilt duct is yet another example of a VTOL concept almost completely left in history if not for the emergence of new aerospace market segments and a revival by modern aerospace technologies. Incentives for AAM and advances in distributed electric propulsion have once again renewed visions for concepts like the VZ-4 and X-22, as government entities and universities have begun to lay the groundwork for new tilt duct designs [100-102]. Although this momentum offers solace to the field of tilt duct design, the demand for new FIW concepts is bound to bottleneck and may altogether be halted by a vacant FIW design methodology if one is not soon developed.

2.4. Problem Statement

Achieving runway-independence with High-Speed Vertical TakeOff and Landing (HSVTOL) aircraft has been a decades long pursuit in both civil and military aviation. The challenge lies in developing a sophisticated system that satisfies the conflicting requirements of efficient hover with high-speed cruise. However, when the cruise portion of flight makes up a large percent of the total mission, the embedded lift-fan or "Fan-In-Wing" (FIW) configuration becomes one of the most compelling HSVTOL solutions due to the concealability of its vertical lift components in forward flight. The FIW concept is able to approach speeds of a conventional jet by stowing its fans away during cruise, which creates a smaller drag profile than comparable rotorcraft. In addition, the design offers lower downwash velocities and demands less hover power in comparison to similarly sized vectored thrust or ejector concepts.

Nonetheless, there exists little in the way of an adequate theory for sizing a fan-in-wing aircraft from scratch. Despite years of progress documented in the development of lift-fan technology, radical approaches to FIW aircraft designs have persisted throughout industry and academia, unguided by a foundational design algorithm that differentiates itself from traditional rotorcraft and fixed-wing design methodologies. Establishing a fan-in-wing specific design methodology is critical to streamlining the initial approach to such concept, increasing confidence in designs pursued, and distinguishing promising configurations from those violating the laws of physics. Therefore, this thesis aims to develop a sizing methodology for the conceptual design of HSVTOL aircraft utilizing FIW propulsion. By compiling data from the existing landscape of lift-fan research and deriving constraint equations for FIW geometry and performance, the objective is to quantify the theoretical and practical boundaries of the fan-in-wing design space. Moreover, this work aims to highlight aspects of the FIW design process that diverge from the conventional fixed-

wing and rotorcraft design guidelines, focusing on conceptual approaches unique to the fan-in-wing concept.

2.5. Objectives

The primary objective of this thesis work is to develop a conceptual design methodology that can be used as a general approach to conceptual fan-in-wing aircraft design. Additional research objectives aligned with completing the primary objective are listed below:

1) Understand the fundamental mission requirements that would entice designers into selecting the FIW concept over other competitive VTOL configurations and elaborate on how the FIW concept sufficiently differs from conventional fixed-wing and rotorcraft designs.

2) Examine the geometric constraints that limit the overall size of the FIW design, thus defining a useful design trade space for the FIW concept.

3) Derive the fundamental cruise and hover performance metrics of the FIW concept in terms of the parameters defining the sizing trade space, so the two may be interconnected for performance analysis.

4) Perform an example design study to demonstrate how the final FIW conceptual design methodology would be used in practice.

2.6. Presented Work Outline

The research performed has been divided into two main sections:

1) Methodology: this section has been subsequently divided into 3 subsections:

- Subsection 1: presents the conceptual design theory behind conventional fixed-wing and rotary wing aircraft. This subsection also brings the FIW design into the equation, and why it matters to form a new design methodology for such concept.
- Subsection 2: presents the geometric considerations involved in sizing the wing planform of a FIW concept, initially from a theoretical standpoint, and then through a more practical lens. This subsection defines the effective FIW sizing trade space between lift-fan disk area and wing reference area.
- Subsection 3: presents the cruise and hover performance metrics that should receive the most consideration based on the top-level mission requirements for the FIW concept. For cruise, this includes total energy, range, and power required, while the hover portion details Figure of Merit and downwash, as well as power required.

2) Results & Discussion: this section presents the amalgamation of all design considerations previously discussed to form a proposed conceptual design methodology. In addition, an example FIW case study demonstrates how the sizing constraints and performance metrics intertwine for a real FIW application.

3. Technical Approach

The following section describes the methods and related FIW theory extracted from the relevant literature that contributed to the development of the FIW conceptual design methodology.

3.1. Aspects of Conceptual Fan-in-Wing Aircraft Design

The entire process of generating a new aircraft design between initialization of the concept to full-scale fabrication can be broken down into three fundamental development stages: conceptual design, preliminary design, and detailed design [103]. Aircraft designers in the conceptual design stage rely on a set of aircraft and mission requirements to brainstorm ideas for defining their "dash-one" configuration. Based on a number of factors, including what has worked in the past, aircraft of similar mission capability, and current state-of-the-art technologies, designers use the conceptual design stage to build out an early model of how their aircraft will look, how much it will weight, what it can do, and subsequently how much it will cost.

In the preliminary and detailed design stages, estimates extracted from the conceptual design stage are verified and further refined. Designers take their time in these development phases to address underlying assumptions and fine tune the aircraft's various components until they satisfy constraints imposed by the entire system. Essentially, the preliminary design stage allows the design to mature, while the detailed design stage prepares the model for manufacturing.

The design considerations procured by this thesis, however, are mostly applicable to the initialization, or conceptual design, of the fan-in-wing concept. Since the crux of the stated problem with FIW design is the lack of a common design framework, attempting to define preliminary and detailed design criteria before establishing a conceptual design methodology would be out-of-line with the conceptual, preliminary, and detail design hierarchical order. Such work would be analogous to trying to build an aircraft before the blueprints are ready – an error-

prone and counterproductive effort. Hence, to prime the development of a fan-in-wing conceptual design methodology, it is worth summarizing the conceptual design processes of conventional airplanes and rotorcraft from which many aspects of fan-in-wing design work stem.

3.1.1.Conceptual Design of Conventional Airplanes

Conceptual airplane designs typically emerge from a set of major aircraft and mission requirements. For the military, the bottom line is aerial defense and superiority, while the commercial sector is principally concerned with maximizing revenue. However, airplane designs are usually tailored to a more descriptive set of requirements specified by the customer, who requests a minimum level of performance and sets the development deadline. In addition to minimum performance, the conventional aircraft designer must also be mindful of costs, as well as the operational, environmental, and safety constraints prescribed by law.

Under these obligations, conceptual design of a conventional airplane molds into the so called "back-of-the-napkin" sketch [103]. If the required payload is of a certain volume, such as a x-standard size cargo pallets or x-number of passengers, the fuselage should be sized accordingly. Likewise, a specified payload weight should drive the overall initial design gross weight. Other requirements with major influences on fixed-wing aircraft design include speed (affecting leading-edge sweep of the wing and powerplant selection), range (affecting required fuel weight and cruise efficiency), and operating conditions (affecting wing, engine, and landing gear layouts).

Simultaneously, inspiration for the first sketch of a conventional airplane should be taken from historical aircraft of like-mission capability. Airplane design textbooks from authors like Raymer [103], Nicolai & Carichner [104], and McCormick [105] have compiled large amounts of statistical aircraft data indicating where major design parameters typically lie for certain airplane types. For instance, Figure 3.1 shows lighter airplanes tend to have higher empty weight fractions, Table 3.1 differentiates between the types of airplanes governed by thrust-to-weight ratio (T/W) as opposed

to power-to-weight ratio (*P/W*), and Table 3.2 reveals that higher performance airplanes tend to have higher wing loadings (*W/S*), translating to more mass per unit wing area [103]. It is quite common for aircraft designers to compile their own statistical databases and base the initial parameters of new designs on the averages of historical figures.

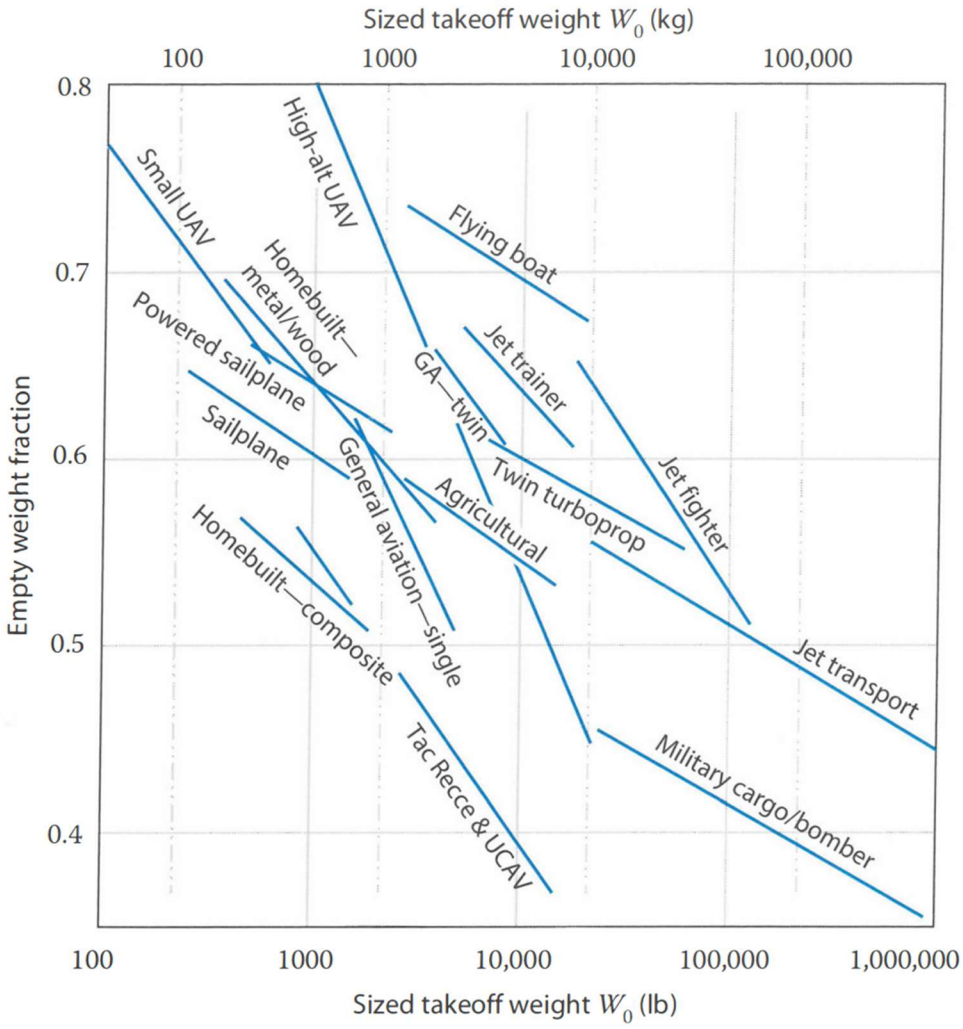

Figure 3.1 Historical trends in airplane empty weight fraction, W_e/W_0, and takeoff weight, W_0 from [103].

Table 3.1 Powerplant performance of historical airplanes and the differences between their power-to-weight *P/W* ratios and thrust-to-weight *T/W* ratios, adapted from [103].

Aircraft Type	Typical P/W	
	[hp/lb]	[kW/kg]
Powered Sailplane	0.04	0.07
Homebuilt	0.08	0.13
General Aviation – Single Engine	0.07	0.12
General Aviation – Twin Engine	0.17	0.3
Agricultural	0.09	0.15
Twin Turboprop	0.2	0.33
Flying Boat	0.1	0.16

Aircraft Type	Typical (Installed) T/W
Jet Trainer	0.4
Jet Fighter	0.6-0.9
Military Cargo/Bomber	0.25
Jet Transport	0.25-0.4

Table 3.2 Historical trends of airplane wing loading, *W/S*, adapted from [103].

Aircraft Type	Typical Takeoff W/S	
	[lb/ft^2]	[kg/m^2]
Sailplane	6	30
Homebuilt	11	54
General Aviation – Single Engine	17	83
General Aviation – Twin Engine	26	127
Twin Turboprop	40	195
Jet Trainer	50	244
Jet Fighter	70	342
Military Cargo/Bomber	120	586
Jet Transport	120	586

Once the top-level airplane layout, powerplant, and total weight has been selected from a host of promising candidates, the initial aircraft design can be further optimized to reveal a final, satisfactory configuration. This is commonly done through the use of classical airplane carpet plots, parametric trade studies, and various optimization techniques. Raymer deems the *T/W* vs. *W/S* carpet plot as the "granddaddy" of airplane optimization, since it reveals the minimum-weight

aircraft design that meets all performance requirements [103]. Optimization of the initial design is the final step in the conceptual design stage of a conventional airplane to harmonize the aircraft's structures, propulsion, and controls requirements and ensure the design is adequately prepared for refinement during preliminary design. An overview of the conventional aircraft design process is presented in Figure 3.2.

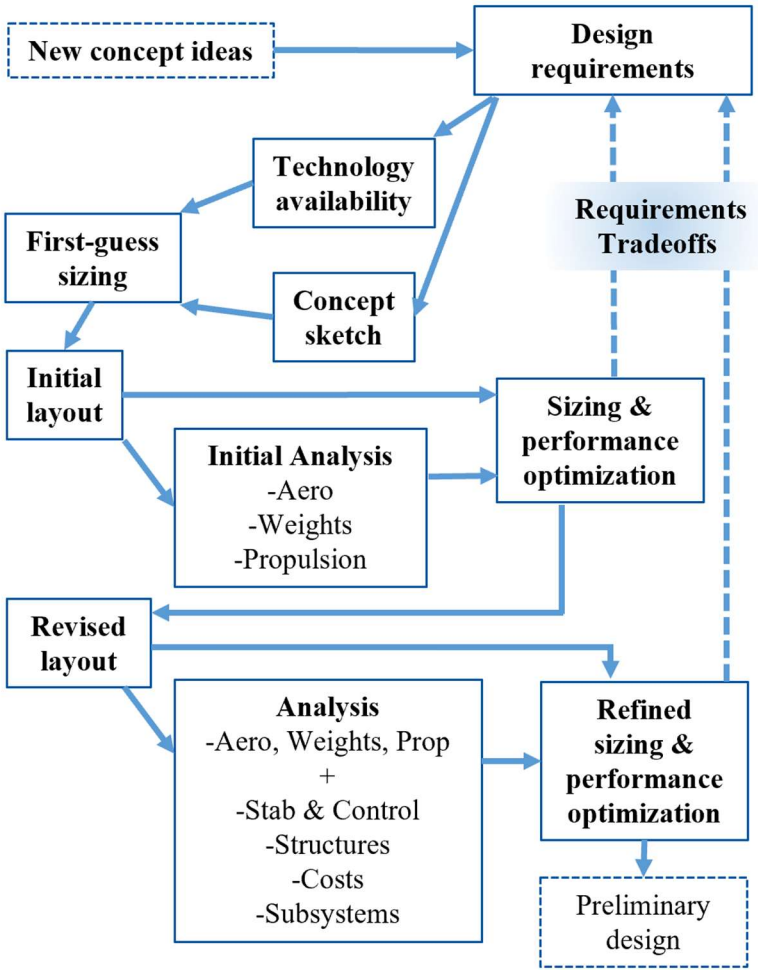

Figure 3.2 Overview of the conceptual design process for conventional airplanes, adapted from [103].

3.1.2.Conceptual Design of Conventional Helicopters

The conceptual design process for helicopters shares many of the same steps involved with conceptual airplane design, for several reasons. First and foremost, helicopters are a type of aircraft, and like airplanes, are considered a highly integrated system of aerodynamics, propulsion, structures, and controls technology. Logistically, helicopters serve the same ultimate purpose of either homeland security or making businesses money. Hence, new helicopter designs usually come from related, mission-specific requirements as well. There is also a wide array of design parameters in helicopter design that makes the design space for helicopters quite large. Consequently, arriving at a satisfactory design requires the same level of detail involved with the conceptual airplane design process, necessitating the same design space reduction and optimization techniques, such as statistical assessments of existing designs and trade studies of pertinent design criteria.

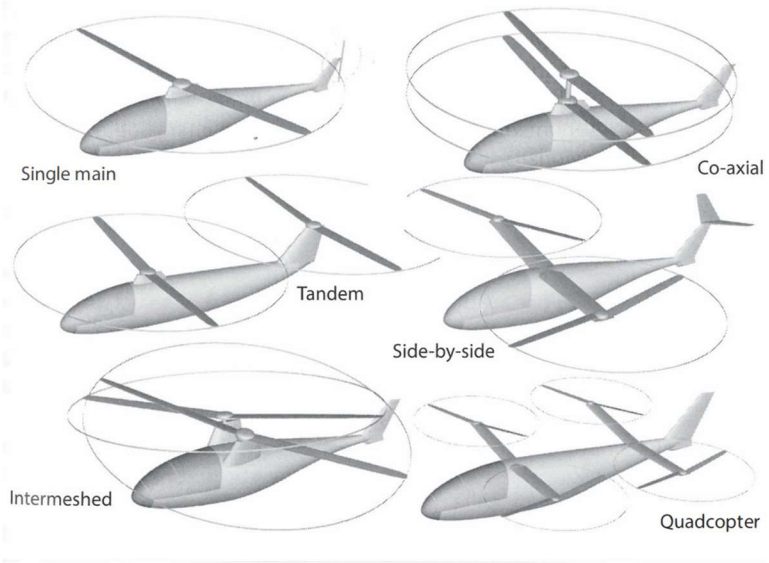

Figure 3.3 Variation in helicopter design from [103].

However, conventional helicopters can (and usually do) serve completely different roles in society. Their biggest differentiator is their ability to take off and land vertically, as well as remain

stationary in space for prolonged periods of time. While airplanes are limited to a minimum stall speed, helicopters' hover capability gives them the distinct advantages of VTOL, position hold, and precision attitude. At the same time, helicopters are limited in many ways that airplanes are not. Most fixed-wing aircraft can fly faster than similarly sized rotorcraft, since helicopters are adversely impacted by the effects of higher parasite drag, advancing blade compressibility, and retreating blade stall. Additionally, most helicopters are altitude-limited by their Hover Out of Ground Effect (HOGE) rating and do not feature pressurized cabins like airliners. Their VTOL ability also comes with the cost of reduced aerodynamic efficiency, which limits their range, among other performance targets.

These differences in mission requirements and functionality further characterize discrepancies in the way helicopters are conceptually designed. Although a helicopter's main rotor system resembles the main wing of an airplane by generating a majority of the required lift, the two are unequivocally unique. Unlike the fixed airplane wing, the rotating helicopter rotor experiences 360 degrees of asymmetric inflow and crossflow in forward flight. As a result, helicopter designers must consider an entirely separate set of design challenges, including main rotor torque balance, autorotation performance, and cyclic/collective control. Such specific design criteria creates additional steps in the conceptual design process solely applicable to the helicopter: namely, tail rotor sizing, main rotor sizing, and main rotor control.

Along the same lines, it is important to note there are fundamental differences in some design parameters that make them critical to helicopters but irrelevant for airplanes. While the definitions of some factors – such as the empty weight fraction, shown in Table 3.3 – are retained across conceptual design methodologies, others differ due to the physical differences between the two concepts. In conceptual helicopter design, the power loading (*W/P*, Table 3.4) and disk loading

(*T/A*, Table 3.5) parameters are weighted as equally important as *P/W* and *W/S*, respectively. However, the power loading and disk loading are indicative of helicopter hover efficiency, which is not the same as the fixed-wing stall, climb, and cruise implications of power-to-weight and wing loading parameters. These parametric sizing differences can be expected to work their way into the respective conceptual design processes as well, further distinguishing the fixed-wing and rotorcraft design methodologies. An overview of the conventional rotorcraft design process is shown in Figure 3.4.

Table 3.3 Historical trends of Empty Weight Fractions, W_e/W_0, adapted from [103].

Helicopter Type	Typical W_e/W_0
Scout/Attack (light armament)	0.5-0.6
Scout/Attack (heavy armament)	0.6-0.8
Transport	0.45-0.55
Civil/Utility	0.45-0.6
Tilt Rotor	0.55-0.7

Table 3.4 Historical trends of Power Loading, *W/P*, adapted from [103].

Helicopter Type	Typical W/P	
	[lb/hp]	[kg/kW]
Scout/Attack	3-5	1.8-3.1
Transport	5-7	3.1-4.3
Civil/Utility	3-8	1.8-4.9
Tilt Rotor	4-5	2.4-3.1
Tilt Wing (propeller)	~3.4	~2.1

Table 3.5 Historical trends of Disk Loading, *T/A*, adapted from [103].

Helicopter Type	Typical T/A	
	[lb/ft^2]	[kg/m^2]
Scout/Attack	8-10	39-49
Transport	6-15	29-73
Civil/Utility (low speed) *	4-6	20-29
Civil/Utility (high speed)	6-10	29-49
Tilt Rotor	15-25	73-122
Tilt Wing (propeller)	~50	~245

*(low speed < 150 kts)

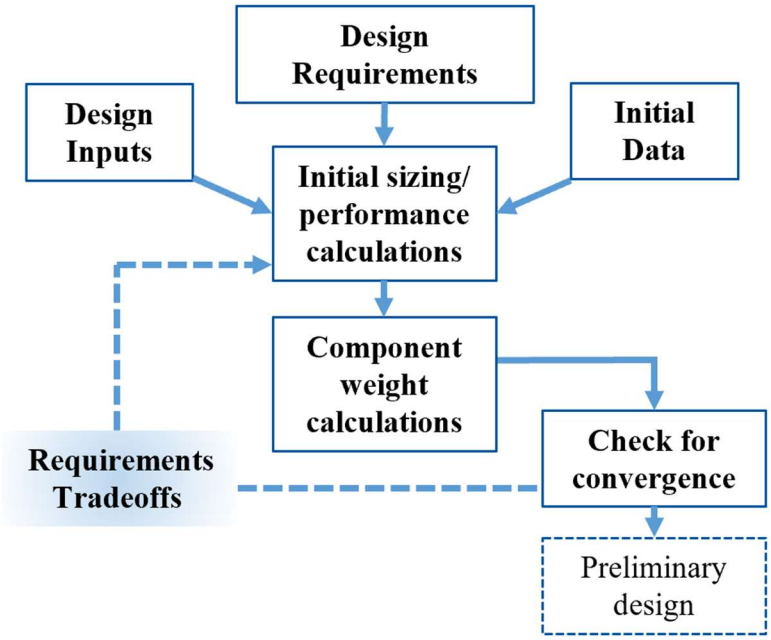

Figure 3.4 Overview of the conceptual design process for conventional rotorcraft, adapted from [111].

3.1.3.Top-Level Requirements for the Fan-in-Wing Concept

Where the capabilities of conventional airplanes and helicopters intersect, the fan-in-wing concept emerges. Yet, defining the steps that constitute a clear, generalized, and effective path to fan-in-wing design is less straightforward than simply superimposing the traditional design algorithms of fixed-wing and rotary-wing aircraft. Since a FIW aircraft is not an exact 50-50 blend of an airplane and a helicopter, it should not be treated as such. Instead, the approach to FIW design should explicitly eliminate conventional steps that are irrelevant to the lift-fan concept, incorporate those uniquely related to it, and retain those shared by all three configurations, as shown in Figure 3.5. Only those steps which are shared among the design processes may be replicated in the FIW design methodology. The points where conventional airplane and helicopter design principles fail the FIW concept, on the other hand, are a little more convoluted. Fortunately, the first step of the

FIW design process is one shared by all engineering processes and is typically a task already completed by the customer; that is, defining the top-level mission and aircraft requirements.

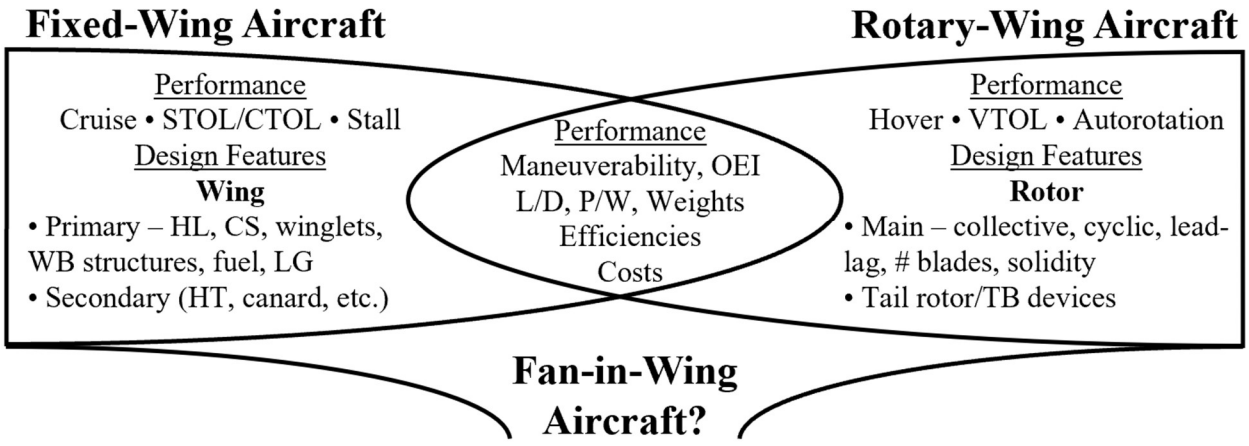

Figure 3.5 The steps to developing a FIW conceptual design methodology lie somewhere between the intersection of fixed-wing and rotary wing aircraft design.

The objectives outlined by a specific mission are all the FIW designer needs to jump right into conceptual design. Important performance metrics shared by aircraft of all types, like speed, payload capacity, and range should certainly be considered. However, there must be specific performance metrics that make the FIW concept more desirable than other aircraft configurations. After all, if the mission requirements favored the modern helicopter, why would the designer not opt to design a new helicopter? In other words, the top-level requirements specify what the aircraft must do, not necessarily what the aircraft must be. Therefore, to understand the process involved in FIW design, one must first understand the requirements that lead to the selection of the FIW concept in the first place.

Arguably, the most important mission requirement that drives a designer toward rotary-winged aircraft is vertical flight. For airplanes, the design space has evolved over 100 years, ranging from record-setting STOL aircraft like the modified Piper Cub [106] to rocket-powered hypersonic vehicles like the North American X-15 [107]. That is to say, if the mission requirements permit

conventional takeoff and landing, the designer should almost certainly pursue some type of fixed-wing airplane to minimize costs and maximize performance. However, helicopters have nearly mastered the art of vertical flight. In terms of pure hover and versatile mission capability, the helicopter is simply unmatched. Hence, to compete with modern airplanes and helicopters, a new VTOL concept must offer the customer a performance package that neither conventional fixed-wing or rotary-wing vehicle can.

Figure 3.6 offers a glimpse of what real LF and FIW aircraft have to offer over other real VTOL designs. Adapted from [108], Figure 3.6 compares the performance of the XV-5A fan-in-wing and F-35B lift-fan concepts to the UH-60M helicopter, MV-22B tiltrotor, CH-47F tandem-rotor helicopter, and the S-97 coaxial helicopter. Each of the five top-level mission requirements were nondimensionalized relative to the mission criteria set forth by the 2023 VFS HSVTOL student design competition, which specified a minimum payload of 5,000 pounds out to a 500 nautical mile combat radius, a cruise speed of 450 knots above 20,000 feet, and a disk loading below 40 lb/ft^2 for acceptable operation over unprepared surfaces [109]. In comparison, both FIW and LF concepts substantially underperform in the downwash department, while the F-35B LF concept clearly dominates the range and payload weight categories over the XV-5A's estimated potential. However, what the FIW and LF concepts lack in downwash, they make up for in high speed and altitude performance, satisfying both requirements and exceeding all competitive designs by substantial margins.

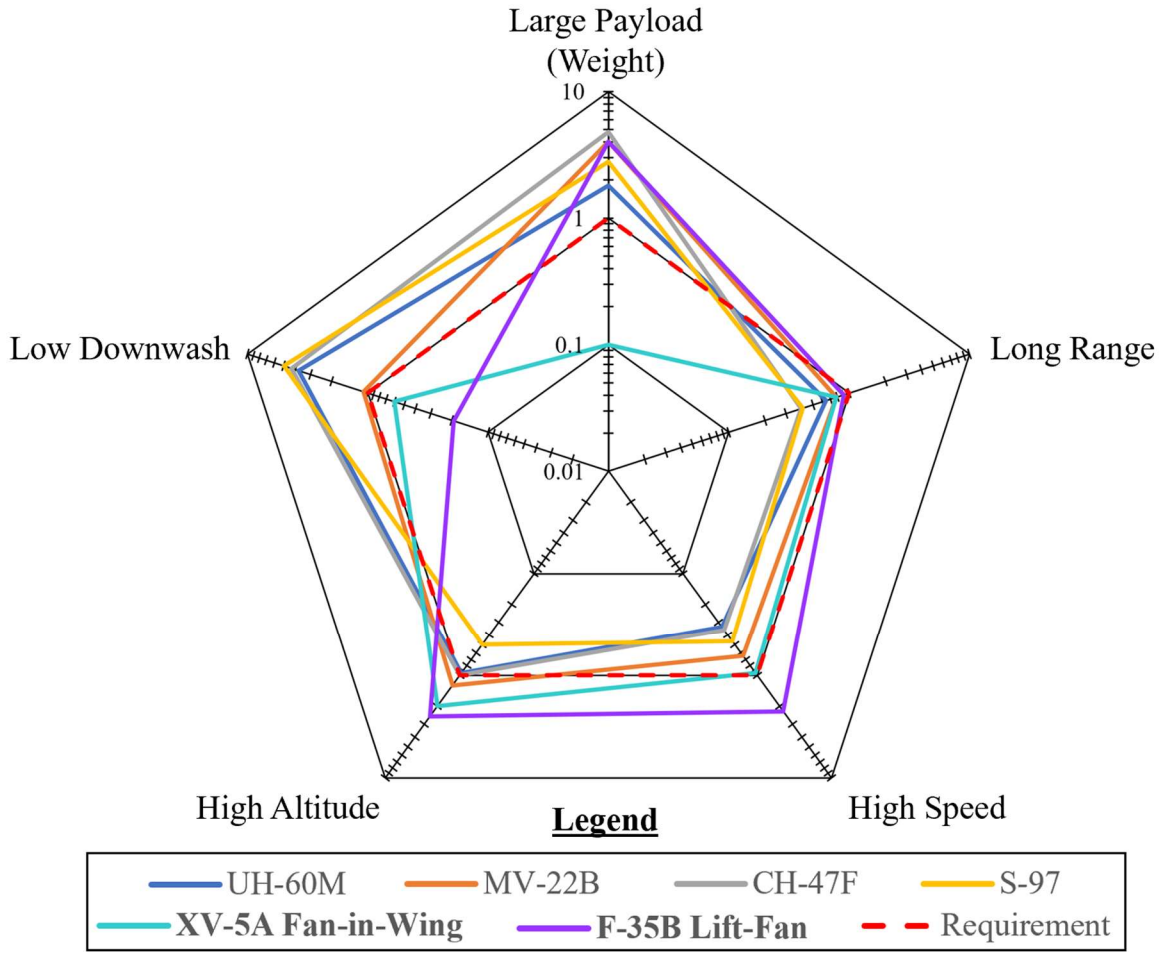

Figure 3.6 Radar chart of the top-level performance metrics of various VTOL aircraft, including the XV-5A FIW and F-35B LF aircraft, adapted from [108].

Upon further investigation, Figure 3.7 reveals the estimated speed and altitude capabilities of the FIW and LF concepts amount to even fixed-wing airplanes of comparable size. By overlaying the anticipated FIW and LF airspeed-altitude envelopes atop those of general helicopter and airplane configurations, Figure 3.7 shows the combined performance potential of the two individual lift-fan concepts falls short only to the most advanced supersonic aircraft [35] and [110-112]. Comparatively, the XV-5A and F-35B both exceed the maximum operating speeds and altitudes of the contending VTOL aircraft, and only lack altitude performance below about Mach 0.3. The expected operational performance of the XV-5A is projected to rival modern commercial

airliners with equivalent altitude and a slight reduction in maximum speed. Yet, the fuselage-embedded lift-fan design allows the F-35B to fly at supersonic speeds and climb to altitudes above 45,000 feet. Such figures in the VTOL aircraft design space are only outmatched by thrust vectoring and ejector type concepts.

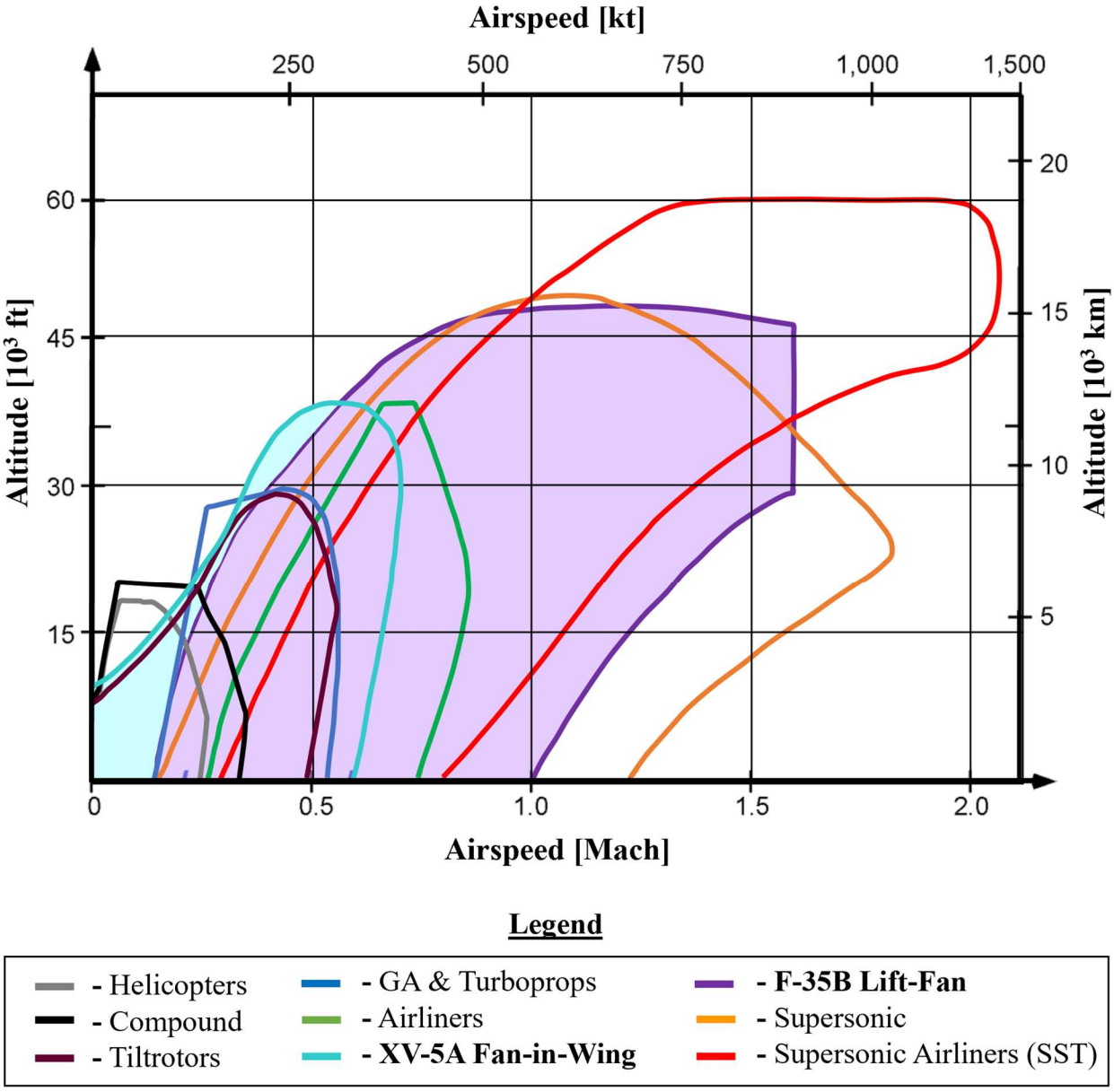

Figure 3.7 Flight envelopes of various conventional and VTOL aircraft, including the (projected) XV-5A FIW and F-35B LF aircraft, adapted from [35] and [110-112].

So, it becomes clear that the FIW and LF concepts cover an exceptional speed and altitude range. However, as mentioned in the conceptual design process of conventional helicopters, there are two important performance metrics also used to indicate the hover efficiency of a VTOL aircraft, namely, power loading and disk loading. Power loading measures the effective weight a rotorcraft can sustain in hover per unit power required, while disk loading refers to the sustainable hover weight per unit disk area. Since hover efficiency is characterized by a high *PL* and low *DL*, the two are inversely proportional, meaning rotorcraft with large disk areas tend to require less power to hover and vice versa.

Oppositely, higher cruise efficiency for VTOL aircraft generally correlates to minimum exposed rotor area. Figure 3.8, adapted from [113] and [114], compares this trend in maximum speed vs. disk loading to the trend observed in power loading for VTOL aircraft. As illustrated by five separate configurations, including the lift-fan concept, Figure 3.8 shows that the aircraft capable of achieving higher speeds are only able to do so at the expense of reduced power loading, and VTOL concepts with superior power loadings suffer in the same way from lower speed capability. This existential performance trade-off is the root of why HSVTOL aircraft design is so challenging.

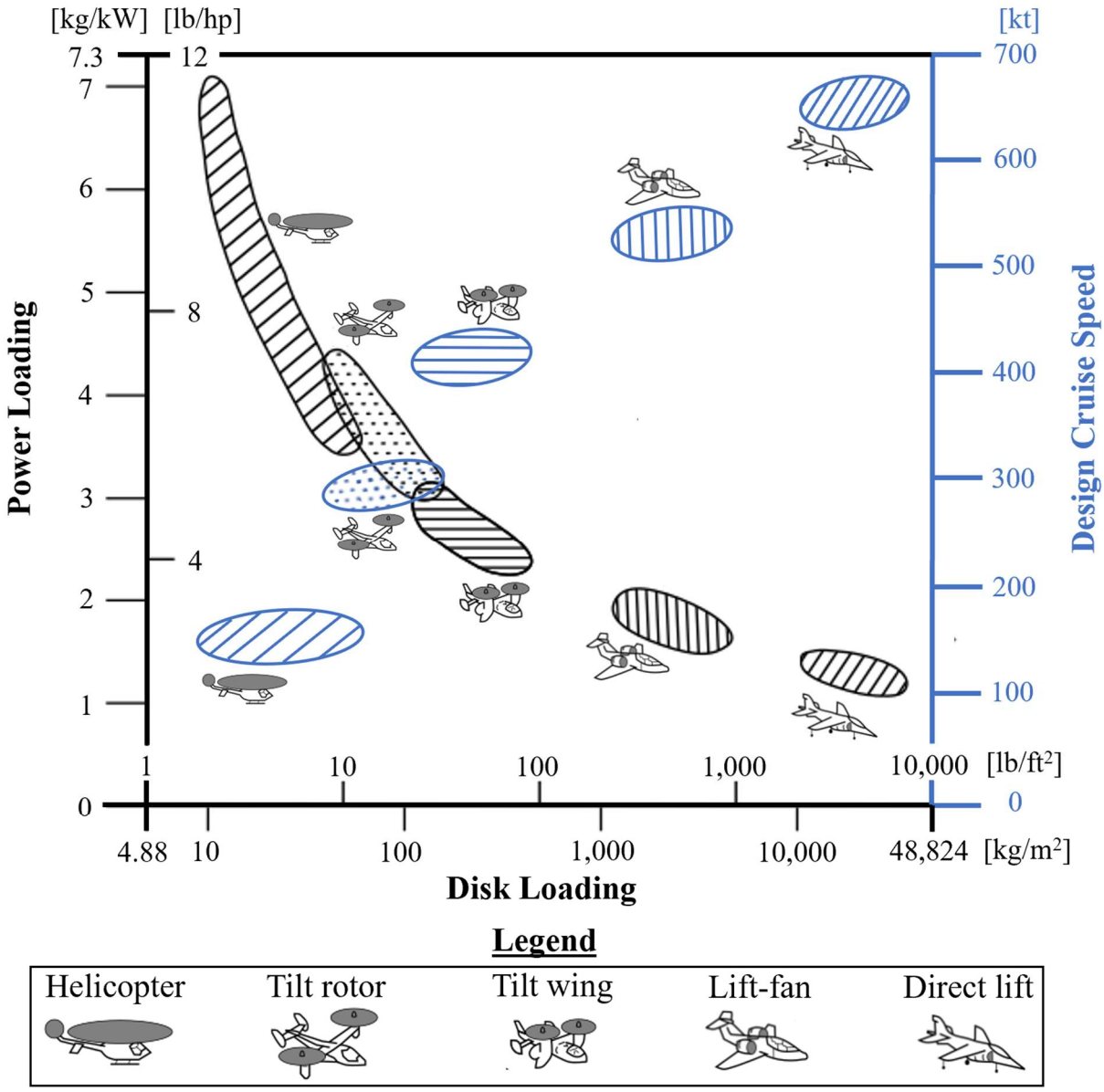

Figure 3.8 Estimated power loading and design cruise speed vs. disk loading of various VTOL concepts, adapted from [113] and [114].

Since the maximum hover and cruise efficiencies for a VTOL aircraft do not coexist at any given disk area, Figure 3.8 suggests that what differentiates the major VTOL concepts from one another is their individual balances in hover-to-cruise efficiency. By this logic, the entire VTOL design spectrum lies between two extremes of VTOL design. On one end, there are the helicopters,

which demonstrate the best hover performance but lowest maximum speeds. On the other end, there are direct lift concepts, featuring the greatest maximum speeds but lowest power loading. With all other types of VTOL aircraft falling in between, it becomes apparent that the VTOL aircraft designer should tailor their choice of concept to the blend in hover-to-cruise efficiency that best matches their mission requirements.

Figure 3.9 illustrates this notion of the hover-to-cruise efficiency spectrum using the same VTOL categories from Figure 3.8. On the x-axis, maximum speed capability (*Vc*) is measured as a percentage of how important the aircraft's High-Speed Cruise (HSC) capability is to the overall mission, while the power loading is measured oppositely as the percentage of how important the hover requirement is to the overall mission. These percentages range from 100%, meaning more important than all other requirements, to 0%, meaning absolutely no importance whatsoever. The y-axis represents the overall optimality of the VTOL design concept relative to the other configurations and is also labeled in units of percentage as well, ranging from 0% meaning completely suboptimal to 100% meaning fully optimized. To make sense of how each total curve was formed, the hover and HSC weighting factors were also plotted using dashed and semi-dashed lines, respectively. The percent optimality of the VTOL concept, $Optimal_x$ % relative to the five VTOL concepts in Figure 3.8 was computed as follows:

$$Optimal_x\% = \left[1 - \left(\frac{PL_x - PL_{val}}{PL_{\max} - PL_{\min}}\right)\right](PL_x\%) + \left[1 - \left(\frac{Vc_x - Vc_{val}}{Vc_{\max} - Vc_{\min}}\right)\right](Vc_x\%) \tag{3.1}$$

where the variables of Equation 3.1 are:

- PL_{max} – maximum relative *PL*
- PL_{min} – minimum relative *PL*
- Vc_{max} – maximum relative *Vc*
- Vc_{min} – minimum relative *Vc*

- $PL_x\%$ and $Vc_x\%$ – importance percentages of the hover and HSC requirements (x-values)
- PL_x and Vc_x – PL and Vc of the VTOL concept in question
- PL_{val} and Vc_{val} – interpolated PL and Vc based on the respective hover and HSC importance percentages

The computations for PL_{val} and Vc_{val} are provided by Equations 3.2 and 3.3:

$$PL_{val} = \left(\frac{PL_{\max} - PL_{\min}}{100\% - 0\%} \right) (PL_x\% - 0\%) + PL_{\min} \tag{3.2}$$

$$Vc_{val} = \left(\frac{Vc_{\max} - Vc_{\min}}{100\% - 0\%} \right) (Vc_x\% - 0\%) + Vc_{\min} \tag{3.3}$$

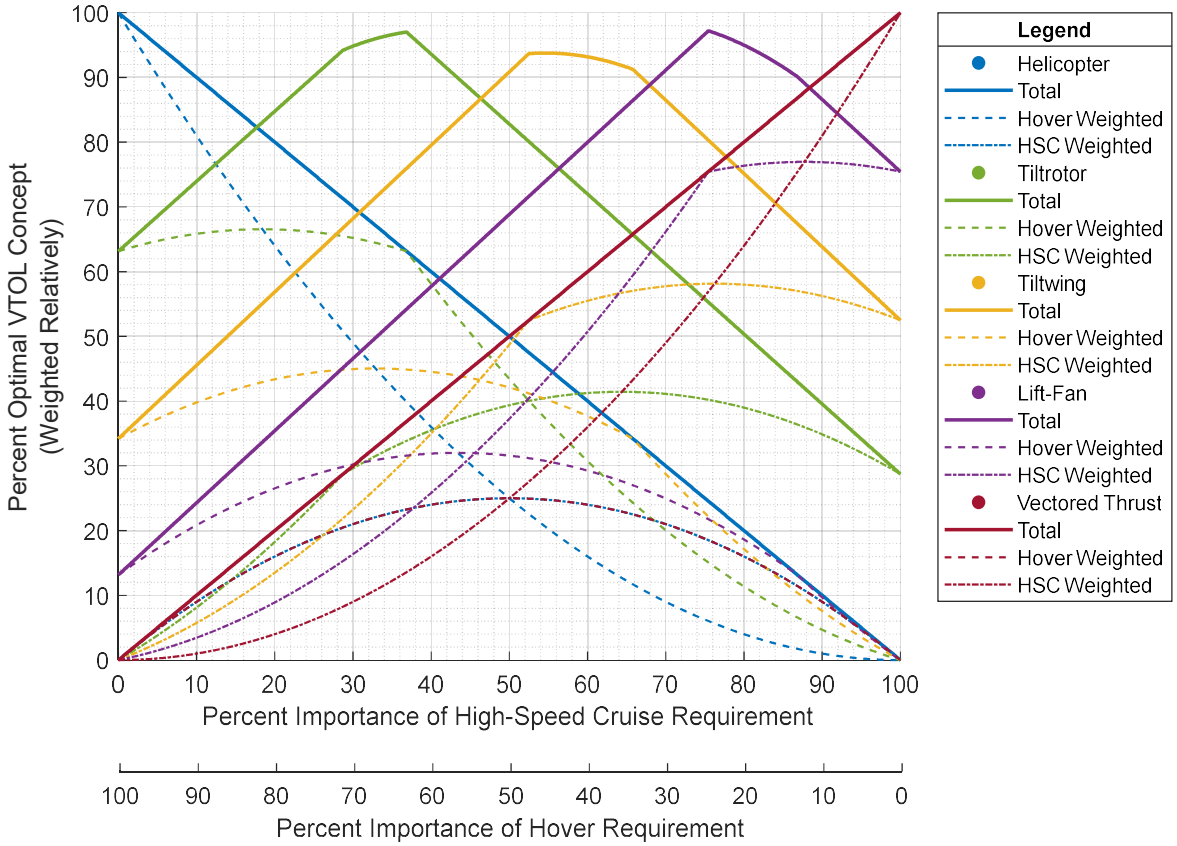

Figure 3.9 Percent optimality of the VTOL concepts presented in Figure 3.8, considering the percent significance of HSC and hover requirements relative to the total mission.

Neglecting all other VTOL concepts and design requirements aside from high-speed cruise and hover, Figure 3.9 reveals that the lift-fan concept becomes the most compelling VTOL design when the HSC requirement is approximately 68%-88% important to the overall design mission, and the hover requirement is roughly 12%-32% important. At the same rate, helicopters appear the most optimal, on average, between HSC importance percentages of 0-18%, while tiltrotors, tiltwing, and vectored thrust concepts occupy the ranges between 18-46%, 46-88%, and 88-100%, respectively. This is also to say that if percentage importance were translated to percentage of the total mission, the lift-fan concept becomes most appealing when the customer envisions an aircraft that spends 68-88% of its total mission in high-speed cruise.

This is an important distinction for the LF concept, as it highlights one of the major reasons why an aircraft designer might be drawn to its performance over other VTOL concepts. While other vectored thrust concepts are able to attain higher speeds and better cruise efficiencies, their performance in terms of downwash and power required in hover is significantly worse than lift-fan concepts, which still matters to the aircraft's functionality as a VTOL aircraft. Moreover, according to [115], the typical aircraft mission profile constitutes about 78% of its total flight in cruise (including the climb portion), which falls directly within the 68-88% HSC window that makes the lift-fan concept the most optimal design over all other VTOL configurations compared in Figure 3.8.

Thus, the fan-in-wing, and more generally the lift-fan concept, becomes of key interest when the design mission is mostly biased to the cruise portion of flight, but not quite to the extent that makes VTOL operation and hover efficiency the lowest priority. In fact, as a VTOL aircraft, the FIW concept offers exceptional low speed flight performance over jets of similar size, particularly during takeoff and landing.

Figure 3.10 shows three separate takeoff techniques demonstrated by the XV-5A research FIW aircraft during the 1960s that allowed the aircraft to clear a 50-foot obstacle and meet the balance field-length definitions prescribed by MIL-C5011A and FAR Part 23 [103] in much less runway distance than comparable civil and military jet trainers. The first was a completely vertical takeoff, enabled by the excess hover power available for the XV-5A to climb vertically with a lift-to-weight ratio of about 1.15 [35]. The second technique was a vertical climb to a 15 ft altitude followed by a forward acceleration from hover into climb, which allowed the XV-5A to clear a 50 ft obstacle in just over 500 ft. The third technique demonstrated by the XV-5A was a conventional ground roll takeoff using wake deflection from the wing fans to help generate lift. At a minimum, such technique was proven to clear the 50 ft obstacle in 1,530 ft. All three techniques were stark evidence of the FIW aircraft's ability to cut the required takeoff distance of conventional jets in half, if not eliminate the need for a runway altogether.

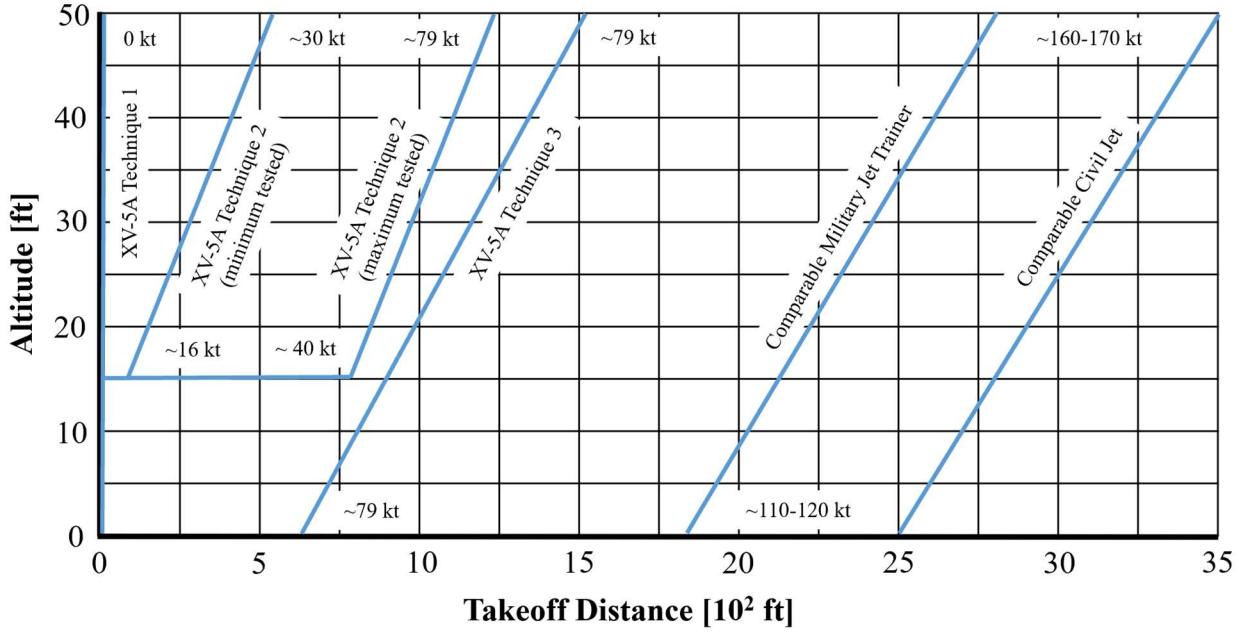

Figure 3.10 Altitude vs. total takeoff distance required of comparable civil and military jet trainers to the XV-5A's three demonstrated takeoff techniques.

Additionally, the FIW concept exhibits substantially reduced downwash speeds compared to most higher speed, vectored thrust VTOL alternatives. Figure 3.11 has been adapted from [109] to include the XV-5A in a comparison of various VTOL designs and their disk loading effects on ground surface erosion. Since disk loading and rotor downwash speeds are directly linked, the disk loading associated with 40 lb/ft^2 is generally considered the acceptable limit of sustainable hover operation near ground personnel. Although FIW aircraft should be expected to operate at disk loadings above this threshold, the onset of surface failures correlated to the disk loadings in Figure 3.11 are only applicable in near-ground effect. Out of ground effect, the XV-5A was able demonstrate the ability to perform water rescues and hovered over ground personnel without any injury to the test subjects. Extrapolations of this hover performance should be acceptable to assume for future lift-fan concepts.

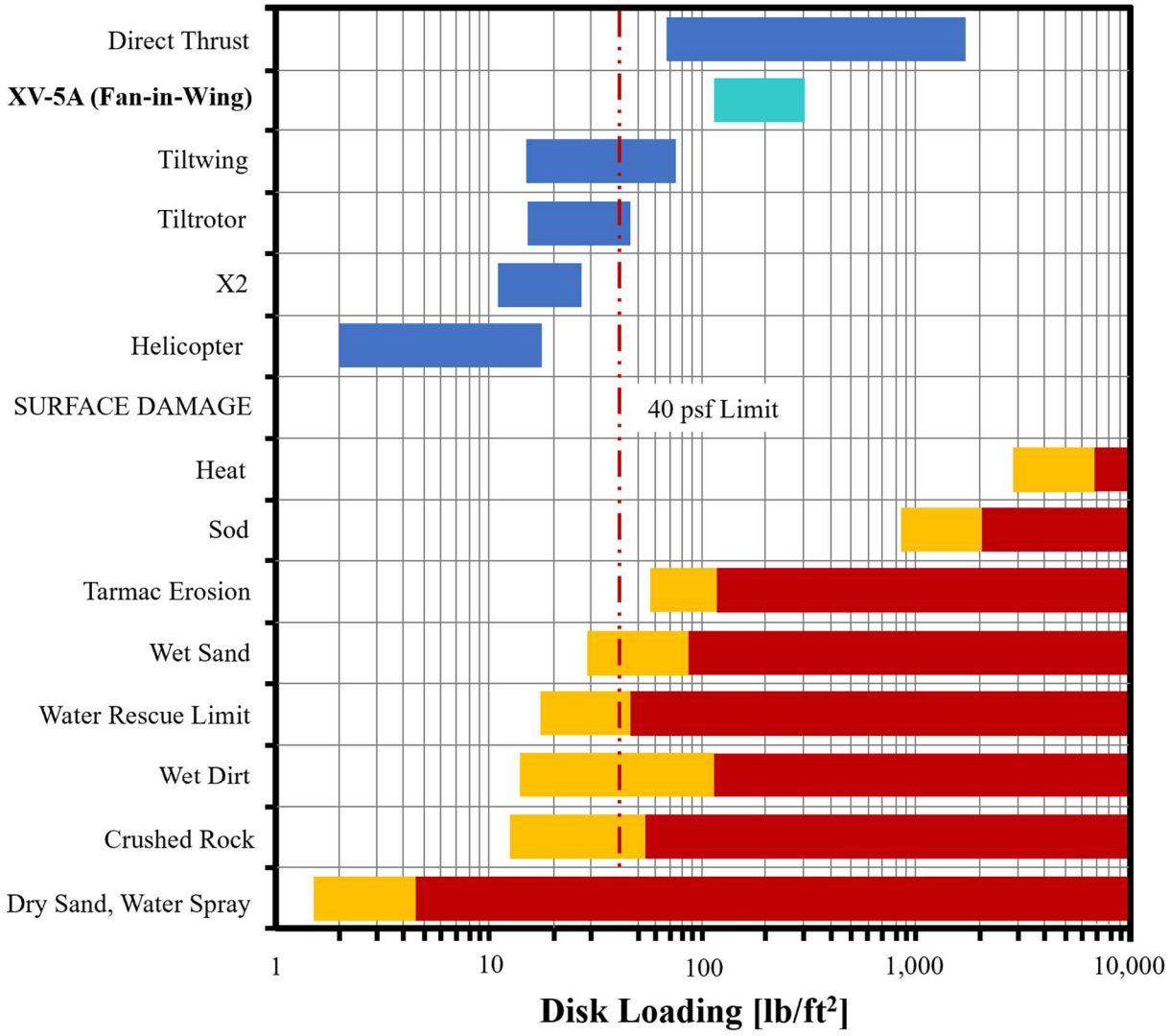

Figure 3.11 Ground surface erosion for select terrains correlated to various VTOL concepts using disk loading, adapted from [109].

3.2. Geometric Considerations

In the conceptual design of fixed-wing aircraft, one of the very first geometric parameters a designer will wish to determine is the wing loading, *W/S*. The wing loading is the ratio of the aircraft's gross weight to its wing reference area. A large *W/S* indicates the aircraft has a smaller wing compared to its overall size, whereas a smaller *W/S* implies a larger wing per unit weight. Typically, the wing loading parameter is determined alongside the thrust-to-weight ratio, since the

two are physically decoupled, yet closely interconnected by aircraft performance. According to [103], an optimal design would emerge from solving for these two parameters simultaneously, but an acceptable secondary approach would be to estimate the first value and calculate the second.

Due to the *T/W* being closely correlated with velocity, it is common for the thrust-to-weight ratio to be initially selected from statistical data and the *W/S* computation to follow. However, when other performance aspects dependent on wing size (like takeoff and landing distance) are deemed more critical, it may be in the designer's best interest to start with an estimate for wing loading instead. This is especially true when the aircraft falls under FAR Part 61, which mandates smaller aircraft must not stall above 61 knots [103]. By incorporating a required stall speed and takeoff density, as well as a first guess at the aircraft's overall C_{Lmax} from an initial airfoil section of the primary wing and assuming lift is equal to weight, the initial takeoff wing loading $(W/S)_{TO}$ can be approximated as:

$$\left(\frac{W}{S}\right)_{TO} = \frac{1}{2}\rho V_{stall}{}^{2} C_{L\max} \tag{3.4}$$

From there, the actual wing reference area is found by simply multiplying the takeoff wing loading by an initial estimate for the takeoff weight. Alternatively, a less reliable yet sufficient method for obtaining a quick wing area estimate based on statistical data for related fixed-wing configurations can be taken from the data of Table 3.2 compiled into Figure 3.12.

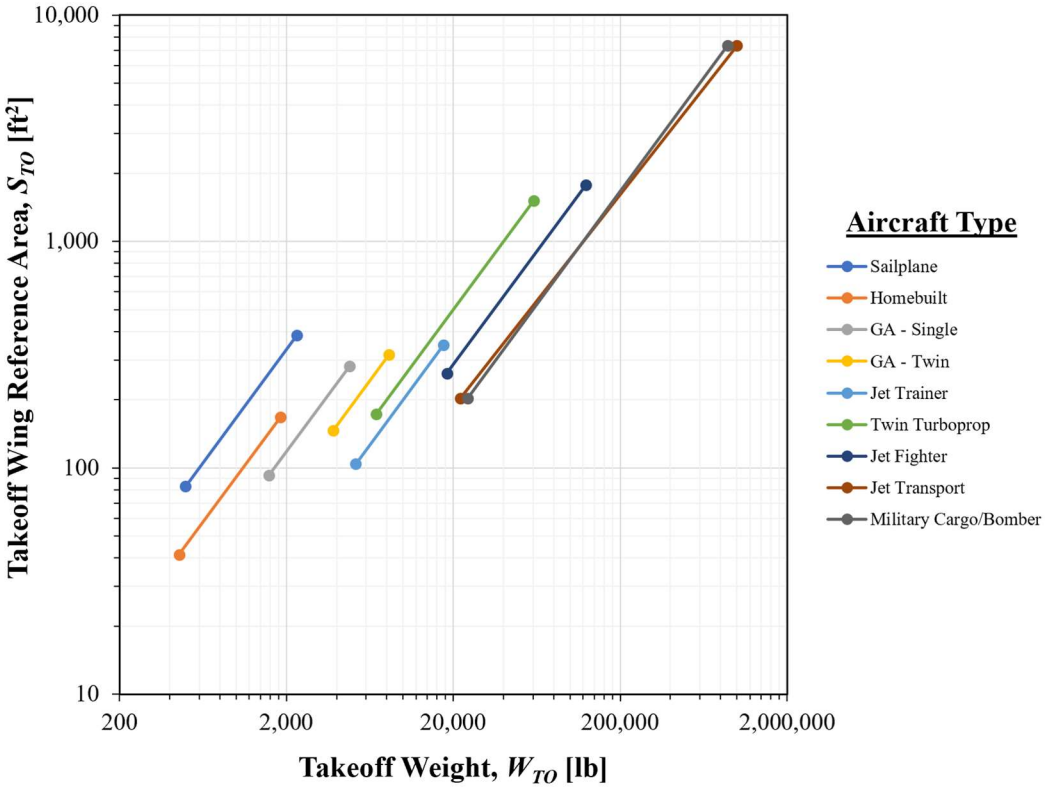

Figure 3.12 Takeoff wing reference area as a function of gross takeoff weight, correlated by Raymer [103].

All fixed-wing aircraft have a respective stall speed that limits their minimum flight velocity on wing lift alone, which generally defines the aircraft's maximum lift coefficient ($C_{L\max}$) and takeoff wing loading. During landing, this stall speed and $C_{L\max}$ also influences the aircraft's approach speed and approach lift coefficient, which directly impacts the runway distance required for the aircraft to come to a complete stop. According to [104], the approach C_L for CTOL aircraft is around 1.5-1.8, whereas a good figure for fixed-wing STOL aircraft is around 4.

However, the FIW concept's VTOL ability allows designers to theoretically decouple the minimum wing loading requirement associated with the initial sizing of conventional airplane wings. Because the FIW configuration can land anywhere between zero airspeed and the stall speed of its conventional wing using additional lift from its lift-fans, it can actually implement any

approach speed for a given wing loading. This also invalidates Equation 3.4 during the aircraft's "fan-mode," because as the approach speed diminishes toward zero, the lift coefficient would rise to infinity in order to maintain the same wing loading.

Conceptually, this means that unlike CTOL and even STOL aircraft where approach speed is a fixed function of wing loading, a VTOL FIW is operational between a range of approach speeds and wing loadings, dependent only on the available lift and gross weight of the vehicle. Figure 3.13 conceptualizes these approach speed and wing loading ranges for the XV-5A as an operational "fan-mode" envelope. In practice, what this implies is that as long as the lift-fans can provide sufficient lift to overcome the weight of the vehicle, the size of the wing itself is not restricted to a takeoff performance requirement.

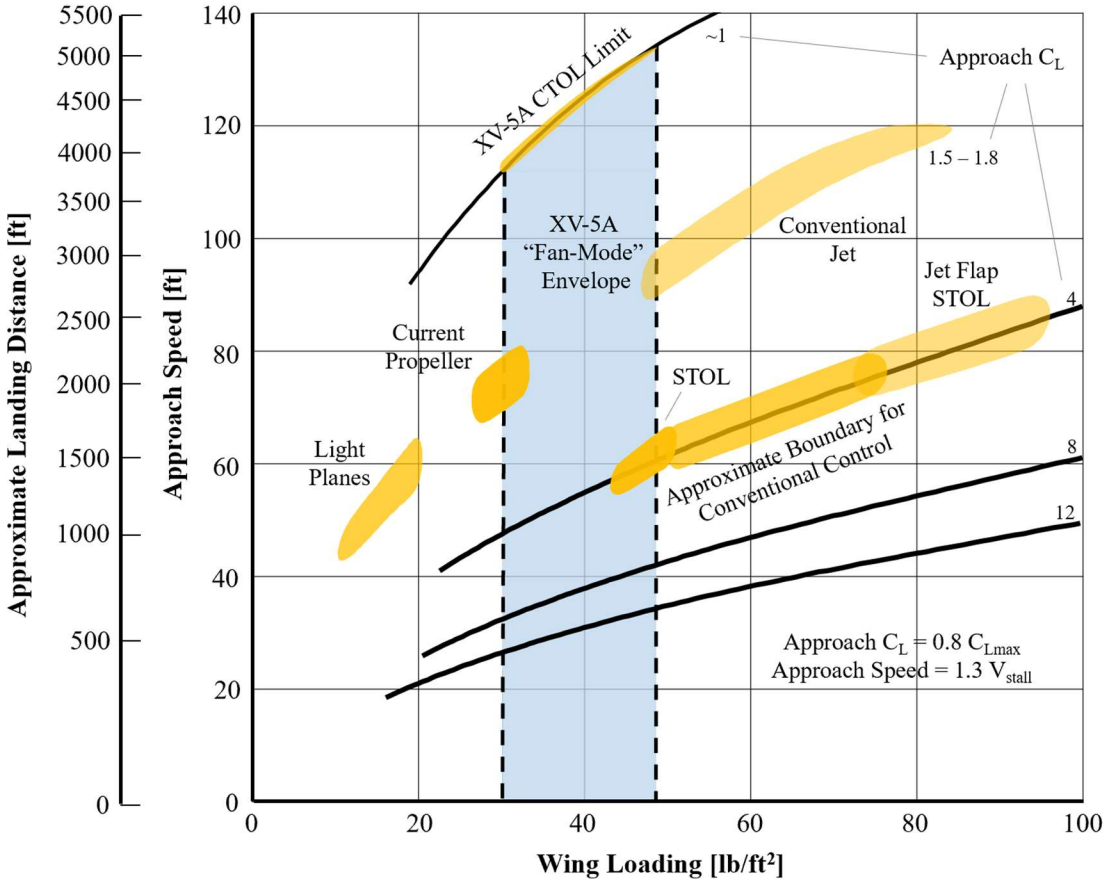

Figure 3.13 Approach speed and approximate landing distance as a function of wing loading, adapted from Nicolai & Carichner [104].

With helicopters, the geometric and aerodynamic equivalent of the wing reference area is the main rotor disk area. The main rotor of a helicopter is perhaps the single most important design feature of the entire helicopter because, unlike airplane propellers and wings, the main rotor duals as both the primary means of lift and propulsion. Sizing the main rotor area of a helicopter requires careful selection of the disk loading and power loading parameters, just like the *W/S* and *T/W* parameters in the aircraft design process. However, helicopters are not limited in low-speed forward flight due to stalling the same way airplanes are. While retreating blade stall does have a limiting effect on a helicopter's maximum speed, the optimal size of its main rotor is highly dependent on an array of other factors.

For maximum hover performance, safe autorotation capability, lower induced velocities, and reduced hover power required, a larger rotor diameter is preferred. Meanwhile, smaller rotors tend to allow helicopters to be more maneuverable, lighter in structural weight, less expensive, more compact, and more efficient in cruise. As a result, the initial size of the main rotor can be difficult to estimate from any one lone performance metric. Nonetheless, trends observed by Leishman [111] and others have found that the main rotor area has historically scaled quite well with the $1/3^{rd}$ power of the helicopter's gross weight, as shown in Figure 3.14. Using this trend is an acceptable place to start in the initial sizing process for a main helicopter rotor.

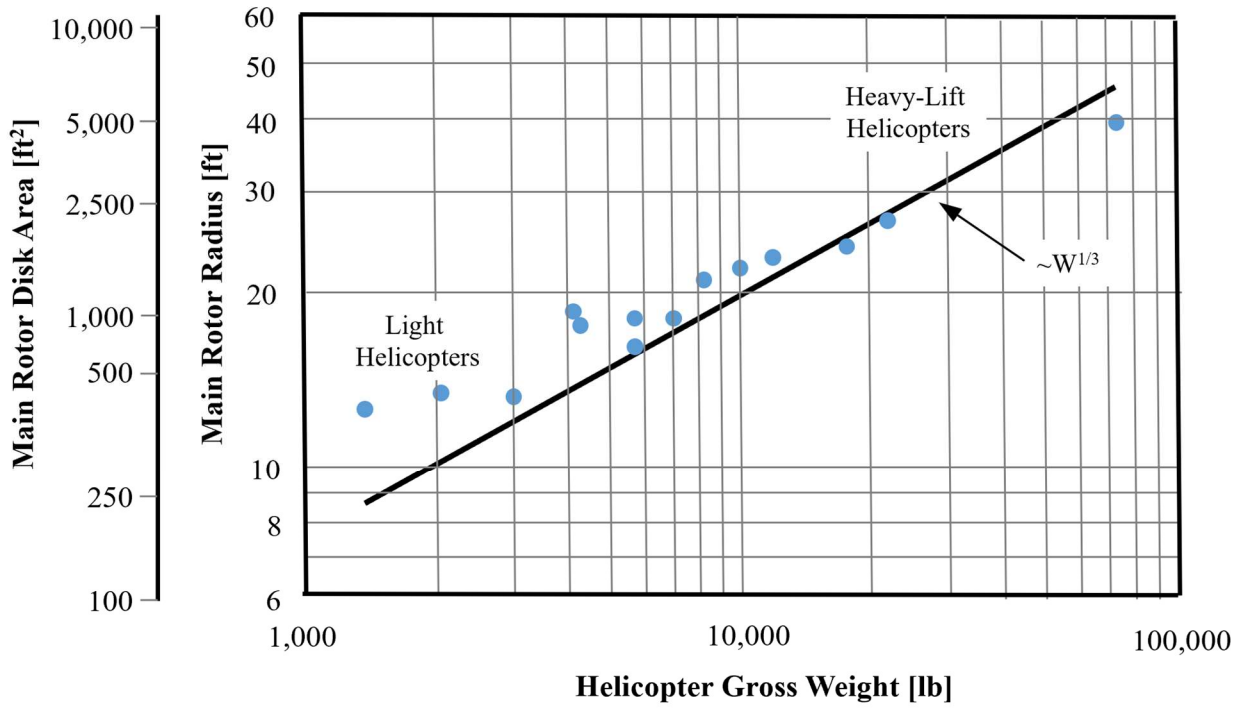

Figure 3.14 General trends in main rotor size (radius) vs. helicopter gross weight, adapted from Leishman [111].

However, unlike helicopter rotors, which can scale independently of all other lifting surfaces onboard the aircraft, the lift-fans of the "fan-in-wing" concept are required to fit within the available reference area of the wing. While the idea of concealing the fans in the wing during cruise to minimize parasitic drag is a strategic design feature, it also introduces special geometric constraints that are only applicable to this specific type of VTOL aircraft.

To understand the limitations of the FIW wing planform design and how it might be affected by this critical constraint, Figure 3.15 was assembled to define the FIW's wing planform trade space in terms of disk area (*Ad*) and wing reference area (*S*). In the case of the FIW concept, the disk area refers to the total 2D planform area of the embedded lift-fans, and the wing area refers to the total wing reference area, including the cutout areas for the lift fans.

By plotting disk area over wing area, the slopes of all lines extending out from the origin in Figure 3.15 represent constant disk-to-wing area (*Ad/S*) ratios. Figure 3.15 was intentionally set up this way to represent the FIW wing planform trade space since a disk-to-wing area ratio of 1 defines a theoretical boundary between the fan-in-wing concept and all other types of compound rotorcraft. When *Ad/S* = 1, this implies that the disk area is equal to the wing area, meaning the lift-fans and the wings are the exact same size. While conceivable in theory, a FIW design with an *Ad/S* of 1 makes little sense in the real world since there would be no excess wing structure to support the enclosure of any lift-fans. At the same time, slopes greater than unity would indicate the disk area is greater than the wing area, which cannot be true for the fans to fit within the wings. Although this red region in Figure 3.15 would hold all VTOL concepts that have larger rotor areas than the total wing reference area, the FIW concept cannot occupy this space. Only below the theoretical *Ad/S* limit is it possible for the FIW design to exist.

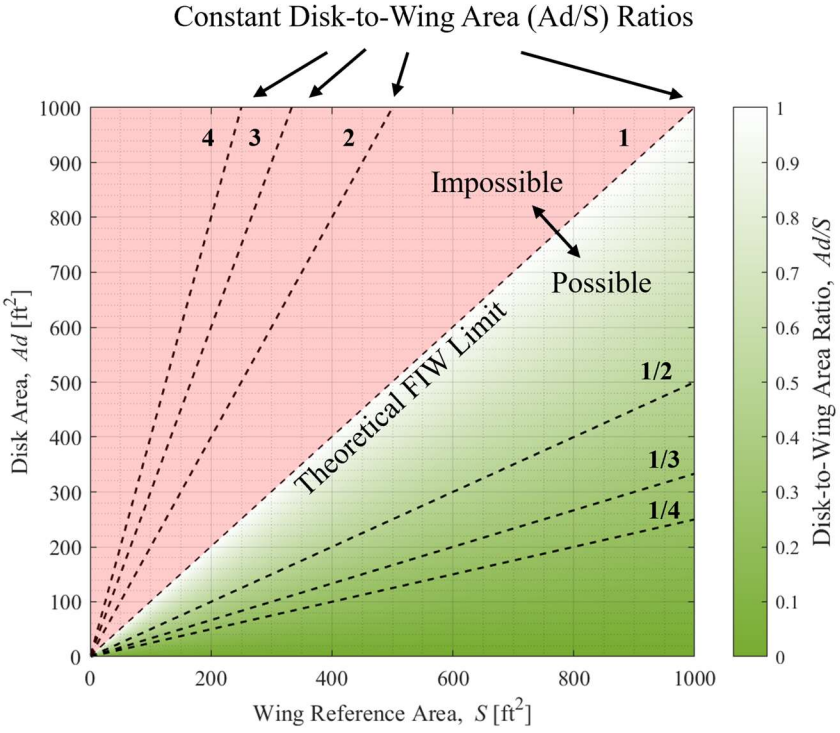

Figure 3.15 Conceptual FIW wing sizing trade space defined by disk area and wing reference area constraints.

However, to claim the FIW disk-to-wing area trade space makes up the entire area under the theoretical *Ad/S* line is an overstatement, because there are practical considerations that have yet to be incorporated. From a pure hovering vantage point, the ideal lift-fan concept would feature a single, large fan that also serves as circular wing planform. This would allow the aircraft to leverage the low power required, minimum fuel consumption, and reduced downwash velocities attainable by large, single-disk helicopters, while simultaneously utilizing the FIW's main principle of covering the rotor with a wing for improved forward flight performance. However, as previously stated, a FIW concept with a perfectly circular wing planform that constitutes an *Ad/S* = 1 is not realistic. Due to structural, aerodynamic, and controllability requirements, it is much more likely that the FIW wing planform will be forced to adopt a more conventional wing planform shape.

Figure 3.16 shows exactly how the wing planform shape affects the disk-to-wing area ratio by illustrating the half-span wing planform of various shapes that can accommodate the maximum single-disk area embedded inside. To the far left, the first configuration represents a twin-disk design (mirroring the right half over the longitudinal axis), where the *Ad/S* = 1. Upon observation, it is evident that this wing configuration lacks the support area and structural integrity to be viable for any realistic FIW design. To the right of that are five additional configurations, showing incremental additions in wing area, and therefore decreasing the *Ad/S* ratio from left to right. Figure 3.17 also marks where these configurations would fall on the disk area vs. wing area graph. This figure reveals that not only does the disk-to-wing area ratio greatly depend on the shape of the wing planform, but as the wing planform increases to resemble more conventional and complex looking wing shapes, the maximum allowable *Ad/S* for the hover-optimal, twin-disk configuration drops substantially.

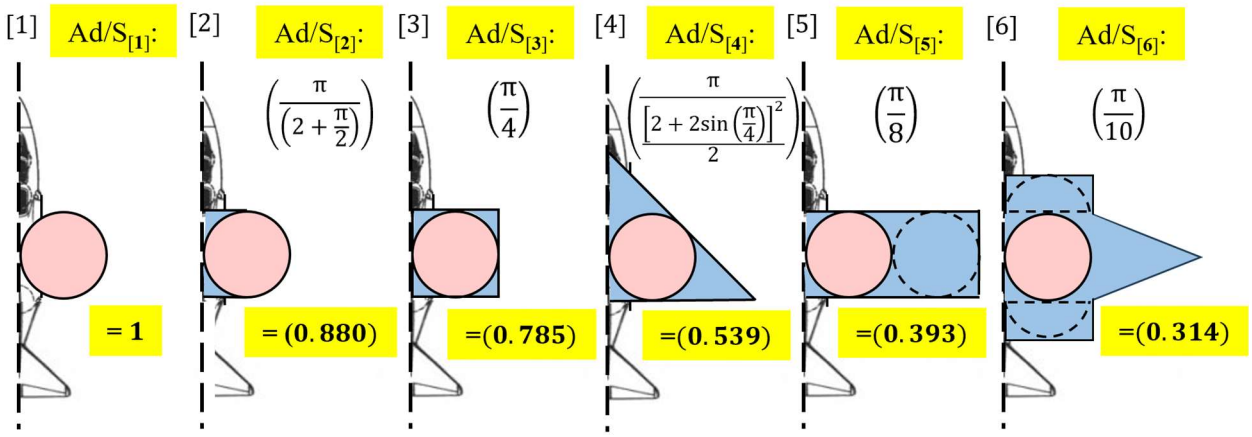

Figure 3.16 Disk-to-wing area ratios for some simplified, twin-disk FIW designs featuring basic wing planforms of various shapes.

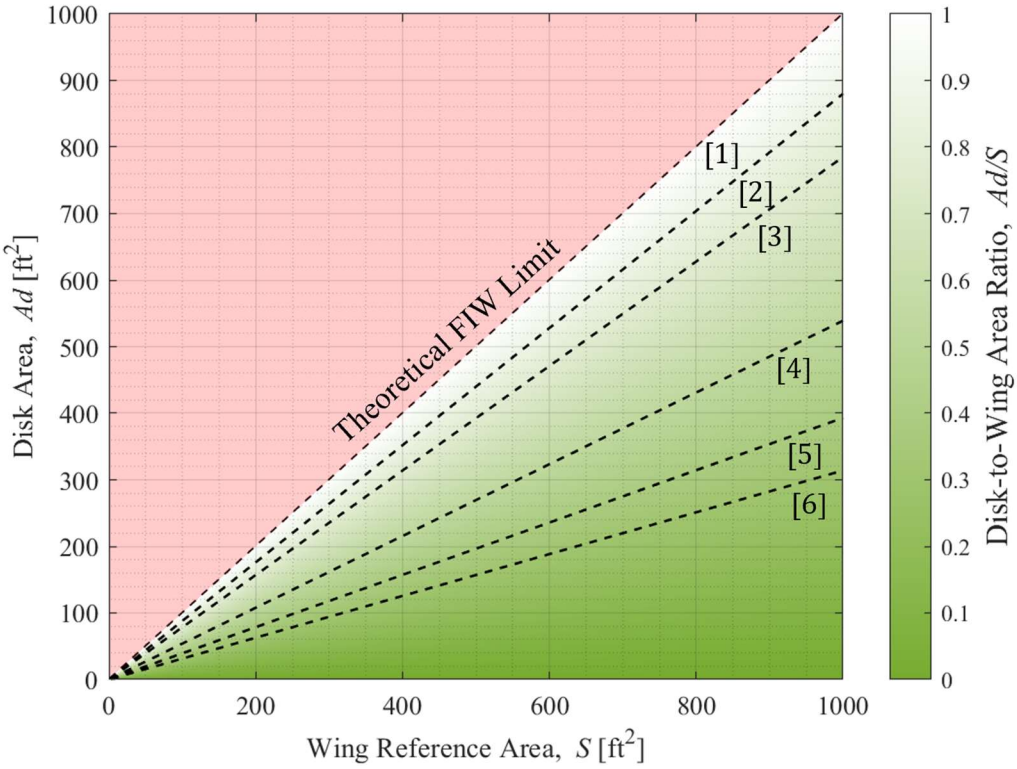

Figure 3.17 FIW design space incorporating the *Ad/S* slopes from Figure 3.16

Another trend that should be of interest to the FIW conceptual designer is how aspect ratio affects this *Ad/S* wing sizing parameter. Aspect ratio, *AR*, is an important parameter to define early in the conceptual design process of a fixed-wing aircraft as it plays a major role in determining the stall speed, maximum speed, and overall lift-to-drag characteristics of the aircraft. Configurations 3 and 5 from Figure 3.16 showed that for a rectangular wing planform, the maximum *Ad/S* (Ad/S_{max}) for the twin-disk configuration is reduced by exactly half as the aspect ratio doubles. This relationship between *Ad/S* and *AR* holds true for all rectangular wing planforms with an *AR* > 1. When the *AR* is exactly 1, meaning a square wing, the rectangular wing planform is at its maximum allowable Ad/S of π/4. For lower aspect ratios, the *Ad/S* is exactly proportional to the aspect ratio by a factor of π/2. Equation 3.5 gives this relationship for rectangular wing planforms as a piecewise function.

For twin-fan rectangular wing planforms:

$$Ad / S_{\max} = \begin{cases} \frac{\pi}{2} AR & \text{if } AR < 1 \\ \frac{\pi}{4} & \text{if } AR = 1 \\ \frac{\pi}{8} \frac{1}{AR} & \text{if } AR > 1 \end{cases} \tag{3.5}$$

When the wing planform is triangular in shape, resembling a delta wing configuration, the maximum *Ad/S* occurs when the half-wing planform forms an isosceles right triangle, as represented by configuration 4 from Figure 3.16. Taking this shape, the half-span wing aspect ratio becomes 2, and the Ad/S_{max} is approximately 0.539. Equation 3.6 gives this relationship for triangular, delta wing planforms as a continuous function.

For twin-fan triangular, delta wing planforms:

$$Ad/S_{\max} = \frac{2\pi AR}{\left(\sqrt{AR^2+1}+AR+1\right)^2} \tag{3.6}$$

Lastly, an equation for the maximum disk-to-wing area ratio has been derived for the elliptical wing planform. Elliptical wings are aerodynamically desirable as they yield the ideal spanwise lift-distribution. However, elliptical wing planforms are typically more difficult and expensive to manufacture compared to simple rectangular and delta wing shapes. Nevertheless, the elliptical wing has considerable merit and offers an equivalent or greater $Ad/S_{\max}$ over the rectangular wing planform at almost every aspect ratio. The maximum Ad/S occurs when AR is approximately 2.214, which yields an $Ad/S_{\max}$ of 0.7698. Due to the nonlinear geometric relation between a circle and an ellipse, the equation for Ad/S_{max} as a function of AR is a piecewise function described by Equation 3.7.

For twin-fan elliptical wing planforms:

$$Ad/S_{\max} = \begin{cases} \dfrac{\pi}{2}AR & \text{if } AR \le 1.794 \\ \dfrac{2}{\pi AR}\left(1-\left(\dfrac{1}{\pi AR}\right)^2\right) & \text{if } AR > 1.794 \end{cases} \tag{3.7}$$

The derivations for each of these $Ad/S_{\max}$ to AR relationships are included in Appendix B for additional reference. However, Figure 3.18 summarizes the above equations by comparing the different wing planform equations in a single $Ad/S_{\max}$ vs. AR plot.

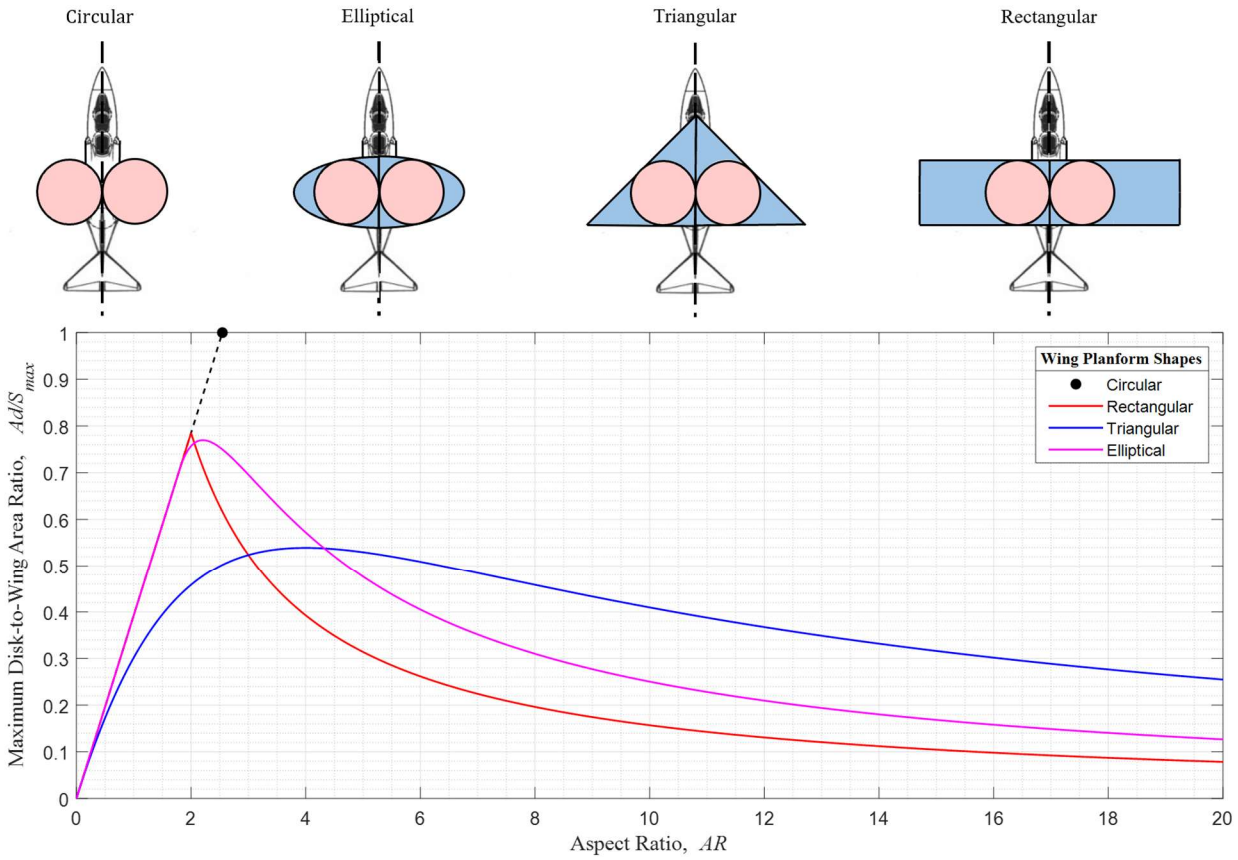

Figure 3.18 Changes in maximum attainable *Ad/S* with aspect ratio for four basic wing planform shapes: circular, rectangular, triangular, and elliptical.

From Figure 3.18, the FIW designer can generate several conclusions. The first is that none of the wing planform shapes described above really come close to the theoretical Ad/S_{max} of 1 inscribed by a perfectly circular wing planform. The closest design is the rectangular wing when $AR = 2$, which is essentially two perfect squares side-by-side, amounting to an Ad/S_{max} of about 0.785. Still, the difference in over 20% *Ad/S* represents a significant gap between the theoretical maximum and practical maximum based on shape alone. The second observation is that the maximum disk-to-wing area ratio is generally largest for low aspect ratios, regardless of wing planform shape. Figure 3.18 shows that all Ad/S_{max} values tend toward zero as *AR* approaches infinity and peaks between aspect ratios of 2 and 4, which are both considerably low. This

observation is a beneficial one for FIW designs that wish to fly fast, because it is easier for aircraft to reach transonic and supersonic speeds when the wing planform features a low *AR* and high leading-edge sweep.

Additionally, each individual wing planform shape appears to make its own case for when it serves most optimal to maximize *Ad/S*. The rectangular wing planform appears to maximize *Ad/S* for aspect ratios ≤ 2, along with the elliptical planform. Yet, the elliptical planform offers superior Ad/S_{max} between and *AR* of 2 and 4, as the disk area quickly shrinks with increasing rectangular wing planform. For all aspect ratios above 4, it seems the triangular design offers the greatest disk area per unit wing area, making triangular delta wings the superb wing shape at higher aspect ratios.

On a final aspect ratio note, one may have noticed that the most common, trapezoidal wing area was not included in this analysis. Such was intentional, because the *Ad/S* for a trapezoidal wing is not just a function of aspect ratio, but also the taper ratio, which means a second variable would have to be introduced to the equation. As a quick work-around to this, one may simply use Figure 3.18 to determine the Ad/S_{max} of a trapezoidal wing by interpolating between the triangular, delta wing curve and the rectangular wing curve, since the taper ratio of a triangular wing is 0 and the taper of a rectangular wing is 1.

For conceptual design purposes, there are at least three additional geometric considerations that, when appropriately included in one's analysis, will yield a higher fidelity estimate of the maximum available disk-to-wing area ratio for a given FIW wing planform shape. These considerations have to do with reducing (or "limiting") the total wing reference area by an amount that is generally considered "off limits" for placement and sizing the FIW aircraft's lift fans.

Therefore, in the proceeding discussion, these constraints on the total available wing reference area for lift fan placement and sizing will be referred to as "limiters."

The first of these limiters to be mentioned and further considered is the unusable wing reference area that passes through the fuselage, also known as the wing-box or "carry-through" area. Although the wing reference area is defined by the entire top view projection of the wing planform, the portion of the wing occupied by the wing box is purely structural and does not support the aircraft in lift generation. Without specific modifications to the fuselage structure that permit embedding the lift-fans within part of the fuselage, like the cutout section used for the F-35B's shaft-driven lift fan, the FIW concept is required to make space for its lift-fans elsewhere on its wing planform. To quantify this first limiter (L_1) as a design variable, consider it equal to the fractional value of the maximum fuselage diameter $d_{f\max}$ over the total wingspan:

$$L_1 = \frac{d_{f\max}}{b} \tag{3.8}$$

The second wing area constraint that should be taken into consideration early on in the design process is additional room for wing control surfaces. Nearly all fixed-wing aircraft feature ailerons for lateral-directional control, and many also incorporate high-lift devices that allow the aircraft to sufficiently increase lift for takeoff and landing performance without requiring a larger wing. While the FIW concept may not need the same caliber of high-lift devices as a CTOL aircraft when operating in fan-mode, it should almost certainly feature some sort of directional control surfaces on its wings if it intends to operate like a conventional aircraft in high-speed forward flight. In such scenario, the second major limiter (L_2), can be defined as the total control surface chord length (c_{cs}) divided by the wing root chord (c_r). Additionally, Figure 3.19 from [103] offers some

historical guidance for scaling aileron chord based on the wing's span and average chord length at the spanwise location of the aileron.

$$L_2 = \frac{c_{cs}}{c_r} \tag{3.9}$$

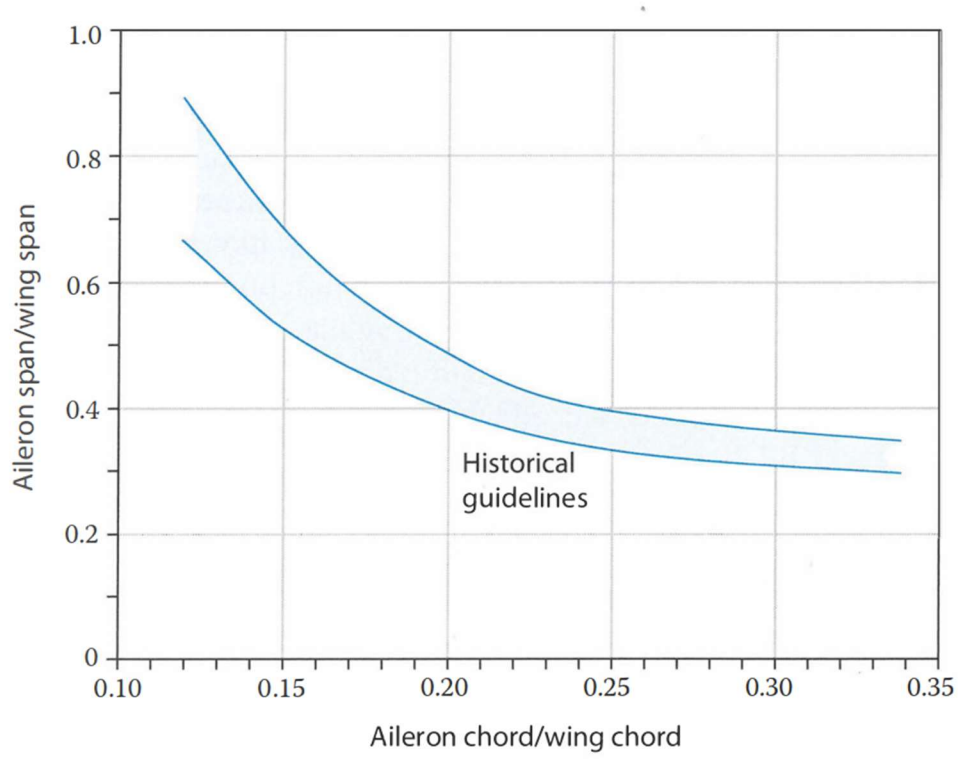

Figure 3.19 Historical aileron scaling trends based on wing dimensions from Raymer [103].

The third major geometric limiter is the additional support structure required to surround and support the lift fans themselves. By choosing to enclose the lift fans within the wings for improved cruise performance, the FIW designer should also consider the additional wing area needed around the perimeter of each lift fan to serve as cover and support material. The nondimensional thickness of this "buffer zone" around each lift fan, denoted L_3, can be quantified by Equation 3.10 as the percent difference between the radius of the lift-fan disk area (r_{lf}) and the anticipated buffer zone edge (r_{bz}). In general, all lift fan buffer zones will depend on the designer's choice of wing skin

thickness, ducting components for the fans, and any critical wing infrastructure such as spars, stringers, and ribs that must come between the lift-fans and the outer edges of the wing.

$$L_3 = 1 - \left(\frac{r_{bz}}{r_{lf}} \right)^2 \tag{3.10}$$

A visual depiction of the three Ad/S_{max} limiters is provided in Figure 3.20:

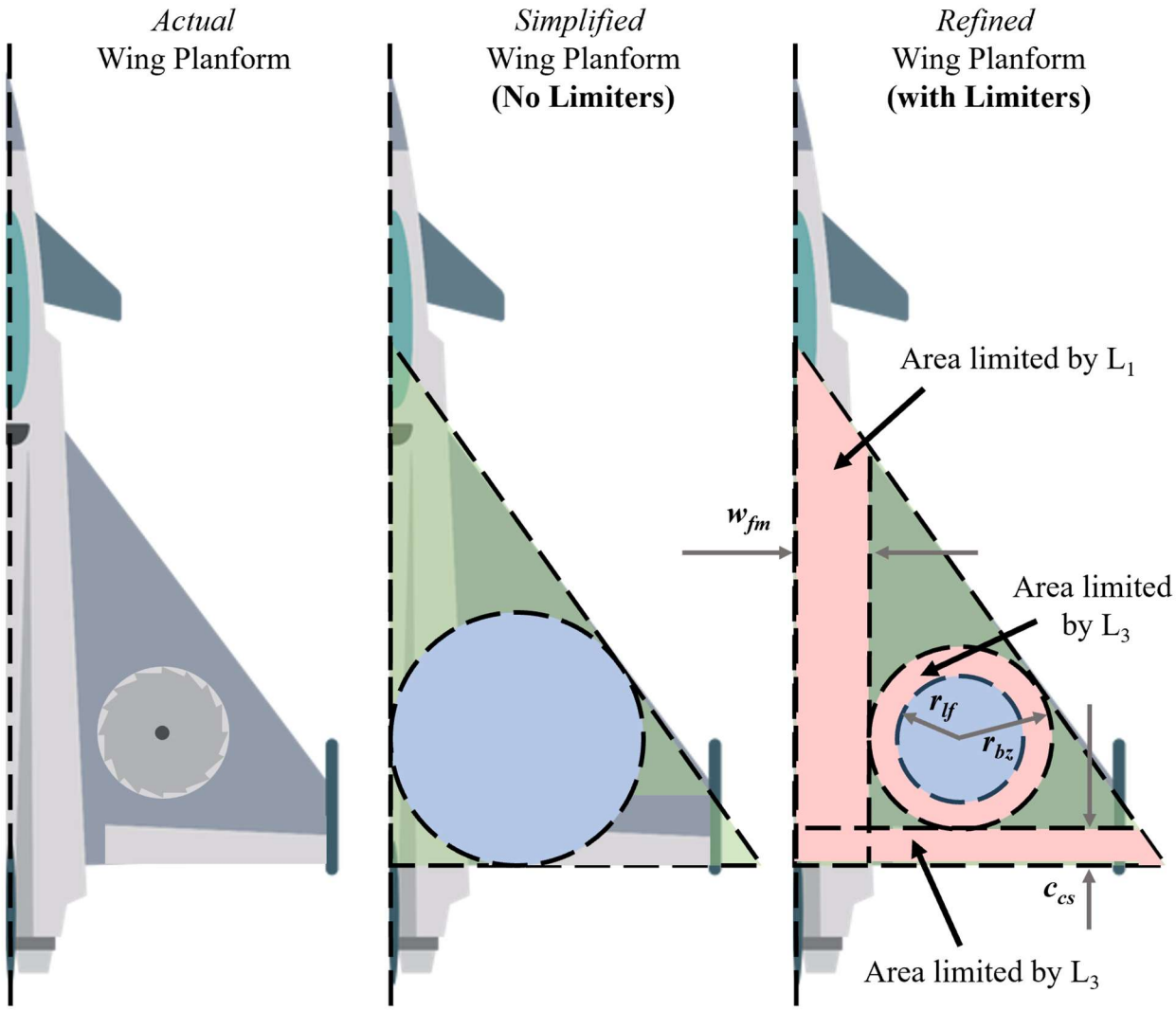

Figure 3.20 Visual description of how the three limiters L_1, L_2, and L_3 reduce the maximum attainable *Ad/S* for a FIW aircraft, adapted from Vexels [116].

In the prior, *simplified* analysis of Ad/S_{max} as a function of wing planform shape and aspect ratio, Equations 3.5-3.7 and Figure 3.18 were derived under the assumption that all existing wing reference area is fair game to make available for the twin-disk FIW lift-fans. This assumption does not account for any wing area lost due to occupation by the fuselage, wing control surfaces, or any fan support structure, which leads to an improper assessment of the actual wing area available to size the lift-fans. For a more accurate estimate, the designer should take these "unusable" wing areas into account by factoring them into a more *refined* analysis.

To demonstrate how this can be done, assume that the design for a new FIW concept calls for a delta wing planform with an *AR* of 2, giving it the isosceles wing shape depicted by configuration 4 of Figure 3.16. The maximum attainable disk-to-fan area for this design was previously proven to be 0.539 with the use of Equation 3.6, but this simplified value neglects any wing area reserved for the wing-box, control surfaces, or fan buffer regions. If these areas were to be included in a refined analysis, one would expect the Ad/S_{max} to be further reduced, but by how much is not clear without properly formulating Ad/S_{max} as a function of L_1, L_2, and L_3.

Interestingly enough, due to the way the conceptual disk-to-wing area limiters L_1, L_2, and L_3 have been defined, the effects of all three limiters on the Ad/S_{max} of the triangular delta wing planform are identical. This can be proven by showing how the maximum disk-to-wing area ratio for a triangular delta-shaped wing is related to the square of the difference between 1 and the limiter value, multiplied by the maximum attainable *Ad/S* for a triangular wing of specified aspect ratio, $C_{A/S}$. As a function of any one of the three L_x limiters, the Ad/S_{max} for the triangular delta wing planform can be rewritten as:

$$Ad/S_{max} = C_{A/S}\left(1 - L_x\right)^2 \tag{3.11}$$

where $C_{A/S}$ for any right-triangle wing planform can be determined using the side lengths of the triangular half-wing shape – a and b – and the hypotenuse length, c:

$$C_{A/S} = \frac{2\pi(a+b)}{3+\left(\sqrt{a+b+c}\right)^3} \tag{3.12}$$

Accordingly, the top line in Figure 3.21 represents Equation 3.11 for the isosceles delta wing planform. As a function of two limiter values, Equation 3.11 becomes Equation 3.13, where L_{x1} is any one of the three Ad/S_{max} limiters (L_1, L_2, or L_3) and L_{x2} is any one of the limiters not selected as L_{x1}.

$$Ad/S_{max} = C_{A/S}\left(1-L_{x1}\right)^2\left(1-L_{x2}\right)^2 \tag{3.13}$$

Hence, the remaining lines in Figure 3.21 are carpet plots of the maximum disk-to-wing area ratio when it becomes a function of two limiters. As expected, Figure 3.21 shows that increasing any of the two limiter values reduces the overall Ad/S_{max}. This figure also allows users to quickly arrive at the same value of Ad/S_{max} whether they first locate L_{x1} and track vertically to find L_{x2} or decide to locate the L_{x2} line first and track down to the right to meet the L_{x1} value. In either scenario, it can be seen that setting any one of the limiters to zero leads the user back to Equation 3.11.

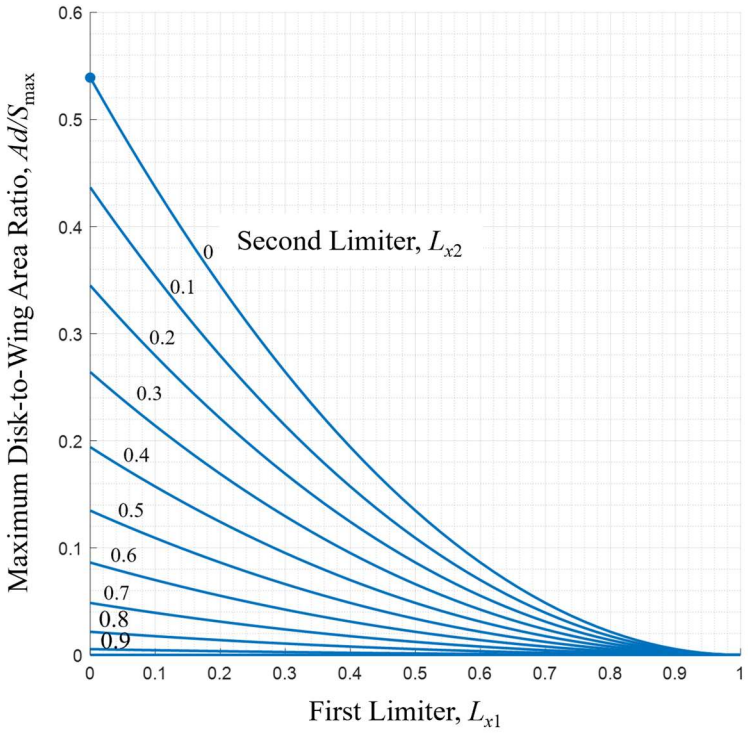

Figure 3.21 Effects of any two of the three described limiters on the maximum attainable *Ad/S*.

If the FIW designer wishes to use a different right triangle for the half-wing planform, Figure 3.21 will change with the $C_{A/S}$ value for their particular shape of choice. Table 3.6 lists five right triangles that have unique relationships between their side lengths and/or angles. When Equation 3.13 for each of these half-wing shapes are plotted over top of each other in the same layout as Figure 3.21, Figure 3.22 is formed to illustrate how the Ad/S_{max} reduces even further when two limiters are applied, *and* the wing's aspect ratio grows further from 1 in either direction.

Table 3.6 List of select special right triangles bound by unique side length or inner angle relationships.

Orientation		**Special Delta Wing Shapes** (Specified by Side Length Multipliers: Side-Side-Hypotenuse)				
		x1 – x1 – x$\sqrt{2}$	x3 – x4 – x5	x1 – x$\sqrt{3}$ – x2	x5 – x12 – x13	x7 – x24 – x25
AR <= 1		$AR = 1$ $\Lambda_{LE} = 45^{\circ}$ 1, $\sqrt{2}$, 1	$AR \approx 5.33$ $\Lambda_{LE} \approx 36.9^{\circ}$ 3, 5, 4	$AR \approx 6.93$ $\Lambda_{LE} = 30^{\circ}$ 1, 2, $\sqrt{3}$	$AR = 9.6$ $\Lambda_{LE} \approx 22.6^{\circ}$ 5, 13, 12	$AR \approx 13.7$ $\Lambda_{LE} = 16.3^{\circ}$ 7, 25, 24
AR >= 1		$AR = 1$ $\Lambda_{LE} = 45^{\circ}$ 1, $\sqrt{2}$, 1	$AR \approx 5.33$ $\Lambda_{LE} \approx 53.1^{\circ}$ 4, 5, 3	$AR \approx 5.33$ $\Lambda_{LE} = 60^{\circ}$ $\sqrt{3}$, 2, 1	$AR \approx 5.33$ $\Lambda_{LE} \approx 67.4^{\circ}$ 12, 13, 5	$AR \approx 5.33$ $\Lambda_{LE} \approx 73.7^{\circ}$ 24, 25, 7

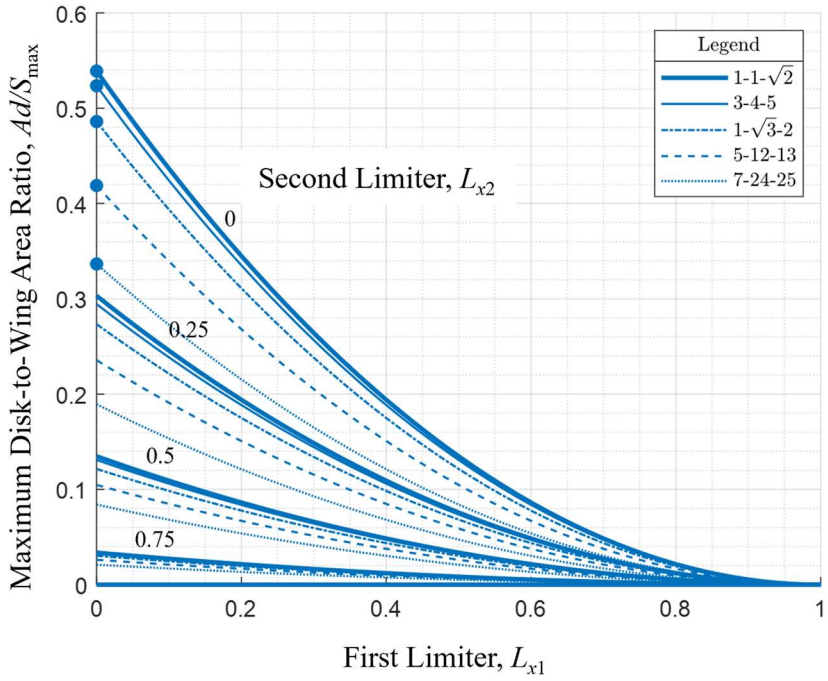

Figure 3.22 Differences in limiter effects due to type of right triangle shape used for a FIW wing planform.

In summary of all the realistic geometric knockdowns to the theoretical disk-to-wing area ratio of the FIW concept which guide FIW designers toward a more practical initial range for conceptual design, Figure 3.23 breaks down the *Ad/S* of the real-world XV-5A and F-35B lift-fan aircraft. While the F-35B's lifting devices are not exactly constrained by the same wing planform restrictions as the XV-5A, the areas of its lift-fan, roll ducts, and swivel nozzle that all contribute to its vertical lift capability are still confined to the concealable area of the aircraft's overall 2D planform. And, interestingly enough, the disk-to-wing area ratios for the XV-5A and F-35B both fall well below the theoretical FIW limit in the design space reproduced in Figure 3.24, even when the disk area outside of the wing reference areas are included in the disk-to-wing area ratio. This is a reassuring indication that, despite the real concepts having plenty of wing area to theoretically grow their lift-fans for better hover performance, there appears to be a significant amount of wing area required to support the embedded lift fans and the functionality of the aircraft in both vertical and horizontal flight.

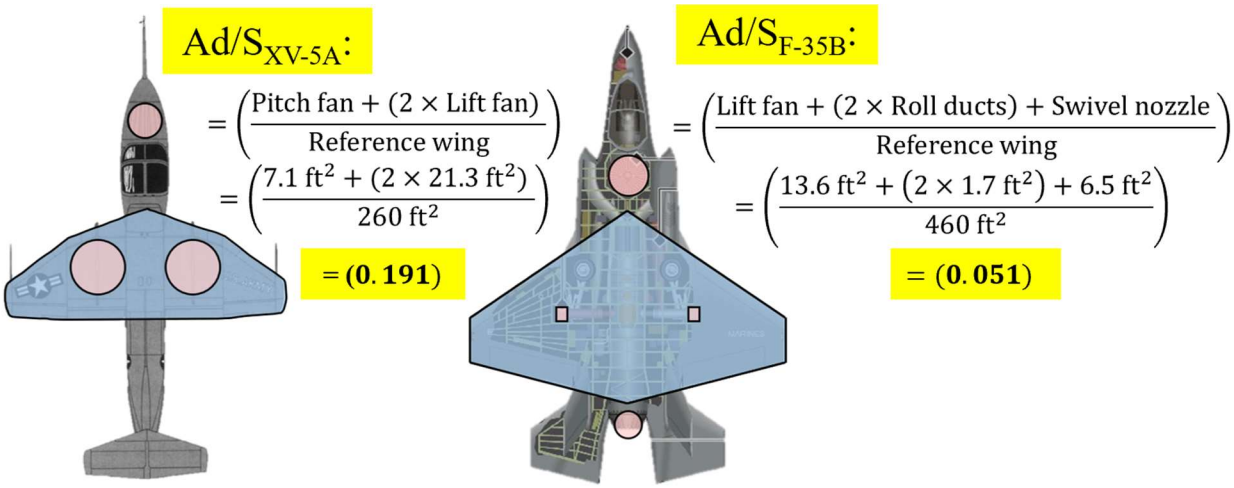

Figure 3.23 Disk-to-wing area ratios for two, real lift-fan aircraft: the XV-5A (left) and F-35B (right).

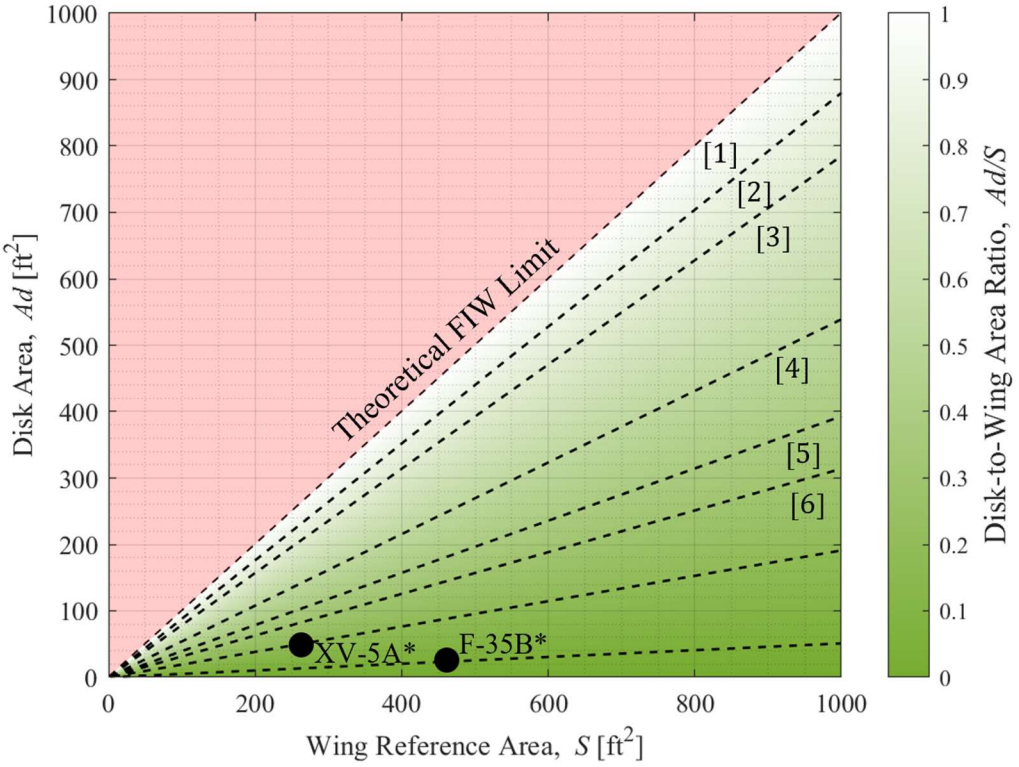

Figure 3.24 Disk-to-wing area design space showing roughly where the XV-5A and F-35B aircraft lie (*including disk area outside the reference wing area).

3.3. Cruise Performance Considerations

The performance of a FIW design, like any other aircraft, is highly dependent on its initial geometric description and weight buildup. Specifically, the performance assessment of a FIW concept is where considerations described in the previous sections coincide to give the designer an idea of how capable their initial configuration truly is. Because conceptual design is an iterative process, it is common for designers to arrive at the performance assessment stage only to find out that their initial configuration fails to meet one or more of the mission requirements, forcing them to revisit the geometric and weight sizing stages. This is to be expected, as refinement of a design takes time.

Nevertheless, performance evaluations are extremely critical in the conceptual stages of aircraft design to ensure that the final conceptual configuration that gets handed off to the preliminary design phase is free of any major issues and avoids a complete rework of the design. In an industry setting, such mistakes result in lost time and money. In the grand scheme of things, the more performance that can be accurately estimated in the initial design stages, the less work will be cut out for the preliminary and detailed designers, and the more believable the design ultimately becomes.

The following performance guidance for a FIW concept has been formulated for designers who already have their initial configurations laid out and are ready to assess the most important performance aspects of their vehicle. In a similar way, this section can be applied to any FIW concepts already available, perhaps any one of the 116 lift-fan eVTOL designs from the VFS eVTOL directory, to gain a rough idea of just how viable the concept really is and how close it actually comes to meeting its performance goals.

The cruise performance of the FIW design is fundamentally the most important aspect of the design to get right, as the top-level mission requirements suggest its high-speed cruise capability makes up its greatest percentage of appeal to designers over similar VTOL concepts. In breaking down the cruise performance of the FIW design, three of the most important metrics that must be estimated in the conceptual design phase are the aircraft's total fuel energy, its cruise power required, and its maximum range performance.

3.3.1.Total Energy

The total energy onboard an aircraft can be estimated by multiplying the total weight of fuel onboard by the specific energy of the fuel, ϵ, which is its energy measured per unit mass. Energy weight matters in aircraft performance, because it is used to determine range, endurance, and loiter capability.

However, there is a distinction between the actual energy available to the aircraft for use during flight and the total energy onboard. Conventional aviation fuels are among the most energy-dense fuel sources on the planet, with the chemical content of liquid avgas possessing a specific energy of approximately 7.3 hp-hr/lb (12,000 Wh/kg) [117]. The only issue is, due to efficiency losses associated with extracting energy from liquid fuels, that chemical value gets substantially knocked down before it can be converted to propulsive energy (around 2.24 hp-hr/lb for an average Rotax engine) [118]. Furthermore, progress in hydrogen fuel cell and battery technologies has advanced to the point where these alternative energy sources may now be considered in modern aircraft. To incorporate these additional energy sources in the energy selection mix, Figure 3.25 summarizes some of the general trends observed in specific energy as a function of propulsion system weight.

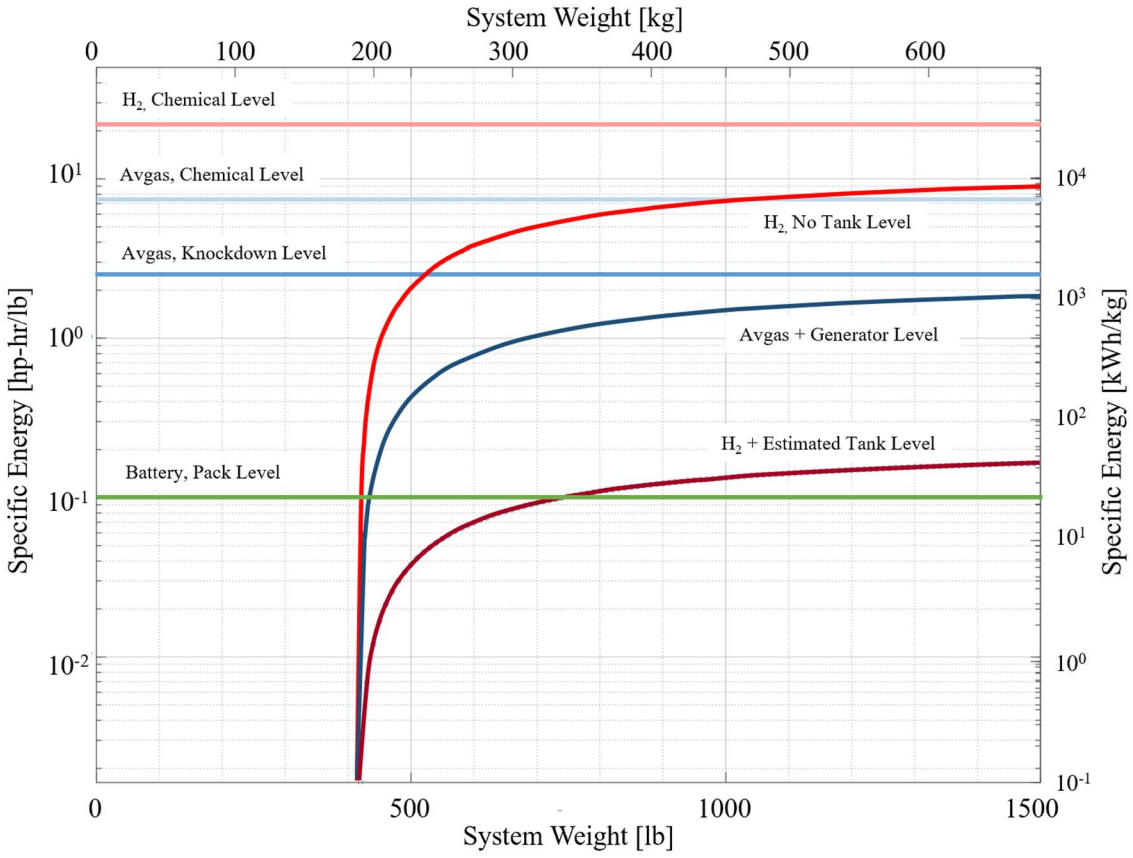

Figure 3.25 Specific energy of various energy sources and propulsion systems, adapted from Anderson et al. [118].

The Breguet Range Equation (BRE) famously specifies range as a function energy weight fraction, which can be used for quick computational purposes to extract the energy weight fraction required to achieve a certain a range specified by the mission requirements [119]. Although the original BRE has two variants that differentiate between propeller and jet thrust range, neither one accounts for battery electric or hybrid-electric variants, which make up a great deal of the FIW concepts currently being proposed.

The BRE for hybrid and battery powered *propeller* aircraft has been derived by Gartenberg [120], which can be applied to prop driven FIW concepts featuring propellers powered by electric motors. However, because the FIW concept is designed to take advantage of high-speed flight, it would seem most appropriate to fit a FIW aircraft with jet engines instead and simply refer to the jet BRE to determine available cruise energy. Although jet aircraft can still employ distributed electric propulsion, a battery pack would mostly be dead weight to a FIW aircraft during high-speed cruise, simply because turbofan and turbojet engines do not require battery power to generate thrust. Therefore, Equations 3.14 and 3.15 offer designers the option to adopt either traditional jet BRE equation or the prop-driven hybrid range equation to estimate the total energy weight fraction (β) of their FIW design:

$$R = \frac{V}{c_t}\left(\frac{L}{D}\right)\ln\left|\frac{1}{1-\beta}\right| \tag{3.14}$$

$$R = \frac{L}{D}\left(\eta_{em}\eta_{em}\varepsilon_{pack}x\beta + \eta_{gt}\varepsilon_{eng}\ln\left(\frac{1}{1-(1-x)\beta}\right)\right) \tag{3.15}$$

where *L/D* is the cruise lift-to-drag ratio, c_t is the thrust specific fuel consumption, x is the percent hybrid factor (0 being fully conventional and 1 being all-electric), ϵ_{pack} and ϵ_{eng} are the specific energies of the battery and conventional engine systems, and η_{em}, η_{bat}, and η_{eng}, are the efficiency values between 0 and 1 of the electric motors, battery pack, and conventional engines,

respectively. Rearranging Equations 3.14 and 3.15 for their energy weight fractions yields Equations 3.16 and 3.17, respectively:

$$\beta = 1 - \frac{1}{e^{\left(\frac{Rc_t}{V}\left(\frac{L}{D}\right)^{-1}\right)}} \quad \text{(from Eq. 3.14)} \tag{3.16}$$

$$\beta = \beta_{bat} + \beta_{gas} \quad \text{(from Eq. 3.15)} \tag{3.17}$$

where the total hybrid energy weight fraction in Equation 3.17 must be found by the summation of the battery pack and liquid fuel energy weight fractions, determined by the range (R_{bat} and R_{gas}) contributions from each:

$$\beta_{bat} = \frac{R_{bat}}{\eta_{em}\eta_{bat}\varepsilon_{pack}x}\left(\frac{L}{D}\right)^{-1} \tag{3.18}$$

$$\beta_{gas} = \left(\frac{1}{1-x}\right)\left(1 - \frac{1}{e^{\left(\frac{R_{gas}}{\eta_{gt}\varepsilon_{eng}}\left(\frac{L}{D}\right)^{-1}\right)}}\right) \tag{3.19}$$

3.3.2.Cruise Power Required

The cruise power required is another performance metric of strong interest to the FIW designer, because it indicates the aircraft's aerodynamic efficiency and the type of propulsion system it requires for cruise. It reasons that to satisfy a given high-speed cruise requirement for an initial FIW configuration, the designer should set the cruise speed equal to the mission required value and let the wing reference area be a variable in solving for the cruise power required.

The general formulation for this starts with the power required of a fixed-wing aircraft in forward flight, which [105] provides via Equation 3.20 as the sum of the aircraft's total induced power (P_{i}) and parasitic power (P_{c}) required at that airspeed.

$$P_c = P_i + P_p = \frac{2}{\rho \pi e}\left(\frac{W}{b}\right)^2\left(\frac{1}{V}\right) + \frac{1}{V}\rho V^3 f \tag{3.20}$$

Note that aside from V_c, Equation 3.20 for P_c is also a function of the cruise altitude (in terms of cruise density, ρ_c), Oswald's efficiency factor (e), wingspan, (b), cruise weight of the aircraft, (W_c), and the equivalent flat plate area, (f). Since the weight of a conventionally fueled aircraft decreases over time as it burns off fuel, and the cruise density changes with altitude, W_c and ρ_c refer to the aircraft gross weight and density at the start of cruise. Meanwhile, the actual Oswald's efficiency factor is a function of the induced power factor (K) and aspect ratio, although Figure 3.26 from [104] can be used to obtain an initial estimate for this value based purely on AR of similar aircraft configurations.

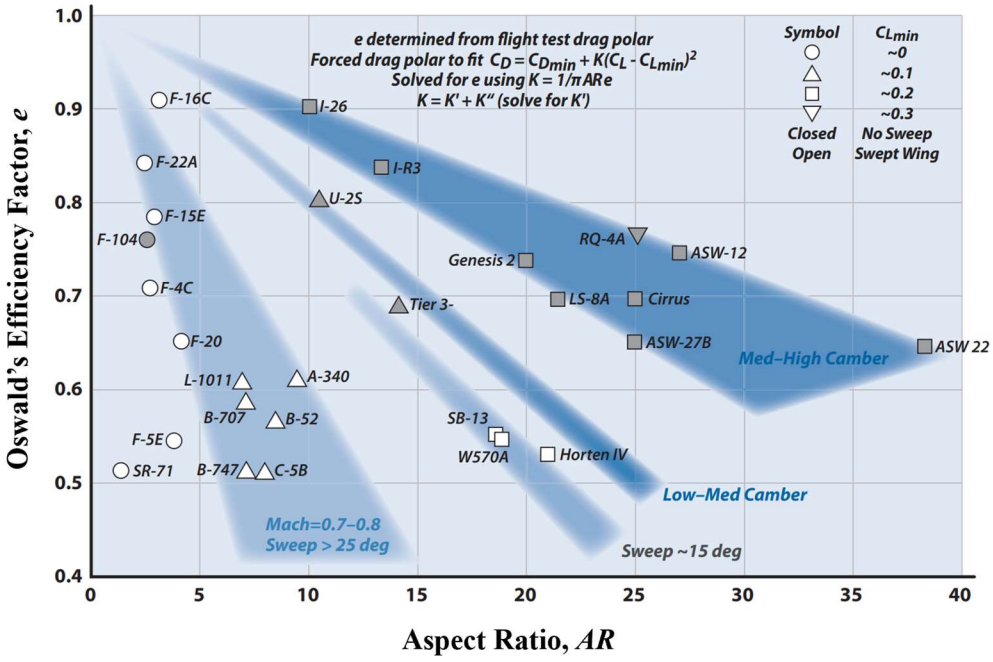

Figure 3.26 Oswald's efficiency factor as a function of aspect ratio for various aircraft at subsonic speeds from Nicolai and Carichner [104].

The flat plate area according to [103] can be defined as the aircraft's average skin friction coefficient (C_F) times the total wetted area, (S_w):

$$f = C_F S_w \tag{3.21}$$

However, the goal is to rearrange Equation 3.20 into a function the wing reference area, S. This can be done for the flat plate area by replacing the wetted area S_w in Equation 3.21 with the equivalent expression of the wetted area to wing reference area ratio (S_w/S) multiplied by S. In doing so, Equation 3.21 transforms into Equation 3.22.

$$f = C_F \left(\frac{S_w}{S} \right) S \tag{3.22}$$

Lastly, the span can also be replaced with an expression for wing area as a function of aspect ratio:

$$b = \sqrt{AR(S)} \tag{3.23}$$

Substituting Equations 3.22 and 3.23 back into Equation 3.20, the cruise power required as a function of wing area becomes:

$$P_c = \frac{2W^2}{\rho \pi e V (AR) S} + \frac{C_F \rho V^3}{2} \left(\frac{S_w}{S} \right) S \tag{3.24}$$

Equation 3.24 assumes AR and S_w/S are constants, meaning the wing shape and rest of the aircraft scales with the wing reference area. If scaling the whole aircraft with the wing area is not the desired effect by the designer, simply undoing the Equation 3.22 substitution will leave the flat plate area as a constant. Vice versa, if the designer would prefer to scale the whole aircraft with S but leave AR as a variable, reverting back to Equation 3.20 before the Equation 3.23 substitution will do the trick. However, in the proceeding analysis, it will be assumed that the designer intends to scale the total aircraft size and wing shape with the wing reference area.

Assuming some example constants for Equation 3.24, the required cruise power as a function of wing area is given by Figure 3.27:

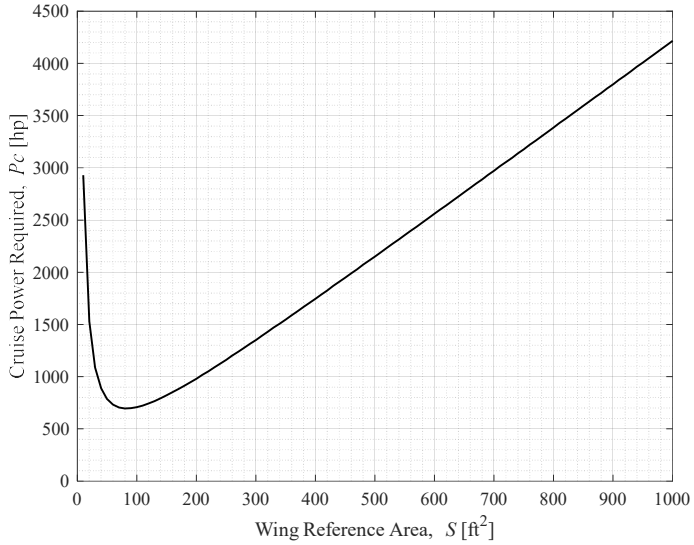

Figure 3.27 Cruise power required for an example FIW aircraft with an initial cruise weight of 10,000 lb.

Moreover, Figure 3.28 shows how the cruise power required varies for different initial cruise weights ranging from 0 to 100,000 lb.

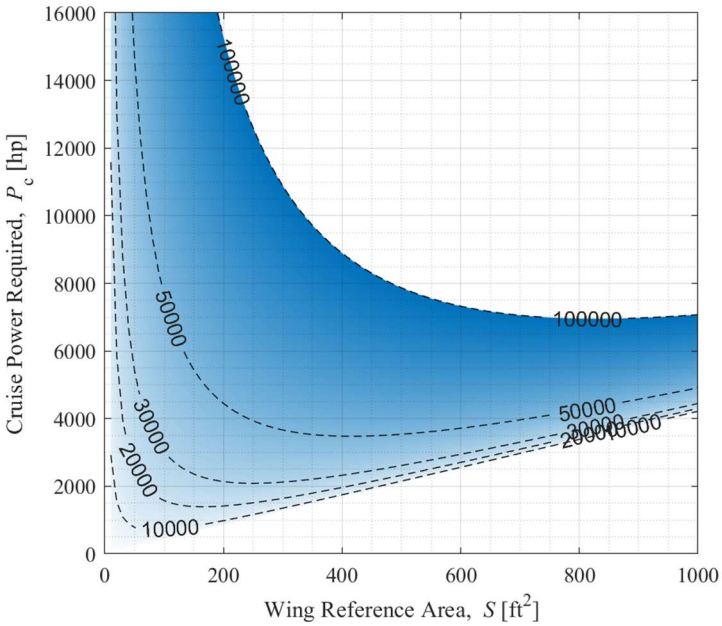

Figure 3.28 Cruise power required for an example FIW aircraft of various initial cruise weight, using the assumptions from Figure 3.27.

In Figure 3.27 and Figure 3.28, it appears that for a given initial cruise weight, there is a specific value of wing reference area that yields the minimum required cruise power. Based on Equation 3.24, it can be proven that there exists an exact wing area that minimizes cruise power required, just as there exists a specific velocity for minimum power. By setting the derivative of Equation 3.24 equal to zero and solving for *S*, the minimum power to cruise at a fixed speed has been found to occur when the wing reference area equals the expression given by Equation 3.25.

$$S = \frac{2W}{\rho V^2}\sqrt{\frac{1}{\pi C_F e(AR)\left(\frac{S_w}{S}\right)}} \tag{3.25}$$

The complete proof of Equation 3.25 is available to view in Appendix B.

3.3.3.Range

Per the top-level mission requirements, it is recommended that the range for a conceptual FIW aircraft be estimated using the BRE for a jet aircraft, since the concept best aligns itself with jet propulsion. This section discusses the quantification of range based on the assumption that the designer has selected a jet powered FIW configuration. In the event that the designer opts to analyze the range performance of a prop-driven design, similar steps can be followed, except starting from the hybrid BRE for propeller driven airplanes, given by Equation 3.15. For brevity, only the jet range analysis has been detailed in this section.

However, to preface the derivation for range as a function of the wing reference area – which is the ultimate goal for aligning range with the derivation for cruise power – an aside must be taken to explain why the designer's choice in either scaling the whole aircraft with the wing reference area or not matters. In essence, the decision boils down to how the drag scales with the wing reference area. If the designer would prefer the entire aircraft to scale with the wing reference area, as assumed in the derivation of cruise power required, then the total zero-lift drag coefficient (C_{D0})

remains fixed, and the maximum attainable range is set based on that value regardless of changes in initial cruise weight. However, if the wing reference area is permitted to scale independently of the total aircraft, then C_{D0} becomes a function of the wing reference area, and the maximum attainable range increases with initial cruise weight. To explain how this occurs, follow the two subsequent derivations for range as a function of wing area:

Derivation 1: ***R = f(S)*** (Assuming S_w/S scales with S)

Starting with an expression from [105] which defines the 3D drag coefficient (C_D) as the summation of the profile drag coefficient (C_{D0}) and the induced drag coefficient (C_{Di}), Equation 3.26 expands C_{Di} using the 3D lift coefficient (C_L) and previously defined parameters e and AR:

$$C_D = C_{D0} + \frac{C_L^{\,2}}{\pi(AR)e} \tag{3.26}$$

Substituting the induced lift coefficient, K for $\frac{1}{\pi(AR)e}$ according to [103] and expanding the zero-lift drag coefficient by $C_{D0} = C_{fe}\frac{S_w}{S} + C_{D\,F\&I} + C_{Dmisc} + C_{D\,L+P} + C_{Dwave}$ [103], the total drag coefficient can be rewritten as:

$$C_D = \left(C_{fe}\frac{S_w}{S} + C_{D\,F+I} + C_{D\,misc} + C_{D\,L+P} + C_{D\,wave} \right) + KC_L^{\,2} \tag{3.27}$$

However, to simplify C_{D0} in equation 3.27, it is within reason to neglect the additional terms that apply to form and interference drag ($C_{D\,F\&I}$), miscellaneous drag (C_{Dmics}), leaks and protuberance drag ($C_{D\,L\&P}$), and wave drag (C_{Dwave}), assuming the FIW cruise speed remains subsonic and below its drag divergence Mach number (M_{DD}). As Figure 3.29 shows, for all

operating speeds below M_{DD}, the skin friction drag contribution $C_{fe}\frac{S_w}{S}$ makes up a significant majority of the total C_{D0}:

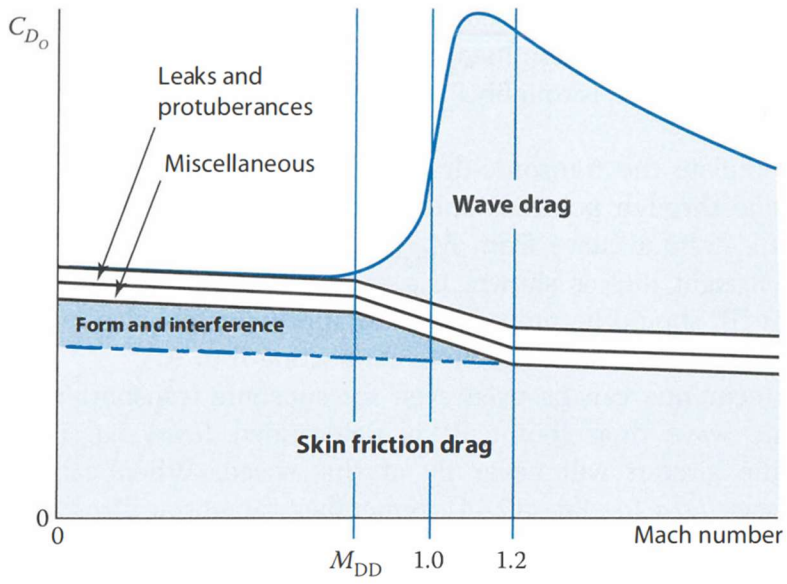

Figure 3.29 Composition of the 3D, zero-lift drag coefficient C_{D0} as a function of Mach number from Raymer [103].

Thus, the total zero-lift drag coefficient reduces to the equivalent skin friction coefficient (C_{fe}) times S_w/S:

$$C_D = C_{fe}\frac{S_w}{S} + KC_L^{\,2} \tag{3.28}$$

However, since S_w/S is assumed to scale with S, and C_{fe} depends only on the aircraft's exposed surface roughness, C_{D0} becomes constant, and Equation 3.28 reduces to:

$$C_D = C_{D0} + KC_L^{\,2} \tag{3.29}$$

Now it is appropriate to reintroduce the Breguet Jet Range Equation from Equation 3.14. However, Equation 3.30 replaces the energy fuel fraction term with the ratio of initial cruise weight

(W_0) to final cruise weight (W_1), and the cruise L/D with the coefficient form C_L/C_D to stay consistent with the prior formulations:

$$R = \frac{1}{c_t} V \left(\frac{C_L}{C_D} \right) \ln \left| \frac{W_0}{W_1} \right| \tag{3.30}$$

If the cruise speed is replaced by the expression $\sqrt{\frac{2W_0}{\rho_0 S C_L}}$ (assuming lift equals weight), the C_L is factored out, and C_D in the denominator is expanded using Equation 3.29, then Equation 3.30 can be rewritten as:

$$R = \frac{1}{c_t} \sqrt{\frac{2W_0}{\rho_0 s}} \frac{\sqrt{C_L}}{C_{D0} + K C_L^{\,2}} \ln \left| \frac{W_0}{W_1} \right| \tag{3.31}$$

The final expression for range as a function of wing reference area, assuming the whole aircraft scales with S, works out to Equation 3.32:

$$R = \frac{\ln \left| \frac{W_0}{W_1} \right|}{c_t \left(C_{D0} \left(\frac{\rho_0 S V}{2W_0} \right) + K \left(\frac{2W_0}{\rho_0 S V^3} \right) \right)} \tag{3.32}$$

Assuming the following example constants for Equation 3.32, the total range as a function of wing area is given by Figure 3.30:

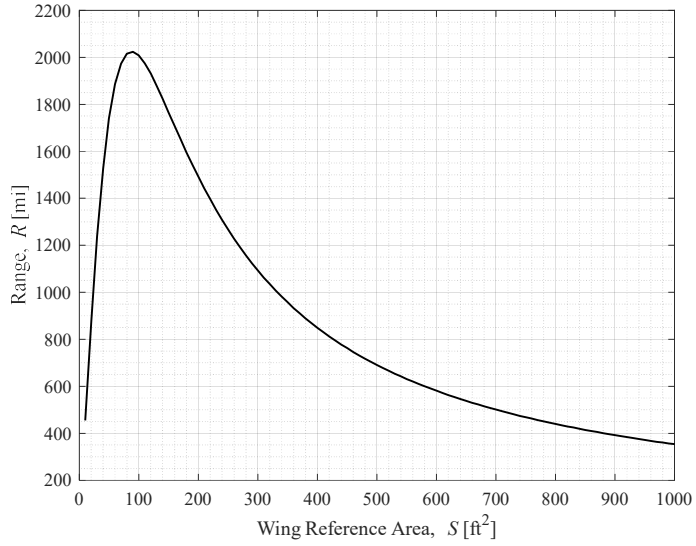

Figure 3.30 Range of an example FIW aircraft with an initial cruise weight of 10,000 lb, assuming constant S_w/S.

Moreover, Figure 3.31 shows how maximum range remains constant for different initial cruise weights ranging from 0 to 100,000 lb.

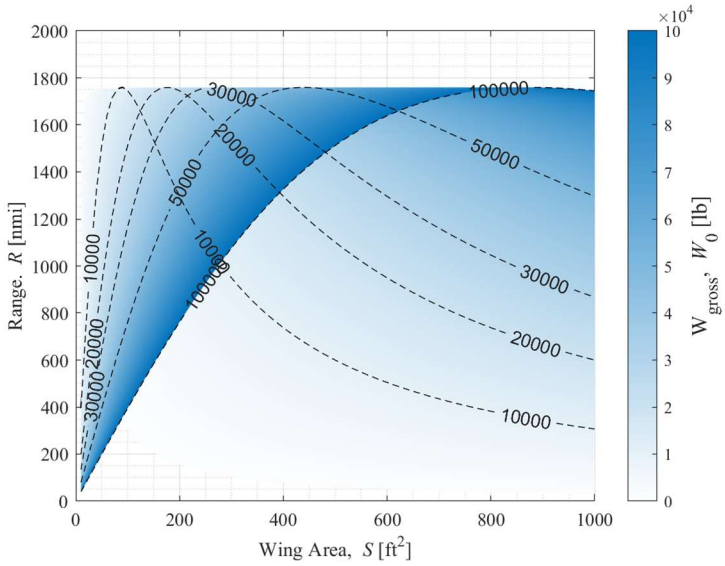

Figure 3.31 Range of an example FIW aircraft of various initial cruise weights, assuming constant S_w/S and the assumptions from Figure 3.30.

In Figure 3.30 and Figure 3.31, it appears that for a given initial cruise weight, there is a specific value of wing area that yields an ideal maximum range. Based on Equation 3.32, it can be proven that there exists an exact wing area that maximizes range, just as there exists a specific velocity for maximum range. By setting the derivative of Equation 3.32 equal to zero and solving for *S*, the maximum range at a fixed speed (when *Sw/S* is constant) has been found to occur when the wing reference area equals the expression given by Equation 3.33:

$$S = \frac{2W_0}{\rho_0 V^2}\sqrt{\frac{K}{C_{D0}}} \tag{3.33}$$

What is compelling about Equation 3.33 is that it states the C_L for maximum range, when speed is fixed and wing area is a variable, occurs when:

$$C_L = \sqrt{\frac{C_{D0}}{K}} \tag{3.34}$$

This is different than the C_L most fixed-wing design textbooks derive for maximum range as a function of airspeed with a fixed wing area, which, according to [103], occurs when:

$$C_L = \sqrt{\frac{C_{D0}}{3K}} \tag{3.35}$$

To understand how these derivations differ, refer to the complete proof and explanation provided in Appendix B.

<u>Derivation 2:</u> ***R = f(S)*** (Assuming S_w/S does <u>*not*</u> scale with *S*)

This second derivation follows Derivation 1 all the way up to Equation 3.28, except beyond this step, it is assumed S_w/S does not scale with *S*, which means S_w/S is not constant, and therefore must be a function of *S*.

Mathematically, S_w/S as a function of *S* simply takes the form 1/x. This expression reasons that as *S* approaches zero, S_w/S goes to infinity, which agrees with the physical interpretation of an

aircraft with no wings. However, as S goes to infinity, the wing physically becomes a flying wing, and thus the total wetted area approaches the sum of the upper and lower surface of the wing reference area, which is approximately 2. Therefore, the equation would also have an asymptote at y = 2.

It is not immediately clear how the slope of such line should be computed, but one approach is to use statistical data and base the slope on a value that must fall on the line. For example, based on [103], the F-4 Phantom has an S_w/S of approximately 4, and according to another figure from [103], a known wing area of 530 ft^2. Therefore, if this point on the equation for S_w/S was known based on a reference aircraft's wing area S_m and reference wetted-to-wing area ratio S_w/S_m, an equation for S_w/S as a function of S in its simplest form can be formulated as:

$$\frac{S_w}{S} = \frac{S_m\left(\frac{S_w}{S_m} - 2\right)}{2} + 2 \tag{3.36}$$

which, for an F-4 type aircraft, would look something like Figure 3.32:

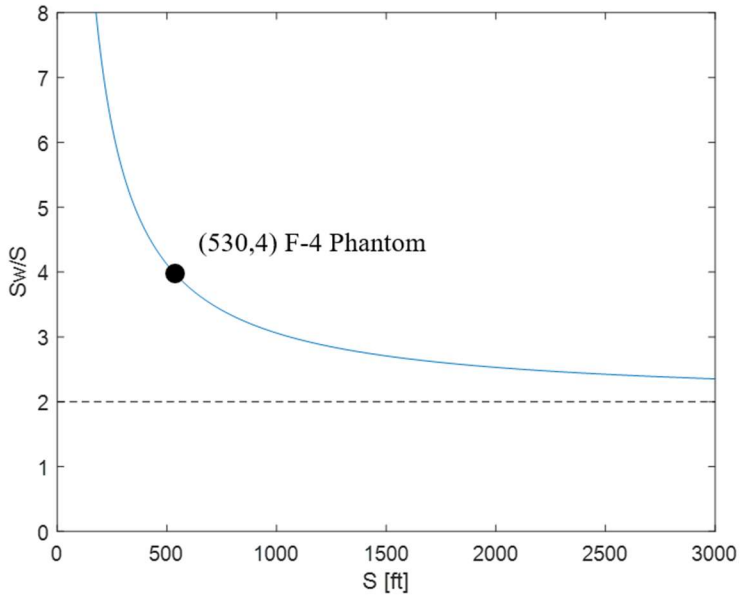

Figure 3.32 Generalized equation for the wetted-to-reference wing area ratio as a function of S for a general, F-4 Phantom shaped aircraft.

More generally, if Equation 3.36 was expanded to other types of fixed-wing aircraft, it would form a viable wetted area region as shown in Figure 3.33.

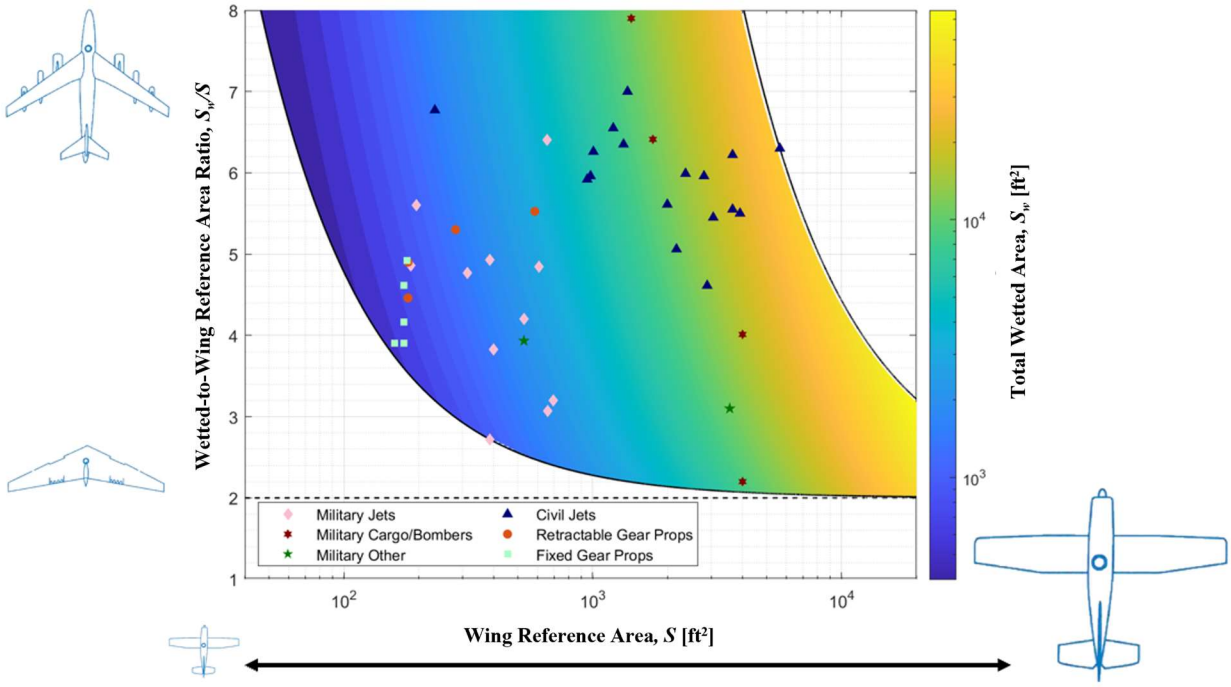

Figure 3.33 Generalized region of wetted-to-reference wing area ratio as a function of S for a variety of conventional aircraft, aircraft images and data from [103].

Thus, as a function of wing reference area, S_w/S can now be substituted back into Equation 3.28:

$$C_D = C_{fe}\left(\frac{S_m\left(\frac{S_w}{S_m} - 2\right)}{2} + 2\right) + KC_L^2 \tag{3.37}$$

From here, if the same steps from Derivation 1 are followed for the jet BRE, except for substituting in the new expression for C_{D0}, the final form of range as a function of wing reference area (when S_w/S does not scale with S) can be rewritten as:

$$R = \frac{\ln\left|\frac{W_0}{W_1}\right|}{c_t\left(C_{fe}\left(S_m\left(\frac{S_w}{S}_m - 2\right)\left(\frac{\rho_0 V}{2W_0}\right) + \frac{\rho_0 SV}{W_0}\right) + K\left(\frac{2W_0}{\rho_0 SV^3}\right)\right)} \tag{3.38}$$

Assuming the following example constants for Equation 3.38, the total range as a function of wing reference area is given by Figure 3.34:

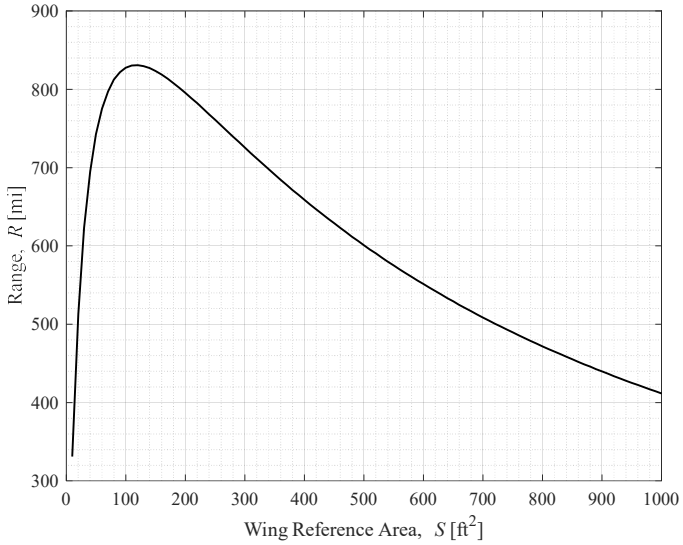

Figure 3.34 Range of an example FIW aircraft with an initial cruise weight of 10,000 lb, assuming variable S_w/S and the assumptions from Figure 3.30.

Moreover, Figure 3.35 shows how maximum range now increases with increasing initial cruise weights ranging from 0 to 100,000 lb.

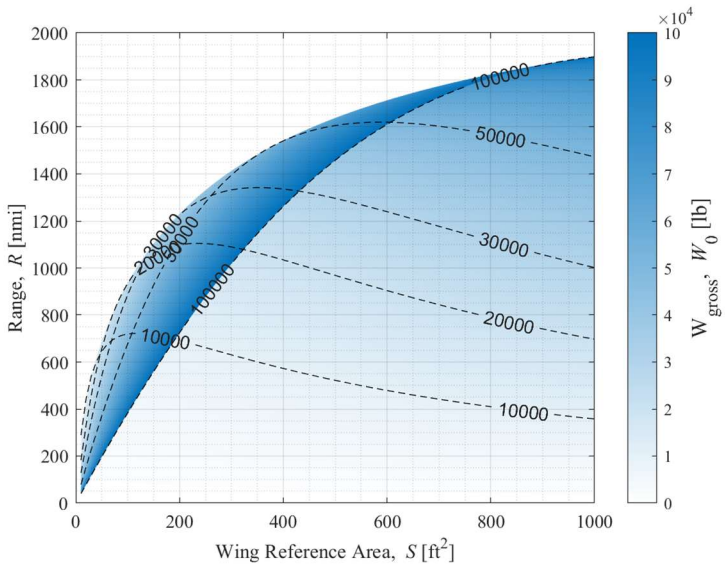

Figure 3.35 Range of an example FIW aircraft with various initial cruise weights, assuming variable S_w/S, and the assumptions from Figure 3.34.

As shown in the previous range derivation, Figure 3.34 and Figure 3.35 appear to show that for a given initial cruise weight, there is a specific value of wing area that yields an ideal maximum range. Based on Equation 3.38, it can be proven that there exists an exact wing area that maximizes range, just as there exists a specific velocity for maximum range. By setting the derivative of Equation 3.38 equal to zero and solving for S, the maximum range at a fixed speed (when S_w/S is not constant) has been found to occur when the wing reference area equals the expression given by Equation 3.39.

$$S = \frac{W_0}{\rho_0 V^2}\sqrt{\frac{2K}{C_{fe}}} \tag{3.39}$$

What is compelling about Equation 3.39 is that it states the C_L for maximum range, when speed is fixed and wing area is a variable, occurs when:

$$C_L = \sqrt{\frac{C_{fe}}{2K}} \tag{3.40}$$

This, again, is different than the C_L most fixed-wing design textbooks derive for maximum range as a function of airspeed with a fixed wing area, which, to reiterate Equation 3.35, occurs when:

$$C_L = \sqrt{\frac{C_{D0}}{3K}} \tag{3.35}$$

To better understand how these derivations differ, refer to the complete proof and explanation provided in Appendix B.

In the analysis to follow, it will be assumed that the designer prefers their total FIW aircraft to scale with increasing wing area. This is aligns with evidence presented in Figure 3.36 [104], which suggests that the total zero-lift drag coefficient is less influenced by the size of the wing and instead more based on the surface area "cleanliness" of the configuration, or C_{fe}.

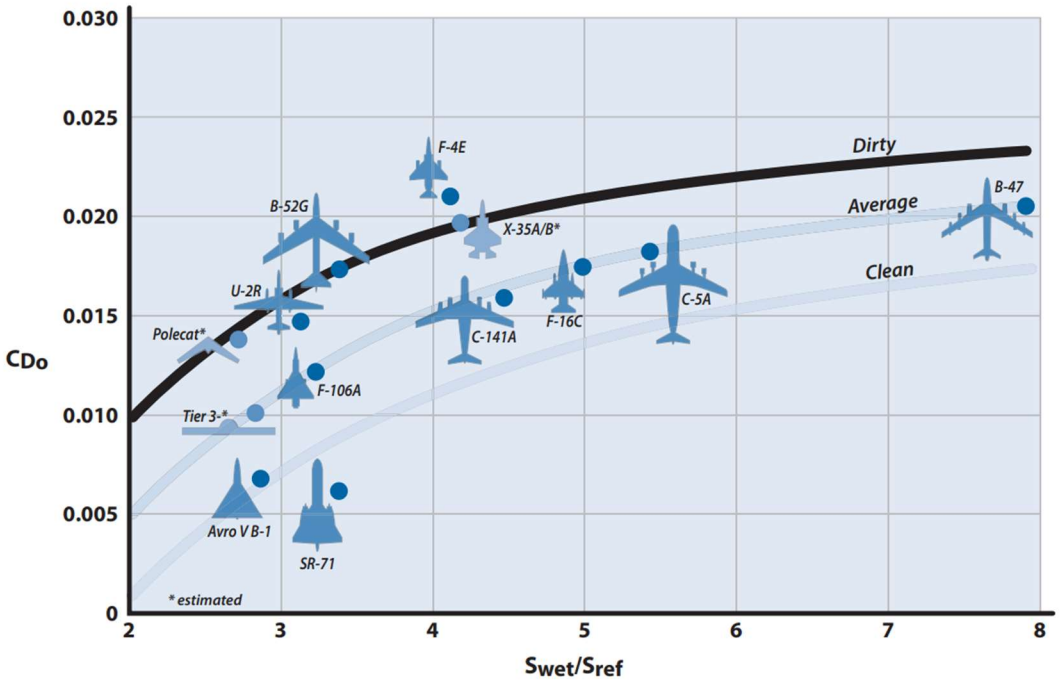

Figure 3.36 Correlation of subsonic C_{D0} from Nicolai and Carichner [104].

3.4. Hover Performance Considerations

FIW hover performance should be considered the second, if not first, most essential performance metric to cruise, because if demonstrated well, can make the concept superior to jets and HSVTOL concepts of similar speed. In breaking down the hover performance of the FIW design, three of the most important metrics that must be considered in the conceptual design phase are the aircraft's hover power required, the figure of merit of its lift fans, and the downwash produced in hover.

3.4.1. Hover Power Required

The hover power required must be known to the FIW designer early in the conceptual design phase because it will suggest the type of propulsion required for hover and indicate how efficiently the lift fans do their job. It reasons that to satisfy a given sustained hover requirement for an initial FIW configuration and as well as the geometric and cruise constraints, the designer should find the power required to hover (P_h) as a function of the total lift-fan disk area (Ad).

However, referring to rotorcraft aerodynamics, it is first important to note that hover power required depends on the tangential tip speed of the lift-fan blades (V_{tip}). The blade tip speed for an individual lift fan can be defined as the disk area radius (r_d) times the rotational speed of the lift fan blades, Ω:

$$V_{tip} = r_d \Omega \tag{3.41}$$

Since Equation 3.41 shows that tip speed is a function of the lift-fan radius, and r_d is proportional Ad, it is not logical to let V_{tip} be proportional to Ad by keeping the rotational speed constant. In such case, V_{tip} would grow to infinity with infinite Ad, which is not feasible. Instead, V_{tip} should be derived using a fixed, average blade lift coefficient (C_l) making V_{tip} inversely proportional to Ad^2.

This relationship can be worked out starting with the definition of the blade thrust coefficient (C_T) from [111]:

$$dC_T = \frac{dT}{\rho(Ad)\left(V_{tip}\right)^2} \tag{3.42}$$

in which case integrating the thrust coefficient along the span of the blades can be done non-dimensionally, assuming an average lift coefficient of C_l and a rectangular blade planform:

$$C_T = \frac{1}{2}\sigma_d \int_0^1 C_l x^2 dx = \frac{1}{6}\sigma_d C_l \tag{3.43}$$

By rearranging Equation 3.42 to isolate the differential thrust force (which in steady-level hover equals the total hover lift and total hover weight, W) and substituting in Equation 3.43 for the integrated C_T, Equation 3.42 becomes:

$$W = \rho A_d \left(V_{tip}\right)^2 \frac{1}{6}\sigma_d C_l \tag{3.44}$$

which means the tip speed can now be rewritten as:

$$V_{tip} = \sqrt{\frac{W6}{\sigma_d \rho(Ad)C_l}} \tag{3.45}$$

It is also possible to show that the thrust coefficient for an ideal hovering rotor of optimum taper and uniform inflow is approximately 1.5 times greater than that of a rectangular blade planform with a solidity (σ_d) equal to the tip solidity of the ideal hovering rotor, using an average blade angle of attack and blade lift coefficient [111]. This means, for the ideal hovering rotor:

$$V_{tip} \cong \sqrt{\frac{W4}{\sigma_d \rho(Ad)C_l}} \tag{3.46}$$

The ideal hovering rotor, however, is difficult to achieve in practice because it requires hyperbolic twist and nonlinear taper, making manufacturing of it more difficult and expensive.

Furthermore, the high degree of twist would be limited by the FIW conceptual tradeoff of trying to keep the wing thickness to chord ratio *t/c* as low as possible. Therefore, for simplicity in the analysis to follow, it will be assumed that the lift-fans employ rectangular blades with tip speeds corresponding to Equation 3.45.

Returning now to the general formulation of P_h as a function of Ad, [111] defines the hover power required for a rotor system in hover as the summation of the total induced power and parasitic power required, which has been expanded in Equation 3.47:

$$P_h = P_i + P_0 = \frac{kW^{3/2}}{\sqrt{2\rho Ad}} + \rho Ad\left(V_{tip}\right)^3\left(\frac{\sigma_d C_{d0}}{8}\right) \tag{3.47}$$

where k is the induced power factor and C_{d0} is the profile drag coefficient of the lift fan blades.

After substitution of Equation 3.45 in for V_{tip} as a function of Ad and simplifying Equation 3.47, Equation 3.48 gives the final form of the hover power required:

$$P_h = \left(\frac{W^{3/2}}{\sqrt{\rho}}\right)\left(\frac{k}{\sqrt{2}} + \frac{C_{d0}}{8\sqrt{\sigma_d}}\left(\frac{6}{C_l}\right)^{3/2}\right)\left(\frac{1}{\sqrt{Ad}}\right) \tag{3.48}$$

Assuming the following example constants for Equation 3.48, the total hover power required as a function of disk area is given by Figure 3.37:

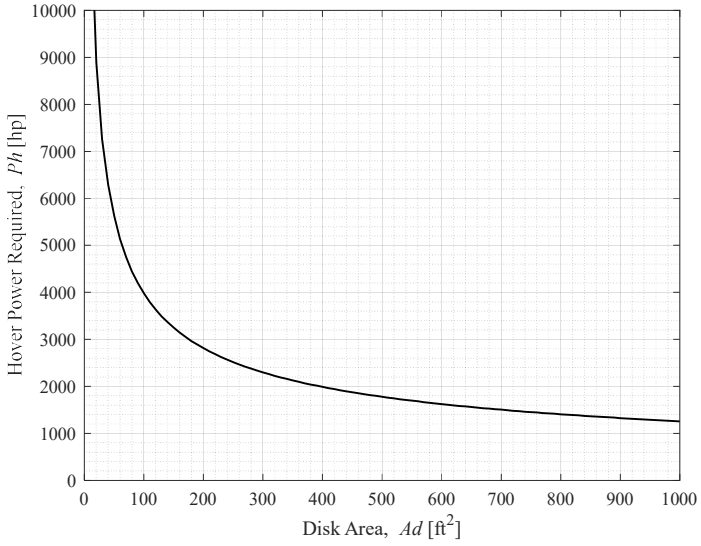

Figure 3.37 Hover power required for an example FIW aircraft with an initial hover weight of 10,000 lb.

Moreover, Figure 3.38 shows how hover power required varies for different initial hover weights ranging from 0 to 100,000 lb.

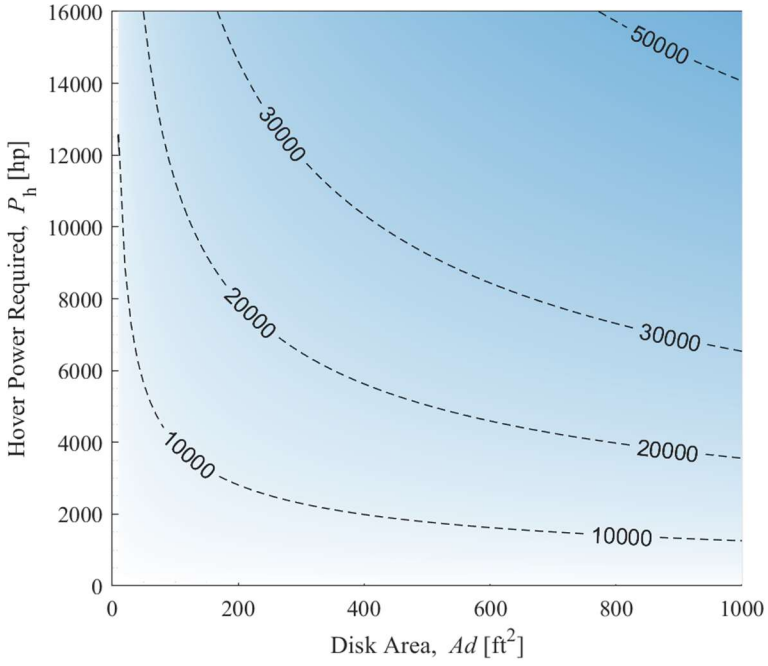

Figure 3.38 Hover power required for an example FIW aircraft of various initial hover weights, using the assumptions from Figure 3.37.

In Figure 3.37 and Figure 3.38, it appears that for a given initial hover weight, there is no singular value of disk area that yields the minimum required hover power. Due to P_h being inversely proportional to the square of Ad, the hover power required will always decrease with increasing disk area. This finding explains why a larger rotor is more power-efficient than a smaller one.

As it concerns the FIW concept, Equation 3.48 confirms that to minimize hover power required, the lift fans should occupy as much area of the wing as possible. Yet, as previously discussed, the maximum allowable disk area is geometrically constrained by the practical size of the wing. While this disk area limitation negatively impacts the concept's maximum hover performance, [111] points out the FIW concept does benefit from an additional reduction in hover power required by embedding its lift fans inside its wings.

Analogous to the way winglets increase aerodynamic efficiency of a fixed-wing aircraft by suppressing the wingtip-induced vortices, the ducting around a shrouded rotor has been proven with momentum theory to limit the contraction of the rotor wake by a certain percentage of the equivalent, open-rotor wake contraction area ($a_w A$). This means that a ducted rotor generates a larger area of the slipstream flow at the outlet (A), as shown in Figure 3.39, due to reduced tip-loss effects. As a result, the ducted rotor consumes less induced power ($P_{i\,FIW}$) than that for a non-ducted fan (P_i) by the wake contraction parameter (a_w):

$$\frac{P_{i\,\mathrm{FIW}}}{P_i} = \frac{1}{\sqrt{2a_w}} \tag{3.49}$$

where a_w varies from 0.5 to 1. When $a_w = 0.5$, the ducting allows no wake contraction to occur, and the total induced power is reduced by an ideal, maximum factor of $1/\sqrt{2}$. When $a_w = 1$, the duct has no effect on the wake contraction, and thus no reduction in power occurs. In theory, the power savings from ducted fans is significant, but in practice, harnessing the full reduced power

potential with a FIW concept will be limited by the duct length required to fit the fan in the wing and additional drive shaft losses [111].

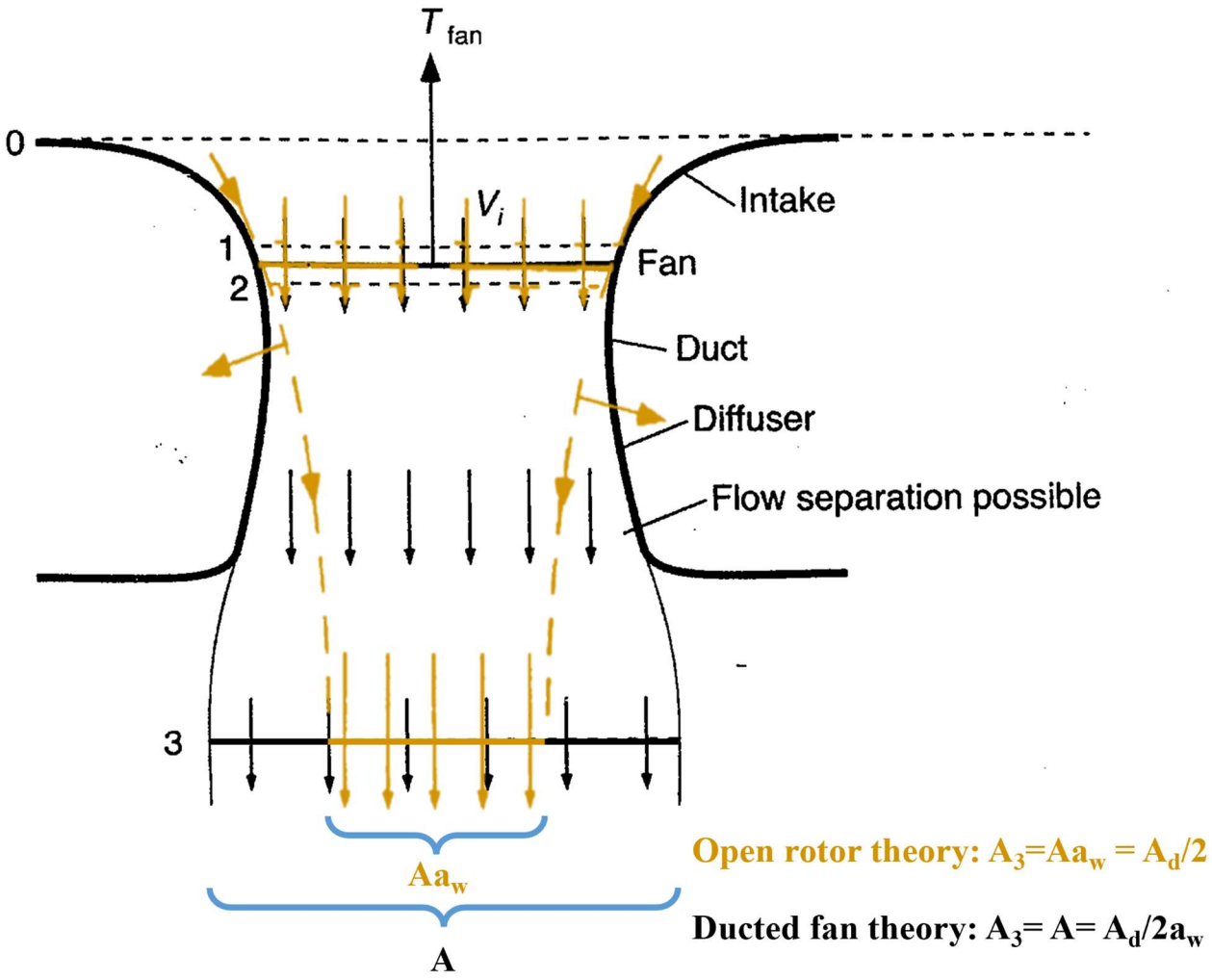

Figure 3.39 Flow model assumed for FIW analysis using momentum theory, adapted from Leishman [111].

3.4.2.Figure of Merit

Another indication of hover efficiency that should be included in the estimated performance of a FIW design as a quick "reality check" is its Figure of Merit (*FM*). The figure of merit of a rotor system is defined as the ratio between its ideal power required to hover and the actual power it consumes during hover. Because the actual P_h of a rotorcraft can never exceed its ideal P_h, the

FM should never exceed 1. Hence, for an adequate reality check to ensure the previously estimated hover power is within reason for a FIW design, its *FM* can be computed using the previously defined power loading and disk loading parameters according to Equation 3.50 [111].

$$FM = PL\sqrt{\frac{DL}{2\rho}} \tag{3.50}$$

Furthermore, when *PL* and *DL* are plotted on a log scale, *FM* contours will appear as diagonal lines. Figure 3.40 shows how this looks, with the *FM* line of unity creating a boundary between the possible and impossible VTOL design space. Below $FM = 1$, lines of decreasing *FM* represent less power-efficient hover designs. Hence, FIW designers can use Figure 3.40 to determine to what degree their design makes use of its ideal hover power required.

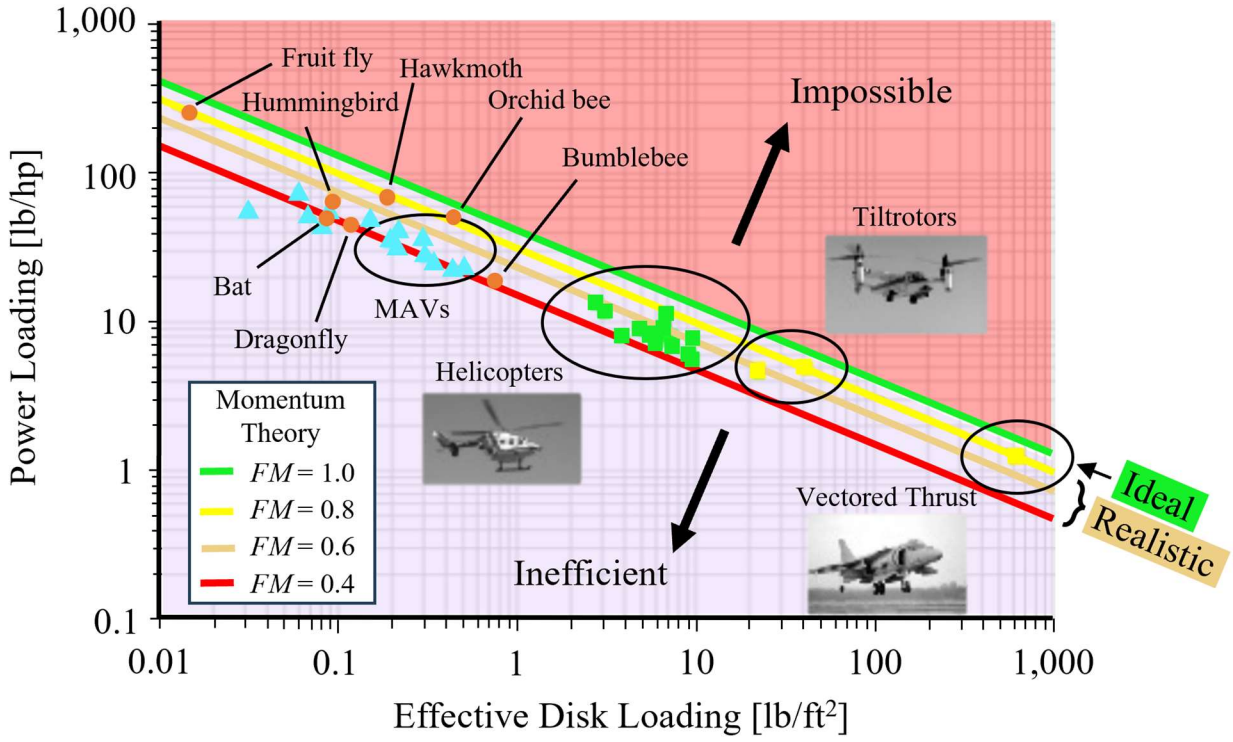

Figure 3.40 Correlating *FM* with hover efficiency, adapted from Leishman [111].

3.4.3.Downwash

The last hover performance consideration worth analyzing is the downwash produced by the FIW concept. Downwash has a huge impact on the terrain a VTOL aircraft can take off and land vertically from, the distance from which it can operate near ground personnel, and the stability of its surrounding environment during hover.

In order to correlate downwash to hover power required, it must also be arranged as a function of disk area. Fortunately, his formulation has been readily prepared by [111], who proves the downwash (w) at the fully developed far wake area ($a_w A$, from Figure 3.39) of a ducted fan is exactly twice the induced velocity (v_i) measured at the rotor disk plane area (Ad), times the wake contraction parameter (a_w):

$$\omega = 2 v_i a_w \tag{3.51}$$

Additionally, the induced velocity at the rotor disk plane is defined as a function of disk area according to Equation 3.52:

$$v_i = \sqrt{\frac{W_h}{2 \rho_h A d}} \tag{3.52}$$

Thus, when Equations 3.51 and 3.52 are combined, the downwash at the far cross-sectional area of the vena contracta for the FIW lift-fan can be expressed as:

$$\omega = a_w \sqrt{\frac{2 W_h}{\rho_h A d}} \tag{3.53}$$

Assuming the following example constants for Equation 3.53, the hover downwash as a function of disk area is given by Figure 3.41:

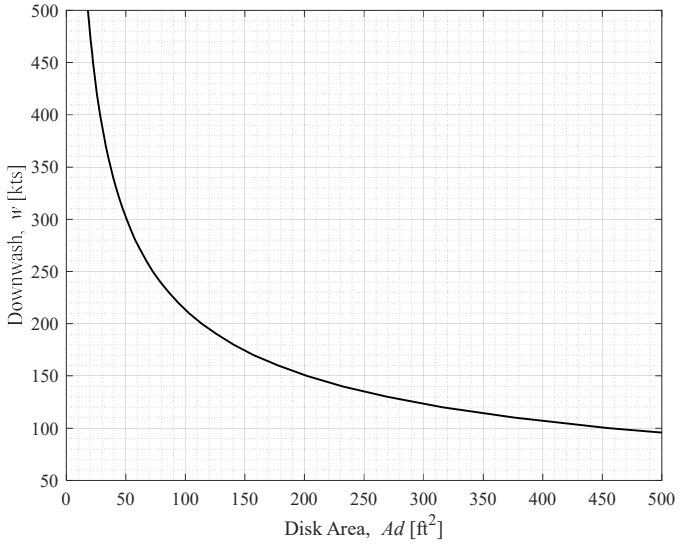

Figure 3.41 Downwash measured at the far vena contraca of the lift-fan wake for an example FIW aircraft with an initial hover weight of 10,000 lb.

Moreover, Figure 3.42 shows how hover downwash varies for different initial hover weights ranging from 0 to 100,000 lb.

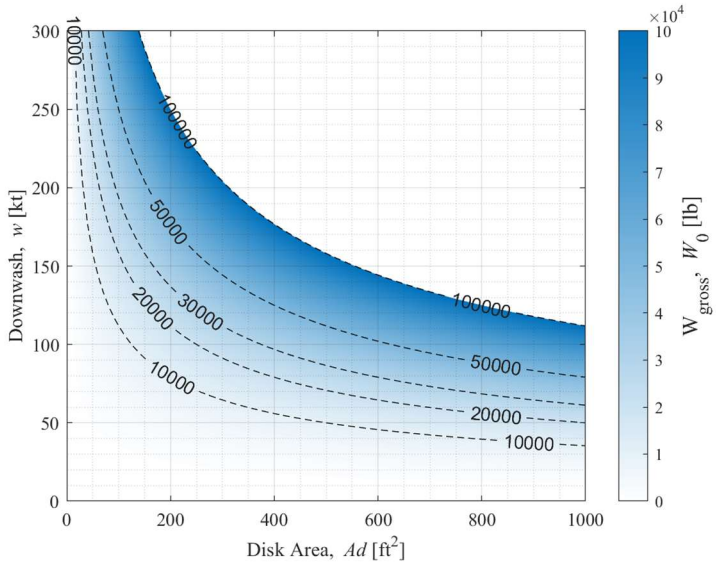

Figure 3.42 Downwash measured at the far vena contracta of the lift-fan wake for an example FIW aircraft of various initial hover weights, using the assumptions from Figure 3.41.

In Figure 3.41 and Figure 3.42, it appears that for a given initial hover weight, there is no singular value of disk area that yields the minimum downwash, just as observed with the required hover power. Due to *w* being inversely proportional to the square of *Ad*, the hover downwash will always decrease with increasing disk area, which supports the conclusion that more rotor area yields a more power-efficient hover performance.

3.5. Total & Excess Power Required

To wrap up the conceptual performance considerations for the FIW concept, one final chart shall prove valuable in the final assessment of the *Ad/S* design space using power required. Since the high-speed cruise and stationary hover mission requirements generally set the maximum power requirements for a VTOL aircraft, it is possible to determine the power limitations of a FIW concept using power to cruise as a function of wing area, power to hover as a function of disk area, and the maximum power available determined by the designer's choice of core powerplant.

Recall the graphical representations of Equations 3.24 and 3.48 illustrated using the previous example values:

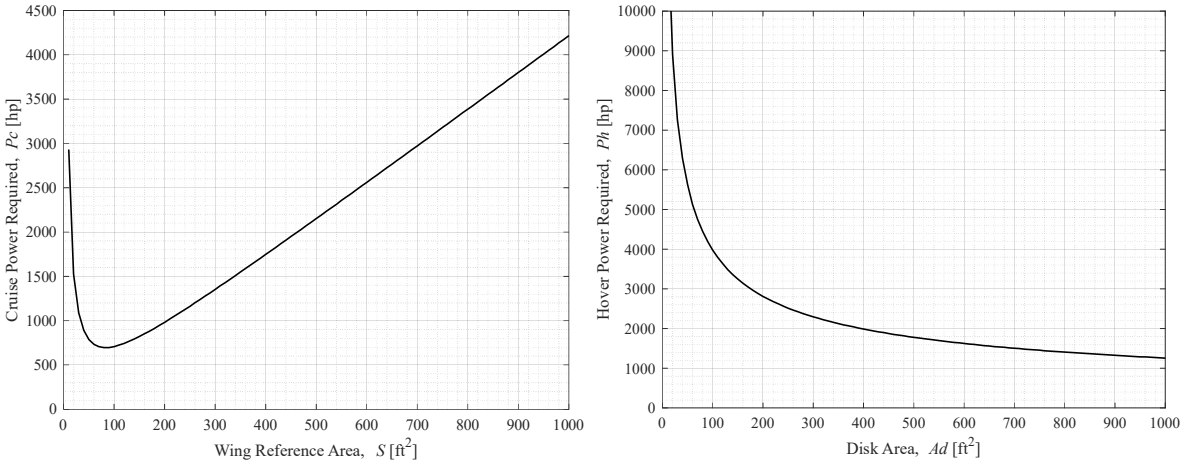

Figure 3.43 Cruise and hover required from the example FIW aircraft represented by Figure 3.27 and Figure 3.37.

On the left of Figure 3.43 is P_c as a function of S, and on the right is P_h as a function of Ad. If a new expression, P_c/P_h, is formed by dividing Equation 3.24 by Equation 3.48 (the left graph divided by the right), the relationship between cruise and hover power required can now be realized as a function of the FIW design parameter Ad/S. Figure 3.44 depicts the cruise-to-hover power ratio of the example aircraft from Figure 3.43 with S and Ad correlated on the x-axis, along with contours showing how the power ratio changes with different values of Ad/S. Note that the exact same relationships shown in Figure 3.44 could equally be shown by plotting P_h/P_c and placing Ad on the primary axis over S. However, since the disk area must be less than or equal to the specified wing area, the power ratio P_c/P_h vs. S has been adopted so that all disk area axes scale within the primary wing reference area axis.

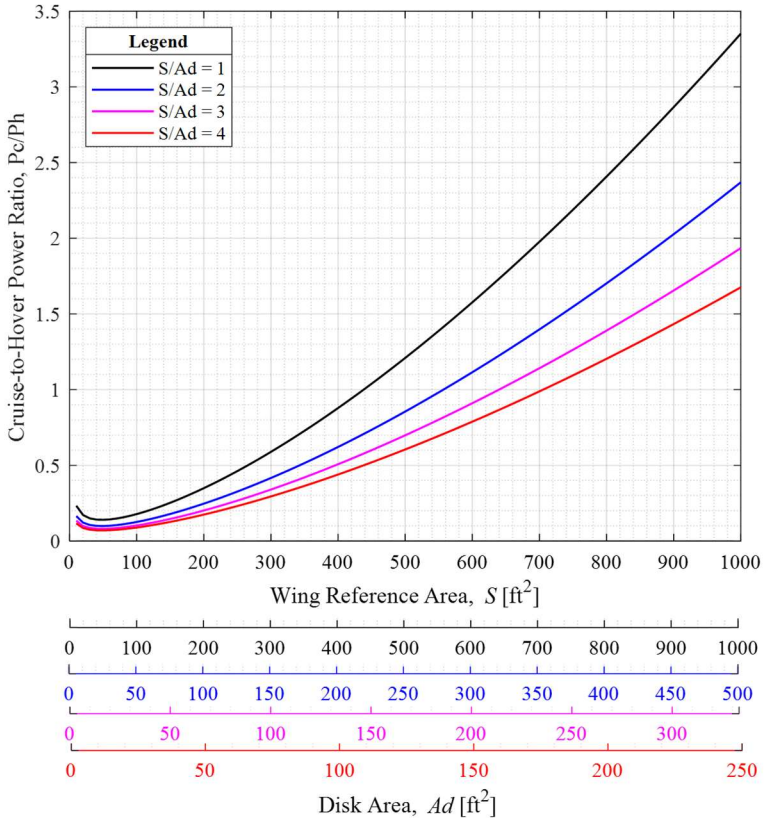

Figure 3.44 Cruise-to-hover power ratio of the example FIW concept with respect to changes in the lift-fan disk area and wing reference area.

Furthermore, if a maximum continuous value for power available (P_a) is known and assumed unchanged between hover and cruise conditions, two more Power Ratios (PR) can be introduced, namely P_a/P_c and P_a/P_h. These available power ratios are of critical importance because they translate to the ratio of power available to power required. When $P_a/P_h > 1$, for instance, it means the aircraft has more power available than what it requires to hover, implying the aircraft has *excess* power. On the other hand, when $P_a/P_h < 1$, it implies the aircraft requires more power to hover than it has available, and therefore, hover is not possible. This makes the condition in which $P_a/P_h = 1$ an operational minimum power limit for hover. The same is true for the available cruise power ratio, P_a/P_c. Figure 3.45 shows how P_a/P_h and P_a/P_c appear on the same graph as Figure 3.44, except only for an Ad/S equal to 1. The points in which the available power ratios equal 1 have also been marked.

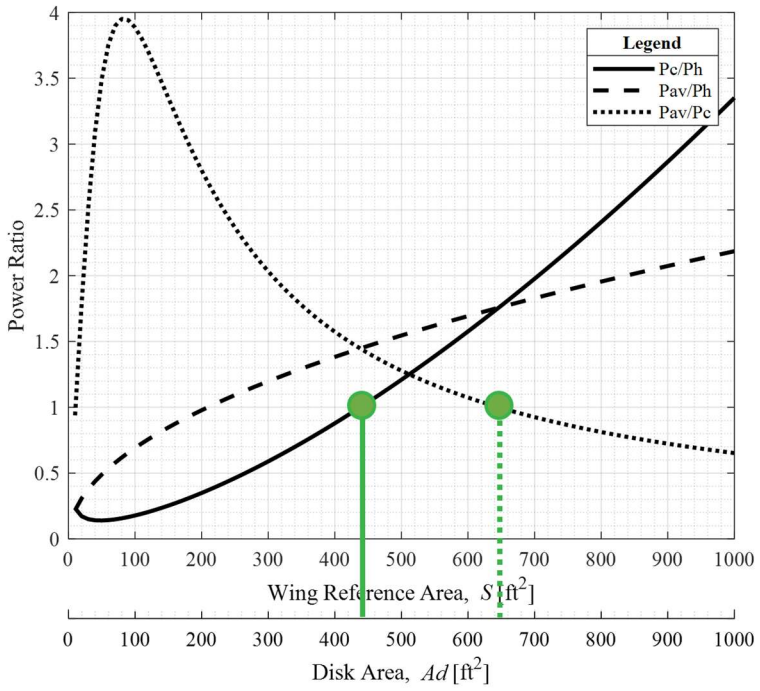

Figure 3.45 Available-to-required cruise and hover power ratios plotted with the cruise-to-hover power ratio for an example FIW aircraft of theoretical $Ad/S = 1$.

When the P_a/P_h and P_a/P_c power ratios are plotted over Figure 3.44 for various Ad/S ratios, a clear trend is observed as Ad/S decreases, as shown in Figure 3.45. With decreasing Ad/S starting from $Ad/S = 1$, it appears the P_a/P_h and P_c/P_h curves bend further to the right, bringing the two points where P_a/P_h and P_a/P_c equal 1 closer together, until at some specific disk-to-wing area ratio, the two coincide. By reducing the Ad/S ratio beyond this point, the P_a/P_h and P_c/P_h curves bend even further right, and consequently, the points where the available power ratios equal 1 cross each other. At the same time, the P_a/P_c curve appears unchanged, but this is simply due to the fact that the wing area axis remains unchanged across the four plots of Figure 3.46.

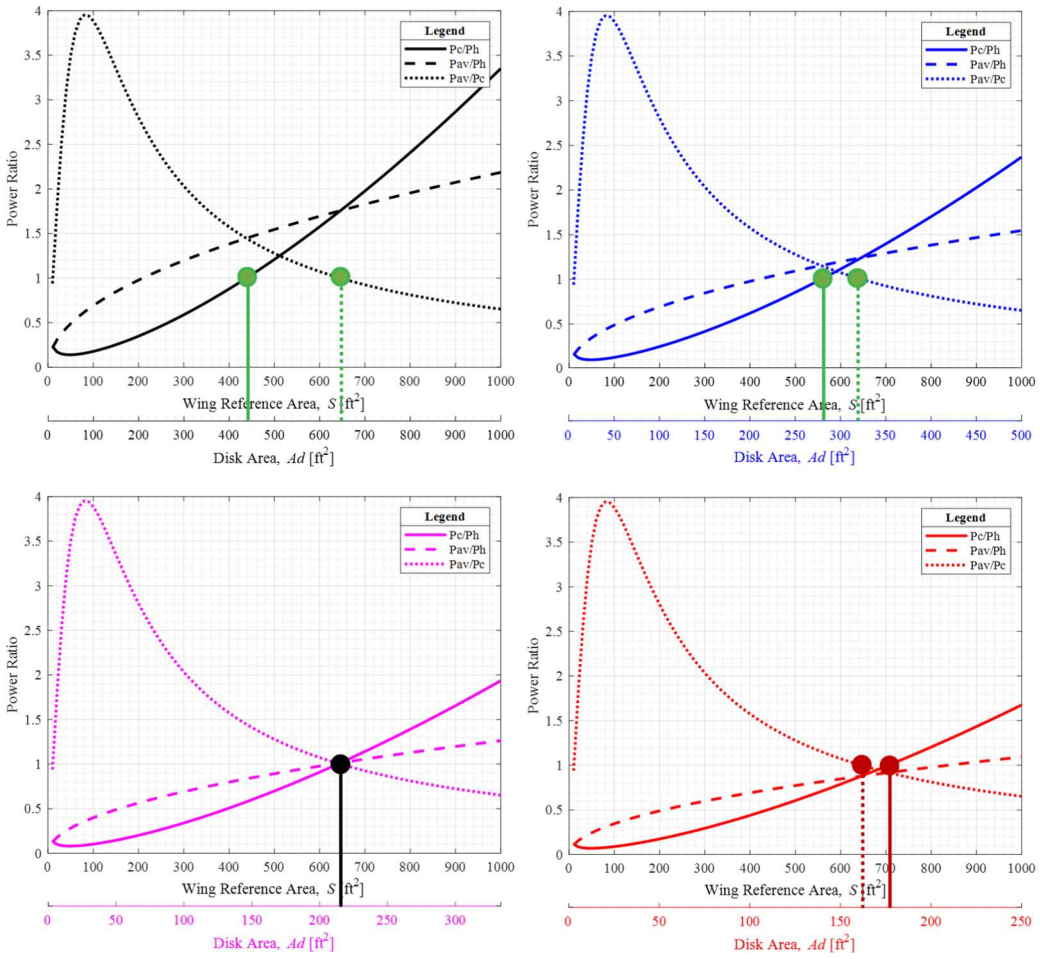

Figure 3.46 Changes to the power ratio curves and possible disk and wing area sizing ranges with diminishing Ad/S.

One may notice in Figure 3.46 that while all x-values associated with each graph represent the same *Ad/S*, they each individually refer to a wing area of different size, and therefore a different corresponding disk area. By tracing the x-values associated with the unity points (where P_a/P_h = 1 and P_a/P_c = 1), Figure 3.46 shows the available range of different *S* and *Ad* values that exist between P_a/P_h = 1 and P_a/P_c = 1 diminishes with decreasing *Ad/S*, until eventually this range completely closes and overlaps. In simpler terms, these size ranges represent the entire design trade space of possible disk and wing area combinations that satisfy the cruise and hover power requirements for a given *Ad/S* ratio. Thus, according to Figure 3.46 and the example aircraft used, the largest geometric design space exists when *Ad/S* = 1. From there, the design space reduces in size with diminishing *Ad/S* until *Ad/S* ≈ 1/3, where only a single combination of *Ad* and *S* satisfy the minimum cruise and hover power requirements for this FIW design. At all *Ad/S* values below 1/3, either P_a/P_c or P_a/P_h dips below 1 for all possible combinations of disk area and wing area size, meaning there is no longer a solution that satisfies both cruise and hover power requirements.

Figure 3.47 summarizes the main takeaways from Figure 3.46 by presenting a final, more user-friendly form of Figure 3.45 for the conceptual design of the example FIW concept used in making the plots of Figure 3.46. In this reconfigured graph, the cruise-to-hover power ratio P_c/P_h lines for each *Ad/S* have been removed for clarity and the P_a/P_c for all *Ad/S* ratios is given by a single line, since it does not vary with disk area. Notice that between the line for P_a/P_c, a power ratio of 1, and each line for P_a/P_h, a unique disk and wing area sizing region exists. Following the pattern observed in Figure 3.46, these design spaces are capped at the theoretical *Ad/S* limit and get smaller with decreasing *Ad/S* until eventually no solution satisfying both the required cruise and hover power requirements exists.

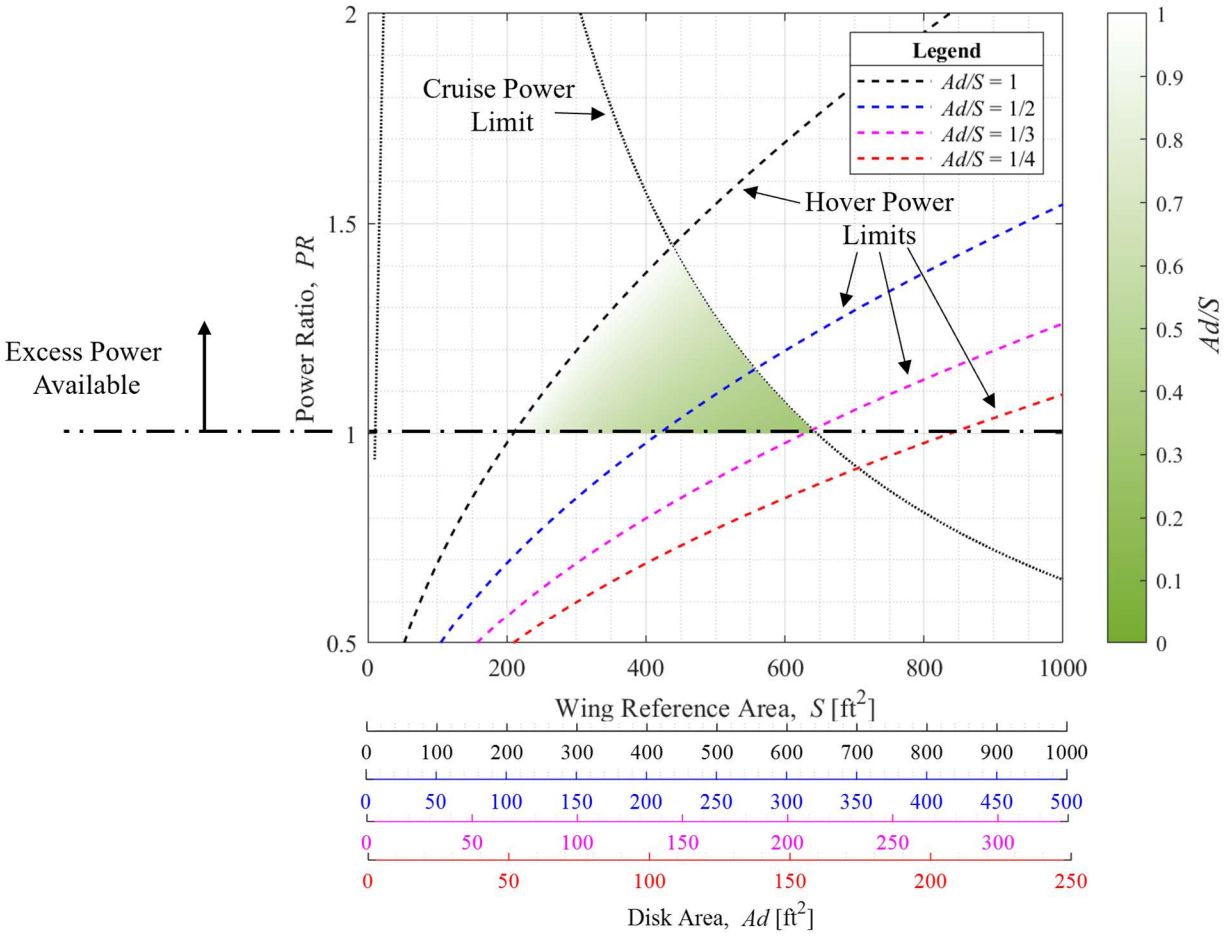

Figure 3.47 Summarized version of Figure 3.46 with annotations describing the various power constraints bounding the available disk and wing area sizing range.

4. Results

As a result of detailing some of the major geometric and performance considerations that uniquely apply to a FIW concept, the conceptual design methods described herein can now be complied to form the basis of a generalized conceptual design methodology for the FIW concept.

4.1. Conceptual Fan-in-Wing Design Methodology

Since FIW aircraft share similar physical attributes, goals, and design challenges with conventional airplanes and helicopters, a generalized design framework for this specific type of aircraft will naturally align its core algorithm with that of all classical aircraft design methodologies. The textbook-defined conceptual aircraft design process [103] suggests that a fresh design always emerges from some combination of mission requirements, performance specifications, and customer requests. The designer is then tasked with taking all factors into consideration and narrowing down the possible design space to just a few most promising aircraft concepts according to some selection criteria. From there, an initial sketch of the "dash-one" is created, and the designer simultaneously begins establishing the aircraft's geometry, powerplant, and overall weight estimates. Once an initial configuration has been thoroughly captured, a series of early performance checks and mission analysis reveal how well the guess configuration does. If any major imbalances in total required thrust, power, or energy are detected, the designer should consider making changes to the design before it proceeds to a refined performance analysis, after which a final configuration can be declared and committed to the preliminary design phase.

The general FIW conceptual design methodology for a single FIW concept follows these exact steps, except the FIW design methodology must also provide guidance on the special considerations necessary to accommodate the lift fans in its wings. These considerations have amounted to the generalized FIW conceptual design methodology presented in Figure 4.1.

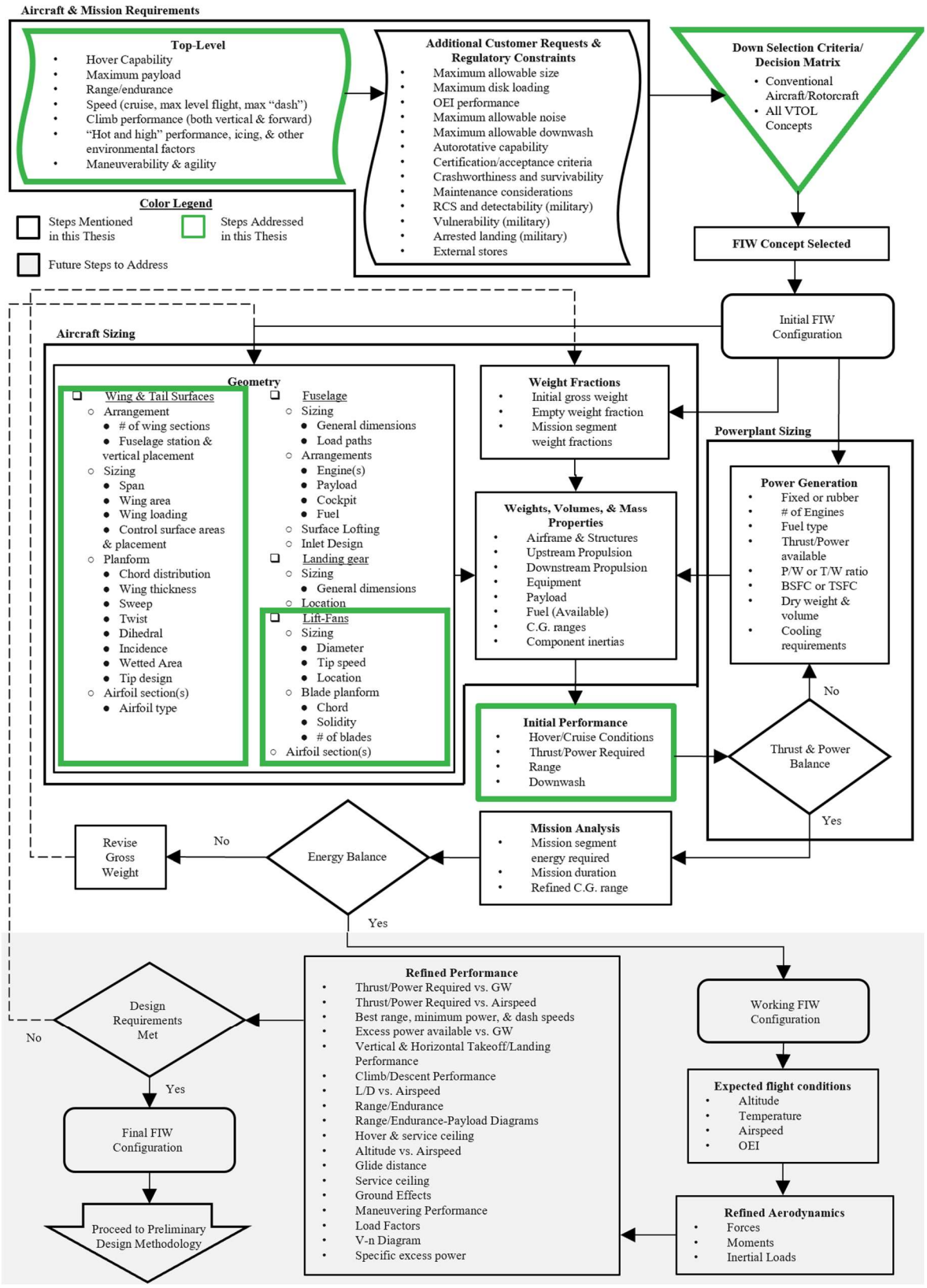

Figure 4.1 Complete generalized FIW conceptual design methodology

Moreover, the methodology surrounding the conceptual FIW design was specifically developed with functionality in mind. This lift-fan specific design process enables designers to estimate the most critical cruise and hover performance metrics of their FIW concept by making simple use of the fundamental *Ad/S* design space and their initial estimates for *Ad* and *S*. Figure 5.2 represents how the plots of Figure 3.15, Figure 3.31, Figure 3.42, and Figure 3.47 can all be tied together to link total avilable power, cruise power required, hover power required, cruise range, and hover downwash using nothing but the aircraft's design hover and cruise conditions, along with the designer's initial estimates of lift fan disk area and wing reference area.

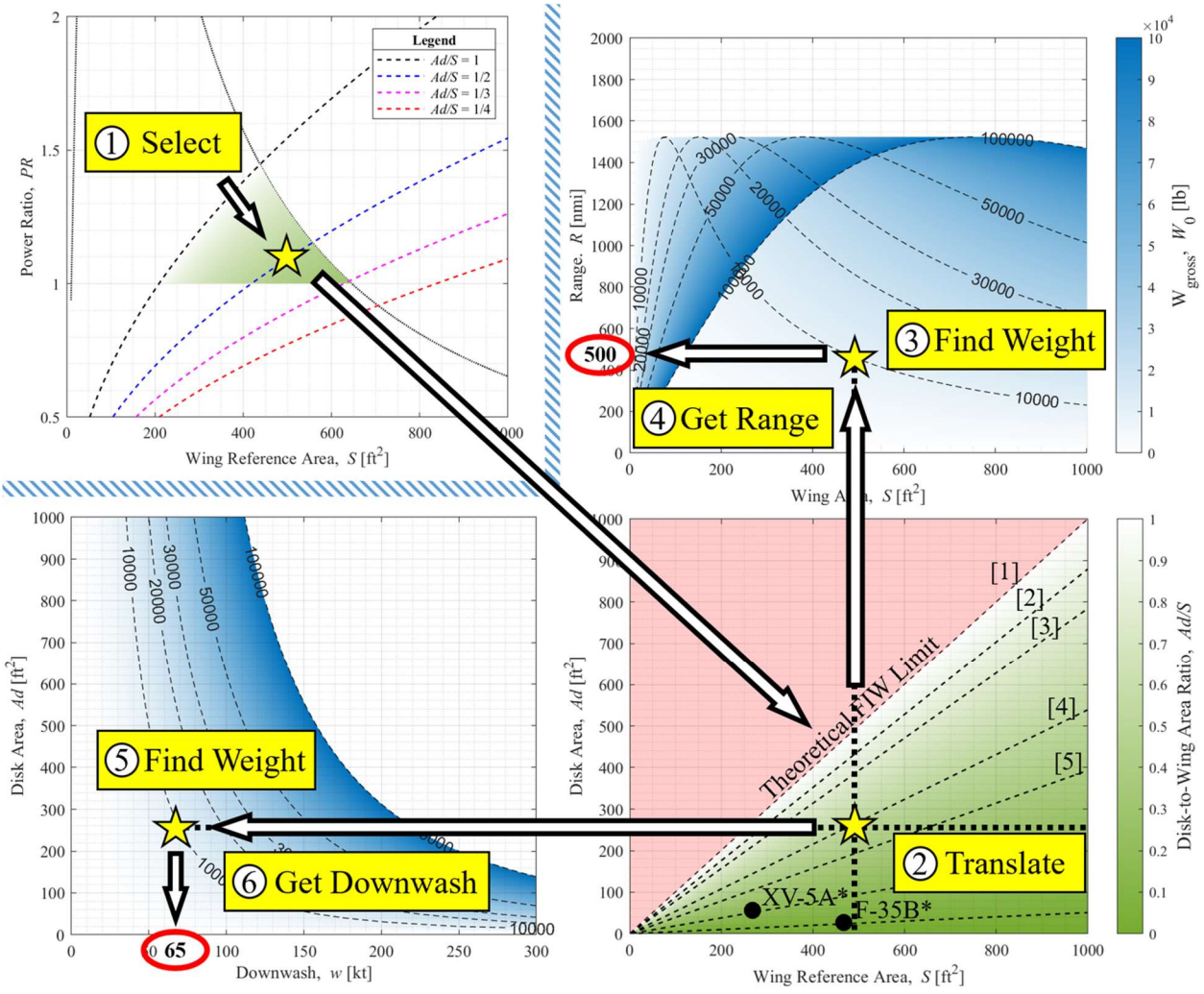

Figure 4.2 General scheme for determining the main cruise and hover performance metrics using the disk-to-wing area relationship for a FIW concept.

To thoroughly illustrate how the geometric and performance derivations from Figure 4.2 may be incorporated into the overall FIW conceptual design process, the following section details an example design study that follows the generalized FIW conceptual design methodology depicted by Figure 4.1.

4.2. Example FIW Design Case and Validation Study

To illustrate how the proposed FIW design methodology may be implemented in real conceptual design work, the example FIW design case presented in this section has been motivated by the rising demand for autonomous HSVTOL military drones. Since the advent of Unmanned Aircraft Systems (UAS), militaries and intelligence agencies around the world have relied on the advanced capabilities of semi-autonomous warfighters to accomplish missions that would otherwise put the pilots and required crew members of manned aircraft in harm's way. As a global reliance on UAS grows and innovations in the fields of autonomy and artificial intelligence continue to redefine modern warfare, the desire for unmanned HSVTOL systems will only further increase in the coming years.

Figure 4.3 further motivates new designs for semi-autonomous HSVTOL aircraft by compiling some of the world's largest and most advanced unmanned aircraft to date [121]. As listed in the legend, the silhouettes in red are aircraft that can achieve speeds greater than or equal to 400 knots, and those capable of vertical flight are shown in blue. Meanwhile, the aircraft capable of both 400 knots and VTOL are filled in purple, and those with neither ability are shown in black. The key takeaway from Figure 4.3 is that although multiple unmanned systems possess the ability to exceed 400 knots or perform VTOL operations, there has yet to be a single large unmanned system that has demonstrated both. With the first high-speed and vertical lift UAS platform still fair game to

any nation, Figure 4.3 reasons why so many of the U.S. initiatives from Table 1.1 are aiming to achieve one first.

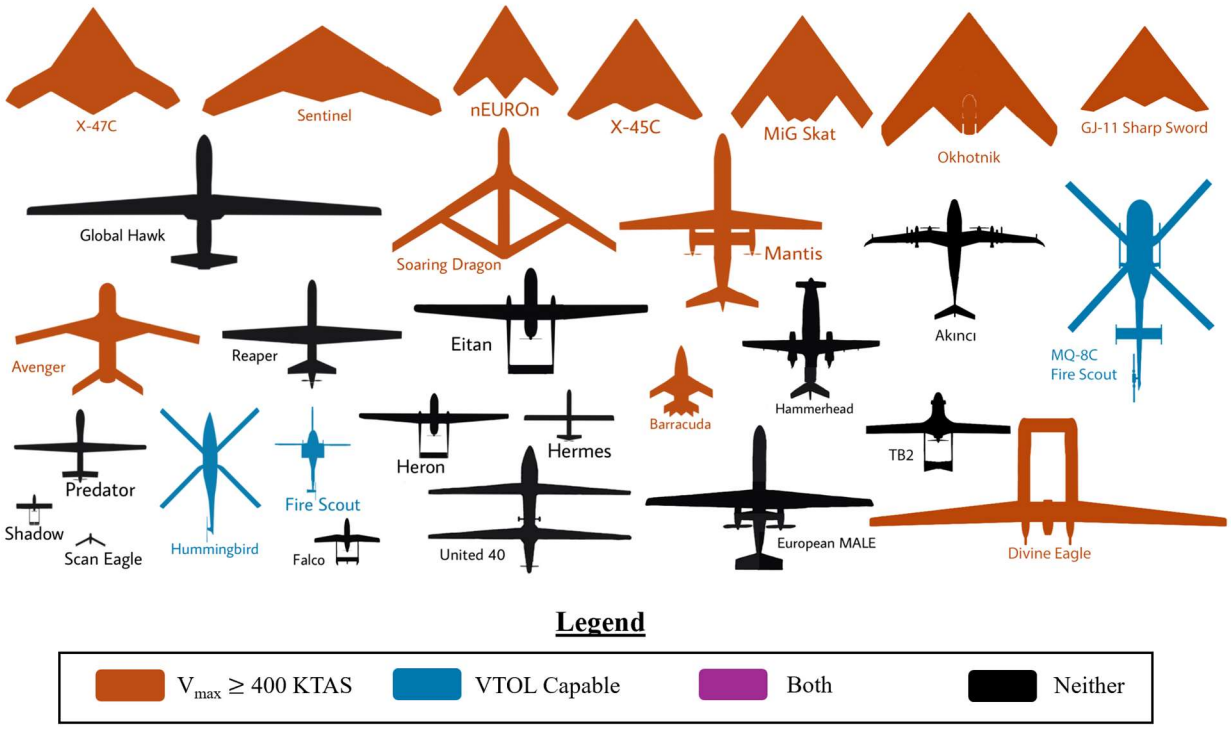

Figure 4.3 Arrangement of the world's largest military drones, categorized as either high-speed capable, VTOL capable, both, or neither, adapted from Saggittarius [121].

Furthermore, the most recent U.S. HSVTOL initiatives have emphasized interest in unmanned systems that are multi-role, scalable, and capable of supporting other mission systems. For instance, the U.S. Air Force just initiated the Collaborative Combat Aircraft (CCA) program in 2022 to develop unmanned aircraft that can work in teams to support manned aircraft operations similar to the loyal wingman concept [122]. A high-speed, semi-autonomous FIW aircraft of this nature could easily support sixth-generation fighters in combat to help increase their survivability or replace current warfighters in high-risk missions while being able to operate in harsh environments with little to no support infrastructure. Thus, the following conceptual FIW design

– given an experimental x-plane project designation "X-EAGLE" as the product of an Embry-Riddle Aeronautical University student – has been proposed to serve the following CCA mission.

Example FIW Design Case for an Unmanned Multi-Role CAA, the "X-EAGLE"

Description:

- HSVTOL Collaborative Combat Aircraft designed to quickly penetrate and evacuate enemy territory upon completing a weapons drop or payload acquisition
- Communicates with both manned aircraft and ground operations teams
- Operable from aircraft carriers, foreign terrain, and destroyed airbases
- Applicable to Search and Destroy, Suppression of Enemy Air Defenses (SEAD), Anti-Submarine Warfare (ASW), and Interdiction missions per MIL-STD-3013

Mission Requirements:

- Payload: 2,000 pounds of armament & electronic warfare equipment
- Cruise speed: 400 knots
- Combat radius: 500 nautical miles
- Acceptable hover downwash: ≤ 108 knots (from Hiller Aircraft Corporation [124])
- Fuel reserves: 10% of mission fuel

Figure 4.4 Image of a notional combat variant XV-5A (left) [125] and Boeing's MQ-25 Stingray aerial refueling drone (right) [126] to illustrate the type of X-EAGLE mission capability desired.

With the top-level aircraft and mission requirements defined, the conceptual design methodology of Figure 4.1 suggests a statistical analysis should be conducted by surveying the existing landscape of aircraft with similar roles to the X-EAGLE to gauge its expected size and performance. However, since Figure 4.3 showed that no unmanned FIW aircraft like the X-EAGLE quite exists, two tables – Table 4.1 and Table 4.2 – have been arranged to satisfy this step in the design process. Table 4.1 lists some existing statistics on large-scale VTOL military drones, and Table 4.2 accounts for large-scale drones with high-speed performance. By considering the aircraft listed in both tables, the "guess" values for initially sizing the X-EAGLE (highlighted in yellow at the bottom of Table 4.2 can be better balanced between its function as both a VTOL and high-speed combat aircraft.

Table 4.1 Statistical database of large-scale, VTOL military drones

Aircraft Name	Gross Takeoff Weight [lb]	Empty Weight [lb]	Max Cruise Speed [kt]	Combat Range [nmi]	Payload (Excluding Fuel) [lb]	Service Ceiling [k ft]	Engine Type	Power [shp]
MQ-8C	6000	3200	140	75	701	20	RR 250-C47B	813
MQ-8B	3150	2073	115	25	600	20	RR 250	420
Eagle Eye	2250	1300	196	400	200	20	PW 207D	641
V-247	29000	16000	300	450	9000	25	NA	5500
A160	6500	2500	140	1125	1000	25	PW207D	550

Table 4.2 Statistical database of large-scale, high-speed military drones

Aircraft Name	Gross Takeoff Weight [lb]	Empty Weight [lb]	Max Cruise Speed [kt]	Combat Range [nmi]	Payload (Excluding Fuel) [lb]	Service Ceiling [k ft]	Engine Type	Thrust [lbf]
Boeing X-45	18000	8000	533	1300	4500	40	Honeywell F124-GA-100	6300
X-47A	5903	3836	533	850	1000	40	PW JT15D-5C	3190

Aircraft Name	Gross Takeoff Weight [lb]	Empty Weight [lb]	Max Cruise Speed [kt]	Combat Range [nmi]	Payload (Excluding Fuel) [lb]	Service Ceiling [k ft]	Engine Type	Thrust [lbf]
X-47B	44500	28837	600	1200	4500	42	PW F100-220U	15000
MQ-25	44500	14000	335	500	16000	39	RR AE 3007N	10000
MQ-20	18200	NA	350	1576	6500	50	PW 545B	3991
EADS Barracuda	7165	5070	562	55	660	20	PW JT15D	3100
XQ-58	6000	2500	476	1500	2300	45	Williams FJ33	2000
Kizilelma-A	18739	NA	590	500	3300	45	I-Progress AI-25TLT	3790
nEUROn	15432	10803	529	NA	1000	45.9	RR Turbomeca Adour	8992
HAL CATS Warrior	4630	NA	600	380	1320	30	(2) HAL HTFE-25	11200
RQ-4	32250	14950	340	6150	3000	60	F137-RR-100	7600
EADS Talarian	22046	7055	340	459	1760	50	NA	NA
WZ-10 Cloud Shadow	7055	5071	334	1080	1900	49	(2) AEF-50E Turbofan	2204
MQ-4C	32250	14945	320	4100	3201	56	RR AE 3007	7000
MiG Skat	10000	NA	432	1075	2000	40	RD-5000B	11340
Initial X-EAGLE Design (“Guess”) Values								
X-EAGLE	9000	5000	400	600	1200	35	(1) Notional Hybrid-Electric Turbofan	4000

Based on the statistical analysis above, target values for the X-EAGLE’s design gross weight, empty weight, cruise speed, combat range, payload, service ceiling, engine type, and maximum static sea-level thrust available have all been arranged. With these figures, the X-EAGLE was sketched as a basis for the initial configuration layout. In this example, the X-EAGLE gathered

inspiration from the XV-5A FIW research aircraft, as well as the unmanned XQ-58A Valkyrie and General Atomics Gambit-1 variant vehicles shown in Figure 4.5. Features used in the X-EAGLE that came from these designs include an engine inlet duct above the fuselage, a V-tail empennage, and lift-fans placed close to the center of the aircraft.

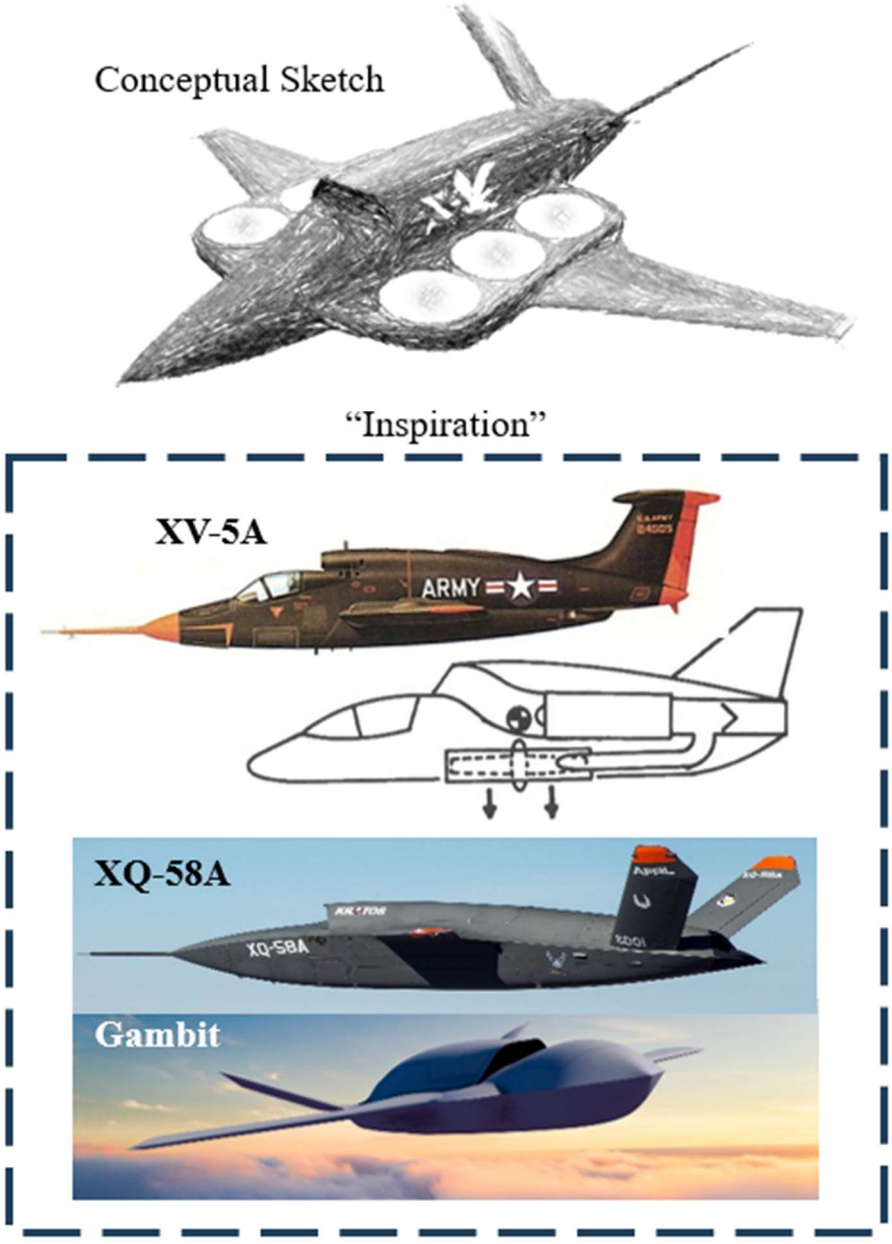

Figure 4.5 Initial conceptual sketch of the X-EAGLE (top) and the aircraft that inspired its design (bottom) [127], [103], [128], and [129].

The initial configuration sketched in Figure 4.5 suggests that the X-EAGLE concept initially featured six fans inside an irregular square-shaped wing planform. However, the number and size of fans shown in Figure 4.5 was purely a guess, because the lift-fan parameters will not be known until the designer has selected a wing planform shape and assigned it a relative aspect ratio. However, the designer can (and should) decide the initial wing planform shape at this stage of the conceptual design process.

In this example, the X-EAGLE's wing planform was divided into three separate areas: an inner, rectangular-shaped area surrounding the fuselage dedicated to sizing the lift-fans, and two outer sections deemed off-limits to lift-fan placement. In general, such wing area segmentation is not required, but in this case, it was included to demonstrate how one may do so in order to keep certain parts of the wing "clean" from fan cutout sections. A top view of the X-EAGLE's wing planform shape and a centerline cross-section view below show the approximate proportions and positions of various external and internal aircraft components.

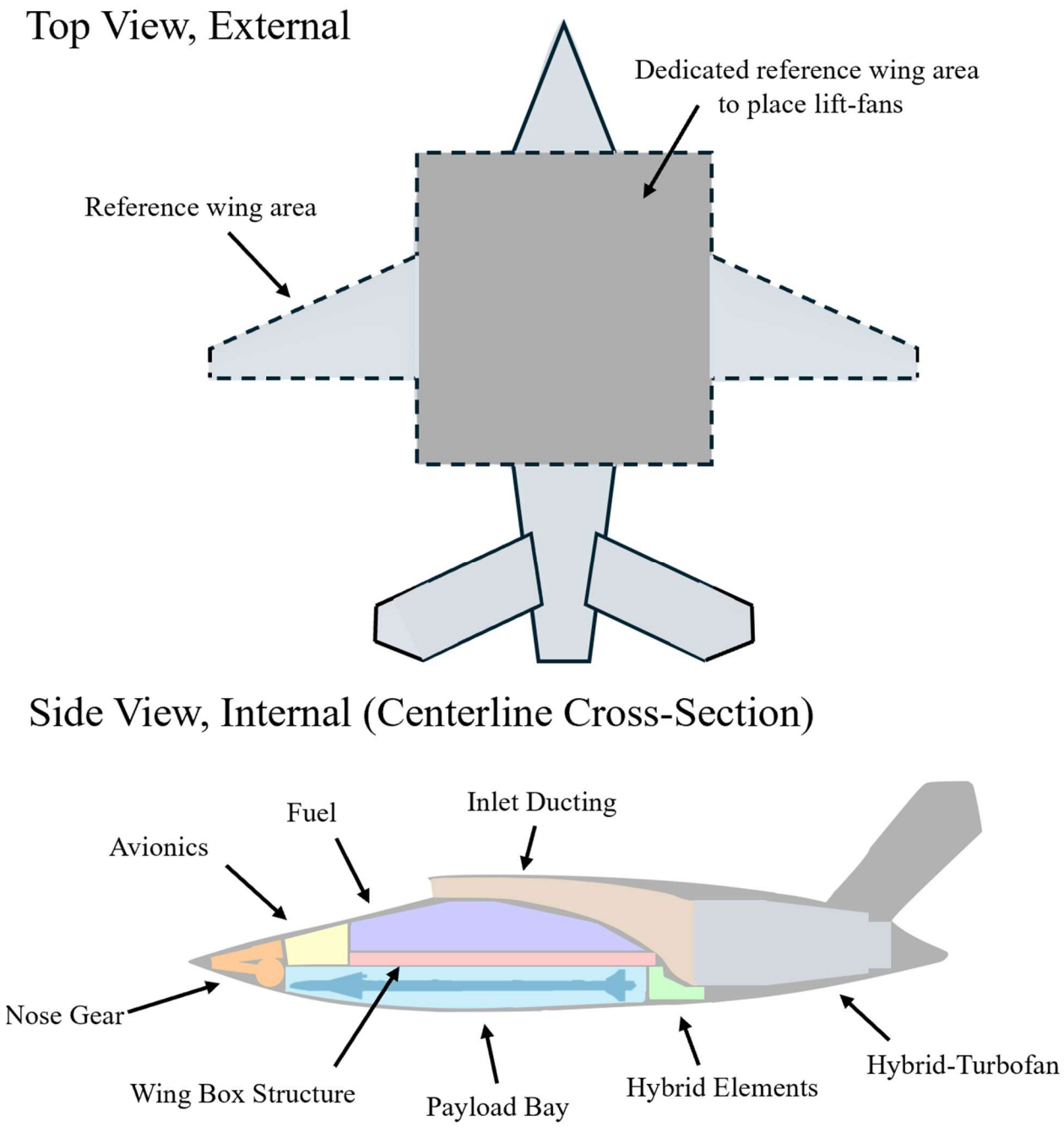

Figure 4.6 Initial configuration layout of the X-EAGLE, showing a top view of the wing planform area (top) and centerline cross-section view showing estimates of various internal aircraft components (bottom).

With the wing planform selected, the X-EAGLE was now ready for sizing its lift fans. Because a specific section of the X-EAGLE's total wing planform was sectioned off for lift-fan sizing, the

first step of the LF sizing process was to establish the lift-fan planform aspect ratio. (Recall that the purpose of giving the wing planform an initial shape and *AR* is to determine the maximum theoretical *Ad* for a single or twin-fan configuration.) For the X-EAGLE, it was determined that its inner, rectangular planform area would arbitrarily have an aspect ratio of 0.48.

The next step was to establish the limiters responsible for reducing the X-EAGLE's maximum theoretical disk area to a more realistic size. To accommodate the wing area cutout by the fuselage, the first limiter L_1 was roughly estimated to be 0.3. and a second limiter of 0.1 was assumed to account for a buffer zone around the lift-fan area. However, a third limiter accounting for area lost to the wing control surfaces was not needed in this example, because the X-EAGLE was assumed to have enough outboard wing area outside the lift-fan sizing zone available for sizing its required ailerons. This was one advantage of having a specific portion of the wing planform isolated from the lift-fan sizing area.

Lastly, once all limiters were determined, the remaining area was used to calculate the remaining space available for additional fans. Based on the rectangular wing planform *AR* and limiter values of the X-EAGLE selected, it was determined that the initial configuration could enclose three lift fans per side, equating to six lift fans total and a final Ad/S_{max} of 0.449. Although this result aligns with the guess configuration shown in Figure 4.5, it only does so in this example by pure coincidence. Figure 4.7 summarizes the lift-fan sizing steps just described with an illustrative step-by-step visual of the X-EAGLE. Similar to Figure 3.20, Figure 4.7 only shows the half-span top view of the aircraft to save space. Additionally, Figure 4.8 shows the same steps graphically as the maximum *Ad/S* changes with respect to the choices made for wing planform *AR*, limiters, and total number of lift-fans.

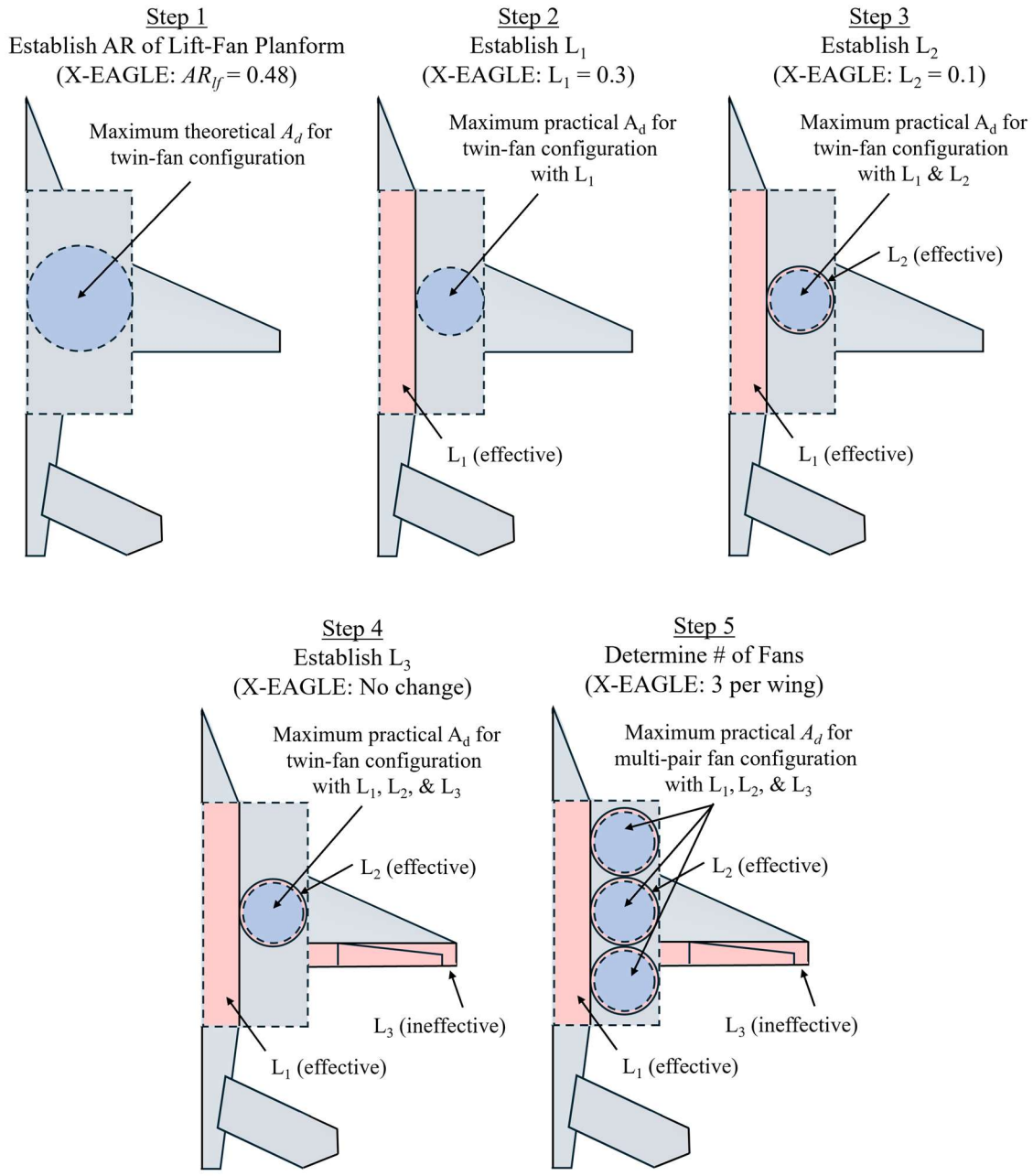

Figure 4.7 FIW planform sizing steps (visual).

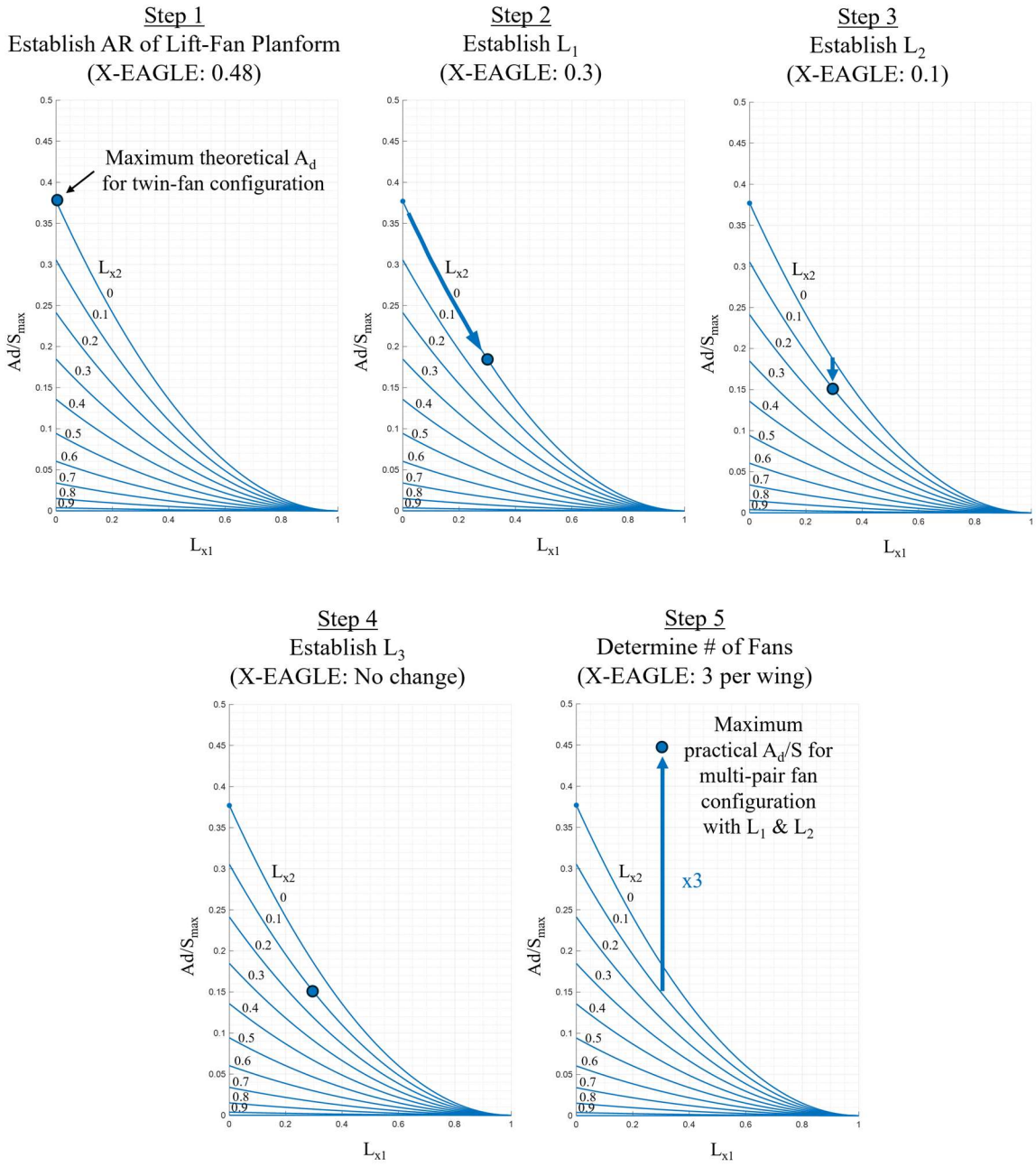

Figure 4.8 FIW planform sizing steps (graphical).

With the wing geometry relatively defined, the next step in the X-EAGLE's conceptual design was to select its powerplant. In this example, a notional parallel hybrid-electric turbofan propulsion system was selected as the top contender for powering the X-EAGLE. While fairly novel in

concept, a parallel hybrid turbofan powertrain offers substantial benefits to HSVTOL military applications [130]. In the case of the X-EAGLE, a hybrid-electric turbofan could provide both sufficient thrust in forward flight and large amounts of electrical power to its lift fans driven by electric motors in hover. Furthermore, if less than maximum power is required during cruise, the X-EAGLE could use the hybrid-electric turbofan's excess electrical capacity to power other electronic warfare and weapons systems. Table 4.3 lists some preliminary statistics of a notional hybrid-electric turbofan engine for the X-EAGLE aircraft, which were loosely based on the similar thrust class VerdeGo Aero VH-5 hybrid-electric turbofan (shown in Figure 4.9) and the conventional Pratt and Whittney PW545-C medium bypass turbofan [131].

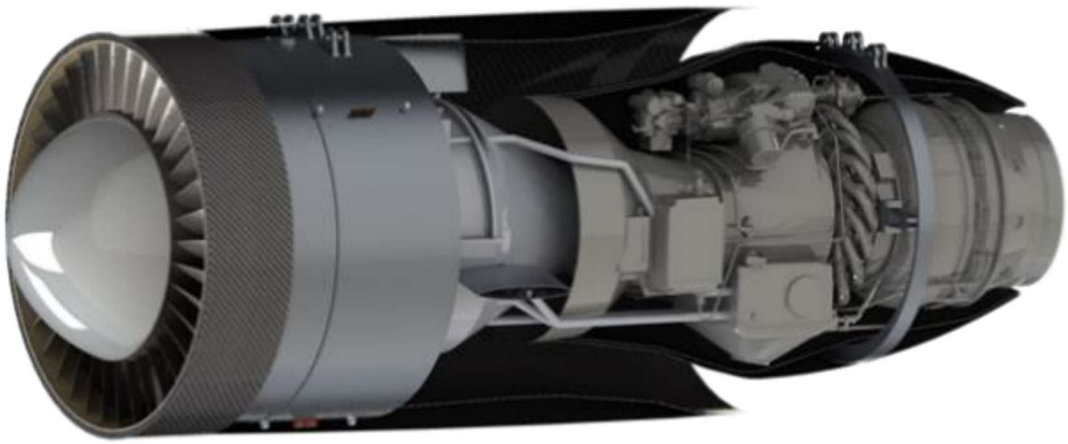

Figure 4.9 The VerdeGo Aero VH-5 hybrid-electric turbofan [132], similar to the notional powertrain envisioned for the X-EAGLE.

Table 4.3 X-EAGLE notional hybrid-electric turbofan preliminary specifications

Engine Specification	Value
Max Continuous Installed Thrust	3,500 lbf
Max Continuous Installed Power	6,650 hp (4.96 MW)
Dry Weight	850 lb
Bypass Ratio	4.12
Overall Pressure Ratio	12.5
Length	5.7 ft
Fan Diameter	2.3 ft

According to Figure 4.1, once the initial aircraft geometry, relative size, and powerplant have been selected, a detailed weights, volume, and mass properties estimate can be made. Table 4.4 compares the initially anticipated weight breakdown of the X-EAGLE with data extrapolated from [110-112] on the XV-5A. In this study, the XV-5A served as the validation case to verify the estimates for the X-EAGLE were within reason.

Table 4.4 Weight breakdown of the X-EAGLE in comparison to the XV-5A

Weight Breakdowns [lb]	**XV-5A**	**X-EAGLE**
Structures		
Forward Fuselage	713	425
Tail & Aft Fuselage	742	250
Landing Gear	482	300
Wing	1003	600
Propulsion		
Engines	975	850
Lift-Fan System	2730	1700
Equipment		
Controls	139	170
Electrical	339	210
Hydraulics	365	245
Avionics & Instrumentation	390	500
Furnishings	110	0
Miscellaneous	75	50
Useful Load		
Crew	400	0
Payload	507	2000
Trapped Fuel	60	60
Reserve Fuel	373	120
Mission Fuel	2817	1020
Maximum Fuel	3250	1200
Totals		
Total Empty Weight	8063	5300
Total Zero-Fuel Weight	8970	7300
Maximum Gross Takeoff Weight	12200	9000

Finally, the initial cruise and hover requirements of the XV-5A were determined and satisfied using the performance evaluation methodology proposed in Figure 4.2. In the X-EAGLE example, the first step of this process involved selecting the power ratio and wing reference area from the

top left chart generated in Figure 4.10. Recall that this design choice of *PR* and *S* must fall within the acceptable bounds of the excess power boundary and along the line corresponding to the disk-to-wing area ratio determined from the lift-fan sizing procedure of Figure 4.7. For clarity, the X-EAGLE design space has been represented in the plots of Figure 4.10 using black lines, the cut off boundaries are represented using thicker vertical lines, and the stars represent the X-EAGLE's selected design points. In this example, the final *PR* and *Ad* values of 1.32 and 222.7 ft^2 were chosen.

With the wing reference area selected, the designer then traces down the wing reference area to the bottom right chart in Figure 4.10 to determine the lift-fan disk area. Recall this chart shows the standard disk area vs. wing reference area design envelope, illustrating where a general FIW design may lie with respect to the maximum theoretical *Ad/S* limit of 1. Because this chart defines the viable wing planform design space for all FIW concepts, it can be universally used for any FIW design and is not specific to the X-EAGLE. Only the region marked by the black line segments in Figure 4.10 will change with individual designs. In the bottom right chart of Figure 4.10, the lift-fan disk area was found to be 100 ft^2 by tracking the intersection of the available design space (solid black line) and the *S* value of 222.7 ft^2.

From there, the total cruise range was found by tracing the starred point from the bottom left chart in Figure 4.10 up to the top right chart where the selected S value intersects the equation for range as a function of wing reference area at the design gross weight of 9,000 pounds. According to Figure 4.10, this resulted in a total available range of 1,144 nautical miles. Similarly, the total hover downwash was found by tracing the starred point from the bottom left chart in Figure 4.10 over to the bottom left chart where the selected *Ad* value intersects the equation for downwash as

a function of disk area at the same design gross weight. Consequently, the minimum total hover downwash was determined to be 106 knots.

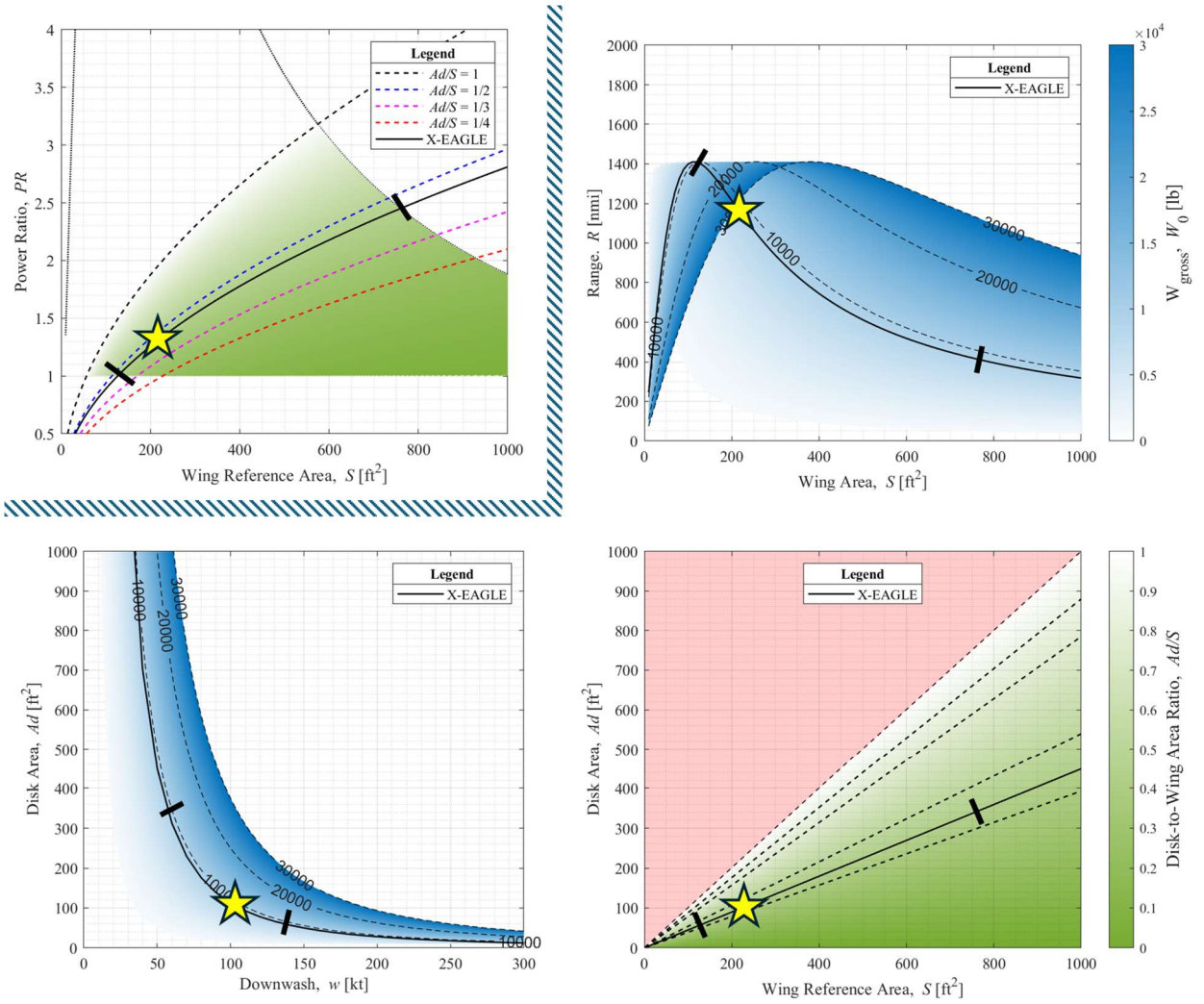

Figure 4.10 Wing planform sizing methodology used to determine the X-EAGLE's anticipated cruise range and hover downwash based on selected *PR* and *Ad/S* values.

To validate this quick cruise and hover performance estimation method, a validation case was conducted using the readily available gross weight, geometry, and available power levels of the XV-5A. Figure 4.11 shows the same methods described by Figure 4.10 used to verify the expected performance of the XV-5A.

The final results summarizing the X-EAGLE's ability to meet the HSVTOL CAA aircraft and design mission requirements are shown in Table 4.5, while results on the success of the performance validation case for the XV-5A are given by the percent error values reported in Table 4.6.

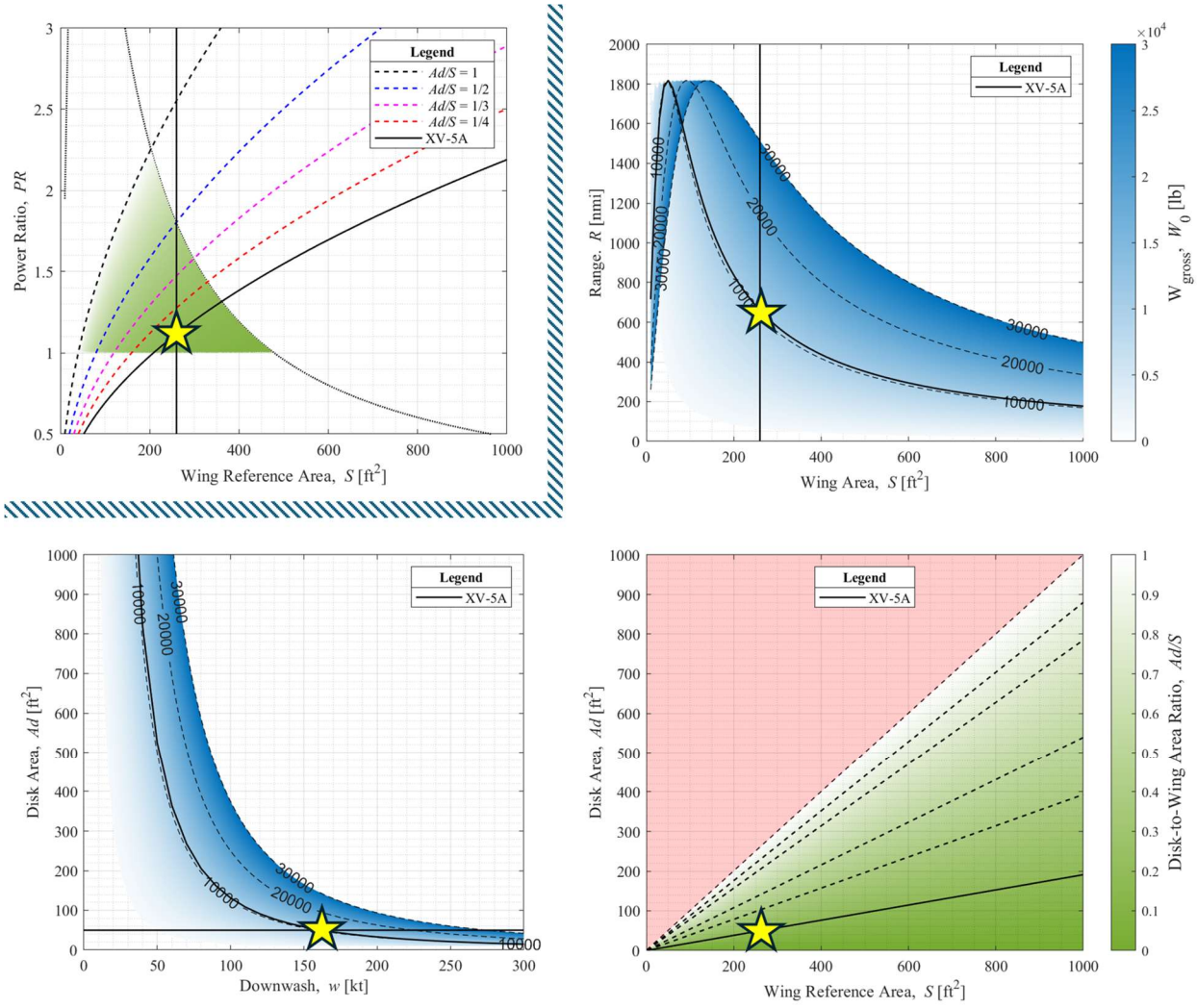

Figure 4.11 Wing planform sizing methodology for performance prediction of the XV-5A research FIW aircraft.

Table 4.5 X-EAGLE required performance evaluation.

	Requirement	X-EAGLE	Requirement Met?
Cruise Speed	≥ 400	400	Yes
Cruise Range (Total)	≥ 1000 nmi	1144 nmi	Yes
Hover Downwash	≤ 108 kt	106 kt	Yes (Conditionally)
Reserve Fuel	≥ 10%	10%	Yes
Payload	≥ 2000 lb	2000 lb	Yes

Table 4.6 XV-5A performance validation.

Validation Case Results	XV-5A Flight Test	XV-5A Estimated	Percent Error
Cruise Range (Sw/S const)	406 nmi	660 nmi	62.6%
Cruise Range (Sw/S var)		439 nmi	8.1%
Average Hover Downwash Velocity	150 kt	160 kt	6.7%
Hover Power Required	7500 hp	8930 hp	19.1%

5. Discussions, Conclusions, and Recommendations

This section summarizes the main finding from this research effort and describes the future work needed to improve on the proposed conceptual FIW design methodology.

5.1. Discussion of Main Results and Conclusions

The main objective of this research was to generalize a conceptual design methodology that adequately describes the conceptual design process of a FIW VTOL aircraft, which an extensive literature review suggests has not been explicitly formulated until now, despite the FIW concept having (1) circulated in the public domain for years, (2) unique design characteristics in need of further detail, and (3) a recent rise in popularity among aircraft designers. By compiling a wide range of relevant geometric relations, classical aircraft design principles, and empirical data used to develop foundational FIW design theory and practical sizing approximations, a generalized conceptual design methodology was procured in the form of Figure 4.1. This conceptual design algorithm was established modeling the core structure of the conventional aircraft design process, yet it incorporates a unique set of design constraints pertaining only to the FIW aircraft.

As a primer to a much larger and in-depth study needed to fully mature the lift-fan design methodology, this work investigated some of the major conceptual design requirements, sizing considerations, and performance metrics applicable to the FIW concept and articulated them in concise terms of lift-fan disk area and wing reference area. Defining the associated equations and FIW design space in this way should prove to be useful to any FIW designer who wishes to iterate quickly on major cruise and performance metrics, as was demonstrated with an example FIW design study and proved successful in scaling the X-EAGLE meet a specified set of FIW design criteria.

It is important to note that in the interest of keeping the discussion in the results section brief, there were several key aspects of the conceptual FIW wing planform sizing and performance

estimation process improperly conveyed or addressed in the results section. The greatest of these items was that while this conceptual FIW design methodology has been developed to streamline the conceptual FIW design process and accelerate the time required to converge on a satisfactory FIW configuration, the quick results presented herein should not downplay the fact that conceptual design work is still a laborious and time-consuming task.

In the X-EAGLE conceptual FIW design example, the initial sketch's surprising resemblance of the final, satisfactory design configuration shown in Figure 5.1 was merely coincidental. In general, most final FIW designs using the proposed conceptual design methodology of Figure 4.1 can expect greater differences in appearance from their initial sketches. This can be due to a number of changes in the wing planform design parameters – such as space for sizing the lift fans, planform shape, aspect ratio, limiters, lift-fan placement, and number of lift fans – that will likely be required to satisfy the aircraft and mission design requirements. These changes must also be incorporated in the performance evaluation stage, resulting in multiple iterations of the charts shown in Figure 4.10 required to find where the star conditions satisfy all design requirements and produce a convergent solution.

Similarly, the FIW designer will be responsible for using the equations presented in the methodology section of this work to produce the charts shown in Figure 4.2. This task was not included in the example conceptual design process for the X-EAGLE but should also be budgeted into a real FIW conceptual design timeline accordingly. Fortunately, the iterations required to update the plots of Figure 4.2 with each design iteration can be quickly arranged by coding the FIW design algorithm using modern computing software like MATLAB.

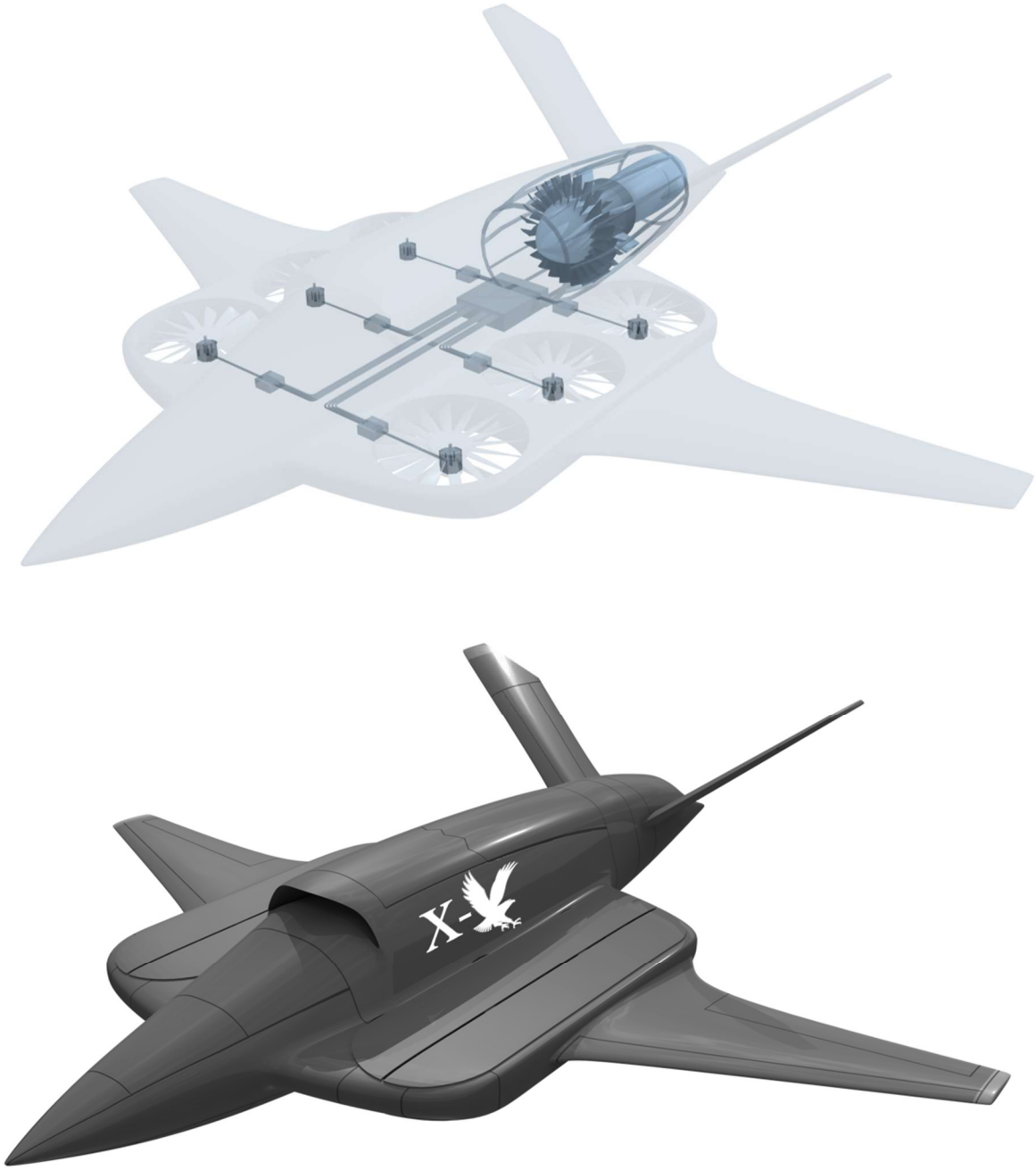

Figure 5.1 3D view of the final, satisfactory X-EAGLE conceptual FIW design. Image credits to VerdeGo Aero.

5.2. Limitations

The general conceptual design methodology summarized by Figure 4.1 should serve FIW designers well as a starting point in their own conceptual design efforts. However, this flowchart must not be mistaken for a complete description of the FIW conceptual design process. The design considerations presented in this work were significantly restricted to the geometric and performance implications of the FIW concept, which, in general, were derived using broad assumptions and left many facets of the FIW design unexplored.

This was in part due to the large breadth of detail conceptual design entails, which simply cannot be constrained to a single thesis. According to Raymer [103], even college textbooks struggle to convey the full conceptual aircraft design process using hundreds of pages of text. Another limitation to this work was the difficulty involved in extracting relevant information from the lift-fan technology studies of the late 20th century. Although many technical documents sharing experimental wind tunnel data on lift-fan models and flight test data from the XV-5A program exist, a large portion of these original documents published by NASA and the U.S. Army have been poorly scanned and recopied, rendering many of their figures and plots illegible. It is believed that a significant contribution to the discrepancies reported in the validation results of Table 4.6 were due to a lack of confirmation on the XV-5A performance figures assumed.

Moreover, the vast majority of technical information on past lift-fan demonstrators has been either completely lost or proprietarily protected. Hence, in addition to there being relatively few lift-fan concepts to have ever successfully flown, the limited availability and useability of existing data was an even greater hindrance to the fidelity of this study. Nonetheless, these limitations in the present work leave ample room for improvement and expansion in the current state of conceptual FIW design.

5.3. Recommendations for Future Work

VTOL designers of the future would certainly benefit from additional efforts to expand upon the presently proposed FIW conceptual design methodolgy. This implies further investigating the various aerodynamic, structural, and control constraints impacting the FIW concept in order to capture a more comprehensive and accurate representation of the available design trade space. While not an exhaustive list, the following subjects make up the most critical topics in need of further research and guidance regarding their specific implications on the conceptual design of a FIW aircraft concept.

Aerodynamics

The complex aerodynamic interactions between lift-fans and surrounding structures is currently a large research field with much room to improve the current methods for evaluating and quantifying FIW performance. To optimize a FIW design for high-speed flight, future work to include transonic and wave drag effects in the cruise performance drag analysis should be considered. In addition to the lift-fan sizing and placement parameters discussed in this work, it would be beneficial to see more discussion on fan solidity, blade planform optimization, rotor scaling limits, fan stacking criteria, and resulting performance reductions from various lift-fan failure modes. Similarly, implications of noise, comfort, and safety to FIW passengers, crew, and ground personnel should be given more consideration as these factors will have a large influence on public perception and acceptability of future FIW concepts.

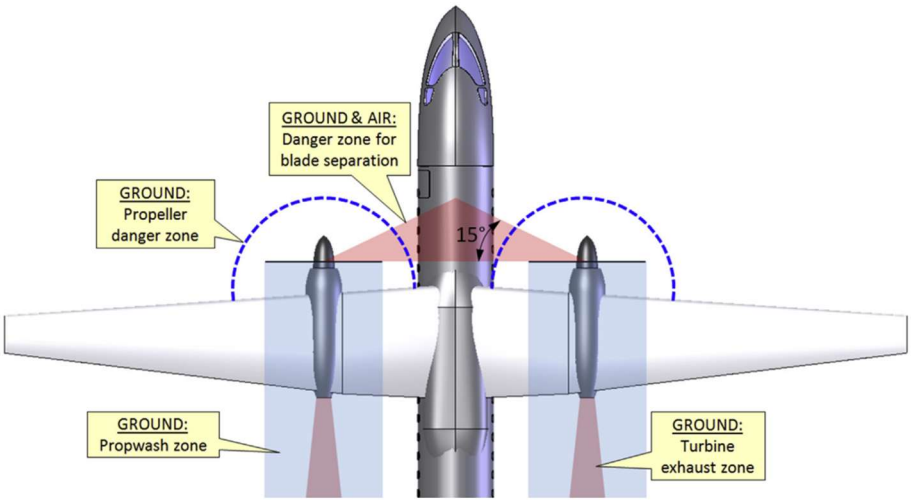

FIGURE 7-15 Danger zones around a typical turboprop.

Figure 5.2 Danger zones for a turboprop aircraft illustrated by [136], which should also be generalized for the FIW concept.

Structures

The principal design conflict with a lift-fan concept is that its fans must be buried in some part of the aircraft structure. As [29] points out, fans embedded in a wing will require a suitable airfoil thickness, and if a short chord is used, the thickness ratio may be too high. In contrast, increasing chord length to reduce the thickness ratio will result in a lower overall aspect ratio. To achieve higher *AR* designs for improved subsonic cruise range without compromising high-speed performance, future work should consider FIW layouts with variable sweep geometry and generalize the expected structural weight impacts. According to [32], the weight penalty for mechanically designing wings to accommodate lift-fans is estimated to be 5% heavier than the weight for a conventional wing. However, this subject was not expanded upon in this research effort. To better understand the structural implications of FIW designs, more research should be published detailing a general FIW weight breakdown and quantifying the representative forces and moments illustrated by Figure 5.3 with shear and moment diagrams.

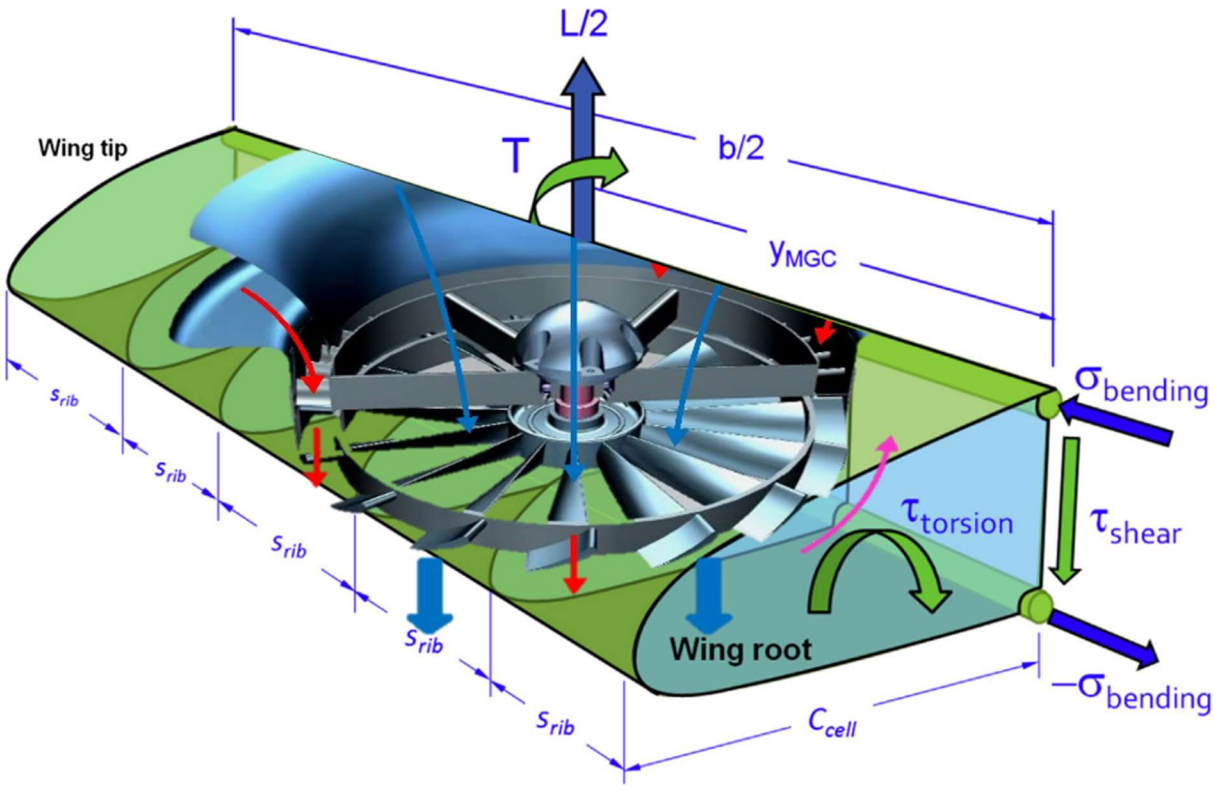

Figure 5.3 Representative illustration of the forces and moments imposed by a wing featuring an embedded lift-fan, adapted from [137] and [138].

Controls

Considerations to ensure static and dynamic stability of FIW configurations were largely neglected in this research effort but would require significant attention in real FIW design efforts. Previous studies have shown that lift-fans exhibit poor stability and handling qualities when placed outboard on the wings for roll control, forward of the aircraft for pitch control, and anywhere near the ground when unsteady ground effects are present [32]. For best management of control and maneuverability in low-speed flight, some studies suggest lift-fans are best located inboard of the wing surface(s) near the aircraft center of gravity and feature additional actuation methods for attitude control, such as the thrust vectoring louvers used on the XV-5A or the roll-control ducts employed by the F-35B. With new control architectures and advanced fly-by-wire systems now

available long after the 1960s-era XV-5A FIW research aircraft, control systems are another FIW field of study with immense potential to be expanded.

Costs, Maintenance, & Development Risks

Finally, no conceptual aircraft design is fully complete without breaking down the costs, maintenance, and development risks associated with its design. The costs of a FIW concept are expected to be greater than conventional aircraft of similar size, but exact figures and projections should be further investigated. According to [139], the F-35B variant's price per unit including depot maintenance, ground support equipment, and spare parts costs was evaluated to be 23% and 16% higher than the CTOL F-35A and F-35C variants, respectively, as of 2021. Additionally, Figure 5.4 from [140] gives an approximate cost breakdown of specific components on the F-35B and its lift-fan system. To provide FIW designers with the most reliable data for compiling project development budgets, future work is required to understand the lifecycle costs and risks of FIW aircraft.

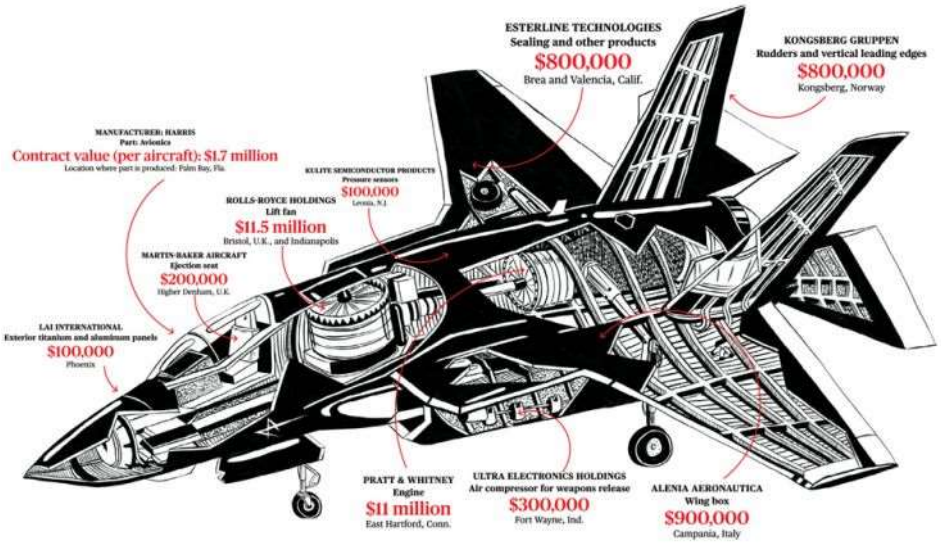

Figure 5.4 Approximate cost breakdown of the F-35B lift-fan aircraft [140].

REFERENCES

[1] Congressional Research Service, "F-35 Joint Strike Fighter (JSF) Program, *CRS Report*, published online May 2022.
https://sgp.fas.org/crs/weapons/RL30563.pdf

[2] Hirshberg, M., "Transitions: From 2011 to 2023 – VFS Behind the Scenes of FVL," *Vertiflight Magazine,* the Vertical Flight Society, Jan.-Feb. 2023.

[3] VFS, "V/STOL Aircraft and Propulsion Concepts," *The Vertical Flight Society*, 2023.
https://vtol.org/vstol/wheel.htm

[4] Nixon, R., *Six Crises*, Doubleday, ISBN: 9780671706197, 1962

[5] VFS, "eVTOL Aircraft Directory," *Electric VTOL News by The Vertical Flight Society*, 2023.
https://evtol.news/aircraft

[6] Aviation Dictionary, "Fan Lift," *Academic Dictionaries and Encyclopedias*, published online 2014.
https://aviation_dictionary.en-academic.com/2689/fan_lift

[7] Mavris, D., Tai, J., Schrage, D., "A Multidisciplinary Design Optimization Approach to Sizing Stopped Rotor Configurations Utilizing Reaction Drive and Circulation Control," *5th Symposium on Multidisciplinary Analysis and Optimization*, Panama City Beach, Florida, Sep. 1994.
https://doi.org/10.2514/6.1994-4296

[8] Lindenbaum, B., Blake, W., "The VZ-9 Avrocar," *Vertiflite-VZ9*, www.vtol.org, published online 2006.

[9] Whittley, D., Garland, D., "Analysis of Tests of the Avrocar in the NASA 40 x 80 ft. Wind Tunnel," *NASA Contractor Report – Avro Aircraft Limited*, No. 271500, Ames Research Center,

[10] Bzuk, "The Avrocar S/N 58-7055 (marked AV-7055) on its rollout," *Wikipedia Commons*, published online Feb. 2012.
https://en.wikipedia.org/wiki/File:Colour_avrocar_59.jpg

[11] Zuk, W., "Avrocar 3-View," *Wikipedia Commons*, published online Feb. 2007.
https://en.m.wikipedia.org/wiki/File:Avrocar_3-view.jpg

[12] Schneider, J., "The Vanguard VTOL Aircraft Concept," *AHS Newsletter*, Oct. 1959.

[13] Quackenbush, T., Keller, J., Whitehouse, G., "Analysis Methods for Advanced V/STOL Configurations," *AHS 72nd Annual Forum*, West Palm Beach, Florida, May 17-19, 2016.

[14] Levy, H., “Vanguard Unveils a Very Unusual VTOL,” *Air Progress Magazine*, Spring Ed., 1960.

[15] Markman, S., Holder, B., “The Vanguard Omniplane: III. Flight Tests and Abandonment,” *Prototypes.com*, published online Aug. 2005. http://xplanes.free.fr/omni/omni-3.html

[16] Kirill, R., “Verticraft Verticar Experimental Aircraft (USA),” *Military Review*, en.topwar.ru, published online Aug. 7, 2017.

[17] S., B., “Tri-Service VTOL Transport proposals (XC-142 competition),” *Secret Projects Forums,* published online Jun. 2020. https://www.secretprojects.co.uk/threads/tri-service-vtol-transport-proposals-xc-142-competition.2591/page-2

[18] RetroMechanix.com, “Verticraft Verticar – Wingless VTOL Transport Aircraft with Airfoil Fuselage, *ARC Forums – Research Corner*, published online Nov. 2011. http://www.arcforums.com/forums/air/index.php?/topic/241151-verticraft-verticar-wingless-vtol-transport-aircraft-with-airfoil-fu/&tab=comments#comment-2295901

[19] Goebel, G., “US VTOL Flat Riser Jets,” *AirVectors*, Vol. 1, published online Jul. 2001. https://www.airvectors.net/avuvto.html

[20] North American Aviation, “Ryan XV-5A Vertifan,” *KerbalX*, published online Jul. 2017. https://kerbalx.com/NorthAmericanAviation/Ryan-XV-5-Vertifan

[21] Bolkcom, C., “Joint Strike Fighter (JSF) Program: Background, Status, and Issues,” *CRS Report for Congress*, published online June 16, 2003. https://apps.dtic.mil/sti/pdfs/ADA472773.pdf

[22] Kukulich, T., Ramsey, J., “Missing Jet: What to Know About the $90M F-35B Missing in SC,” *Post and Courier,* published online Sep. 2023. https://www.postandcourier.com/news/the-f-35b-what-you-should-know-about-the-90m-fighter-jet-that-went-missing/article_04b9781e-5629-11ee-a9a7-d7eb80dee7c7.html

[23] Bender, J., “The F-35B Can’t Carry It’s Most Advanced Weapon Until 2022,” Business Insider – Military & Defense, published online Mar. 2015. https://www.businessinsider.com/the-f-35b-cant-carry-its-most-advanced-weapon-2015-3

[24] Janes, “UrbanAero X-Hawk,” *Jane’s All the World’ Aircraft*, 2007-2008.

[25] Tactical Robotics, “The Cormorant By Tactical Robotics,” *cdn.exiteme.com*, published online Nov .2013. https://cdn.exiteme.com/exitetogo/www.tactical-robotics.com/userfiles/files/CORMORANT-SPCS.pdf

[26] Hirshberg, M., “Project Zero Unveiled,” *Vertiflight Magazine*, May-Jun. 2013.

[27] The Vertical Flight Society, “Leonardo Helicopters Project Zero (defunct),” Electric VTOL News, published online 2018.

[28] General Electric Company, “Analysis and Test Results of Division of Power Between Lift Fan and Jet Nozzle,” *U.S. Army Transportation Research Command*, Fort Eustis, VA, Dec. 1962.

[29] Peterson, J., M., “Lift Fan V/STOL Concept of Future Applications,” *AIAA General Aviation Aircraft Design and Operations Meeting*, Wichita, Kansas, May 25-27, 1964. https://doi.org/10.2514/3.43624

[30] Gerdes, R. M., “Lift-Fan Aircraft - Lessons Learned from the Pilot's Perspective,” *NASA Contractor Report,* 177620, Aug. 1993.

[31] Morgan, W. R., True, H. C., Starkey, H. B., “The Army XV-5A Lift Fan Flight Research Airplane,” *Automotive Engineering Congress*, Detroit, MI, Jan 13-17, 1964.

[32] Clark, D., Smith, E., “Lift Fan Flight Test Experience,” *AIAA Propulsion Joint Specialist Conference*, AIAA Paper No. 65-603, Colorado Springs, CO, Jun. 14-18, 1965.

[33] Pittsburgh Univ., PA. Research Staff, “XV-5A Lift Fan Flight Research Aircraft Interim Report,” *USAAMRDL*, TIR 18.1.3.1, Apr. 1966.

[34] Finnestead, R., Ferrel, K., Welter, W., Anderson, W., “Engineering Flight Research Evaluation of the XV-5A Lift-Fan Aircraft - Part 1 Stability and Control,” *U.S. Army Aviation Test Activity*, Edwards Air Force Base, CA, Aug. 1966.

[35] Ferrel, K., Welter, W., “Engineering Flight Research Evaluation of the XV-5A Lift-Fan Aircraft - Part 2 Performance,” *U.S. Army Aviation Test Activity*, Edwards Air Force Base, CA, Aug. 1967.

[36] Hickey, D., Ellis, D., “Wind-Tunnel Tests of a Semispan Wing with a Fan Rotating in the Plane of the Wing,” *NASA Ames Research Center*, TN D-88, Moffet Field, CA, Oct. 1959.

[37] Przedpelski, Z., “Lift Fans for Advanced VSTOL Aircraft,” *CASI/AIAA Low-Speed Flight Meeting*, AIAA Paper No. 65-708, Montreal, Canada, Oct. 18-19, 1965.

[38] Peterson, J., M., “Tailoring the Lift Fan VSTOL Concept to Mission Requirements,” *National Aeronautic Meeting*, Washington D.C., Apr. 12-15, 1965.

[39] Pickerell, D., Cresswell, R., “Powerplant Aspects of a High-Speed, Inner City VTOL

Aircraft," *CASI/AIAA 10th Anglo-American Aeronautical Conference*, AIAA Paper No. 67-745, Log Angeles, CA, Oct. 18-20, 1967.

[40] Moss, R., "Boulton Paul," *British Aviation - Projects to Production*, uploaded online Aug. 2020.
http://www.britishaviation-ptp.com/b/boulton_paul.html

[41] Drew, "Grumman FAAV," *Secret Project Forums*, published online Jan 2023.
https://www.secretprojects.co.uk/threads/grumman-faav.3986/

[42] Wu, J., McMahon, H., Hubbart, J., "Potential Flow Studies of Lift-Fan Inflow Interference Phenomena," *First Quarterly R&D Status Report*, No. E-16-622, Wright-Patterson AFB, Ohio, Mar. 1972.

[43] Heyson, H., "Theoretical and Experimental Investigation of the Performance of a Fan-in-Wing VTOL Configuration," *NASA Langley Research Center*, TN D-7498, Dec. 1973.

[44] Hicks, R., Henne, P., "Wing Design by Numerical Optimization," *AIAA Aircraft Systems and Technology Conference,* AIAA Paper 77-1247, Seattle, WA, Aug. 22-24, 1978.

[45] Roelke, R., Zigan, S., "Design Studies of Lift Fan Engines Suitable for Use in Civilian VTOL Aircraft," *Gas Turbine and Fluids Engineering Conference & Products Show*, San Francisco, CA, Mar. 26-30, 1972.

[46] Deckert, W., Evans, R., "NASA Lift Fan V/STOL Transport Technology Status," *SAE International Journal*, Vol. 81, Sec. 4, No. 720856, pp. 2548-2557, 1972.
https://www.jstor.org/stable/44716260

[47] Thomas, J., Hoad, D., Croom, D., "Aerodynamic Effects of Five Lift-Fan Pod Arrangements on an Unpowered V/STOL Transport Model," *NASA Langely Research Center and U.S. Army Air Mobility R&D Laboratory,* TN D-7199, Jun. 1973.

[48] Zabinsky, J., et al., "V/STOL Lift Fan Commercial Short-Haul Transports," *NASA Contractor Report – Boeing Commercial Airplane Company*, CR-2437, Jul. 1974.

[49] Cavage, R., et al., "Conceptual Design Study of Improved 1985 Remote Lift-Fan VSTOL Commercial Transports," *NASA Contractor Report – Rockwell International Corporation*, CR-2481, Jan. 1975.

[50] Benzakein, M., Volk, L., "Study Program for Lift Fan Noise Reduction and Suppression," *NASA Contractor Report – General Electric Company*, CR-1493, Mar. 1970.

[51] Kirk, J., Hall, L., Hodder, B., "Aerodynamics of Lift Fan VSTOL Aircraft," *NASA Ames Research Center and U.S. Army Air Mobility Research and Development Laboratory*, TM X-62,086, Sep. 1971.

[52] Gerdes, R., Hynes, C., "Factors Affecting Handling Qualities of a Lift-Fan Aircraft During Steep Terminal Area Approaches," 27th *Annual Forum of the American Helicopter Society*, NASA Ames Research Center, Moffet Field, CA, May 1971.

[53] Atencio Jr., A., "Noise Measurements from a Large-Scale Lift Fan Transport in the 40- by 80- Foot Wind Tunnel," *NASA Ames Research Center*, TM X-62,284, Moffett Field, CA, Mar. 1973.

[54] Lieblein, S., "Problem Areas for Lift Fan Propulsion for Civil VTOL Transports," *DGLR Symposium on VTOL Propulsion*, NASA TM X-52907, Munich, Germany, Oct. 22-23, 1970.

[55] Ford, J., "Lift-Fan Propulsion-Control System," *SAE International Journal*, Vol. 82, Sect. 2, No. 730360, pp. 1229-1242, 1973.
https://www.jstor.org/stable/44717537

[56] Scott, M., "Summary of Technology Needs for High-Speed," *AIAA/SAE/ASME/ASEE 27th Joint Propulsion Conference*, AIAA Paper No. 91-2148, Sacramento, CA, June 24-26,1991.

[57] Rutherford, J., O'Rourke, M., Martin, C., Lovenguth, M., "Technology Needs for High-Speed Rotorcraft," *NASA Contractor Report – McDonnel Douglas Helicopter Company*, CR-177578, Apr. 1991.

[58] Scott, M., "Technology Needs for High-Speed Rotorcraft (2)," *NASA Contractor Report – Sikorsky Aircraft*, CR-177590, Aug. 1991.

[59] Jack DeTore, Conway, S., "Technology Needs for High-Speed Rotorcraft (3)," *NASA Contractor Report – Bell Helicopter Textron*, CR-177592, Oct. 1991.

[60] Corgiat, A., Lind, G., Hartsel, J., "Fan-in-Wing Technology, From the XV-5A to the Present," *American Institute of Aeronautics*, AIAA Paper No. 93-4839-CP, 1993.

[61] Cook, W., "Summary of Lift and Lift-Cruise Fan Powered Lift Concept Technology," *NASA Contractor Report – Retired NASA Ames Researcher*, CR-177619, Aug. 1993.

[62] Hickey, D., Kirk, J., "Survey of Lift-Fan Aerodynamic Technology," *NASA Contractor Report – NASA Ames Research Center*, CR-177615, Sep. 1993.

[63] Stockman, N., Loeffler, I., Lieblein, S., "Effect of Rotor Design Tip Speed on Aerodynamic Performance of a Model VTOL Lift Fan Under Static and Crossflow Conditions," *Gas Turbine Conference and Products Show*, Paper No. 73-GT-2, Washington D.C., Apr. 8-12, 1973.

[64] Diedrich, J, Clough, N., Lieblein, S., "Installation Effects on Performance of Multiple

Model V/STOL Lift Fans," *AIAA/SAE 8th Joint Propulsion Specialist Conference*, Paper No. 72-1175, New Orleans, LA, Nov 29-Dec. 1, 1973.

[65] Lieblein, S., Yuska, J., Diedrich, J., "Performance Characteristics of a Model VTOL Lift Fan in Crossflow," *JA Aircraft*, Vol. 10. No. 3, Mar. 1973. https://doi.org/10.2514/3.44357

[66] Thouault, N., Breitsamter, Adams, N., "Numerical Investigation of Inlet Distortion on a Wing-Embedded Lift Fan," *Journal of Power and Propulsion*, Vol. 27, No. 1, Jan. 2011. https://doi.org/10.2514/1.46046

[67] Jiany, Y., Zhang, B., Huang, T., "CFD Study of an Annular-Ducted Fan Lift System for VTOL Aircraft," *MDPI Aerospace Journal*, Vol 2., No. 555-580, 2015. https://doi.org/10.3390/aerospace2040555

[68] Lee, H., Prasad, R., Choi, S., "Aerodynamic Analysis for Conceptual Design of a Lift Fan Type Aircraft," *AIAA Aviation Forum, 34th AIAA Applied Aerodynamics Conference,* Washington D. C., Jun. 13-17, 2016. https://doi.org/10.2514/6.2016-3408

[69] Thouault, N., Breitsamter, C., Adams, N., "Numerical and Experimental Analysis of a Generic Fan-in-Wing Configuration," *Journal of Aircraft*, Vol. 46, No. 2, Mar. 2009. https://doi.org/10.2514/1.39750

[70] Thouault, N., Breitsamter, C., Adams, N., Gologan, C., Seifert, J., "Experimental Investigation of the Aerodynamic Characteristics of Generic Fan-In-Wing Configurations," *The Aeronautical Journal*, Vol. 113, No. 1139, Paper No. 3338, 2009. https://doi.org/10.1017/S0001924000002736

[71] Thouault, N., Breitsamter, C., Adams, N., Gologan, C., "Numerical analysis of design parameters for a generic fan-in-wing configuration," *Elsevier Aerospace Science and Technology Journal*, Vol. 14., Paper No. 65-77, 2010. https://doi.org/10.1016/j.ast.2009.10.004

[72] Bevilaqua, P., "Joint Strike Fighter Dual-Cycle Propulsion System," *Journal of Propulsion and Power*, Vol. 21, No. 5, Sep. 2005. https://doi.org/10.2514/1.15228

[73] Sylvester, T., Brown, R., Connor, C., "F-35B Lift Fan Inlet Development," *AIAA Centennial of Naval Aviation Forum,* AIAA Paper No. 2011-6940, Virginia Beach, VA, Sep. 21-22, 2011.

[74] Finger, D., Braun, C., Bil, C., "A Review of Configuration Design for Distributed Propulsion Transitioning VTOL," *Asia-Pacific International Symposium on Aerospace Technology*, Seoul, Korea, 2017.

[75] Jiang, Y, Zhang, B., "CFD Study of a New Annular Lift Fan Configuration with High Lift Efficiency," *MDPI Aerospace Journal*, Vol. 4, No. 13, 2017. https://doi.org/10.3390/aerospace4010013

[76] Jiang, Y, Zhang, B., "Numerical Assessment of a High Disk Landing Annular Lift Fan Aircraft," *Journal of the American Helicopter Society*, Vol. 63, Paper No. 042000, 2018. https://doi.org/10.4050/JAHS.63.042000

[77] Posva, D., Neuhas, R., Wilhelm, P., Leyland, P., "Design and Aerodynamic Considerations about the Civil VTOL Aircraft Ray," *International Powered Lift Conference, the American Helicopter Society*, Philadelphia, PA, Oct. 5-7, 2010.

[78] Ohanian III, O., "Ducted Fan Aerodynamics and Modeling, with Applications of Steady and Synthetic Jet Flow Control," *Master's Thesis Dissertation*, Viginia Polytechnic Institute and State University, Blacksburg, VA, 2011.

[79] Jhou, Y., Huang, G., Xia, C., "Analysis of Fixed-Wing VTOL Aircraft with Gas-Driven Fan Propulsion System," Elsevier Aerospace Science and Technology Journal, Vol. 104, Paper No. 105984, 2020. https://doi.org/10.1016/j.ast.2020.105984

[80] Hoeveler, B., Bauknecht, A., Wolf, C., Janser, F., "Wind-Tunnel Study of a Wing-Embedded Lifting Fan Remaining Open in Cruise Flight," *AIAA Journal of Aircraft*, Vol. 57, No. 4, Jul. 2020. https://doi.org/10.2514/1.C035422

[81] Chakraborty, I., Mishra, A., "Design and Sizing of an Electrified Lift-Plus-Cruise Ducted Fan," *AIAA Journal of Aircraft*, Vol. 60, No. 3, May 2023. https://doi.org/10.2514/1.C036811

[82] Liu, P., "Computational Fluid Dynamics," *A General Theory of Fluid Mechanics*, Springer, Singapore, published online Apr. 2, 2021. https://doi.org/10.1007/978-981-33-6660-2_4

[83] Captain Electro, "Why Electric Aircraft Could be the Next Big Thing in Aviation," *Captain Electro – Aircraft*, published online Jun. 12, 2023. https://www.captainelectro.com/aircraft/why-electric-aircraft-could-be-the-next-big-thing-in-aviation

[84] Rolls, L., Gerdes, R., "Flight Evaluation of Tip-Turbine-Driven Fans for Lateral Control in a Hovering VTOL Aircraft," *NASA Ames Research Center*, TN D-5491, Moffett Field, CA, Oct. 1969.

[85] Zhou, Z. et al., "Design of Thrust Vectoring Vertical/Short Takeoff and Landing Aircraft Stability Augmentation Controller Based on L1 Adaptive Control," *Recent Progress in Robot Control Systems: Theory and Applications*, MDPI, published online Sep 4, 2022.

https://doi.org/10.3390/sym14091837

[86] Gal-Or, B., "Fundamental Concepts of Vectored Propulsion," *Journal of Propulsion and Power*, AIAA, Vol. 6, No. 6, pp. 673-800, published online Nov. 1990. https://doi.org/10.2514/3.23281

[87] Ferris, J., "EWR VJ 101C a Groundbreaking Supersonic Aircraft," *Plane Historia*, published online Nov. 2023. https://planehistoria.com/vj-101c/

[88] Whitemule, "Dornier Do 31 E-1: Two "Harriers" under the wings + 8 more engines," *Word Press*, published online Dec. 2012. https://elpoderdelasgalaxias.wordpress.com/2012/12/14/dornier-do-31-e-two-harriers-under-the-wings-8-more-engines/

[89] Kirk, B., "Lockheed XV-4 Hummingbird: America's Failed VTOL Rival to the Original Harrier," *Auto Evolution News*, published online Dec. 2022. https://www.autoevolution.com/news/lockheed-xv-4-hummingbird-america-s-failed-vtol-rival-to-the-original-harrier-206016.html

[90] Tosaka, "Yak-38 Lift Engines NT," *Wikimedia Commons*, published online Aug. 2008. https://en.m.wikipedia.org/wiki/File:Yak-38_Lift_Engines_NT.PNG

[91] Tosaka, "F-35B Joint Strike Fighter (thrust vectoring nozzle and lift fan)," *Wikimedia Commons*, published online Jul. 2008. https://en.m.wikipedia.org/wiki/File:F35B_Joint_Strike_Fighter_(thrust_vectoring_nozzle_and_lift_fan).PNG

[92] Ruh, M., et al., "Large-Scale Multidisciplinary Design Optimization of the NASA Lift-Plus-Cruise Concept Using a Novel Aircraft Design Framework," *VFS Autonomous VTOL Technical Meeting*, Mesa, Arizona, Jan 24-26, 2023. https://ar5iv.labs.arxiv.org/html/2304.14889

[93] Charkraborty, I., Mishra, A., "Sizing and Analysis of a Lift-Plus-Cruise Aircraft with Electrified Propulsion," *Aerospace Research Central*, published online Nov. 1, 2022. https://doi.org/10.2514/1.C037044

[94] Cha, W., et al., "Design of a Lift+Cruise eVTOL Aircraft Reflecting the Geometry and Structural Details Regarding Battery Locations," *VFS 79th Annual Forum & Technology Display*, West Palm Beach, Florida, May 16-18, 2023. https://doi.org/10.4050/F-0079-2023-18000

[95] Underwood Photo Archives, "Hiller Flying Platform (VTOL) 1962," *Superstock*, published online 2024. https://www.superstock.com/asset/hiller-flying-platform-vtol/1035-142

[96] Shetty, T., "Moller M200G Volantor," *Alchetron*, published online Feb. 2024. https://alchetron.com/Moller-M200G-Volantor

[97] Dodda, J., Srinivasulu, N., Reddy, B., "Various Developments in the Design of Hovercrafts: A Review," *Smart Innovation, Systems and Technologies*, Vol. 213, pp. 519-528, Springer, Singapore, 2021. https://doi.org/10.1007/978-981-33-4443-3_50

[98] Doak Aircraft Co., Inc., "Doak 16-Army VZ-4DA VTOL," *VFS Publications*, released Jun. 1959. https://gallery.vtol.org/image/PD5Dn

[99] U.S. Army, Defense.gov, "Bell X-22 Ducted Fan," *Wikimedia Commons*, published online Apr. 2023. https://en.m.wikipedia.org/wiki/File:Bell_X-22_ducted_fan.jpg

[100] Whiteside, S., Pollard, B., "Conceptual Design of a Tiltduct Reference Vehicle for Urban Air Mobility," *Aeromechanics for Advanced Vertical Flight Technical Meeting*, NASA Langley Research Center, San Jose, California, Jan. 25-27, 2022.

[101] Armutcuoglu, O., Kavsaoglu, M., Tekinalp, O., "Tilt Duct Vertical Takeoff and Landing
Uninhabited Aerial Vehicle Concept Design Study," Journal of Aircraft, Vol. 41, No. 2, Mar.-Apr. 2004 https://doi.org/10.2514/1.271

[102] Zhang, J. et al., "Conceptual Design and System Level Analysis of Tilt-Duct eVTOL Aircraft," *Asia-Pacific International Symposium on Aerospace Technology*, Korea, published online Aug. 31, 2022. https://doi.org/10.1007/978-981-19-2689-1_14

[103] Raymer, D., P., *Aircraft Design: A Conceptual Approach*, 6th ed., AIAA, Reston, VA, 2018.

[104] Nicolai, L. M., Carichner, G. E., *Fundamentals of Aircraft and Airship Design*, Vo1. 1 Aircraft Design, AIAA, Reston VA, 2010.

[105] McCormick, B. W., *Aerodynamics, Aeronautics, and Flight Mechanics*, 2nd ed. John Wiley & Sons, New York, 1995.

[106] Collins, M., "Valdez STOL Distances Get Shorter, 2018 Event Sees New Takeoff, Landing Records," AOPA, published online May 2018. https://www.aopa.org/news-and-media/all-news/2018/may/17/valdez-stol-distances-get-shorter

[107] Uri, J., "65 Years Ago: First Factory Rollout of the X-15 Hypersonic Rocket Plane,"

NASA, Johnson Space Center, published online Oct. 2023.
https://www.nasa.gov/history/65-years-ago-first-factory-rollout-of-the-x-15-hypersonic-rocket-plane/

[108] Yang, X., "Comparative Evaluation of Propulsive Power Transmission Technologies for
High-Speed Vertical Takeoff and Landing (HSVTOL) Cargo Aircraft," *Doctoral Dissertations and Master's Theses, ERAU*, 2023.
https://commons.erau.edu/edt/783

[109] The Vertical Flight Society, "High-Speed Vertical Takeoff and Landing (HSVTOL) Aircraft," *40th Annual Student Design Competition Request For Proposals*, Sikorsky, 2022-2023.
https://vtol.org/files/dmfile/rfp_sikorskyhvstol_40thsdc_2022-23_final.pdf

[110] Leishman, J. G., *Introduction to Aerospace Flight Vehicles*, Sec. 10., Ch. 42, Embry-Riddle Aeronautical University, published online 2023.
https://doi.org/10.15394/eaglepub.202

[111] Leishman, J. G., *Principles of Helicopter Aerodynamics*, 2nd ed., Cambridge University Press, New York, NY, 2006.

[112] Parsons, D., Eckstein, A., Azevedo, J., "F-35 Aerodynamic Performance Verification," *AIAA Aviation Technology, Integration, and Operations Conference*, Atlanta, GA, Jun. 25-29, 2018.
https://doi.org/10.2514/6.2018-3679

[113] Filipenko, M., "Back to the Future: A rough comparison of 70s VTOL concepts to current eVTOL designs," *LinkedIn*, published online May 2020.
https://www.linkedin.com/pulse/back-future-rough-comparison-70s-vtol-concepts-evtol filipenko/

[114] Maisel, M., Giulianetti, D., Dugan, D., "The History of the XV-15 Tilt Rotor Research Aircraft: From Concept to Flight," *NASA SP-2000-4517*, Washington, D. C., published online 2000.
https://www.nasa.gov/wp-content/uploads/2023/04/sp-4517.pdf

[115] Schmidt, M., K. Plötner, O., Pornet, C., Isikveren, A. T., Hornung, M., "Contributions of Cabin Related and Ground Operation Technologies Towards Flightpath 2050," *Deutscher Luft-und Raumfahrtkongress*, Document-ID: 1299, 2013.
https://www.researchgate.net/publication/274704939_Contributions_of_Cabin_Related_and_Ground_Operation_Technologies_Towards_Flightpath_2050

[116] Vexels, "Airplane Top View Simple Icon PNG Design," *Vexels.com*, published online Dec. 2019.
https://www.vexels.com/png-svg/preview/195247/airplane-top-view-simple-icon

[117] Air BP, “Aviation Fuels and Methanol/Water Mixtures,” *BP Products Handbook*, Air BP Ltd., pp. 10-16, United Kingdom, 2000.

[118] Anderson, R., Steinfeldt B., Lewis, R., “Hybrid Propulsion of a Cargo VTOL Aircraft,” *First International Conference on Advanced Air Mobility Systems (ICAAMS-1),* The Vertical Flight Society & Rotary Wing Society of India, Bengaluru, India, Dec. 4-6, 2023.

[119] Smith, H., *Aircraft Flight Mechanics*, Range and Endurance, published online 2022. https://aircraftflightmechanics.com/AircraftPerformance/RangeandEndurance.html

[120] Gartenberg, L., "Battery Centric Serial Hybrid Aircraft Performance and Design Space," *Doctoral Dissertations and Master's Theses*, *ERAU*, 2017. https://commons.erau.edu/edt/327

[121] Saggittarius A, “A Comparison of Many Unmanned Aerial Vehicles,” *Wikipedia Commons*, published online Nov. 2019. https://en.wikipedia.org/wiki/File:UAV_Comparison.jpg

[122] Waterman, S., “General Atomics Exec: CCA Will ‘Go Down in History’ for Putting Drones Front and Center,” *Air & Space Forces Magazine*, published online Mar. 2024. https://www.airandspaceforces.com/general-atomics-cca-drones-front-and-center/

[123] Department of Defense, *MIL-STD-3013A*, Feb. 2003.

[124] Hiller Aircraft Corporation, “VTOL Downwash Impingement Study Surface Erosion Tests,” *U.S. Army Transportation Research Command*, TR No. 60-67, Fort Eustis, VA, Oct. 1960.

[125] SDASM Archives, “Ryan Aeronautical Image,” *flickr*, published online May. 2017. https://www.flickr.com/photos/sdasmarchives/34369889362/in/dateposted/

[126] Boeing, “MQ-25 Refuels F-35C,” *Wikipedia Commons*, published online Sep. 2021. https://media.defense.gov/2021/Sep/14/2002853456/-1/-1/0/210914-N-NO101-0151.JPG

[127] Panzer, “Ryan XV-5A Vertifan,” *Armed Conflicts*, published online in 2016. https://www.valka.cz/Ryan-XV-5-Vertifan-t190500#550968

[128] 88 Air Base Wing Public Affairs, “XQ-58A Valkyrie Demonstrator Completes Inaugural Flight,” *Wright-Patterson AFB*, published online Mar. 2019. https://www.wpafb.af.mil/News/Article-Display/Article/1777743/xq-58a-valkyrie demonstrator-completes-inaugural-flight/

[129] General Atomics Aeronautical Systems, Inc., “General Atomics Aeronautical’s Gambit Series Lets U.S. Forces Move Fast and Move First,” *Breaking Defense*, published online February 2024.

https://breakingdefense.com/2024/02/general-atomics-aeronauticals-gambit-series-lets-u-s-forces-move-fast-and-move-first/

[130] VerdeGo Aero, "The VH-5 Makes a New Class of Ultra-High Performance Electrified Aircraft Possible," *1MW+ High-Speed Hybrids*, published online in 2023. https://verdegoaero.com/product/vh5/

[131] EASA, "Type-Certificate Data Sheet," *Pratt and Whittney Canada PW545 Series Engines,* Document Number IM.E.013, Issue 2, Feb. 2009.

[132] Bartsch, E., "Hybridization – Making Electric Flight Practical," *11th Annual Electric VTOL Symposium*, *eVTOL Session 4: Electric Propulsion*, Santa Clara, California, Feb. 6-8, 2024.

[133] General Electric, "Quarterly Technical Progress Report No. 9," *Defense Documentation Center for Scientific and Technical Information*, AD 447839, Cameron Station, Alexandria, VA, Jan. 1964.

[134] General Electric, "Quarterly Technical Progress Report No. 10," *Defense Documentation Center for Scientific and Technical Information*, AD 461017, Cameron Station, Alexandria, VA, Jul. 1964.

[135] General Electric, "Quarterly Technical Progress Report No. 11," *Defense Documentation Center for Scientific and Technical Information*, AD 461455, Cameron Station, Alexandria, VA, Oct. 1964.

[136] Gudmundsson, S., *General Aviation Aircraft Design: Applied Methods and Procedures*, Elsevier, 2014.

[137] Xiang, X., Huang, G., Chen, J., Li, L., Lu, W., "Numerical Investigations of Tip Turbine Aerodynamic Design in a Propulsion System for VTOL Vehicles," *MDPI Energies Journal,* Vol. 12, No. 15, published online Aug. 2019. https://doi.org/10.3390/en12153003

[138] Murcia, D.C, "Study: 3D modeling and initial structural analysis of a light aircraft," *Semantic Scholar*, Corpus ID: 213678550, published online Jun. 2019. https://www.semanticscholar.org/paper/Study%3A-3D-modeling-and-initial-structural-analysis-Murcia/9cd25aecdb967a3fa02169150f7310935b648e7f

[139] Lockheed Martin, "Fact Sheet: Joint-Strike Fighter: Costs and Challenges," Center for Arms Control and Non-Proliferation, published online Apr. 2016. https://armscontrolcenter.org/f-35-joint-strike-fighter-costs-challenges/

[140] Levinson, R., "The F-35's Global Supply Chain," *Bloomberg Businessweek*, published online Sep. 2011. https://www.bloomberg.com/news/articles/2011-09-01/the-f-35-s-global-supply-chain

6. APPENDIX A - ADDITIONAL TABLES AND FIGURES

This Appendix was reserved for all additional tables and figures deemed necessary to include at the end of this thesis for further reference in support of the main material.

6.1. eVTOL Classification Table

The following table details the classification of each aircraft concept from the VFS eVTOL directory [5] into classes of "embedded fan," "ducted fan," manned," unique aircraft," and "unique concept" using binary digits to indicate what classes, if any, each concept falls into.

Table 6.1 Classification of aircraft concepts from the VFS eVTOL directory [5]

#	Concept Aircraft	Embedded Fan	Ducted Fan	Manned	Unique Concept	Unique Organization
1	1. A2-Cal Aptos Blue	0	0	1	1	1
2	2. Ace VTOL GT Slipstream (concept design)	1	1	1	1	1
3	3. Ace VTOL Slipstream Elite (concept design)	1	1	1	1	0
4	4. Ace VTOL Trinity (concept design)	1	1	1	1	0
5	5. ACS Aviation Z-300	0	0	1	1	1
6	6. Advanced Research Foundation Cyclocar	0	0	1	1	1
7	7. Advanced System Engineering - FIPSI BX4	0	0	1	1	1
8	8. Advanced System Engineering - FIPSI WX4	0	0	1	0	0
9	9. Advanced Tactics Barracuda	0	0	1	1	1
10	10. Aerofugia Technology Co. Ltd. (Geely) AE200 X01 (technology demonstrator)	0	0	1	1	1
11	11. aeroG Aviation aG-4 Liberty	0	0	1	1	1
12	12. aeroG Aviation UV-4	0	0	1	0	0
13	13. Aeronext Flying Gondola	0	0	1	1	1
14	14. Airbus Acubed Vahana Alpha One (defunct)	0	0	1	1	1
15	15. Airbus Acubed Vahana Alpha Two (defunct)	0	0	1	0	0
16	16. Airbus Acubed Vahana Beta (concept design)	0	0	1	0	0
17	17. AIR AIR ONE (technology demonstrator)	0	0	1	1	1
18	18. Air Race E Unnamed eVTOL Racer	0	1	1	1	1

#	Concept Aircraft	Embedded Fan	Ducted Fan	Manned	Unique Concept	Unique Organization
19	19. Airis Aerospace AirisOne	1	1	1	1	1
20	20. Airspace Experience Technologies (ASX) MOBi-One V1 (concept design)	0	0	1	1	1
21	21. Airspace Experience Technologies (ASX) MOBi-One V2 (concept design)	0	0	1	0	0
22	22. Airspace Experience Technologies (ASX) MOBi-One V3 (concept design)	0	0	1	0	0
23	23. Airspace Experience Technologies (ASX) Sigma-6 (prototype)	0	0	1	1	0
24	24. Airspace Experience Technologies (ASX) Sigma-6 Cargo Drone (concept design)	0	0	0	0	0
25	25. Alauda Airspeeder Mk4 (hydrogen-electric)	0	1	1	1	1
26	26. Aliptera APV-1	1	1	1	1	1
27	27. Alwinart (Sagstuen) Tesla eVTOL Concept	1	1	1	1	1
28	28. American Aerospace Engineering Eversor	0	0	1	1	1
29	29. AMSL Aero Vertiia	0	0	1	1	1
30	30. ARC Aerosystems HUMA (concept design)	0	0	1	1	1
31	31. ARC Aerosystems e-Starling Jet (concept design)	1	1	1	1	0
32	32. ARC Aerosystems Starling Cargo (concept design)	1	1	1	0	0
33	33. ARC Aerosystems Starling Cargo S5M (demonstrator)	1	1	1	0	0
34	34. ARC Aerosystems Starling Jet (concept design)	0	0	1	0	0
35	35. ARC Aerosystems UAV Starling (concept design)	1	1	1	1	0
36	36. Archer Maker (technology demonstrator)	0	0	1	1	1
37	37. Archer Midnight (production aircraft)	0	0	1	0	0
38	38. Aston Martin Volante	1	1	1	1	1
39	39. Aufeer Design Flying Taxi	1	1	1	1	1
40	40. Aurora Flight Sciences LightningStrike (defunct)	0	1	1	1	1
41	41. Autonomous Flight Y6S	0	0	0	1	1
42	42. Autonomous Flight Y6S Plus	0	0	0	0	0
43	43. AVIC General Aviation eVTOL	0	0	1	1	1
44	44. Avioneo Robotics Avioneo 2345	0	0	1	1	1
45	45. Baaz Concept Design	0	1	1	1	1
46	46. Baaz Production Model	0	1	1	0	0
47	47. Bartini (technology demonstrator)	0	1	1	1	1
48	48. Bartini (two passenger concept design)	0	1	1	0	0

#	Concept Aircraft	Embedded Fan	Ducted Fan	Manned	Unique Concept	Unique Organization
49	49. Bartini (four passenger concept design)	0	1	1	1	0
50	50. Bartini (production aircraft)	0	1	1	0	0
51	51. Bell Autonomous Pod Transport (APT)	0	0	0	1	1
52	52. Bell Nexus 4EX	0	1	1	1	1
53	53. Bell Nexus 6HX	0	1	1	1	0
54	54. Bellwether Industries Antelope	1	1	1	1	1
55	55. Beta Technologies Ava XC (technology demonstrator)	0	0	1	1	1
56	56. Blueflite Slate	0	1	1	1	1
57	57. Cadillac VTOL	1	1	1	1	1
58	58. CFC AirCAR	0	1	1	1	1
59	59. Chatillon Buzzaxe H5 (concept design)	1	1	1	1	1
60	60. Chatillon Ciconia (concept design)	0	0	1	1	0
61	61. Chatillon Le Colibri (concept design)	0	0	1	1	0
62	62. Chatillon Tritan Jet T1 (concept design)	0	0	1	1	0
63	63. Chatillon Tritan Jet TQ (concept design)	0	0	1	1	0
64	64. Coflow Jet CFJ-VTOL (concept design)	0	0	1	1	1
65	65. Coflow Jet CFJ-VTOL eCargo (concept design)	0	0	1	0	0
66	66. Coflow Jet CFJ-VTOL TW (concept design)	0	0	1	0	0
67	67. Collaborative Mini-Bee	1	1	1	1	1
68	68. Chongqing Flying Car (prototype)	0	0	1	1	1
69	69. CycloTech Passenger Demonstrator	0	0	1	1	1
70	70. CycloTech UAV Demonstrator	0	0	0	0	0
71	71. DARPA Ancillary Tactical Drone (proposer)	0	1	0	1	1
72	72. Davies Tesla Concept Model V	1	1	1	1	1
73	73. Davies Tesla Concept Model V2	1	1	1	0	0
74	74. Deep Blue Aviation MX 18 Silhouette 5	1	1	1	1	1
75	75. Deep Blue Aviation MX 18 Silhouette M	1	1	1	1	0
76	76. Deep Blue Aviation MX 18 Silhouette X	1	1	1	1	0
77	77. Deep Blue Aviation Sky Cruiser	1	1	1	1	0
78	78. Delft University of Technology Aether (concept design)	0	0	1	1	1

#	Concept Aircraft	Embedded Fan	Ducted Fan	Manned	Unique Concept	Unique Organization
79	79. Delft University of Technology Wigeon (concept design)	0	0	1	1	0
80	80. DeLorean Aerospace DR-7	1	1	1	1	1
81	81. Detroit Flying Cars WD-1	0	1	1	1	1
82	82. Didia Atlas (concept design)	0	1	1	1	1
83	83. Didia Blueflite	0	1	1	0	0
84	84. Didia Mantas (concept design)	0	1	1	1	0
85	85. Didia Titan (concept design)	0	1	1	1	0
86	86. Digi Robotics DroFire	0	0	0	1	1
87	87. Digi Robotics Droxi	0	0	0	1	0
88	88. Dufour Aerospace aEro 2 (defunct)	0	0	1	1	1
89	89. Dufour Aerospace Aero2 (cargo drone)	0	0	0	0	0
90	90. Dufour Aerospace aEro 3 (defunct)	0	0	1	0	0
91	91. Dufour Aerospace Aero3 (production design)	0	0	1	0	0
92	92. Dufour Aerospace VTOL Technology Demonstrator	0	0	1	1	0
93	93. Eco'Trip (concept design)	0	1	1	1	1
94	94. Edea 22/1 Jay	1	1	1	1	1
95	95. Electric Airspace Y6	0	0	1	1	1
96	96. Embraer Pulse Concept	0	0	1	1	1
97	97. EVA X01	0	1	1	1	1
98	98. EVA Valkyr	1	1	1	1	0
99	99. Flexcraft RPV	0	0	1	1	1
100	100. Flexcraft VERA	0	0	1	1	0
101	101. Freedom Transports Zero G eCruzer	0	0	1	1	1
102	102. Gizio CellCraft G150	0	1	1	1	1
103	103. Gizio CellCraft G450	0	1	1	1	0
104	104. Gizio DDRH/DDVL	0	1	1	1	0
105	105. Gizio EJ11 ElectroJet	0	1	1	1	0
106	106. Grug Group Business eVTOL Jet	1	1	1	1	1
107	107. Grug Group Ghost X V1	0	1	1	1	0
108	108. Grug Group Ghost X V2.2	0	1	1	0	0

#	Concept Aircraft	Embedded Fan	Ducted Fan	Manned	Unique Concept	Unique Organization
109	109. Grug Group Ghost X V3	1	1	1	0	0
110	110. Grug Group Personal eVTOL Jet	1	1	1	1	0
111	111. Grug Group SBX	0	1	1	1	0
112	112. Hemanth Sudhakaran AVEM	0	1	1	1	1
113	113. Highgate AeroDesign Targa VTOL	0	0	1	1	1
114	114. HopFlyt Venturi	0	0	1	1	1
115	115. HopLite Aviation	1	1	1	1	1
116	116. Imaginactive Transvolution	1	1	1	1	1
117	117. Industry Network Cocooon X-1	0	0	1	1	1
118	118. IO Aircraft Challenger SC	0	1	1	1	1
119	119. IO Aircraft Chippewa 350E	0	0	1	1	0
120	120. IO Aircraft Chippewa 350M	0	0	1	0	0
121	121. Ion Aircraft eVTOL-CHe (concept design)	0	1	1	1	1
122	122. Ion Jet EVTOL (concept design)	0	1	1	1	0
123	123. Jantschke Megacity Aviation (concept design)	0	1	1	1	1
124	124. JAXA Hornisse 2B	1	1	1	1	1
125	125. Jetcopter VTOL Technologies Sky Bridge	0	1	1	1	1
126	126. Jetcopter VTOL Technologies Sky Cargo	0	1	1	1	0
127	127. Jetcopter VTOL Technologies Sky Commuter	0	0	1	1	0
128	128. Jetcopter VTOL Technologies Sky Connect	0	1	1	1	0
129	129. Jetcopter VTOL Technologies Sky Executive	0	0	1	1	0
130	130. Jetcopter VTOL Technologies Sky Hopper	1	1	1	1	0
131	131. Jetcopter VTOL Technologies Sky Mod	1	1	1	1	0
132	132. Jetcopter VTOL Technologies Sky Path	0	0	1	1	0
133	133. Jetcopter VTOL Technologies Sky Shadow	0	0	1	1	0
134	134. Jetcopter VTOL Technologies Sky Skimmer	0	1	1	1	0
135	135. Jetcopter VTOL Technologies Sky Slider	0	0	1	1	0
136	136. Jetcopter VTOL Technologies Sky View	1	1	1	1	0
137	137. Jetoptera J2000	0	0	1	1	1
138	138. JETX Vector E	1	1	1	1	1

#	Concept Aircraft	Embedded Fan	Ducted Fan	Manned	Unique Concept	Unique Organization
139	139. JETX Vector F	0	0	1	1	0
140	140. JETX Vector MADE	0	0	1	1	0
141	141. JETX Vector MAPE	0	0	1	1	0
142	142. JETX Vector MPE	0	0	1	1	0
143	143. Joby Aviation Monarch (defunct)	0	0	1	0	1
144	144. Joby Aviation Lotus (defunct)	0	0	1	0	0
145	145. Joby Aviation S2 (defunct)	0	0	1	0	0
146	146. Joby Aviation S4 1.0 (technology demonstrator)	0	0	1	0	0
147	147. Joby Aviation S4 2.0 (pre-production prototype)	0	0	1	0	0
148	148. Joby Aviation S4 (production prototype)	0	0	1	1	0
149	149. KARI Optionally Piloted PAV	0	0	1	1	1
150	150. Kelekona Unnamed eVTOL	0	1	1	1	1
151	151. KineticCo Aerospace and Advanced Technologies	0	0	1	1	1
152	152. Kitty Hawk Heaviside (defunct)	0	0	1	0	1
153	153. Kitty Hawk Heaviside 2 (H2) (concept design)	0	0	1	1	0
154	154. Korea Aerospace Industries (KAI) Night Intruder	0	0	1	1	1
155	155. Korea Aerospace Industries (KAI) Unnamed (prototype)	0	0	1	1	0
156	156. Kozloff Pegasus	0	0	1	1	1
157	157. Kozloff Ship to Shore Air Limo	0	0	1	1	0
158	158. Kronstadt Air Taxi	0	1	1	1	1
159	159. Leonardo Unnamed eVTOL	0	0	1	1	1
160	160. Leonardo Helicopters Project Zero (formerly AgustaWestland)	1	1	1	1	0
161	161. Lilium Dragon (defunct)	0	1	1	0	1
162	162. Lilium Eagle (defunct)	0	1	1	0	0
163	163. Lilium Falcon (defunct)	0	1	1	0	0
164	164. Lilium Jet (7-seater)	0	1	1	1	0
165	165. Lilium Jet (16-seater)	0	1	1	1	0
166	166. Lilium Phoenix (defunct)	0	1	1	0	0
167	167. Limosa LimoConnect	0	0	1	1	1
168	168. LuftCar (concept design)	0	0	1	0	1

#	Concept Aircraft	Embedded Fan	Ducted Fan	Manned	Unique Concept	Unique Organization
169	169. LuftCar (production model)	0	0	1	1	0
170	170. Macchina Volontis Flying Car	0	1	1	1	1
171	171. Maglev Aero (HyperDrive Propulsion System)	1	1	1	1	1
172	172. Manta Aircraft ANN Cargo	0	1	1	1	1
173	173. Manta Aircraft ANN Drone	0	1	0	0	0
174	174. Manta Aircraft ANN1 (defunct)	0	1	1	0	0
175	175. Manta Aircraft ANN2	1	1	1	0	0
176	176. Manta Aircraft ANN4	0	1	1	1	0
177	177. Micor Technologies Advanced Individual VTOL Aircraft (AIVA)	0	0	1	1	1
178	178. Micor Technologies Advanced Multi-passenger VTOL Aircraft (AMVA)	0	0	1	1	0
179	179. Micor Technologies Variable Geometry VTOL aircraft (VAGEV)	0	0	1	1	0
180	180. MGI Engineering MGI Cargo (technology demonstrator)	0	0	1	1	1
181	181. Moller Skycar® 200 (prototype)	0	1	1	0	1
182	182. Moller Skycar® 400 (prototype)	0	1	1	1	0
183	183. Moscow Team AI Kamchatka	0	1	1	1	1
184	184. Moviation Vonaer (concept design)	0	0	1	1	1
185	185. MyDraco	0	1	1	1	1
186	186. NASA Greased Lightning	0	0	1	1	1
187	187. NASA LA-8 eVTOL Testbed	0	0	1	1	0
188	188. NEAE-GSI eVTOL-BUS	0	1	1	1	1
189	189. NEAE-GSI eVTOL-Taxi	0	1	1	1	0
190	190. Neoptera eOpter	0	0	1	1	1
191	191. Next Green Xcar Cuba	0	0	1	1	1
192	192. Node-Air Node	0	1	1	1	1
193	193. NFT ASKA 1.0 (concept design)	1	1	1	0	1
194	194. NFT ASKA 2.0 (concept design)	1	1	1	0	0
195	195. NFT ASKA 3.0 (concept design)	0	0	1	1	0
196	196. NFT ASKA™ A5 (production model)	0	0	1	1	0
197	197. Odys Aviation Unnammed eVTOL	0	0	1	1	1
198	198. Ola Electric Ola AirPro (concept design)	0	0	1	1	1

#	Concept Aircraft	Embedded Fan	Ducted Fan	Manned	Unique Concept	Unique Organization
199	199. Orca Aerospace Orca eVTOL	0	0	1	1	1
200	200. Overair Butterfly (concept design)	0	0	1	0	1
201	201. Overair Butterfly (production model)	0	0	1	1	0
202	202. Paragon VTOL Aerospace Soar	1	1	1	1	1
203	203. Paragon VTOL Aerospace T21 Raptor (defunct)	1	1	1	1	0
204	204. Pantuo Aviation Pantala Concept H	1	1	1	1	1
205	205. Pantuo Aviation Demonstrator T1	1	1	1	1	0
206	206. PDRL AeroHans 2S	0	1	1	1	1
207	207. PDRL AeroHans 4S	0	1	1	1	0
208	208. Phractyl Macrobat	0	0	1	1	1
209	209. Plana CP-01	0	0	1	1	1
210	210. Porsche (unnamed)	1	1	1	1	1
211	211. PteroDynamics Transwing	0	0	1	1	1
212	212. Quaternion Group Compact Personal Aircraft	0	0	1	1	1
213	213. Ravatia Aerospace Unnamed Cargo Drone	0	0	0	1	1
214	214. Ray VTOL Aircraft	1	1	1	1	1
215	215. Robathan LVI eVTOL	0	1	1	1	1
216	216. Robathan Range Rover eVTOL	0	0	1	1	0
217	217. Robathon SAI eVTOL	0	0	1	1	0
218	218. Robathan SIH eVTOL	0	1	1	1	0
219	219. Robathan VEL eVTOL	0	1	1	1	0
220	220. Rolls-Royce EVTOL	0	0	1	1	1
221	221. Sabrewing Draco-2 (dormant)	0	1	1	1	1
222	222. Sabrewing Rhaegal	0	1	1	1	0
223	223. SASTRA University Mistral (concept design)	0	0	1	1	1
224	224. Scienex Flyter	0	0	1	1	1
225	225. Shaanxi Huayu Xianxiang Intelligent Technology Co Subscale Demonstrator	0	0	1	1	1
226	226. Sierra Technical Services Fledermauser FM1 (concept design)	0	1	1	0	1
227	227. Sierra Technical Services Fledermauser FM2 (concept design)	0	1	1	0	0
228	228. Sierra Technical Services Fledermauser FM3 (concept design)	0	1	1	1	0

#	Concept Aircraft	Embedded Fan	Ducted Fan	Manned	Unique Concept	Unique Organization
229	229. Sirrandalot Emerald Flyer	0	1	1	1	1
230	230. Sky Chaser (concept design)	0	0	1	0	1
231	231. Sky Chaser (technology demonstrator)	0	0	1	1	0
232	232. SkyBoom eVTOL Automobiles	0	0	1	1	1
233	233. Skyfly Technologies Axe	0	0	1	1	1
234	234. SKYLYS Aircraft AO	0	0	1	1	1
235	235. Skynet Project Genesys X-1	0	0	1	0	1
236	236. Skynet Project Genesys X-2	0	0	1	1	0
237	237. Smolensk Aviation Plant AeroTaxi	0	0	1	1	1
238	238. Smolensk Joint Development eVTOL	0	0	1	1	0
239	239. Streamlined Main Dynamics AAVa	0	1	1	1	1
240	240. Stuttgart Aerospace Apollo	0	1	1	1	1
241	241. Stuttgart Aerospace Eolos	0	1	1	1	0
242	242. Stuttgart Aerospace Eolos 1	0	1	1	0	0
243	243. Stuttgart Aerospace Eolos 2	0	1	1	1	0
244	244. Stuttgart Aerospace Parmenion	0	1	1	1	0
245	245. Stuttgart Aerospace VMax	0	1	1	1	0
246	246. Supernal (Hyundai) S-A1	0	0	1	1	1
247	247. Supervolant Pegasus	0	0	1	1	1
248	248. Tcab Tech E20	0	0	1	1	1
249	249. Terrafugia TF-2 Tiltrotor	0	0	1	1	1
250	250. Terrafugia TF-X	0	0	1	1	0
251	251. Textron eAviation Nexus (concept design)	0	0	1	1	1
252	252. Transcend Air Vy 400	0	0	1	1	1
253	253. Trek Aerospace Scorpion	0	1	1	1	1
254	254. Trek Aerospace Tern	0	1	1	1	0
255	255. Tupan Aircraft Tupan 1000	0	1	1	1	1
256	256. Turkey Demirkanat Helicopter Team (concept design)	0	1	1	1	1
257	257. Uber Elevate eCRM-001	0	0	1	1	1
258	258. Uber Elevate eCRM-004	0	0	1	1	0

#	Concept Aircraft	Embedded Fan	Ducted Fan	Manned	Unique Concept	Unique Organization
259	259. Umiles Next Concept Integrity	0	0	1	1	1
260	260. Umiles Next Integrity 3	0	0	1	1	0
261	261. University of Illinois Illini Air Shuttle	0	0	1	1	1
262	262. University of Maryland Starling (concept design)	0	0	1	1	1
263	263. VerdeGo Aero PAT200	0	0	1	1	1
264	264. Vertical Aerospace VX4 (production model)	0	0	1	1	1
265	265. VertiLectric Volpire GF	0	0	1	1	1
266	266. Vickers WAVE eVTOL	0	0	1	1	1
267	267. Vimana AAV	0	0	1	1	1
268	268. Vision VTOL	0	1	1	1	1
269	269. Volerian	1	1	1	1	1
270	270. Volerian Century	1	1	1	1	0
271	271. Volerian Cosmopolitan	0	1	1	1	0
272	272. Volerian Echo	1	1	1	1	0
273	273. Volerian Lander	1	1	1	1	0
274	274. Voyzon e-VOTO	1	1	1	1	1
275	275. VRCO NeoXCraft	0	1	1	1	1
276	276. Wisk Aero Generation 6	0	0	1	1	1
277	277. Xagon Solutions XC Heavy	0	1	1	1	1
278	278. Xeriant Halo	0	1	1	1	1
279	279. XTI Aircraft Trifan 200	1	1	1	0	1
280	280. XTI Aircraft Trifan 600	1	1	1	1	0
281	281. Yee Flying Car (concept design)	0	1	1	1	1
282	282. Zenith Altitude EOPA (defunct)	0	0	1	1	1
283	283. Zero Gravity ZG-T6	0	0	1	1	1
284	284. Zeva Z2	0	0	1	1	1
285	285. Zeva Zero	0	0	1	1	0
286	286. Zuri 2.0 (production model)	0	0	1	1	1
287	1. Aerofex Aero-X	0	1	1	1	1
288	2. Aerofex Aero-X Drone	0	1	0	1	0

#	Concept Aircraft	Embedded Fan	Ducted Fan	Manned	Unique Concept	Unique Organization
289	3. Aerofex Aero-X Motorcycle	0	1	1	1	0
290	4. Aerofex Aero-X Nautical	0	1	1	1	0
291	5. Aeroxo ERA Aviabike - I, II	0	1	1	1	0
292	6. Air Transportation Technology Catapult One - I, II	1	1	1	1	1
293	7. Airborne Motorworks AeroRunner	0	1	1	1	1
294	8. A.L.I. Technologies Hover Bike	1	1	1	1	1
295	9. A.L.I. Technologies XTURISMO	0	1	1	0	0
296	10. A.L.I. Technologies XTURISMO LE	0	1	1	1	0
297	11. Aliptera ADR-1 Dragon Rider	0	1	1	1	1
298	12. Ascend Dynamics SkyPak V1	0	0	1	0	1
299	13. Ascend Dynamics SkyPak V2	0	1	1	1	0
300	14. Ascend Dynamics SkyPak X1	0	1	1	1	0
301	15. Assen Aeronautics A1 Explorer (defunct)	0	1	1	0	1
302	16. Assen Aeronautics A2 Avenger	0	1	1	1	0
303	17. Athena Aero	1	1	1	1	1
304	18. Aviaereo Aereo-bee	0	0	1	1	1
305	19. Bay Zoltán Flike	1	1	1	0	1
306	20. Bay Zoltán Flike 2	0	0	1	1	0
307	21. Chatillon Haut QuadrAxes (concept design)	0	1	1	1	1
308	22. Chatillon Le Frelon V01 (concept design)	1	1	1	1	0
309	23. Chatillon MotoFly (concept design)	0	1	1	1	0
310	24. Chatillon NautiQuad (concept design)	0	1	1	1	0
311	25. Chatillon TriAxes (concept design)	0	1	1	1	0
312	26. Colin Furze Hoverbike	0	0	1	1	1
313	27. Concept Aircraft Aircycle	0	0	1	1	1
314	28. CopterPack CopterPack	0	1	1	1	1
315	29. DragonAir Airboard 1	0	0	1	0	1
316	30. DragonAir Airboard 2 - II	0	0	1	0	0
317	31. DragonAir Airboard 3	0	0	1	1	0
318	32. Edea 22/2 Squid – II	0	1	1	1	1

#	Concept Aircraft	Embedded Fan	Ducted Fan	Manned	Unique Concept	Unique Organization
319	33. Edea 22/3 Kamino – III	0	1	1	1	0
320	34. ElectraFly ElectraFlyer	0	0	1	1	1
321	35. Electric Jet Aircraft EJ-1B Jetpack (defunct)	0	1	1	0	1
322	36. Electric Jet Aircraft EJ-1H Jetpack	0	1	1	0	0
323	37. Electric Jet Aircraft EJ-1S Jetpack	0	1	1	1	0
324	38. Electric Jet Aircraft VertiCoupe	0	1	1	1	0
325	39. Electric Jet Aircraft VertiCycle	0	1	1	1	0
326	40. EosFlight (unnamed)	0	0	1	1	1
327	41. FanFlyer	0	1	1	1	1
328	42. FBike Flying Bike (technology demonstrator)	0	1	1	1	1
329	43. Flyt Aerospace FlytCycle	0	1	1	1	1
330	44. Georgia Tech HummingBuzz - I	0	1	1	1	1
331	45. Hero Flyer (Defunct)	0	0	1	1	1
332	46. Horus Hoverbike	0	1	1	1	1
333	47. Hover Drone Taxi R-1	0	0	1	1	1
334	48. Hover Scorpion	0	0	1	0	1
335	49. Hover Scorpion D	0	1	1	1	0
336	50. IO Aircraft Hornet	0	0	1	1	1
337	51. Innowings Aerospace PKOK	0	0	1	1	1
338	52. Innowings Aerospace (unnamed)	0	0	1	1	0
339	53. Jayu	0	0	1	1	1
340	54. Jetson ONE	0	0	1	1	1
341	55. Jetson Prototype	0	0	1	0	0
342	56. Jump Aero JA1 Pulse	0	0	1	1	1
343	57. Kalashnikov (unnamed)	0	0	1	1	1
344	58. Kitty Hawk Flyer (defunct prototype)	0	0	1	1	1
345	59. Kovacs Flike	1	1	1	1	1
346	60. Kovacs Racer I	1	1	1	0	0
347	61. Kovacs Racer II	1	1	1	1	0
348	62. Leap Vantage - I	0	0	1	1	1

#	Concept Aircraft	Embedded Fan	Ducted Fan	Manned	Unique Concept	Unique Organization
349	63. Lovenie Fly Kart	0	1	1	1	1
350	64. Malloy Aeronautics Hoverbike (defunct)	0	1	1	1	1
351	65. Micor Technologies Advanced Individual Backpack VTOL Aircraft (AIBVA)	0	1	1	1	1
352	66. Micor Technologies Advanced Individual Propellerpack VTOL Aircraft (AIPVA)	0	0	1	1	0
353	67. NASA Puffin	0	0	1	1	0
354	68. Neva Aerospace AirQuadOne	0	1	1	1	1
355	69. Omni Hoverboards Prototype 1	0	0	1	0	1
356	70. Omni Hoverboards Prototype 2	0	0	1	1	0
357	71. Opener Aero BlackFly V1	0	0	1	0	1
358	72. Opener Aero BlackFly V2	0	0	1	0	0
359	73. Opener Aero BlackFly V3	0	0	1	1	0
360	74. Penn State University Blue Sparrow - I	0	0	1	1	1
361	75. Raven - III	0	1	1	1	1
362	76. Ray Research Dart Flyer	0	1	1	1	1
363	77. rFlight rWing	0	1	1	0	1
364	78. rFlight N217RL	0	1	1	1	0
365	79. Ryerson (Helium Aero) Paragon – II, III	0	0	1	1	1
366	80. Scoop Pegasus 1 - I	0	0	1	1	1
367	81. Silverwing S1 - I, II	0	1	1	1	1
368	82. Skyflow	1	1	1	1	1
369	83. SkyKar Rebel	0	0	1	1	1
370	84. Subaru Land-and-Air	1	1	1	1	1
371	85. Talaria Hermes I	0	0	1	1	1
372	86. teTra 3 - I	0	1	1	1	1
373	87. Teledrone	0	0	1	1	1
374	88. Teledrone Mark I (defunct) – II	0	0	1	0	0
375	89. Teledrone Mark II (defunct) – III	0	0	1	0	0
376	90. Teledrone Mark III (defunct)	0	0	1	0	0
377	91. Teledrone Mark IV (defunct)	0	0	1	0	0
378	92. Teledrone Mark V (scale)	0	0	1	0	0

#	Concept Aircraft	Embedded Fan	Ducted Fan	Manned	Unique Concept	Unique Organization
379	93. Teledrone Mark VI (subscale demonstrator)	0	0	1	1	0
380	94. Texas A&M University Harmony - I, II	0	0	1	1	1
381	95. The Real Guys Flying Bathtub	0	0	1	1	1
382	96. ThrustCycle GyroDrone	0	1	1	1	1
383	97. Tianjin Banlan Aviation Technology Company eVTOL	0	0	1	1	1
384	98. Trek Aerospace Dragonfly	0	1	1	1	1
385	99. Trek Aerospace FlyKart 2 - I, II	1	1	1	1	0
386	100. Trek Aerospace SoloTrek XFVC	0	1	1	0	0
387	101. Trek Aerospace SoloTrek XFVM	0	1	1	1	0
388	102. Trek Aerospace Springtail	0	1	1	1	0
389	103. University of Kansas Mamba - I	1	1	1	1	1
390	104. V_Space V Speeder	0	0	1	0	1
391	105. V_Space V Speeder V2	0	0	1	0	0
392	106. V_Space V Speeder V3	0	0	1	1	0
393	107. WatFly Atlas - II	0	1	1	1	1
394	108. X-Aero X-Craft	0	0	1	1	1
395	109. XPeng AeroHT Magic Cloud (defunct)	0	0	1	1	1
396	110. XPeng AeroHT Sport (concept design)	0	0	1	1	0
397	1. Aergility Atlis Gen 1 (prototype)	0	0	1	0	1
398	2. Aergility Atlis Gen 2 (prototype)	0	0	1	0	0
399	3. Aergility Atlis Gen 3 (prototype)	0	0	1	1	0
400	4. Aerial Vehicle Automation Winged X8	0	0	0	1	1
401	5. Aerofugia Technology Co. Ltd. (Geely) Air Car (concept design)	0	0	1	1	1
402	6. Aerofugia Technology Co. Ltd. (Geely) TF-2	0	0	1	1	0
403	7. Aerofugia Technology Co. Ltd. (Geely) Transporter (concept design)	0	0	1	1	0
404	8. AeroMech Incorporated AM-20 (research eVTOL)	0	1	1	1	1
405	9. AeroMobil 5.0	0	0	1	1	1
406	10. Airbus CityAirbus NextGen (technology demonstrator)	0	0	1	1	0
407	11. ARC Aero Systems C-150 (production model)	0	0	0	1	1
408	12. ARC Aerosystems C-600 (production model)	0	0	0	1	0

#	Concept Aircraft	Embedded Fan	Ducted Fan	Manned	Unique Concept	Unique Organization
409	13. ARC Aerosystems Q-Starling (concept design)	1	1	1	1	0
410	14. Ascendance Flight Technologies ATEA (concept design)	1	1	1	0	1
411	15. Ascendance Flight Technologies ATEA (production aircraft)	1	1	1	1	0
412	16. Aurora Flight Sciences Pegasus PAV	0	0	1	1	1
413	17. Autoflight BAT600 (defunct)	0	0	1	1	1
414	18. Autoflight Prosperity I (V1500M)	0	0	1	1	0
415	19. Autoflight V400 Albatross	0	0	1	1	0
416	20. Autoflight V600 (prototype)	0	0	1	1	0
417	21. Autoflight V880CG (prototype)	0	0	1	1	0
418	22. Autoflight V1000	0	0	1	1	0
419	23. Autoflight V1200 (concept design)	0	0	1	1	0
420	24. Beta Technologies ALIA-250	0	0	1	1	0
421	25. Braunwagner SkyCab	0	1	1	1	1
422	26. CargoTron PD250	0	0	1	1	1
423	27. Central Aerohydrodynamic Institute ERA	0	1	1	1	1
424	28. Chatillon Drone Air Cargo (concept design)	0	0	1	1	1
425	29. Chatillon Jet (concept design)	1	1	1	1	0
426	30. Colugo Systems ARC 500	0	0	1	1	1
427	31. COMAC ET120	0	0	1	1	1
428	32. COMAC ET480	0	0	1	1	0
429	33. COMAC Tian Gong	0	0	1	1	0
430	34. Dahir Insaat Azur Rail	0	0	1	1	1
431	35. Dahir Insaat BleuClair Rail	0	0	1	1	0
432	36. Dahir Insaat Mauve Rail	0	0	1	1	0
433	37. Dahir Insaat Rouge Rail	0	1	1	1	0
434	38. Didia Scout (concept design)	0	1	1	1	1
435	39. Doroni Aerospace H1	1	1	1	1	1
436	40. Ecolibri	0	0	1	1	1
437	41. EHang VT-25	0	0	1	1	1
438	42. EHang VT-30	0	0	1	1	0

#	Concept Aircraft	Embedded Fan	Ducted Fan	Manned	Unique Concept	Unique Organization
439	43. Electrofluidsystems H2PlasmaRay 6.66	1	1	1	1	1
440	44. Elroy Air Chaparral (technology demonstrator)	0	0	1	1	1
441	45. Elroy Chaparral C1	0	0	1	1	0
442	46. eMagic Aircraft Copter (testbed)	0	0	1	0	1
443	47. eMagic Aircraft eMagic Next (production aircraft)	0	0	1	1	0
444	48. eMagic Aircraft eMagic One (demonstrator)	0	0	1	0	0
445	49. Eve Air Mobility Eve (military model)	0	1	1	1	1
446	50. Eve Air Mobility Eve (production model)	0	1	1	1	0
447	51. Eve Air Mobility Eve V2 (concept design)	0	1	1	0	0
448	52. Eve Air Mobility Eve V3 (concept design and formerly EmbraerX & DreamMaker)	0	1	1	0	0
449	53. ePlane Company e200	0	1	1	1	1
450	54. Esprit Aeronautics Heavy Lift Cargo Utility Platform	0	0	1	1	1
451	55. Esprit Aeronautics Lancer ePAV	0	0	1	1	0
452	56. Fei Peng FP-981C	0	0	1	1	1
453	57. Flexcraft Utility Concept	1	1	1	0	1
454	58. Flexcraft VERA II	0	0	1	1	1
455	59. Flyter PAC VTOL 420-120	0	0	1	1	1
456	60. Flyter PAC VTOL 720-200	0	0	1	1	0
457	61. Gadfin Spirit X	0	0	1	1	1
458	62. Georgia Institute of Technology Balto (concept design)	0	0	1	1	1
459	63. Gestalt Aeronauticals VTOL	1	1	1	1	1
460	64. Happy Takeoff CitiFlex (defunct)	0	0	1	0	1
461	65. Happy Takeoff Prism	0	0	1	1	0
462	66. Hi-Lite Lynx-us	0	0	1	1	1
463	67. Honda eVTOL	0	1	1	1	1
464	68. Horizon Aircraft Cavorite X5	1	1	1	1	1
465	69. Horyzn Aerospace Silencio Gamma	0	0	1	1	1
466	70. Hover Formula 2 Winged	1	1	1	1	1
467	71. Hover Formula 5	1	1	1	1	0
468	72. Hover Formula Subscale Prototype	0	1	1	1	0

#	Concept Aircraft	Embedded Fan	Ducted Fan	Manned	Unique Concept	Unique Organization
469	73. Ianis/Mansell Processor 007	1	1	1	1	1
470	74. Jetcopter VTOL Technologies SDR-500	1	1	1	1	1
471	75. Jetcopter VTOL Technologies Sky Force	1	1	1	1	0
472	76. Kaite-VTOL 100	1	1	1	1	1
473	77. Kaite-VTOL 500	1	1	1	1	0
474	78. Katla Aero Katla 700	0	0	1	1	1
475	79. Korea Aerospace Industries (KAI) Unnamed (concept design)	1	1	1	1	1
476	80. Korean Air KUS-VS	0	0	1	1	1
477	81. Leap Aeronautics	0	0	1	1	1
478	82. Leo Flight Corporation Leo Coupe	1	1	1	1	1
479	83. Leo Flight Corporation Lynx	1	1	1	1	0
480	84. Lyte Aviation LA-44 SkyBus	0	0	1	1	1
481	85. Micor Technologies Advanced Multi-Passenger UAM VTOL Aircraft (AMUVA)	0	1	1	1	1
482	86. Micor Technologies Advanced Vehicle VTOL Jet Aircraft (AVVJA)	0	1	1	1	0
483	87. Micor Technologies Advanced Vehicle VTOL Large Jet Aircraft (AVVLJA)	0	1	1	1	0
484	88. Micor Technologies Cargo AVU	0	0	1	1	0
485	89. MightyFly Cento (production model)	0	0	1	1	1
486	90. MightyFly MF-100 (production model)	0	0	1	1	0
487	91. Mojave Mystery eVTOL Aircraft A	0	0	1	1	1
488	92. MuYu eVTOL	0	0	1	1	1
489	93. Napoleon Aero VTOL	1	1	1	1	1
490	94. NEX Aero NEX	0	0	1	1	1
491	95. Packwing (Single Rotor)	1	1	1	0	1
492	96. Packwing (Twin Rotor)	1	1	1	1	0
493	97. Pegasus Universal Aerospace Vertical Business Jet	1	1	1	1	1
494	98. PFV Personal Flying Vehicle #1	1	1	1	1	1
495	99. Pipistrel Vertical Solutions 801 (concept design)	1	1	1	1	1
496	100. Pipistrel Vertical Solutions eVTOL (concept design)	1	1	1	0	0
497	101. Pipistrel Vertical Solutions Nuuva V300	0	0	1	1	0
498	102. Prime Design Consultancy Services Haricopter X1-Q	1	1	1	1	1

#	Concept Aircraft	Embedded Fan	Ducted Fan	Manned	Unique Concept	Unique Organization
499	103. Rensselaer Polytechnic Institute Oliwhoper (concept design)	0	0	1	1	1
500	104. Rosario Hyperlight Aeros	1	1	1	1	1
501	105. Sahand eVTOL Air Taxi	0	1	1	1	1
502	106. SpyDar Drakar	1	1	1	1	1
503	107. SpyDar M-Star	1	1	1	1	0
504	108. Swallow VTOL	0	1	1	1	1
505	109. Swallow VTOL - 3 thruster version	0	1	1	1	0
506	110. Talyn Air Unnamed	0	0	1	1	1
507	111. TechXGeek Marie	0	0	1	1	1
508	112. Terrafugia TF-2	0	0	1	0	1
509	113. Terrafugia TF-2.0 Lift + Push	0	0	1	0	0
510	114. Terrafugia TF-2A (demonstrator)	0	0	1	0	0
511	115. Terrafugia TF-2A (production aircraft)	0	0	1	1	0
512	116. teTra Aviation Mk-5	0	0	1	1	1
513	117. Toyota Cargo Drone	0	0	0	1	1
514	118. Trek Aerospace Tyrannos	1	1	1	1	1
515	119. Uber Elevate eCRM-002	0	0	1	1	0
516	120. Uber Elevate eCRM-003	0	0	1	1	0
517	121. Urban Aeronautics CityHawk	1	1	1	1	1
518	122. Vertaxi Matrix 1 (prototype)	0	0	1	1	1
519	123. Volant Aerotech VE25 X1 (technology demonstrator)	0	0	1	1	1
520	124. Volant Aerotech VT-25 Tiny (proof of concept)	0	0	1	0	0
521	125. Volkswagen Group China V.MO Flying Tiger (Prototype 1)	0	1	1	0	1
522	126. Volkswagen Group China V.MO Sky Garden (full scale mockup)	0	0	1	1	0
523	127. Volocopter VoloRegion	0	1	1	1	1
524	128. VOX Aircraft M400	1	1	1	1	1
525	129. VTOL Aviation Abhiyaan (concept design)	0	1	1	1	1
526	130. VTOL Aviation India Abhiyaan ENM800	0	0	1	0	1
527	131. VTOL Aviation India Abhiyaan ENU800	1	1	1	1	0
528	132. VTOL Aviation India Abhigyaan NX (mock-up)	0	0	1	1	0

#	Concept Aircraft	Embedded Fan	Ducted Fan	Manned	Unique Concept	Unique Organization
529	133. VTOL Aviation India Akshaj HNX150	0	0	1	1	0
530	134. VTOL Aviation India Akshansh HNX300	0	0	1	1	0
531	135. VTOL Aviation India Akshat HNX75	0	0	1	1	0
532	136. VTOL Aviation India Kirtiman HNM2500	0	0	1	1	0
533	137. WEFLY	0	0	1	1	1
534	138. Wisk Aero (formerly Zee Aero) POC (Generation 1)	0	0	1	0	1
535	139. Wisk Aero (formerly Zee Aero) Z-P1 (Generation 2)	0	0	1	0	0
536	140. Wisk Aero (formerly Zee Aero) Z-P2 (Generation 3)	0	0	1	0	0
537	141. Wisk Aero (formerly Kitty Hawk) Cora (Generation 4)	0	0	1	0	0
538	142. Wisk Aero Cora (Generation 5)	0	0	1	1	0
539	143. Zee Aero (now Wisk) Z-P2	0	0	1	1	1
540	144. Zero Gravity ZG-VC2	0	0	1	1	1
541	145. Zeva Aero Argon	0	0	1	1	1
542	146. Zuri (concept design)	0	0	1	0	1
543	147. Zuri (technology demonstrator)	0	0	1	1	0
544	1. 3D Molier Cargo Quadrocopter Drone (concept design)	0	1	1	1	1
545	2. Advanced Tactics AFRL Transformer	0	0	1	1	1
546	3. Advanced Tactics Black Knight Transformer	0	0	1	1	0
547	4. Advanced Tactics Transporter	0	0	1	1	0
548	5. Aeolus Aerospace Air Car	0	1	1	1	1
549	6. Aeras 51 (technology demonstrator)	0	0	1	1	1
550	7. Aerial Vehicle Automation X8	0	0	1	1	1
551	8. Aerodyne Group Vector (concept design)	0	1	1	1	1
552	9. Aerodyne Group Vector Concept (concept design)	0	1	1	1	1
553	10. Airborne Motorworks AeroRise	0	1	1	1	1
554	11. Airborne Motorworks Air Ambulance	0	1	1	1	0
555	12. Airborne Motorworks AirCommuter	0	1	1	1	0
556	13. Airborne Motorworks Genesis	1	1	1	1	0
557	14. Airborne Motorworks Grocery Drone	0	1	1	1	0
558	15. Airborne Motorworks Intermodal Drone	0	1	1	1	0

#	Concept Aircraft	Embedded Fan	Ducted Fan	Manned	Unique Concept	Unique Organization
559	16. Airborne Motorworks Phoenix	0	1	1	1	0
560	17. Airbus Helicopters CityAirbus (technology demonstrator)	0	1	1	1	1
561	18. AirCar (production model)	0	0	1	1	1
562	19. AirCar (concept design)	0	0	1	0	0
563	20. Airflight	0	1	1	1	1
564	21. Alaka'i Technologies Skai	0	0	1	1	1
565	22. Alauda Airspeeder Mk1	0	0	1	0	1
566	23. Alauda Airspeeder Mk2	0	0	1	0	0
567	24. Alauda Airspeeder Mk3	0	0	1	0	0
568	25. Alauda Airspeeder Mk4	0	0	1	1	0
569	26. Ambular Drone	0	0	0	1	1
570	27. Ambular Pod	0	0	0	1	0
571	28. Ambular 2.0	0	0	0	0	0
572	29. Ambular 3.0	0	0	1	0	0
573	30. Applied VTOL Concepts Epiphany™ FLYING CARpet	0	1	1	1	1
574	31. Astro Aerospace Alta	0	0	1	1	1
575	32. Astro Aerospace Elroy	0	0	1	1	0
576	33. AstroX Racer	0	0	1	1	1
577	34. Aura Aerospace Guardian 103 (prototype)	0	0	1	0	1
578	35. Aura Aerospace Guardian G1 (production model)	0	0	1	1	0
579	36. Aura Aerospace Guardian G2 (production model concept design)	0	0	1	0	0
580	37. Autoflight F240 Hot Wheels	0	0	1	1	1
581	38. Avianovations Hepard	1	1	1	1	1
582	39. Aviation and Space Technologies Yurik	0	0	1	1	1
583	40. AXIX SkyRider Horizon	0	0	1	1	1
584	41. Axix SkyRider SuvA	0	0	1	1	0
585	42. Baykar Cezeri	0	1	1	1	1
586	43. Bee Flights Bee-1	0	1	1	1	1
587	44. Boeing Cargo Aerial Vehicle	0	0	1	1	1

#	Concept Aircraft	Embedded Fan	Ducted Fan	Manned	Unique Concept	Unique Organization
588	45. B-Technology Beccarii	0	0	1	1	1
589	46. CAPS Concept Design	0	0	1	1	1
590	47. CAPS Production Aircraft	0	1	1	1	0
591	48. Cartivator SkyDrive (technology demonstrator)	0	1	1	1	1
592	49. Cartivator SkyDrive (concept design)	0	1	1	1	0
593	50. Central Aerohydrodynamic Institute Flying Taxi	0	0	1	1	1
594	51. chAIR Multicopter	0	0	1	1	1
595	52. Champagne and Ciprian Onyx eVTOL	0	1	1	1	1
596	53. Chatillon Gyrobulance (concept design)	0	1	1	1	1
597	54. Chatillon H10 EMS (concept design)	0	0	1	1	0
598	55. Chatillon HexaDeka (concept design)	0	1	1	1	0
599	56. Chatillon Livraison Express (cargo drone concept design)	0	0	1	1	0
600	57. Chatillon Mon Nouveau (concept design)	0	1	1	1	0
601	58. Chatillon Quadraxes Air Racer	0	0	1	1	0
602	59. Chatillon Rescq (concept design)	0	1	1	1	0
603	60. Chatillon Triton (series of concept design aircraft)	1	1	1	1	0
604	61. Chatillon Whisper (concept design)	0	0	1	1	0
605	62. CHRDI AVIC Sylan	0	0	1	1	1
606	63. CityJumper	0	0	1	1	1
607	64. Cognitive Bird HDP01	0	0	1	0	1
608	65. Cognitive Bird HDP02	0	0	1	0	0
609	66. Cognitive Bird HDP03	0	0	1	1	0
610	67. Dahir Insaat AzureQuad Rail	1	1	1	1	1
611	68. Dahir Insaat Fire Rescue	1	1	1	1	0
612	69. Dahir Insaat OrQuad Rail	0	1	1	1	0
613	70. Daymak Avvenire Skyrider	1	1	1	1	1
614	71. DaVinci Technology ZeroG (technology demonstrator)	0	0	1	0	1
615	72. DaVinci Technology ZeroG V1 (concept design)	0	1	1	0	0
616	73. DaVinci Technology ZeroG V2 (concept design)	0	1	1	0	0
617	74. DaVinci Technology ZeroG V3 (production model)	0	1	1	1	0

#	Concept Aircraft	Embedded Fan	Ducted Fan	Manned	Unique Concept	Unique Organization
618	75. Dekatone (unnamed)	1	1	1	1	1
619	76. Didia Combat Scout (concept design)	0	1	1	1	1
620	77. Didia Dragonfly (concept design)	0	1	1	1	0
621	78. Didia Monarch Flyer (concept design)	0	1	1	1	0
622	79. Doroni Aerospace Carbon One	0	1	1	1	1
623	80. Doroni Aerospace X8	1	1	1	1	0
624	81. Doroni Aerospace Yellowjacket Y6	0	1	1	1	0
625	82. Drone Champions Big Drone	0	0	1	1	1
626	83. EAC Whisper	0	0	1	1	1
627	84. EAM Hel eCrane	0	0	1	1	1
628	85. EFC iUFO	1	1	1	1	1
629	86. EHang 116 (production aircraft)	0	0	1	1	1
630	87. EHang 184 (defunct)	0	0	1	0	0
631	88. EHang 216 (production aircraft)	0	0	1	1	0
632	89. EHang 216L (logistics)	0	0	0	1	0
633	90. Electric Jet Aircraft VertiPod IV	0	0	0	1	1
634	91. Eve Air Mobility Eve V1 (concept design)	0	1	1	1	1
635	92. Event 38 Heavy-lift Drone	0	0	1	1	1
636	93. EXA Air Car	0	1	1	1	1
637	94. Flutr Motors Flutr	0	1	1	1	1
638	95. Frogs 282	0	0	1	1	1
639	96. Full Throttle Aerial Scorpion	0	0	1	1	1
640	97. Galvani Fly Citycopter (concept design)	0	1	1	1	1
641	98. Garudeus Aviation KiiRA	0	0	1	1	1
642	99. Gelisim University Tusi Technology Demonstrator	0	0	1	1	1
643	100. Gelisim University Tusi	0	0	1	1	1
644	101. Gizio EJ420 ElectroJet	0	0	1	1	1
645	102. Green Aerotechnics Research Institute Gatri	0	0	1	1	1
646	103. GroundAero Sport Utility Aircraft (defunct)	0	0	1	1	1
647	104. Guangzhou Automobile Group Gove (prototype)	0	0	1	1	1

#	Concept Aircraft	Embedded Fan	Ducted Fan	Manned	Unique Concept	Unique Organization
648	105. Hi-Fly Cargo	0	1	1	1	1
649	106. Hi-Fly S700	0	0	1	1	0
650	107. Hover Formula 2	1	1	1	1	1
651	108. Hover Formula 2 Prototype	0	1	1	0	0
652	109. Hover Scorpion Air Taxi	0	1	1	1	0
653	110. Hover Scorpion Cargo Drone	0	0	0	1	0
654	111. Imaginactive Ambular	0	1	1	1	1
655	112. International Aviation Center Begaero Technology Demonstrator	0	0	1	1	1
656	113. IO Aircraft Aelous	0	0	1	1	1
657	114. IO Aircraft BlackJack-E	0	1	1	0	0
658	115. IO Aircraft BlackJack-H	0	1	1	1	0
659	116. IO Aircraft BlackJack-T	0	1	1	1	0
660	117. IO Aircraft QC-1	0	1	1	1	0
661	118. IO Aircraft Skyline	0	1	1	0	0
662	119. IO Aircraft Skyline-H	0	1	1	1	0
663	120. Jetpack Aviation Blade Runner (defunct)	0	0	1	1	1
664	121. Kármán XK-1	0	1	1	1	1
665	122. Kenyan Passenger Drone	0	0	1	1	1
666	123. Kitty Hawk Flyer (defunct)	0	0	1	1	1
667	124. Kovacs Element Drone	0	1	0	1	1
668	125. Kovacs Heavy Duty Drone	0	1	0	1	0
669	126. Lazzarini FD-One	0	1	1	1	1
670	127. Lazzarini Hover Coupé	0	1	1	1	0
671	128. Lazzarini I.F.O.	1	1	1	1	0
672	129. Lazzarini Linux	0	1	1	1	0
673	130. Lazzarini Stratosfera	0	1	1	1	0
674	131. LIFT Aircraft HEXA	0	0	1	1	1
675	132. LIFT Aircraft HEXA Cargo	0	0	1	0	0
676	133. LIFT Aircraft HEXA EMS	0	0	1	0	0
677	134. LIFT Aircraft HEXA Fire	0	0	1	0	0

#	Concept Aircraft	Embedded Fan	Ducted Fan	Manned	Unique Concept	Unique Organization
678	135. LIFT Aircraft HEXA Military	0	0	1	0	0
679	136. LIFT Aircraft HEXA Police	0	0	1	0	0
680	137. LIFT Aircraft HEXA SAR	0	0	1	0	0
681	138. MACA Aviation & Aerospace 11	0	0	1	0	1
682	139. MACA Aviation & Aerospace S11	0	0	1	1	0
683	140. Malloy Aeronautics T150	0	0	1	1	1
684	141. Malloy Aeronautics T400	0	0	1	1	0
685	142. Malloy Aeronautics T650	0	0	1	1	0
686	143. ManDrone	0	0	0	1	1
687	144. Merk Heli T-Arrow (concept design)	1	1	1	1	1
688	145. Merk T Copter Car 8 (concept design)	0	1	1	1	0
689	146. Merk T Copter Car 25 (concept design)	0	1	1	1	0
690	147. Merk T Copter Voiture 44 (concept design)	0	1	1	1	0
691	148. Merk T Hover School Bus 02 (concept design)	0	1	1	1	0
692	149. Micor Technologies Advanced Vehicle VTOL Aircraft (AVVA)	0	1	1	1	1
693	150. Moog SureFly	0	0	1	1	1
694	151. My Flying Car	0	0	1	1	1
695	152. National Polytechnic Institute of Cambodia Human Carrier Drone	0	0	1	1	1
696	153. NEC Corporation eVTOL Testbed	0	1	1	1	1
697	154. Neo Aeronautics Crimson S8	0	0	1	0	1
698	155. Neo Aeronautics Crimson S8-SR	0	0	1	1	0
699	156. NeXt iFLY	0	1	1	1	1
700	157. NUS Snowstorm	0	0	1	1	1
701	158. OVER LLC	0	0	1	1	1
702	159. PAV-X PAV-UL Ultralight (defunct)	0	0	1	1	1
703	160. PAV-X (defunct)	0	0	1	1	0
704	161. Piasecki Air Scout	0	1	1	1	1
705	162. Ponti Design Studio Kite	0	1	1	1	1
706	163. Pop.Up Next	0	1	1	1	1
707	164. PR-DC Flying Car	1	1	1	1	1

#	Concept Aircraft	Embedded Fan	Ducted Fan	Manned	Unique Concept	Unique Organization
708	165. Prime Design Consultancy Services Haricopter X1-B	1	1	1	1	1
709	166. Renault AIR4	0	0	1	1	1
710	167. Rosario Vultran Tyger 1	0	1	1	1	1
711	168. Rotor X Dragon (production model)	0	0	1	1	1
712	169. Rotor X Dragon (prototype)	0	0	1	0	0
713	170. RYSE Aero Technologies Recon	0	0	1	1	1
714	171. Schumacher-Lehner PLC28 Chopper (concept design)	0	1	1	1	1
715	172. Shenzhen UFO Flying Saucer Technology UFO eVTOL	1	1	1	1	1
716	173. Star 8 Green ECAV 50 (cargo drone)	0	0	1	1	1
717	174. Star 8 Green ECAV 100 (cargo drone)	0	0	1	1	0
718	175. Star 8 Green ECAV 150 (cargo drone)	0	0	1	1	0
719	176. Star 8 Green EMAV-2 Flying Car	0	0	1	0	0
720	177. Star 8 Green EMAV-2 Flying Taxi	0	0	1	1	0
721	178. Star 8 Green EMAV-4 Flying Taxi	0	0	1	1	0
722	179. Star 8 Green EMAV Sports Flyer	0	0	1	1	0
723	180. Star 8 Green Hoverboard V1.0	0	0	1	0	0
724	181. Star 8 Green Hoverboard V2.0	0	0	1	1	0
725	182. Star 8 Green Koncepto Millenya	0	0	1	1	0
726	183. Star 8 Green Rescue Drone	0	0	0	1	0
727	184. Stuttgart Aerospace Cargo Box	0	0	1	1	1
728	185. Stuttgart Aerospace Hephestos	0	1	1	1	0
729	186. SkyDrive SD-01 (technology demonstrator)	0	1	1	0	1
730	187. SkyDrive SD-02 (technology demonstrator)	0	0	1	0	0
731	188. SkyDrive SD-03 (technology demonstrator)	0	0	1	0	0
732	189. SkyDrive SD-05 (production model)	0	0	1	1	0
733	190. SkyDrive SD-XX (concept design)	1	1	1	0	0
734	191. SkyDrive SKYDRIVE (production model)	0	0	1	1	0
735	192. SkyDrive SkyLift (cargo drone)	0	0	1	1	0
736	193. Skypod Aerospace Skypod	0	1	1	1	1
737	194. Sky-Hopper	0	0	1	1	1

#	Concept Aircraft	Embedded Fan	Ducted Fan	Manned	Unique Concept	Unique Organization
738	195. Swarm Multicopter	0	0	1	1	1
739	196. Trek Aerospace DuoTrek 1.0	0	1	1	0	1
740	197. Trek Aerospace DuoTrek 2.0	0	1	1	1	0
741	198. Trek Aerospace Mule	0	1	1	1	0
742	199. Trek Aerospace Nightingale	0	1	1	1	0
743	200. Trek Aerospace OAV-II	0	1	1	1	0
744	201. Turkish Technic Esinti	0	0	1	1	1
745	202. Umiles Next New Concept (prototype) - formerly Tecnalia	0	0	1	1	1
746	203. Uniqopter Inc. Uniqopter	0	1	1	1	1
747	204. Vadar X-H1	0	1	1	1	1
748	205. Varon V200	1	1	1	1	1
749	206. Varon V210	0	0	1	1	0
750	207. Vertical Aerospace VA-X1 (proof of concept)	0	1	1	0	1
751	208. Vertical Aerospace VA-X2 (prototype)	0	0	1	1	0
752	209. Vinata Aeromobility	0	0	1	1	1
753	210. Vinata Aeromobility Cargo Drone	0	0	1	1	0
754	211. Volocopter (e-volo) VC007 (defunct)	0	0	1	0	1
755	212. Volocopter (e-volo) VC1 (defunct)	0	0	1	0	0
756	213. Volocopter (e-volo) VC2 (defunct)	0	0	1	0	0
757	214. Volocopter (e-volo) VC100 (defunct)	0	0	1	0	0
758	215. Volocopter (e-volo) VC400 (defunct)	0	0	1	0	0
759	216. Volocopter (e-volo) uVC100 cargo (defunct)	0	0	1	0	0
760	217. Volocopter (e-volo) uVC200 cargo (defunct)	0	0	1	0	0
761	218. Volocopter (e-volo) uVC400 cargo (defunct)	0	0	1	0	0
762	219. Volocopter (e-volo) VC Evolution 1P (defunct)	0	0	1	0	0
763	220. Volocopter (e-volo) VC Evolution 2P (defunct)	0	0	1	0	0
764	221. Volocopter 2X	0	0	1	1	0
765	222. Volocopter VC200 (defunct)	0	0	1	0	0
766	223. Volocopter VoloCity	0	0	1	1	0
767	224. Volocopter VoloDrone	0	0	0	1	0

#	Concept Aircraft	Embedded Fan	Ducted Fan	Manned	Unique Concept	Unique Organization
768	225. Voltline Skyla (prototype)	0	0	1	0	1
769	226. Voltline Skyla_V1 (prototype)	0	0	1	0	0
770	227. Voltline Skyla_V2 (production aircraft)	0	0	1	1	0
771	228. Walliams Chitty Chitty Bang Bang	0	0	1	1	1
772	229. Weslax HyLift	0	0	1	1	1
773	230. Weslax HySky	0	0	1	1	0
774	231. Weslax Proof of Concept	0	0	1	0	0
775	232. XPeng AeroHT Air F1 (defunct)	0	0	1	1	1
776	233. XPeng AeroHT Cruiser (concept design)	0	0	1	1	0
777	234. XPeng AeroHT Flying Car (concept design)	0	0	1	1	0
778	235. XPeng AeroHT Skimmer (concept design)	0	0	1	1	0
779	236. XPeng AeroHT Snow Flyer (concept design)	0	0	1	1	0
780	237. XPeng AeroHT T1 (production model)	0	0	1	1	0
781	238. XPeng AeroHT Voyager X1 (production model)	0	0	1	0	0
782	239. XPeng AeroHT Voyager X2 (production model)	0	0	1	1	0
783	240. XPeng AeroHT X3 (prototype)	0	0	1	1	0
784	241. Zapata AirScooter	0	0	1	1	1
785	242. Zero Gravity ZG-ONE	0	0	1	1	1
786	243. Zhuhai Svffi Aviation SF-80 (cargo drone)	0	0	1	1	1
787	244. Zhuhai Svffi Aviation SF-DL-180 (production model)	0	0	1	1	0
788	245. Zhuhai Svffi Aviation SF-X8-F23K-75 (production model)	0	0	1	1	0
789	246. Zhuhai Svffi Aviation SVF-180 (production model)	0	0	1	1	0
790	1. Amo ZEROº (concept design)	0	0	1	1	1
791	2. ARC Aero Systems Linx P03	0	1	1	1	1
792	3. ARC Aerosystems Linx P9	0	0	1	1	0
793	4. Aquinea ENAC Volta	0	0	1	1	1
794	5. AutoGyro eCavalon	0	0	1	1	1
795	6. Aviation Artur Trendak T6 (prototype)	0	0	1	1	1
796	7. Carter Aviation Air Taxi (defunct)	0	0	1	1	1

#	Concept Aircraft	Embedded Fan	Ducted Fan	Manned	Unique Concept	Unique Organization
797	8. China Helicopter Research and Development Institute Electric Helicopter (CHRDI AVIC)	0	0	1	1	1
798	9. Composite-FX XE-Volt Mosquito (proof-of-concept)	0	0	1	1	1
799	10. CycloTech Compound Helicopter	0	0	1	1	1
800	11. EADS (Airbus) eCO2avia (mock-up)	0	0	1	1	1
801	12. Edea 22/4 REVTOL	0	0	1	1	1
802	13. eJet Aerospace GJet AEon	0	0	1	1	1
803	14. eJet Aerospace GJet Koan	0	0	1	1	0
804	15. FlyNow Aviation FlyNow PAV	0	0	1	1	1
805	16. Fraundorfer Aeronautics Tensor	0	0	1	1	1
806	17. Fraundorfer Aeronautics Tensor 600X	0	0	1	1	0
807	18. Hirobo Bit	0	0	1	1	1
808	19. Horizon AutoCopters Auto-Copter	0	0	1	1	1
809	20. Infinity Motions Electri-Copter 650 Impulse	0	0	1	1	1
810	21. Jaunt Air Mobility Journey	0	0	1	1	1
811	22. Jaunt Air Mobility MAV55	0	0	1	1	0
812	23. Kocyba Hummel	0	1	1	1	1
813	24. Liaoning General Aviation Academy HX1E Electric Helicopter	0	0	1	1	1
814	25. Luminati Aerospace XRON	0	0	1	1	1
815	26. Orlando Helicopter Airways electric S-52 (defunct)	0	0	1	1	1
816	27. PAL-V International Liberty	0	0	1	1	1
817	28. Pennsylvania State University MG-76 Catacopter (concept design)	0	0	1	1	1
818	29. Piasecki HAXEL (demonstrator)	0	0	1	1	1
819	30. Piasecki PA-890	0	0	1	1	0
820	31. Prades GyroBike	0	1	1	1	1
821	32. Prades GyroPack	0	1	1	1	0
822	33. Rotor X eTransporter	0	0	1	1	1
823	34. Rotor X eA600	0	0	1	1	0
824	35. Rotor X eJavelin	0	0	1	1	0
825	36. Sikorsky Firefly	0	0	1	1	1

#	Concept Aircraft	Embedded Fan	Ducted Fan	Manned	Unique Concept	Unique Organization
826	37. Sikorsky Aircraft Hybrid-Electric Demonstrator (HEX)	0	0	1	1	0
827	38. Sikorsky VERT	0	0	1	1	0
828	39. Stielau Electric Helicopter	0	0	1	1	1
829	40. Skyworks Aeronautics eGyro	0	0	1	1	1
830	41. Skyworks Aeronautics GyroLiner	0	0	1	1	0
831	42. Skyworks Aeronautics ScoutHawk	0	0	1	1	0
832	43. Skyworks Aeronautics Vertijet	0	0	1	1	0
833	44. Solution F Electric Helicopter	0	0	1	1	1
834	45. Tier 1 Engineering e-R44 1st Generation	0	0	1	0	1
835	46. Tier 1 Engineering e-R44 2nd Generation	0	0	1	0	0
836	47. Tier 1 Engineering e-R44 3rd Generation	0	0	1	1	0
837	48. UASystems eZELOS 300 POC	0	0	1	1	1
838	49. UASystems eZELOS Air Taxi	0	0	1	1	0
839	50. UASystems eZELOS Twin-Hybrid Air Taxi	0	1	1	1	0
840	51. UASystems eZELOS Twin-Hybrid Cargo	0	1	0	1	0
841	52. UAVOS SumoAir	0	1	1	1	1
842	53. University of Maryland Blitzen (concept design)	0	0	1	1	1
843	54. VEA Aviation PA-890	0	0	1	1	1
844	55. Vinati F-Helix	0	0	1	1	1
845	56. Wenzhou Duofu Aviation Industry Group Co. Pegasus	0	0	1	1	1
Total		**116**	**352**	**817**	**699**	**467**

7. APPENDIX B – PROOFS & DERIVATIONS

This Appendix details several derivations of important geometric and performance criteria about the FIW concept that has been excluded from the main text but supports the proposed methodology and may be used as additional guidance in the FIW conceptual design process.

7.1. Twin-Fan Ad/S_{max} Derivation for Basic Wing Planform Shapes of Varying AR

The following geometric derivations have been provided to prove the maximum twin-fan *Ad/S* and *AR* relationships between the basic wing planform shapes described by Figure 3.18. Assuming the aircraft is symmetrical from a top view across its butt line, the half-span disk-to-wing reference area ratio for a twin-fan configuration is the same as its full-span *Ad/S*. Therefore, to simplify things, the derivations below were first found using the half-span aspect ratio ($AR_{/2}$) and then converted to the full aspect ratio (*AR*) equations at the end.

7.1.1. Rectangular Wings

Consider the half-span rectangular wing planform of a twin-fan FIW aircraft that maximizes *Ad/S* and how the disk-to-wing area ratio changes visually with *AR* according to Figure 7.2.

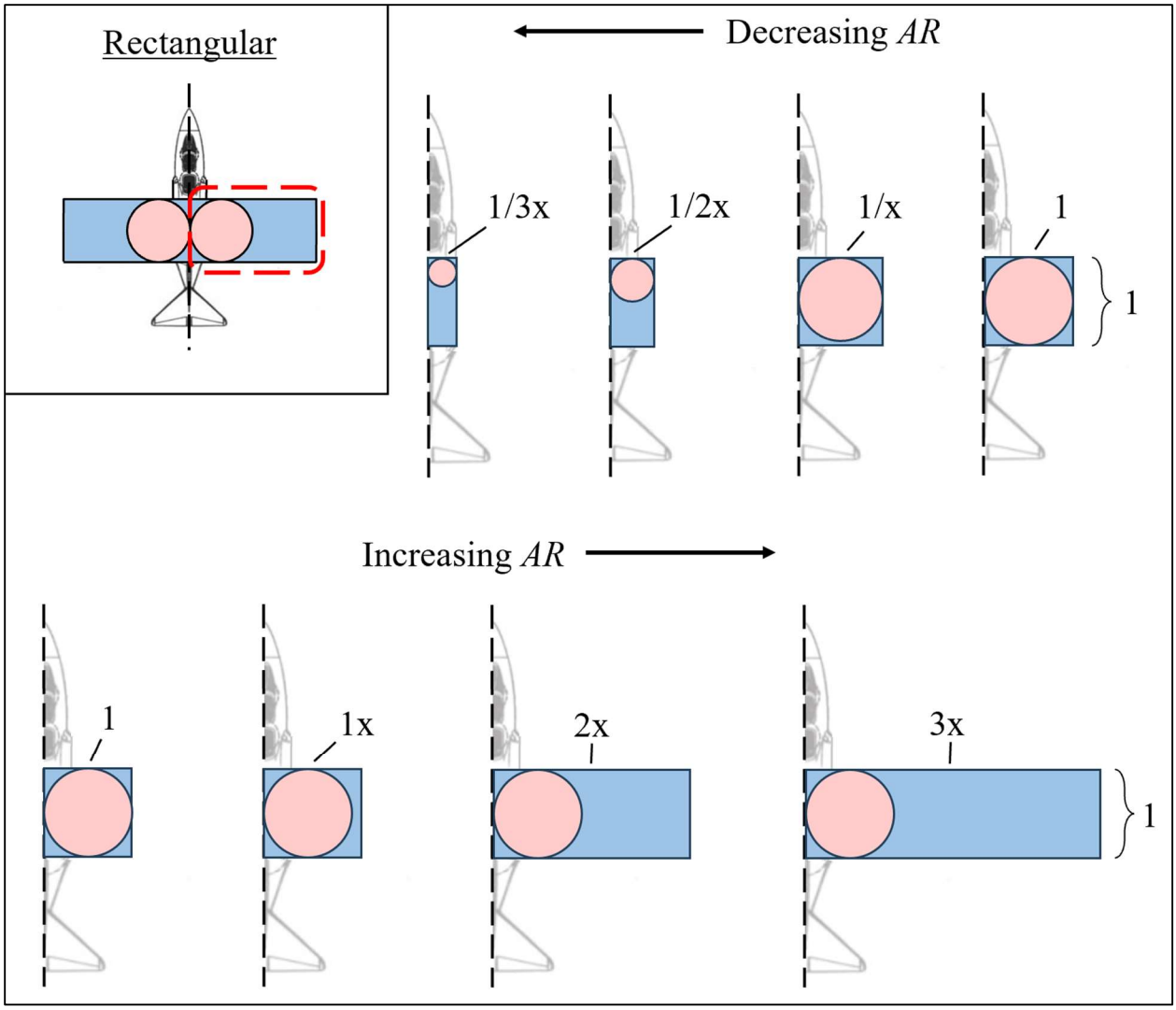

Figure 7.1 Changes in the half-span wing planform of a rectangular-shaped, twin-fan FIW configuration maximizing *Ad/S* as *AR* decreases and increases.

The relationship between the maximum *Ad/S* and $AR_{/2}$ of this rectangular wing planform can be quantified as follows:

1) Starting with the area for a circular disk:

$$Ad = \pi r^2 \tag{8.1}$$

2) Area of a rectangular half-wing, assuming the root chord side is *a* and semispan is *b*:

$$S = ab \tag{8.2}$$

3) Definition of aspect ratio for the rectangular half-wing planform:

$$AR_{/2} = \text{semispan}^2 / \text{area} = b^2 / ab = b / a \tag{8.3}$$

4) Find S as a function of the rectangular half-wing planform $AR_{/2}$ by substituting b for the span, S for the area, and rearranging:

$$S = b^2 / AR_{/2} \tag{8.4}$$

5) Divide Equation 8.1 by Equation 8.2 and simplify:

$$\frac{Ad}{S} = \frac{\pi r^2}{b^2} AR_{/2} \tag{8.5}$$

As shown by Figure 7.1, the maximum disk diameter that fits within the rectangular wing planform is always the same as at least one side length of the rectangle. In other words, the radius of $Ad_{\max}$ is always half the length of one of the rectangle's side lengths. When the rectangular half-wing has equal side lengths (square) so that $AR_{/2} = 1$, Ad/S is maximized at:

$$\left(\frac{Ad}{S}\right)_{\max} = \frac{\pi(1/2)^2(1)}{(1)^2} = \frac{\pi}{4} \quad (\text{for } AR_{/2} = 1) \tag{8.6}$$

When the semispan is shorter than the root chord ($AR_{/2} < 1$), the radius of $Ad_{\max}$ is half the semispan. Thus, Ad/S is maximized at:

$$\left(\frac{Ad}{S}\right)_{\max} = \frac{\pi(b/2)^2 AR_{/2}}{b^2} = \frac{\pi}{4} AR_{/2} \quad (\text{for } AR_{/2} < 1) \tag{8.7}$$

When the semispan is longer than the root chord ($AR_{/2} > 1$), the radius of $Ad_{\max}$ is half the root chord. Thus, Ad/S is maximized at:

$$\left(\frac{Ad}{S}\right)_{\max} = \frac{\pi(a/2)^2 AR_{/2}}{b^2} = \frac{\pi}{4} \frac{1}{AR_{/2}} \quad (\text{for } AR_{/2} > 1) \tag{8.8}$$

6) The full-wing equation can now be expressed by doubling the semispan aspect ratio, leading to the final result of Equation 3.5:

$$Ad / S_{\max} = \begin{cases} \frac{\pi}{2} AR & \text{if } AR < 1 \\ \frac{\pi}{4} & \text{if } AR = 1 \\ \frac{\pi}{8} \frac{1}{AR} & \text{if } AR > 1 \end{cases} \tag{3.5}$$

7.1.2.Triangular – Delta Wing

Consider the half-span rectangular wing planform of a twin-fan FIW aircraft that maximizes *Ad/S* and how the disk-to-wing area ratio changes visually with *AR* according to Figure 7.2.

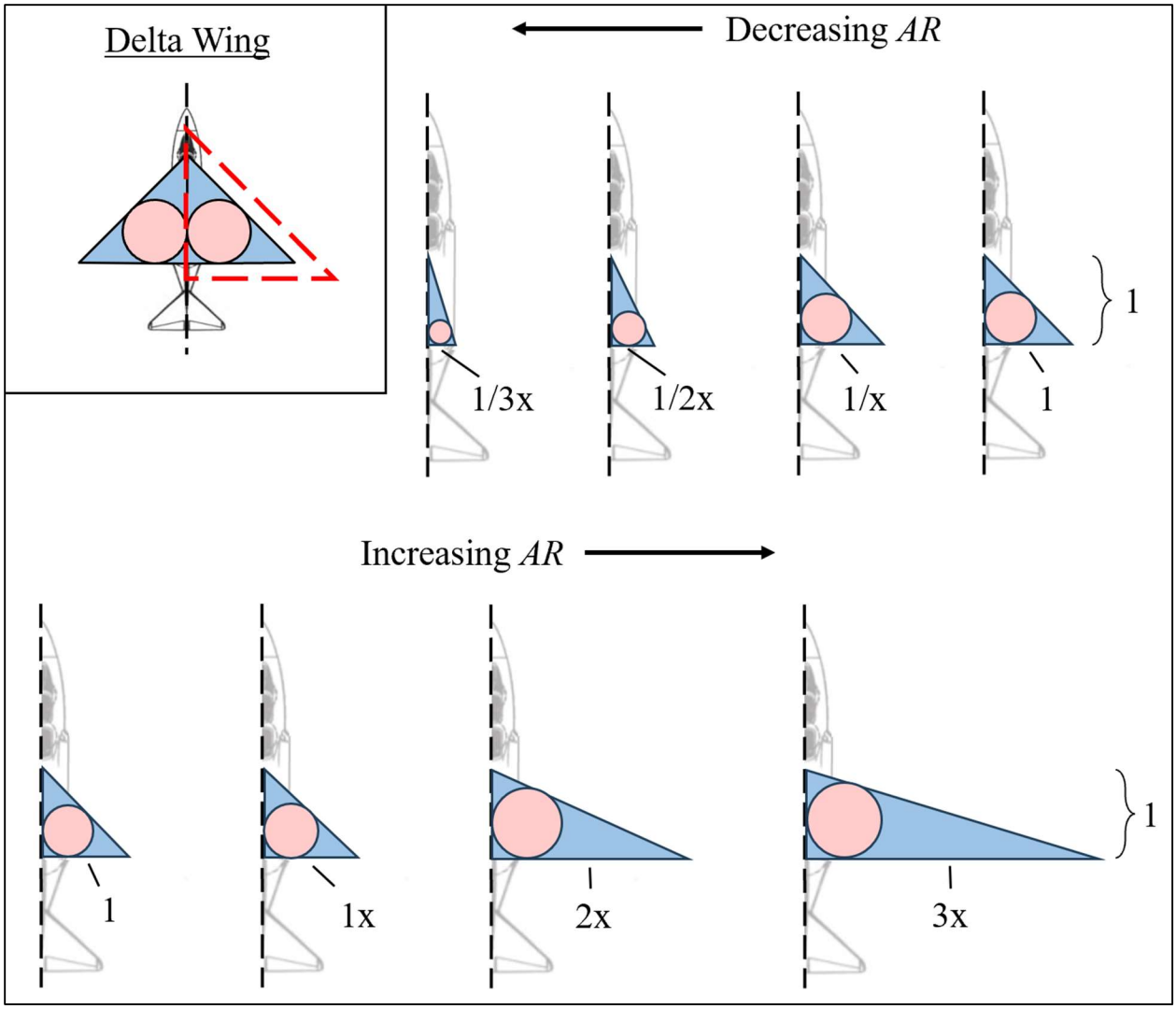

Figure 7.2 Changes in the half-span wing planform of a triangular, delta wing-shaped, twin-fan FIW configuration maximizing *Ad/S* as *AR* decreases and increases.

The relationship between the maximum *Ad/S* and $AR_{/2}$ of this triangular, delta wing planform can be quantified as follows:

1) Area of a triangular, delta half-wing, assuming the root chord length is *a* and semispan is *b*:

$$S = ab / 2 \tag{8.9}$$

2) Definition of aspect ratio for the triangular, delta half-wing planform:

$$AR_{/2} = \text{semispan}^2 / \text{area} = b^2 / (ab/2) = 2b/a \tag{8.10}$$

3) The general expression for Ad/S as a function of $AR_{/2}$ and the area for a circular disk are similar to the rectangular half-wing planform:

$$\frac{Ad}{S} = \frac{\pi r^2}{b^2} AR_{/2} \tag{8.11}$$

The radius of the largest disk that fits within any triangle is a geometric property called the inradius. The unknown inradius, in this case, can be resolved with the geometric relationship between the inradius and triangle area by the triangle's semiperimeter, s.

$$r = \frac{S}{s} \tag{8.12}$$

where:

$$s = \frac{1}{2}(a+b+c) \tag{8.13}$$

and a, b, and c are the triangle's side lengths, respectively. By combining Equations 8.12 and 8.13. and using Pythagorean's theorem to find c as a function of a and b, Equation 8.11 can be rewritten as:

$$\frac{Ad}{S} = \frac{\pi\left(\frac{ab}{\left(a+b+\sqrt{a^2+b^2}\right)}\right)^2}{b^2} AR_{/2}$$

which simplifies to:

$$\frac{Ad}{S} = \frac{\pi a^2}{\left(a+b+\sqrt{a^2+b^2}\right)^2} AR_{/2} \tag{8.14}$$

When the semispan and root chord of the triangular, delta half-wing are equal so that $a = b$ and $AR_{/2} = 2$, Ad/S is maximized at:

$$\frac{Ad}{S}_{\max} = \frac{\pi b^2}{\left(b + b + \sqrt{b^2 + b^2}\right)^2}(2) = \frac{\pi}{3 + \left(\sqrt{2}\right)^3} \quad (\text{for } AR_{/2} = 2) \tag{8.15}$$

For all other $AR_{/2}$ values, Equation 8.14 can be rearranged using Equation 8.10 to produce Equation 8.16:

$$\frac{Ad}{S}_{\max} = \frac{4\pi AR_{/2}}{\left(\sqrt{AR_{/2}{}^2 + 4} + AR_{/2} + 2\right)^2} \tag{8.16}$$

The full-wing equation can now be expressed by doubling the aspect ratio, leading to the final result of Equation 3.6:

$$Ad/S_{\max} = \frac{2\pi AR}{\left(\sqrt{AR^2 + 1} + AR + 1\right)^2} \tag{3.6}$$

7.1.3.Elliptical

Consider the half-span elliptical wing planform of a twin-fan FIW aircraft that maximizes *Ad/S* and how the disk-to-wing area ratio changes visually with *AR* according to Figure 7.3.

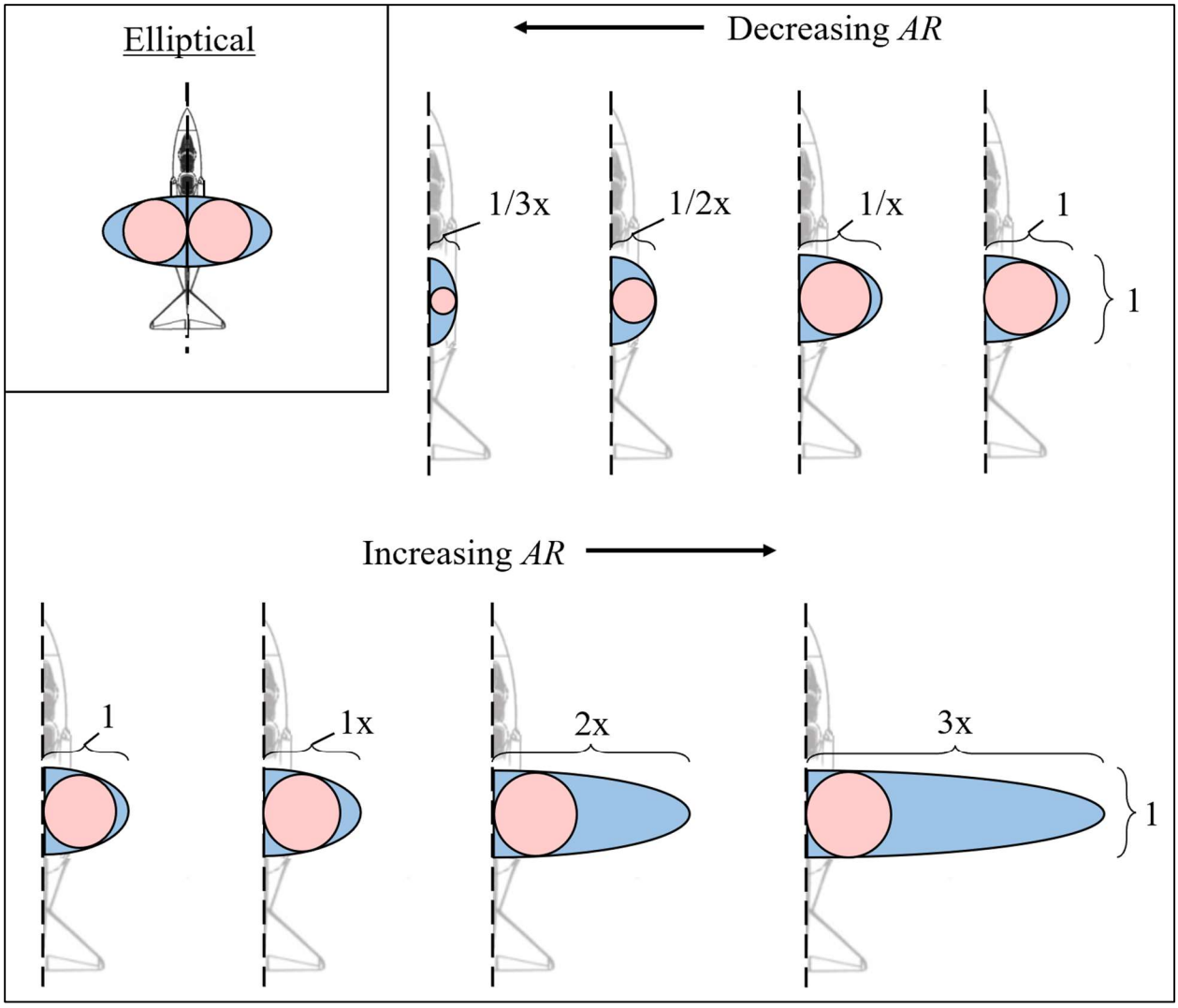

Figure 7.3 Changes in the half-span wing planform of a triangular, delta wing-shaped, twin-fan FIW configuration maximizing *Ad/S* as *AR* decreases and increases.

The relationship between the maximum *Ad/S* and $AR_{/2}$ of this elliptical wing planform can be quantified as follows:

1) Area of an elliptical half-wing, assuming the root chord length (semi minor length) is $2a$ and semispan (semi major length) is b:

$$S = \pi ab / 2 \tag{8.17}$$

2) Definition of aspect ratio for the elliptical half-wing planform:

$$AR_{/2} = \text{semispan}^2 / \text{area} = b^2 / (\pi ab / 2) = 2b / \pi a \tag{8.18}$$

3) The general expression for Ad/S as a function of $AR_{/2}$ and the area for a circular disk are similar to the rectangular half-wing planform:

$$\frac{Ad}{S} = \frac{\pi r^2}{b^2} AR_{/2} \tag{8.19}$$

Note that in Figure 7.3, there is a crossover point where the perimeter of the maximum disk inscribed in the ellipse half-wing goes from coinciding with two points on the ellipse perimeter to just one. This is due to the differences in curvature. Because of this effect, the two different cases can be treated separately. In the first case where the largest inscribed disk intersects two points on the ellipse, the radius of maximum disk area can be found by combining the following line equations for an ellipse (Equation 8.20) and a circle (Equation 8.21) described below as functions of cartesian coordinates x and y:

$$b^2 y^2 + a^2 x^2 = a^2 b^2 \tag{8.20}$$

$$x^2 + b^2 y^2 = a^2 b^2 \tag{8.21}$$

By solving both equations for x and setting them equal to each other, one will find that the result produces a quadratic formula with the variable y. By taking the determinant of this equation, what is left is just the inner disk radius as a function of ellipse parameters a and b:

$$r^2 = a^2 - \frac{a^4}{b^2} \tag{8.22}$$

By plugging Equation 8.22 back into Equation 8.19 and simplifying with the use of Equation 8.18, the maximum Ad/S for which the inscribed circle intersects two points on the ellipse is given below:

$$\frac{Ad}{S}_{\max} = \left(\frac{4}{\pi AR_{/2}}\right)\left(1-\left(\frac{2}{\pi AR_{/2}}\right)^2\right) \tag{8.23}$$

The second case, where the inscribed disk only intersects one point on the ellipse, is simpler, because this point occurs at the very tip of the ellipse. This means the diameter of the circle must be the same length as the semispan. Accordingly, the *Ad/S* in this case simply becomes:

$$\frac{Ad}{S}_{\max} = \frac{\pi}{4} AR_{/2} \tag{8.24}$$

The transition point between the two has not been derived herein but is proven to be around a semispan $AR_{/2}$ of around 0.897. Doubling this value for the full-wing equations ordinarily results in a value of 1.794. The full-wing equation can now be expressed by doubling the aspect ratio in Equations 8.23 and 8.24 as well, leading to the final result of Equation 3.6:

$$Ad/S_{\max} = \begin{cases} \dfrac{\pi}{2} AR & \text{if } AR \le 1.794 \\ \dfrac{2}{\pi AR}\left(1-\left(\dfrac{1}{\pi AR}\right)^2\right) & \text{if } AR > 1.794 \end{cases} \tag{3.7}$$

7.2. Derivation of Airplane Power Required as a Function of Wing Area

1) Starting with the cruise power required for an airplane, from [105]:

$$P_c = P_i + P_p = \frac{2}{\rho\pi e}\left(\frac{W}{b}\right)^2\left(\frac{1}{V}\right) + \frac{1}{V}\rho V^3 f \tag{8.25}$$

2) Replace *b* and *f* with equivalent terms involving wing reference area from [105]:

$$P_c = \frac{2W^2}{\rho\pi eV(AR)S} + \frac{1}{2}\rho V^3\left(C_F\left(\frac{S_w}{S}\right)S\right) \tag{8.26}$$

3) Rearrange terms:

$$P_c = \frac{2W^2}{\rho \pi e V (AR) S} + \frac{C_F \rho V^3}{2}\left(\frac{S_w}{S}\right) S \tag{8.27}$$

4) Simplify by forming constant coefficients **a** and **b**:

$$P_c = \frac{a}{S} + bS \tag{8.28}$$

where:

$$a = \frac{2W^2}{\rho \pi e V (AR)},\ \text{b} = \frac{C_F \rho V^3}{2}\left(\frac{S_w}{S}\right)$$

Graphical form of equation:

$$y = \frac{a}{x} + bx \tag{8.29}$$

According to the equation above, the wing area required for minimum cruise power occurs where $dPc/dS = 0$.

5) Take the first derivative of P_c with respect to S, set the expression equal to zero, and simplify:

$$\frac{dP_c}{dS} = 0 \tag{8.30}$$

$$\left[P_c\right]\frac{dP_c}{dS} = \left[\frac{a}{S} + bS\right]\frac{dP_c}{dS} = 0$$

$$\left[b - \frac{a}{S^2}\right] = 0$$

$$S = \sqrt{\frac{a}{b}} \tag{8.31}$$

6) Substitute *a* & *b*:

$$S = \sqrt{\frac{a}{b}} = \sqrt{\frac{\frac{2W^2}{\rho \pi e V (AR)}}{\frac{C_F \rho V^3}{2}\left(\frac{S_w}{S}\right)}} \tag{8.32}$$

7) Reduce to simplest expression:

$$S = \sqrt{\frac{4W^2}{\rho^2 \pi C_F e V^4 (AR)\left(\frac{S_w}{S}\right)}}$$

$$S = \frac{2W}{\rho V^2}\sqrt{\frac{1}{\pi C_F e (AR)\left(\frac{S_w}{S}\right)}} \tag{3.25}$$

7.3. Derivation of Range as a Function of Wing Reference Area

7.3.1. *R(S)*, Assuming Fuselage Scales with Wing Area

Fixed assumptions (constants):

- V – cruise speed
- ρ_0 – beginning-of-cruise density (altitude) for cruise-climb range
- AR – aspect ratio
- e – oswald's efficiency factor
- c_t – TSFC
- W_0 – beginning-of-cruise weight
- W_1 – end-of-cruise weight
- C_{fe} – equivalent skin friction coefficient (neglecting Reynold's number effects)
- $\frac{S_w}{S}$ – total wetted area to wing reference area ratio
    - (must be constant to assume fuselage scales with wing area)

1) Starting with the 3D drag coefficient:

$$C_D = C_{D0} + kC_L{}^2 + \frac{C_L{}^2}{\pi (AR)}(1+\delta) \tag{8.26}$$

Note, spanwise efficiency: $e = \frac{1}{(1+\delta)}$

2) Factor out $C_L{}^2$:

$$C_D = C_{D0} + \left(\frac{k(AR)\pi + 1 + \delta}{\pi(AR)} \right) C_L{}^2 \tag{8.27}$$

3) Substitute Oswald's efficiency factor: $e = \frac{1}{1+\delta+k(AR)\pi}$

$$C_D = C_{D0} + \frac{C_L{}^2}{\pi(AR)e} \tag{8.28}$$

4) Substitute induced lift coefficient: $K = \frac{1}{\pi(AR)e}$

$$C_D = C_{D0} + KC_L{}^2 \tag{8.29}$$

5) Expand zero-lift drag coefficient: $C_{D0} = C_{fe}\frac{S_w}{S} + C_{Dmisc.} + C_{D\,L+P}$

$$C_D = \left(C_{fe}\frac{S_w}{S} + C_{Dmisc} + C_{D\,L+P} \right) + KC_L{}^2 \tag{8.30}$$

6) Neglect form, interference, miscellaneous, and L&P drag at high subsonic cruise speed as small contributions to total parasite drag, indicated by Figure 3.29. Assume wave drag also negligible. Reduce and simplify final expression for drag coefficient:

$$C_D = C_{fe}\frac{S_w}{S} + KC_L{}^2 \tag{8.31}$$

In the case where the fuselage is assumed to scale with the wings, the ratio between aircraft's total wetted area and wing reference area remains constant. Therefore, if an average overall C_{fe} is assumed, the entire C_{D0} term becomes constant, and Equation 3.31 reduces back the form presented by Equation 3.29.

7) Introduce Breguet (Jet Range) Equation:

$$R = \frac{1}{c_t} V \frac{C_L}{C_D} \ln\left|\frac{W_0}{W_1}\right| \tag{8.32}$$

8) Expand: $V = \sqrt{\frac{2W_0}{\rho_0 S C_L}}$

$$R = \frac{1}{c_t} \sqrt{\frac{2W_0}{\rho_0 S C_L}} \frac{C_L}{C_D} \ln\left|\frac{W_0}{W_1}\right| \tag{8.33}$$

9) Factor out C_L:

$$R = \frac{1}{c_t} \sqrt{\frac{2W_0}{\rho_0 C_L}} \frac{\left(C_L\right)^{0.5}}{C_D} \ln\left|\frac{W_0}{W_1}\right| \tag{8.34}$$

10) Expand: $C_D = C_{D0} + K{C_L}^2$

$$R = \frac{1}{c_t} \sqrt{\frac{2W_0}{\rho_0 S}} \frac{\sqrt{C_L}}{C_{D0} + K{C_L}^2} \ln\left|\frac{W_0}{W_1}\right| \tag{8.35}$$

11) Expand: $C_L = \frac{2W_0}{\rho_0 S V^2}$

$$R = \frac{1}{c_t} \sqrt{\frac{2W_0}{\rho_0 S}} \frac{\sqrt{\frac{2W_0}{\rho_0 S V^2}}}{C_{D0} + K\left(\frac{2W_0}{\rho_0 S V^2}\right)^2} \ln\left|\frac{W_0}{W_1}\right| \tag{8.36}$$

12) Reduce like terms:

$$R = \frac{1}{c_t V} \left(\frac{2W_0}{\rho_0 S}\right) \frac{1}{C_{D0} + K\left(\frac{4{W_0}^2}{{\rho_0}^2 S^2 V^4}\right)} \ln\left|\frac{W_0}{W_1}\right| \tag{8.37}$$

13) Distribute $\left(\frac{2W_0}{\rho_0 S}\right)$:

$$R = \frac{1}{c_t V} \frac{1}{C_{D0}\left(\frac{\rho_0 S}{2W_0}\right) + K\left(\frac{2W_0}{\rho_0 S V^4}\right)} \ln\left|\frac{W_0}{W_1}\right| \tag{8.37}$$

14) Distribute $\left(\frac{1}{V}\right)$:

$$R = \frac{1}{c_t\left(C_{D0}\left(\frac{\rho_0 VS}{2W_0}\right) + K\left(\frac{2W_0}{\rho_0 SV^3}\right)\right)} \ln\left|\frac{W_0}{W_1}\right|$$

$$R = \frac{\ln\left|\frac{W_0}{W_1}\right|}{c_t\left(C_{D0}\left(\frac{\rho_0 VS}{2W_0}\right) + K\left(\frac{2W_0}{\rho_0 SV^3}\right)\right)} \tag{8.38}$$

15) Simplify by forming constant coefficients **a**, **b**, & **c**:

$$R = \frac{a}{\left(bS + \frac{c}{S}\right)} \tag{8.39}$$

where:

$$a = \ln\left|\frac{W_0}{W_1}\right|, \quad b = c_t C_{D0}\left(\frac{\rho_0 V}{2W_0}\right), \quad c = c_t K\left(\frac{2W_0}{\rho_0 V^3}\right)$$

Graphical form of equation:

$$y = \frac{a}{\left(bx + \frac{c}{x}\right)} \tag{8.40}$$

Wing area required for maximum range occurs were dR/dS = 0:

$$\frac{dR}{dS} = 0 \tag{8.40}$$

$$\frac{dR}{dS}[R] = \frac{dR}{dS}\left[\frac{a}{\left(bS + \frac{c}{S}\right)}\right] = 0$$

$$-\frac{a\left(b-\frac{c}{S^2}\right)}{\left(bS+\frac{c}{S}\right)^2}=0$$

$$S=\sqrt{\frac{c}{b}} \tag{8.41}$$

16) Substitute c & b:

$$R=\sqrt{\frac{c}{b}}=\sqrt{\frac{c_t K\left(\frac{2W_0}{\rho_0 V^3}\right)}{c_t C_{D0}\left(\frac{\rho_0 V}{2W_0}\right)}} \tag{8.42}$$

17) Reduce to simplest expression:

$$S=\sqrt{\frac{K\left(\frac{4W_0{}^2}{\rho_0{}^2 V^4}\right)}{C_{D0}}}$$

$$S=\frac{2W_0}{\rho_0 V^2}\sqrt{\frac{K}{C_{D0}}} \tag{8.43}$$

Using the following constants…

- $V = 400$ kts
- Cruise-climb starting at h_0 = 30k ft ($\rho_0 = 8.91 \times 10^{-4}$slug/ft^3)
- AR = 8.33
- e = 0.8
- c_t = 0.69 lb/lb/hr
- W_0 = 10,000 lb
- W_1/W_0 = 0.967
    - For W_0 = 10,000 lb… W_1 = 9,670 lb. (330 lb. fuel for cruise)
- C_{fe} = 0.0042
- $\frac{S_w}{S}$ = 4

Plot $R = f(S)$:

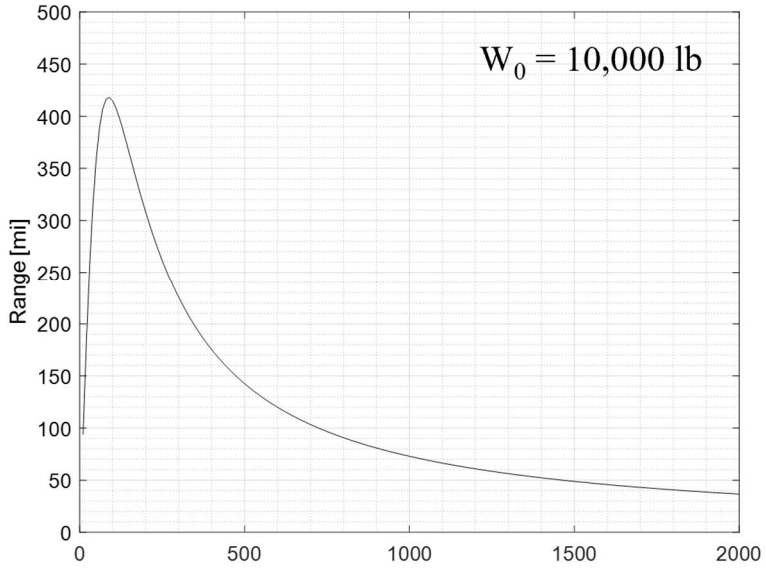

Plot $R = f(S)$ *varying* W_0:

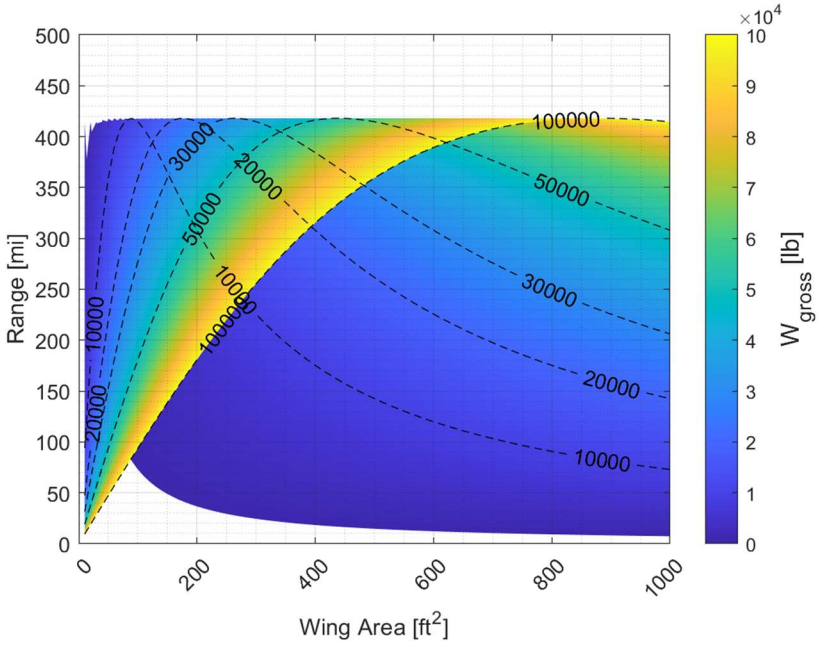

Plot $R = f(S)$ along with L/D to see what L/D maximizes range:

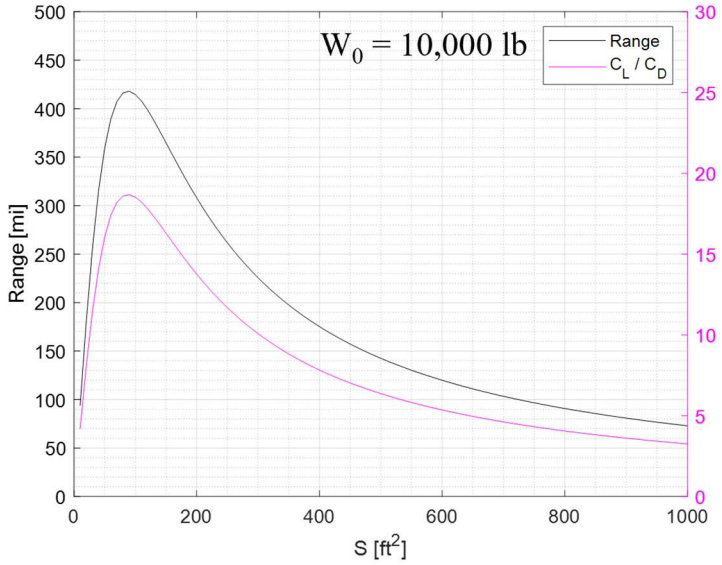

It appears $R = f(S)$ is maximized at L/D_{max}. This is different from the maximum jet range as a function of airspeed, $R = f(V)$, which is maximized at $L^{0.5}/D$

Range vs. Wing Area and Airspeed:

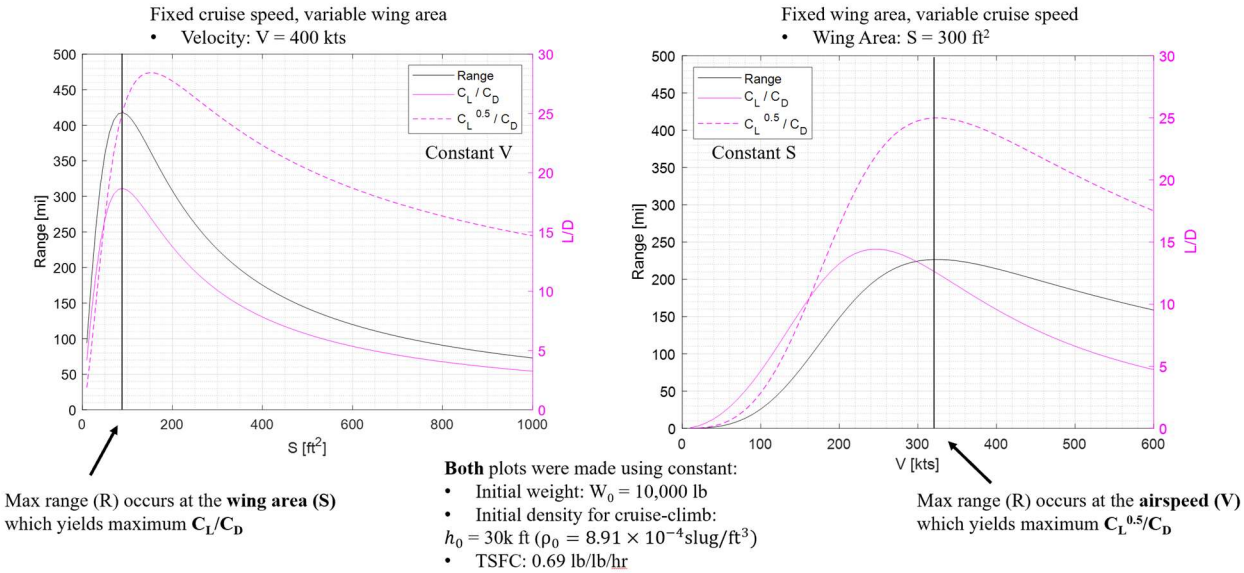

(Proof on next page)

R(S)

$$R = \frac{\ln\left|\frac{W_0}{W_1}\right|}{c_t\left(C_{D0}\left(\frac{\rho_0 SV}{2W_0}\right)+K\left(\frac{2W_0}{\rho_0 SV^3}\right)\right)}$$

Simplify by forming coefficients **a**, **b**, & **c**:

$R = \frac{\boldsymbol{a}}{\left(\boldsymbol{b}S+\frac{\boldsymbol{c}}{S}\right)}$, where: $\boldsymbol{a} = \ln\left|\frac{W_0}{W_1}\right|$,

$\boldsymbol{b} = c_t C_{D0}\left(\frac{\rho_0 V}{2W_0}\right), \boldsymbol{c} = c_t K\left(\frac{2W_0}{\rho_0 V^3}\right)$

Wing area required for maximum range occurs where dR/dS = 0:

$$\frac{dR}{dS}[R] = \frac{dR}{dS}\left[\frac{\boldsymbol{a}}{\left(\boldsymbol{b}S+\frac{\boldsymbol{c}}{S}\right)}\right] = 0$$

$$-\frac{\boldsymbol{a}\left(\boldsymbol{b}-\frac{\boldsymbol{c}}{S^2}\right)}{\left(\boldsymbol{b}S+\frac{\boldsymbol{c}}{S}\right)^2} = 0$$

$$S = \sqrt{\frac{\boldsymbol{c}}{\boldsymbol{b}}}$$

Substitute c & b:

$$S = \sqrt{\frac{\boldsymbol{c}}{\boldsymbol{b}}} = \sqrt{\frac{c_t K\left(\frac{2W_0}{\rho_0 V^3}\right)}{c_t C_{D0}\left(\frac{\rho_0 V}{2W_0}\right)}}$$

Reduce to simplest expression:

$$S = \sqrt{\frac{K\left(\frac{4{W_0}^2}{\rho_0{}^2 V^4}\right)}{C_{D0}}}$$

$$S = \frac{2W_0}{\rho_0 V^2}\sqrt{\frac{K}{C_{D0}}}$$

C_L for maximum range:

$$C_L = \sqrt{\frac{C_{D0}}{K}}$$

R(V)

$$R = \frac{\ln\left|\frac{W_0}{W_1}\right|}{c_t\left(C_{D0}\left(\frac{\rho_0 SV}{2W_0}\right)+K\left(\frac{2W_0}{\rho_0 SV^3}\right)\right)}$$

Simplify by forming coefficients **a**, **b**, & **c**:

$R = \frac{\boldsymbol{a}}{\left(\boldsymbol{b}V+\frac{\boldsymbol{c}}{V^3}\right)}$, where: $\boldsymbol{a} = \ln\left|\frac{W_0}{W_1}\right|$,

$\boldsymbol{b} = c_t C_{D0}\left(\frac{\rho_0 S}{2W_0}\right), \boldsymbol{c} = c_t K\left(\frac{2W_0}{\rho_0 S}\right)$

Airspeed required for maximum range occurs where dR/dS = 0:

$$\frac{dR}{dS}[R] = \frac{dR}{dS}\left[\frac{\boldsymbol{a}}{\left(\boldsymbol{b}S+\frac{\boldsymbol{c}}{S}\right)}\right] = 0$$

$$-\frac{\boldsymbol{a}\left(\boldsymbol{b}-\frac{3\boldsymbol{c}}{V^4}\right)}{\left(\boldsymbol{b}V+\frac{\boldsymbol{c}}{V^3}\right)^2} = 0$$

$$V = \sqrt[4]{\frac{3\boldsymbol{c}}{\boldsymbol{b}}}$$

Substitute c & b:

$$V = \sqrt[4]{\frac{3\boldsymbol{c}}{\boldsymbol{b}}} = \sqrt[4]{\frac{3c_t K\left(\frac{2W_0}{\rho_0 S}\right)}{c_t C_{D0}\left(\frac{\rho_0 S}{2W_0}\right)}}$$

Reduce to simplest expression:

$$V = \sqrt[4]{\frac{3K\left(\frac{4{W_0}^2}{\rho_0{}^2 S^2}\right)}{C_{D0}}}$$

$$V = \sqrt{\frac{2W_0}{\rho_0 S}\sqrt{\frac{3K}{C_{D0}}}}$$ Raymer (Eq. 17.25)

C_L for maximum range:

$$C_L = \sqrt{\frac{C_{D0}}{3K}}$$ Raymer (Eq. 17.26)

7.3.2. *R(S),* Assuming Fuselage Does Not Scale with Wing Area

Fixed assumptions (constants):

- V – cruise speed
- ρ_0 – beginning-of-cruise density (altitude) for cruise-climb range
- AR – aspect ratio
- e – oswald's efficiency factor
- c_t – TSFC
- W_0 – beginning-of-cruise weight
- W_1 – end-of-cruise weight
- C_{fe} – equivalent skin friction coefficient (neglecting Reynold's number effects)

1) Follow the same steps presented in the previous *R(S)* derivation to arrive at Equation 8.31 for the drag coefficient:

$$C_D = C_{fe}\frac{S_w}{S} + KC_L^{\,2} \tag{8.31}$$

2) Now, to assume the fuselage does not scale with the wing, $\frac{S_w}{S}$ must no longer be constant and must instead be a function of wing area *S*. Using [103] as a reference, we know that the function $\frac{S_w}{S} = f(S)$ would take the form shown below:

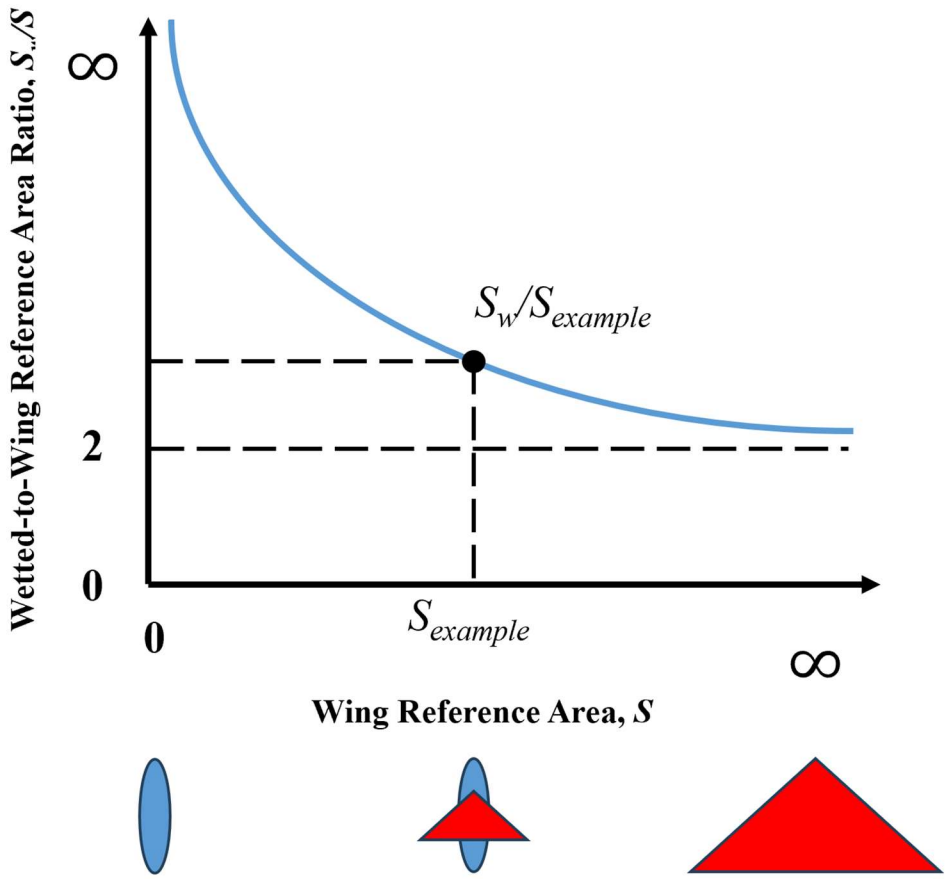

By using a real aircraft datapoint as a point on the curve, we can define the slope of $\frac{S_w}{S} = f(S)$ and create an analytical solution. Consider the F-4 Phantom as an example, since we know $S = 530$ ft^2 for this aircraft, and $\frac{S_w}{S} = 4$ according to [103]. In its simplest form, the $\frac{S_w}{S} = f(S)$ equation for an aircraft of this shape would be:

$$y = \frac{(530\ \text{ft}^2)(4-2)}{x} + 2$$

which looks like:

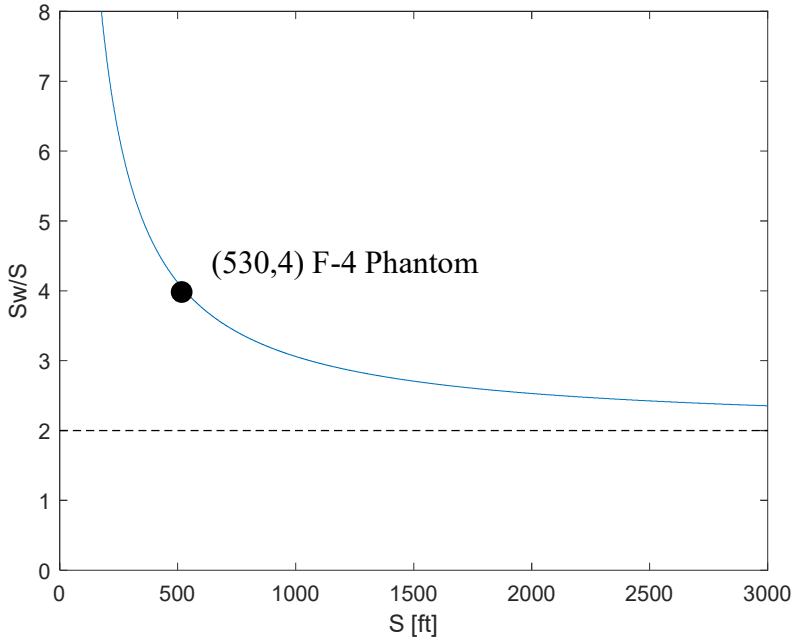

To generalize this curve for any reference aircraft, we can use:

$$\frac{S_w}{S} = \frac{S_m\left(\frac{S_w}{S}_m - 2\right)}{S} + 2 \tag{8.44}$$

in which S_m and $\frac{S_w}{S}_m$ are the wing reference area and wetted-to-wing area ratio for a reference aircraft denoted with the subscript 'm'. Now, as a function of S, we can substitute $\frac{S_w}{S}$ back into Equation 8.31 for C_D:

$$C_D = C_{fe}\left(\frac{S_m\left(\frac{S_w}{S}_m - 2\right)}{S} + 2\right) + KC_L^{\,2} \tag{8.45}$$

3) Introduce Breguet (Jet Range) Equation:

$$R = \frac{1}{c_t} V \frac{C_L}{C_D} \ln\left|\frac{W_0}{W_1}\right| \tag{8.46}$$

4) Follow previous steps 8-15 from Derivation 1 to arrive at:

$$R = \frac{\ln\left|\frac{W_0}{W_1}\right|}{c_t\left(C_{D0}\left(\frac{\rho_0 VS}{2W_0}\right)+K\left(\frac{2W_0}{\rho_0 SV^3}\right)\right)} \tag{8.47}$$

5) Expand: $C_{D0} = C_{fe}\left(\frac{S_m\left(\frac{S_w}{S_m}-2\right)}{S}+2\right)$

$$R = \frac{\ln\left|\frac{W_0}{W_1}\right|}{c_t\left(\left(C_{fe}\left(\frac{S_m\left(\frac{S_w}{S_m}-2\right)}{S}+2\right)\right)\left(\frac{\rho_0 VS}{2W_0}\right)+K\left(\frac{2W_0}{\rho_0 SV^3}\right)\right)} \tag{8.47}$$

6) Distribute $\left(\frac{\rho_0 SV}{2W_0}\right)$ across first term in the denominator and simplify:

$$R = \frac{\ln\left|\frac{W_0}{W_1}\right|}{c_t\left(C_{fe}\left(S_m\left(\frac{S_w}{S_m}-2\right)\left(\frac{\rho_0 V}{2W_0}\right)+\frac{\rho_0 VS}{W_0}\right)+K\left(\frac{2W_0}{\rho_0 SV^3}\right)\right)} \tag{8.47}$$

7) Simplify by forming constant coefficients **a**, **b**, **c, & d**:

$$R = \frac{a}{\left(b+cS+\frac{d}{S}\right)} \tag{8.47}$$

where:

$$a = \ln\left|\frac{W_0}{W_1}\right|$$

$$b = c_t\left(C_{fe}\right)S_m\left(\frac{S_w}{S_m}-2\right)\left(\frac{\rho_0 V}{2W_0}\right)$$

$$c = c_t\left(C_{fe}\right)\left(\frac{\rho_0 V}{W_0}\right)$$

$$d = c_t K\left(\frac{2W_0}{\rho_0 V^3}\right)$$

Graphical form of equation:

$$y = \frac{a}{\left(b + cx + \frac{d}{x}\right)} \tag{8.40}$$

Wing area required for maximum range occurs were dR/dS = 0:

$$\frac{dR}{dS} = 0 \tag{8.40}$$

$$\frac{dR}{dS}[R] = \frac{dR}{dS}\left[\frac{a}{\left(b + cS + \frac{d}{S}\right)}\right] = 0$$

$$-\frac{a\left(c - \frac{d}{S^2}\right)}{\left(b + cS + \frac{d}{S}\right)^2} = 0$$

$$S = \sqrt{\frac{d}{c}} \tag{8.41}$$

8) Substitute c & d:

$$R = \sqrt{\frac{d}{c}} = \sqrt{\frac{c_t K\left(\frac{2W_0}{\rho_0 V^3}\right)}{c_t C_{fe}\left(\frac{\rho_0 V}{W_0}\right)}} \tag{8.42}$$

9) Reduce to simplest expression:

$$S = \sqrt{\frac{K\left(\frac{2W_0^{\,2}}{\rho_0^{\,2}V^4}\right)}{C_{fe}}}$$

$$S = \frac{W_0}{\rho_0 V^2}\sqrt{\frac{2K}{C_{fe}}} \tag{8.43}$$

Using the following constants…

- $V = 400$ kts
- Cruise-climb starting at h_0 = 30k ft ($\rho_0 = 8.91 \times 10^{-4}$slug/ft^3)
- AR = 8.33
- e = 0.8
- c_t = 0.69 lb/lb/hr
- W_0 = 10,000 lb
- W_1/W_0 = 0.967
    - For W_0 = 10,000 lb… W_1 = 9,670 lb. (330 lb. fuel for cruise)
- C_{fe} = 0.0042

Plot *R = f(S):*

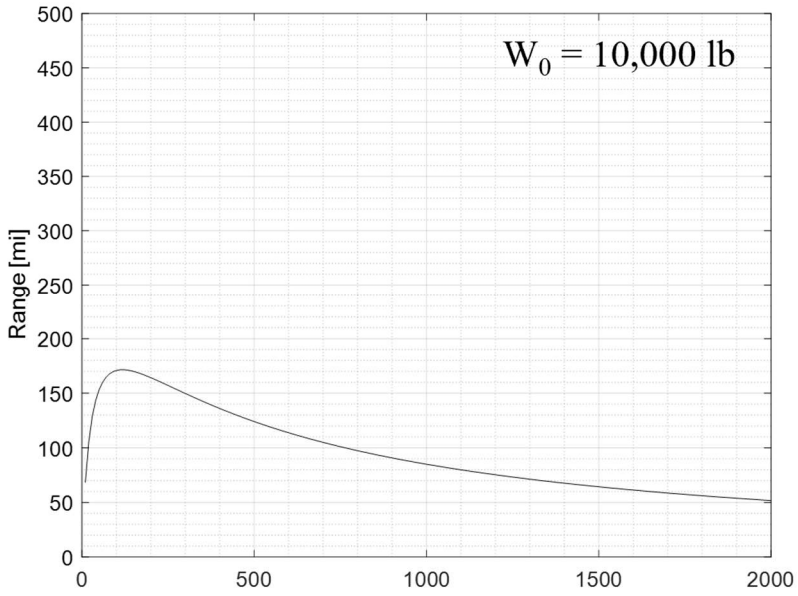

Plot $R = f(S)$ *varying* W_0:

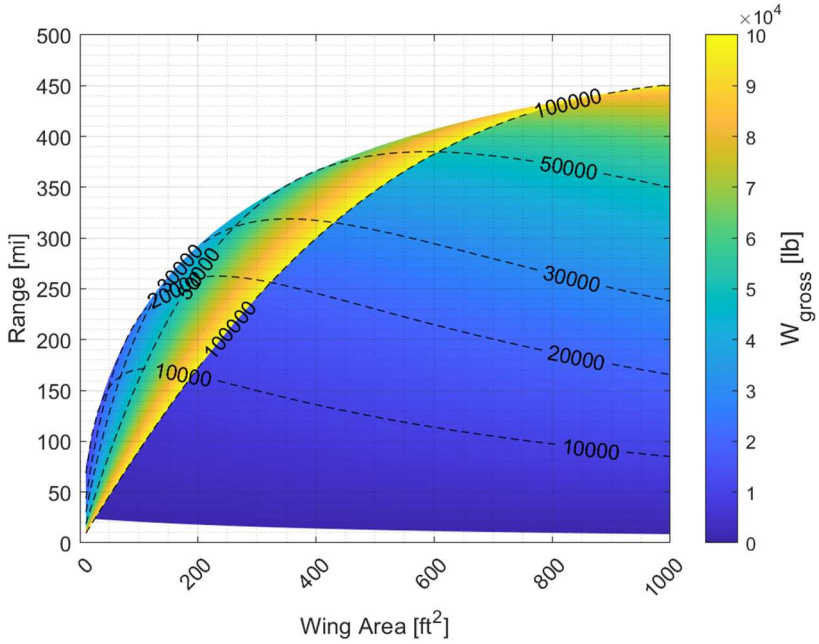

Plot $R = f(S)$ along with L/D to see what L/D maximizes range:

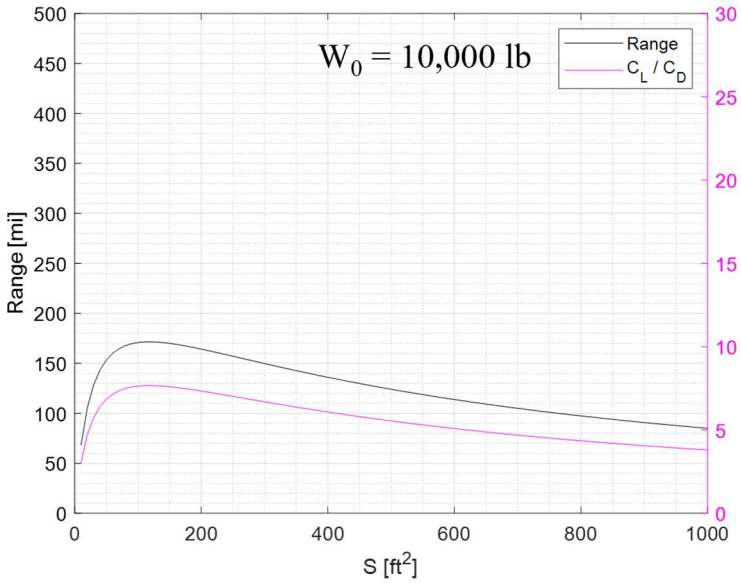

It appears $R = f(S)$ is maximized at L/D_{max}. This is different from the maximum jet range as a function of airspeed, $R = f(V)$, which is maximized at $L^{0.5}/D$.

Range vs. Wing Area and Airspeed:

Fixed cruise speed, variable wing area

- Velocity: V = 400 kts

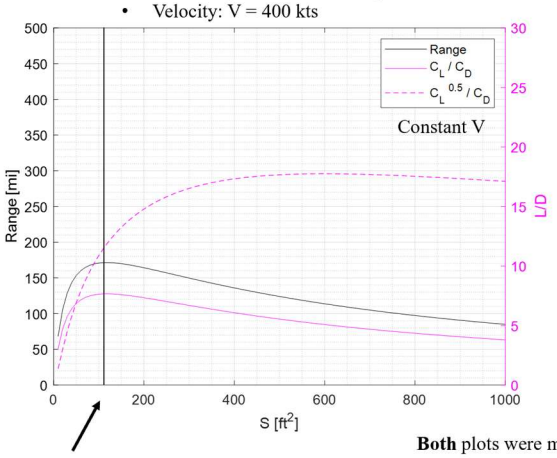

Max range (R) occurs at the **wing area (S)** which yields maximum $\mathbf{C_L/C_D}$

Fixed wing area, variable cruise speed

- Wing Area: S = 300 ft^2

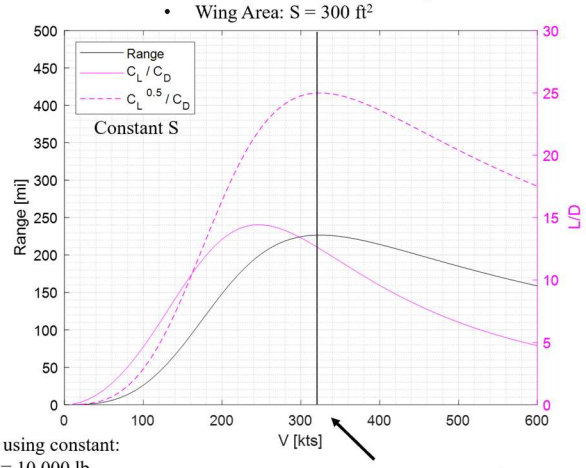

Max range (R) occurs at the **airspeed (V)** which yields maximum $\mathbf{C_L^{0.5}/C_D}$

Both plots were made using constant:

- Initial weight: W_0 = 10,000 lb
- Initial density for cruise-climb: h_0 = 30k ft ($\rho_0 = 8.91 \times 10^{-4}$slug/ft^3)
- TSFC: 0.69 lb/lb/hr

(Proof on next page)

R(S)

$$R = \frac{\ln\left|\frac{W_0}{W_1}\right|}{c_t\left(\left(C_{fe}\left(S_m\left(\frac{S_w}{S}_m - 2\right)\left(\frac{\rho_0 V}{2W_0}\right) + \frac{\rho_0 SV}{W_0}\right)\right) + K\left(\frac{2W_0}{\rho_0 SV^3}\right)\right)}$$

Simplify by forming coefficients **a**, **b**, **c, & d**:

$R = \frac{\boldsymbol{a}}{\left(\boldsymbol{b}+\boldsymbol{c}S+\frac{\boldsymbol{d}}{S}\right)}$, where: $\boldsymbol{a} = \ln\left|\frac{W_0}{W_1}\right|$,

$\boldsymbol{b} = c_t(C_{fe})S_m\left(\frac{S_w}{S}_m - 2\right)\left(\frac{\rho_0 V}{2W_0}\right)$

$\boldsymbol{c} = c_t(C_{fe})\left(\frac{\rho_0 V}{W_0}\right), \quad \boldsymbol{d} = c_t K\left(\frac{2W_0}{\rho_0 V^3}\right)$

Wing area required for maximum range occurs where dR/dS = 0:

$$\frac{dR}{dS}[R] = \frac{dR}{dS}\left[\frac{\boldsymbol{a}}{\left(\boldsymbol{b}+\boldsymbol{c}S+\frac{\boldsymbol{d}}{S}\right)}\right] = 0$$

$$-\frac{\boldsymbol{a}\left(\boldsymbol{c}-\frac{\boldsymbol{d}}{S^2}\right)}{\left(\boldsymbol{b}+\boldsymbol{c}S+\frac{\boldsymbol{d}}{S}\right)^2} = 0$$

$$S = \sqrt{\frac{\boldsymbol{d}}{\boldsymbol{c}}}$$

Substitute c & b:

$$S = \sqrt{\frac{\boldsymbol{d}}{\boldsymbol{c}}} = \sqrt{\frac{c_t K\left(\frac{2W_0}{\rho_0 V^3}\right)}{c_t C_{fe}\left(\frac{\rho_0 V}{W_0}\right)}}$$

Reduce to simplest expression:

$$S = \sqrt{\frac{K\left(\frac{2{W_0}^2}{\rho_0{}^2 V^4}\right)}{C_{fe}}}$$

$$S = \frac{W_0}{\rho_0 V^2}\sqrt{\frac{2K}{C_{fe}}}$$

C_L for maximum range:

$$C_L = \sqrt{\frac{C_{fe}}{2K}}$$

R(V)

$$R = \frac{\ln\left|\frac{W_0}{W_1}\right|}{c_t\left(C_{D0}\left(\frac{\rho_0 SV}{2W_0}\right) + K\left(\frac{2W_0}{\rho_0 SV^3}\right)\right)}$$

Simplify by forming coefficients **a**, **b**, & **c**:

$R = \frac{\boldsymbol{a}}{\left(\boldsymbol{b}V+\frac{\boldsymbol{c}}{V^3}\right)}$, where:

$\boldsymbol{a} = \ln\left|\frac{W_0}{W_1}\right|, \quad \boldsymbol{b} = c_t C_{D0}\left(\frac{\rho_0 S}{2W_0}\right)$

$\boldsymbol{c} = c_t K\left(\frac{2W_0}{\rho_0 S}\right)$

Airspeed required for maximum range occurs where dR/dS = 0:

$$\frac{dR}{dS}[R] = \frac{dR}{dS}\left[\frac{\boldsymbol{a}}{\left(\boldsymbol{b}S+\frac{\boldsymbol{c}}{S}\right)}\right] = 0$$

$$-\frac{\boldsymbol{a}\left(\boldsymbol{b}-\frac{3\boldsymbol{c}}{V^4}\right)}{\left(\boldsymbol{b}V+\frac{\boldsymbol{c}}{V^3}\right)^2} = 0$$

$$V = \sqrt[4]{\frac{3\boldsymbol{c}}{\boldsymbol{b}}}$$

Substitute c & b:

$$V = \sqrt[4]{\frac{3\boldsymbol{c}}{\boldsymbol{b}}} = \sqrt[4]{\frac{3c_t K\left(\frac{2W_0}{\rho_0 S}\right)}{c_t C_{D0}\left(\frac{\rho_0 S}{2W_0}\right)}}$$

Reduce to simplest expression:

$$V = \sqrt[4]{\frac{3K\left(\frac{4{W_0}^2}{\rho_0{}^2 S^2}\right)}{C_{D0}}}$$

$$V = \sqrt{\frac{2W_0}{\rho_0 S}}\sqrt{\frac{3K}{C_{D0}}} \quad \text{Raymer (Eq. 17.25)}$$

CL for maximum range:

$$C_L = \sqrt{\frac{C_{D0}}{3K}} \quad \text{Raymer (Eq. 17.26)}$$

End of Document